IMAGE-GUIDED RADIOTHERAPY OF LUNG CANCER

Edited by

James D. Cox

Joe Y. Chang

Ritsuko Komaki

informa
healthcare

Image-Guided Radiotherapy of Lung Cancer

IMAGE-GUIDED RADIOTHERAPY OF LUNG CANCER

Edited by

James D. Cox

The University of Texas M.D. Anderson Cancer Center
Houston, Texas, USA

Joe Y. Chang

The University of Texas M.D. Anderson Cancer Center
Houston, Texas, USA

Ritsuko Komaki

The University of Texas M.D. Anderson Cancer Center
Houston, Texas, USA

informa

healthcare

New York   London

Preface

Lung cancer is the leading cause of cancer death in the United States and the world. The five-year survival rate for all lung cancer patients over the past 20 years was around 15%. Approximately 15–20% of non–small cell lung cancer (NSCLC) patients present with stage I/II disease that is considered surgically resectable. However, most patients present with locally advanced disease requiring combined modality treatment including radiotherapy. In addition, patients with stage I/II NSCLC who cannot tolerate surgical resection due to co-morbidity are treated with definitive radiotherapy. For conventional radiotherapy, local control has been reported to be around 30–50% for stage I/II disease and 30% for stage III. Uncontrolled loco-regional disease is a major source for continuous seeding to distant organs and causes eventual treatment failure and cancer death. Eradication of loco-regional disease is an essential step for cure. There are three main reasons for local failure after radiotherapy: 1) geographic misses due to inadequacy of imaging tools for staging and radiotherapy planning; 2) respiratory tumor motion during radiotherapy; and 3) inadequate radiation dose due to concerns of significant toxicity. Novel approaches to improve radiotherapy in lung cancer are urgently needed.

The recent development of image-guided radiotherapy (IGRT) has introduced a new era of radiotherapy for lung cancer. PET/CT has been shown to improve targeting accuracy in 25–50% of cases, and 4-dimensional CT scanning has helped to individualize patients' radiotherapy based on tumor motion. Intensity modulated radiation therapy (IMRT) may allow us to escalate radiotherapy dose without increasing toxicity. Stereotactic body radiation therapy (SBRT) has opened the door to achieving higher than 90% local control by focused, hypofractionated, high biologically equivalent dose of radiotherapy. Proton radiotherapy may hold promise for lung cancer due to its physical characteristics that lead to high and conformal dose distribution in the tumor while reducing the entrance dose and stopping the beam distal to the target. These novel approaches were considered experimental just a couple of years ago. However, because of the potentially significant improvement in clinical outcome and accumulating clinical data, they are beginning to become standard treatment for lung cancer at major cancer centers.

In this book, we focus on novel approaches using IGRT, particularly PET/CT, 4-D CT, gated radiotherapy, stereotactic body radiation therapy, IMRT, and proton radiotherapy in lung cancer. We provide our recommended dose, fractionation, target volume delineation, treatment techniques, and normal tissue tolerances. Our intention is to provide disease stage-specific treatment guidelines and step-by-step techniques so that radiation oncologists may incorporate these new techniques into their clinical practice.

James D. Cox
Joe Y. Chang
Ritsuko Komaki

Acknowledgments

Contents

Contributors

Peter Balter   Department of Radiation Physics, University of Texas M.D. Anderson Cancer Center, Houston, Texas, U.S.A.

Keith R. Britton   Department of Radiation Physics, University of Texas M.D. Anderson Cancer Center, Houston Texas, U.S.A.

Joe Y. Chang   Department of Radiation Oncology, University of Texas M.D. Anderson Cancer Center, Houston, Texas, U.S.A.

James D. Cox   Department of Radiation Oncology, University of Texas M.D. Anderson Cancer Center, Houston, Texas, U.S.A.

Lei Dong   Department of Radiation Physics, University of Texas M.D. Anderson Cancer Center, Houston, Texas, U.S.A.

Roy Herbst   Department of Thoracic/Head and Neck Medical Oncology, University of Texas M.D. Anderson Cancer Center, Houston, Texas, U.S.A.

Ritsuko Komaki   Department of Radiation Oncology, University of Texas M.D. Anderson Cancer Center, Houston, Texas, U.S.A.

Zhongxing Liao   Department of Radiation Oncology, University of Texas M.D. Anderson Cancer Center, Houston, Texas, U.S.A.

Helen H. Liu   Department of Radiation Physics, University of Texas M.D. Anderson Cancer Center, Houston, Texas, U.S.A.

Radhe Mohan   Department of Radiation Physics, University of Texas M.D. Anderson Cancer Center, Houston, Texas, U.S.A.

Jack A. Roth   Department of Thoracic and Cardiovascular Surgery, University of Texas M.D. Anderson Cancer Center, Houston, Texas, U.S.A.

George Starkschall   Department of Radiation Physics, University of Texas M.D. Anderson Cancer Center, Houston, Texas, U.S.A.

Image Guidance of Screening, Staging, and Combined Modality Management of Non–Small Cell Lung Cancer

Joe Y. Chang and Ritsuko Komaki
Department of Radiation Oncology, University of Texas M.D. Anderson Cancer Center, Houston, Texas, U.S.A.

Jack A. Roth
Department of Thoracic and Cardiovascular Surgery, University of Texas M.D. Anderson Cancer Center, Houston, Texas, U.S.A.

Roy Herbst
Department of Thoracic/Head and Neck Medical Oncology, University of Texas M.D. Anderson Cancer Center, Houston, Texas, U.S.A.

James D. Cox
Department of Radiation Oncology, University of Texas M.D. Anderson Cancer Center, Houston, Texas, U.S.A.

INTRODUCTION

Lung cancer is the most common cancer worldwide and accounts for the most cancer-related deaths (1). The United States 2006 cancer statistics (2) showed that lung cancer is the second most common cancer for men and women but the number one cancer killer in both sexes. The most common lung cancer is non–small cell lung cancer (NSCLC), which accounts for 80% of all lung cancer cases. The 5-year survival rate of patients with lung cancer in the United States is only 15% according to the Surveillance, Epidemiology, and End Results program. Early diagnoses and more effective treatments are urgently needed.

Radiotherapy is crucial in the treatment of lung cancer and is required in 40% of patients with lung cancer. The poor outcome of lung cancer radiotherapy is caused by three major problems:

1. *Geographic miss*: The target is missed because of inadequate imaging and poor target delineation. Positron emission tomography/computed tomography (PET/CT) provides a more accurate image for stage and target delineation and has been reported to change the management of NSCLC, including target delineation in 25–50% of cases.
2. *Tumor motion*: Lung cancer moves during and between radiotherapy. If tumor motion is not considered, the target is missed and normal tissues are overexposed to radiation.
3. *Inadequate radiation dose*: We know that current standard doses are not high enough to achieve good local control. Dose escalation improves local control and possibly survival. However, toxic effects associated with dose escalation are significant, particularly when concurrent chemotherapy is given.

Image-guided radiation therapy (IGRT) allows more accurate tumor targeting and reduces toxic effects. IGRT with radiation dose escalation/acceleration may significantly improve the clinical outcome for patients with lung cancer. With the advancement of new systemic therapy, particularly molecular targeting therapy with a low occurrence of toxic effects, the combination of IGRT with novel systemic therapy may begin a new era for lung cancer management.

Recent innovations in imaging technology have changed the management of lung cancer, including screening, determining stage, designing radiotherapy regimens, and evaluating treatment response. IGRT, particularly in lung cancer, has been actively investigated, and preliminary data have demonstrated its efficacy in improving targeting accuracy and reducing toxic effects. In this chapter, we discuss image-guided lung cancer screening, staging, and combined modality management and follow-up of NSCLC.

NSCLC CLINICAL PRESENTATION AND PATTERNS OF SPREAD

Carcinoma of the lung is among the most insidious of all neoplasms. Some patients present with an asymptomatic lesion discovered incidentally by chest radiography or CT. Most lung cancers, however, are discovered because of the development of a new or worsening clinical symptom or sign. Although no set of signs or symptoms is pathognomonic for lung

cancer, the signs and symptoms may be divided into three categories based on progression or spread pattern: those due to local tumor growth and intrathoracic spread; those due to distant metastases; and those that are due to systemic effects, or paraneoplastic syndromes. Lung cancer may spread via hematogenous routes or locally within the lymphatics. In most cases, lymph node metastases seem to occur earlier than distant hematogenous spread. When patients present with symptoms or signs, the disease has usually reached an advanced stage, and thus, the chance of cure is much lower than it would have been if the disease had been detected earlier. Therefore, early diagnosis is crucial to improve clinical outcome.

IMAGE-GUIDED LUNG CANCER SCREENING

Efforts to detect lung cancers in earlier stages through screening programs had been unsuccessful until recently (3,4) partly because imaging technology has improved over the past two decades. Recently, the International Early Lung Cancer Action Program Investigators (5) reported the results of their large, collaborative, 12-year lung cancer screening study using spiral CT. Of 31,567 symptomatic participants at high risk of lung cancer, 484 were found to have lung cancer, which was of clinical stage I in 85% of cases. The estimated 10-year survival rate was 88% for all patients and 92% for the patients who underwent surgical resection within 1 month after diagnosis. The investigators concluded that annual spiral CT screening can detect lung cancer while it is still curable and that this procedure is cost effective (5).

The National Lung Screening Trial (NLST), sponsored by the National Cancer Institute (NCI), is a randomized controlled trial (6) to test whether low-dose CT scanning can reduce lung cancer mortality in asymptomatic individuals. The subjects are being randomly selected to undergo screening with low-dose CT or chest X-ray. The NLST will enroll 50,000 heavy smokers (and former heavy smokers who quit within 15 years before randomization) at high risk of lung cancer who are 55–74 years old. Participants will undergo an initial screening and two subsequent annual screenings and will be observed for at least 4.5 years. Final analyses are expected in 2009 (6).

IMAGE-GUIDED DIAGNOSTIC AND STAGING WORKUP

Determination of stage is important for therapeutic decisions and prognoses. Careful initial diagnostic evaluation to localize the disease and determine the extent of primary and metastatic tumor involvement is critical for patient care and radiotherapy treatment planning. Staging procedures include recording the patient's medical history, performing a physical examination, evaluating routine laboratory tests, and performing a chest X-ray and chest CT scan with contrast. The CT scan should extend inferiorly to include the upper abdomen and adrenal glands.

Additional tests such as bone scans and CT or magnetic resonance imaging of the brain may be performed if initial assessments suggest metastases, or they may be performed for patients with stages II–III disease who are under consideration for aggressive local and combined modality treatments. Mediastinoscopy or endobronchial ultrasound guided biopsies (EBUS) of mediastinal lymph nodes is considered standard if accurate evaluation of the nodal status is needed to determine therapy.

Radiologic Image Modality: CT and PET/CT

The wider availability and use of fluorodeoxyglucose positron emission tomography (FDG-PET) for staging has led to its use in evaluating mediastinal lymph nodes and distant metastases (43). The combination of CT scanning and PET scanning has greater sensitivity and specificity than CT scanning alone, and PET scanning should be considered a standard staging procedure. A prospective trial studied the effect of FDG-PET on disease staging for 102 patients with NSCLC. The investigators found that for the detection of mediastinal metastases, FDG-PET alone yielded a sensitivity of 91%, a specificity of 86%, a negative predictive value of 95%, and a positive predictive value of 74%, as compared with CT scanning alone, which had a sensitivity of 75% and a specificity of 66% (7). False-positive results were often caused by the presence of benign inflammatory disease, such as abscesses and active granulomatous diseases. Treatment-induced hypermetabolic inflammatory changes also may lead to difficulty in differentiating between treatment effects and those of the residual tumor. False-negative results have occurred primarily in tumors with a low-glucose metabolism (carcinoid and bronchioloalveolar carcinoma) and in small tumors, owing to the limited spatial resolution of current PET scanners. For patients with clinically operable NSCLC, a biopsy of the mediastinal lymph nodes is recommended for nodes in which the shortest transverse axis is >1.0 cm as shown on a chest CT scan or for nodes positive on an FDG-PET scan. Biopsy with mediastinoscopy or EBUS is necessary for the detection of cancer in mediastinal lymph nodes when the results of the CT scan and FDG-PET do not corroborate each other. In addition, FDG uptake by cancer cells revealed on PET scans has been shown to have independent prognostic value in newly diagnosed NSCLC and will help clinician to individualized patient management (8–10).

Table 1 TNM Descriptors[a]

Primary tumor (T)

TX Primary tumor cannot be assessed, or tumor proven by the presence of malignant cells in sputum or bronchial washes but not visualized by imaging or bronchoscopy

T0 No evidence of primary tumor

Tis Carcinoma in situ

T1 Tumor 3 cm or less in greatest dimension, surrounded by lung or visceral pleura, without bronchoscopic evidence of invasion more proximal than the lobar bronchus[a] (i.e. not in the main bronchus)

T2 Tumor with any of the following features of size or extent: more than 3 cm in greatest dimension; involves main bronchus, 2 cm or more distal to the carina; invades the visceral pleura; associated with atelectasis or obstructive pneumonitis that extends to the hilar region but does not involve the entire lung

T3 Tumor of any size that directly invades any of the following: chest wall (including superior sulcus tumors), diaphragm, mediastinal pleura, or parietal pericardium; or tumor in the main bronchus less than 2 cm distal to the carina, but without involvement of the carina; or associated atelectasis or obstructive pneumonitis of the entire lung

T4 Tumor of any size that invades any of the following: mediastinum, heart, great vessels, trachea, esophagus, vertebral body, or carina; or tumor with a malignant pleural or pericardial effusion,[b] or with satellite tumor nodule(s) within the ipsilateral primary tumor lobe of the lung

Regional lymph nodes (N)

NX Regional lymph nodes cannot be assessed

N0 No regional lymph-node metastasis

N1 Metastasis to ipsilateral peribronchial and/or ipsilateral hilar lymph nodes, and intrapulmonary nodes involved by direct extension of the primary tumor

N2 Metastasis to ipsilateral mediastinal and/or subcarinal lymph node(s)

N3 Metastasis to contralateral mediastinal, contralateral hilar, ipsilateral or contralateral scalene, or supraclavicular lymph node(s)

Distant metastasis (M)

MX Presence of distant metastasis cannot be assessed

M0 No distant metastasis

M1 Distant metastasis[c]

[a] The uncommon superficial tumor of any size with its invasive component limited to the bronchial wall, which may extend proximal to the main bronchus, also is classified T1.

[b] Most pleural effusions associated with lung cancer are the result of tumor. However, there are a few patients in whom multiple cytopathologic examinations of pleural fluid are negative for tumor. In these cases, the fluid is nonbloody and is not an exudate. When these elements are clinical judgment dictate that the effusion is not related to the tumor, the effusion should be excluded as a staging element and the patient should be staged T1, T2, and T3. Pericardial effusion is classified according to the same rules.

[c] Separate metastatic tumor nodule(s) in the ipsilateral nonprimary tumor lobe(s) of the lung are also classified M1.

Abbreviation: TNM, tumor, node, metastasis.

Source: From Ref. 69.

Staging

The American Joint Committee on Cancer has adopted the tumor, node, metastasis (TNM) classification, originally proposed by Mountain et al. (11), which is based primarily on surgical findings. This staging system, which was adopted by the American Joint Committee on Cancer and the International Union Against Cancer in 1997, was recently revised (Tables 1 and 2 and Fig. 1) (12,13). The staging system serves as a guide for treatment modality and prognosis.

Pathologic Classification and Prognostic Factors

The histologic classfication of lung tumors was revised in 1999 and in 2004 (Table 3). The histologic types are based on analysis by light microscopy and by standard staining techniques. The four major types are squamous cell carcinoma, adenocarcinoma, large-cell carcinoma (collectively known as NSCLC and reflecting 90% of cases), and small-cell undifferentiated carcinoma.

Prognostic factors for patients with lung cancer can be classified by patient-, tumor-, and treatment-specific variables. In the V.A. Lung Group Protocols, Stanley (14) evaluated 77 prognostic factors in approximately 5000 patients with inoperable carcinoma of the lung. The three most important prognostic factors affecting survival were patient-specific variables: performance status (Karnofsky score), disease stage, and weight loss. It is generally believed that squamous cell carcinoma has the best prognosis, followed by adenocarcinoma and undifferentiated large-cell carcinoma. Until recently, undifferentiated small-cell carcinoma had the poorest prognosis, but that prognosis has improved since the advent of more aggressive combined modality treatments.

COMBINED MODALITY MANAGEMENT OF NSCLC

In patients with NSCLC, the most important prognostic factor is tumor stage. This factor largely determines treatment. Surgery is the standard treatment for patients with stage I or II tumors and for selective patients with stage III tumors who can tolerate surgery. Neoadjuvant or adjuvant therapy is recommended for

Table 2 Stage Grouping: TNM Subsets

Stage	TNM subset		
Stage 0	Carcinoma in situ		
Stage IA	T1 N0 M0		
Stage IB	T2 N0 M0		
Stage IIA	T1 N1 M0		
Stage IIB	T2 N1 M0	T3 N0 M0	
Stage IIIA	T3 N1 M0	T1 N2 M0	
	T2 N2 M0	T3 N2 M0	
Stage IIIB	T4 N0 M0	T4 N1 M0	T4 N2 M0
	T1 N3 M0	T2 N3 M0	T3 N3 M0
	T4 N3 M0		
Stage IV	Any T, any N, any M		

Abbreviation: TNM, tumor, node, metastasis.
Source: From Ref. 69.

many patients with stage II or III disease. Only about 20% of all patients with lung cancer are suitable candidates for curative surgery. The use of combined modality therapy including radiotherapy and chemotherapy is recommended for locally advanced stage III disease. Patients with stage IV disease receive chemotherapy, palliative radiotherapy, or supportive therapy alone. Patients with histologically documented unresectable or medically inoperable stages I–III NSCLC are evaluated for undergoing definitive radiotherapy with or without chemotherapy. If there are pressing symptomatic needs for palliation, such as significant obstruction of a major airway, severe hemoptysis, superior vena cava obstruction, painful bony metastases in the weight-bearing areas, or symptomatic brain metastases, the initial treatment is radiotherapy with or without chemotherapy. If a patient has evidence of disseminated disease and there is no pressing need for radiotherapy, the approach includes consideration of systemic chemotherapy or supportive therapy alone if the patient's general condition is not suitable for systemic chemotherapy.
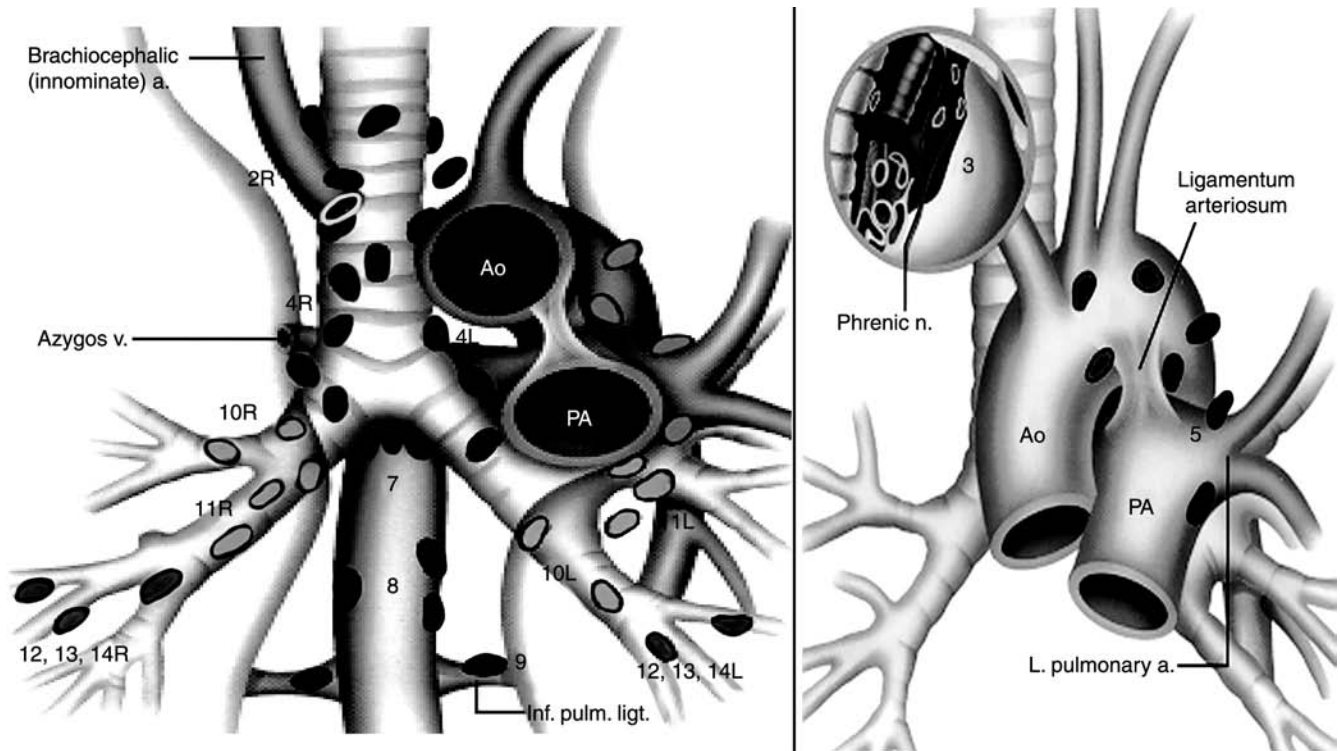

Figure 1 Regional nodal stations for lung cancer staging. N2 nodes include stations 1–9. N1 nodes include stations 10–14.

Table 3 WHO Lung Cancer Classification

  I. Epithelial tumors
    A. Benign
      1. Papillomas
      2. Adenoma
    B. Dysplasia/carcinoma *in situ*
    C. Malignant
      1. Squamous cell carcinoma
        a. Spindle cell variant
      2. Small-cell carcinoma
        a. Oat cell carcinoma
        b. Intermediate cell type
        c. Combined oat cell carcinoma
      3. Adenocarcinoma
        a. Acinar
        b. Papillary
        c. Bronchioalveolar
        d. Solid carcinoma with mucin formation
      4. Large cell carcinoma
        a. Giant cell carcinoma
        b. Clear cell carcinoma
      5. Adenosquamous carcinoma
      6. Carcinoid tumor
      7. Bronchial gland carcinoma
      8. Others
 II. Soft-tissue tumors
III. Mesothelial tumors
    A. Benign
    B. Malignant
IV. Miscellaneous tumors
    A. Benign
    B. Malignant
  V. Secondary tumors
 VI. Unclassified tumors
VII. Tumor-like lesions

Abbreviation: WHO, World Health Organization.
Source: From Ref. 70.

SURGICAL RESECTION AS A DEFINITIVE TREATMENT FOR NSCLC

Stages I and II NSCLC

Surgical resection with mediastinal lymph node dissection or sampling has been considered standard treatment for operable stage I or II NSCLC. The Lung Cancer Study Group reported a randomized comparison of an anatomic lobectomy versus a limited (wedge or segmental) resection for peripheral T1 pulmonary carcinomas (15). The locoregional recurrence rate was three times greater in the limited resection group (17%) than in the lobectomy group (6%). In the lobectomy group, there was a survival benefit for patients with tumors larger than 3 cm (15). For this reason, an anatomic lobectomy is recommended in patients who are able to tolerate the procedure. The average 5-year survival rate for patients with stage I NSCLC is approximately 65% (range 55–90%). The average 5-year survival rate for patients with stage II disease was 41% (range 29–60%) (13,16).

Stage III NSCLC

Approximately 25–40% of patients with NSCLC have stage III disease. Of these, approximately one-third present with potentially resectable disease, stage IIIA (T1-3 N2, T3 N1). The median survival duration for all patients with stage IIIA (clinical or surgical stage) disease treated with surgical resection alone is 12 months, and the 5-year survival rate is 9–15%. Within the stage IIIA subset, however, survival rates vary widely (13,16).

Patients with clinical (preoperative) N0 or N1 disease but pathologic (postresection) N2 disease survive longer than patients with clinical N2 disease. If patients have N2 disease at diagnosis, combined modality management is generally recommended, and participation in clinical trials is encouraged. Patients with stage IIIB disease are not considered candidates for surgical resection except for those with selective T4 tumors involving the carina and the superior vena cava, aorta, or atrium or those with satellite lesions in the same lobe and having limited vertebral involvement. However, special expertise in this type of surgery is required, and combined modality treatment is recommended.

Patients with stage II disease and lymph node involvement (T1 N1 and T2 N1) who have low 5-year survival rates (25–50%) after surgical resection alone and those with stage III disease who have a very low 5-year survival rate might benefit from neoadjuvant therapy. At M.D. Anderson Cancer Center, 60 patients with stage III NSCLC were randomized to undergo either neoadjuvant chemotherapy (three cycles of cyclophosphamide, etoposide, and cisplatin) and then surgery or surgery alone originally reported in 1994 (17). An update of the analysis with a median potential follow-up of 82 months, showed 36% 5-year survival for the neoadjuvant chemotherapy group compared to 15% for the surgery alone groups which retained statistical significance ($P < 0.05$). Rosell and et al. (18) of Barcelona reported similar result in their randomized study.

A trial approach similar to those mentioned for stage IIIA disease was also reported by Rusch et al. (19), who administered neoadjuvant treatment consisting of cisplatin plus etoposide and concurrent irradiation, followed by surgery, to 51 patients with stage IIIB NSCLC [a subset of patients from a Southwest Oncology Group (SWOG) protocol]. Thirty-two patients (63%) underwent resection of the primary tumor; the operative mortality rate was 5.2%. The 2-year survival rate for the total group of 51 patients was 39%. Most of the recurrences were distant. This study demonstrated the feasibility of such an approach in patients with advanced disease (19).

To study the issue of surgical resection after induction chemoradiotherapy, the SWOG conducted a

phase II trial of induction concurrent chemotherapy, cisplatin, and etoposide with thoracic radiotherapy (TRT) in 74 patients with biopsy-proven stage IIIA (N2) NSCLC. Study results suggested that this approach may improve patient survival with reasonable toxic effects. Median survival duration was 13 months, the 2-year survival rate was 37%, and the 3-year survival rate was 27%. The median survival duration of the patients who had pathologic complete response of nodal disease was 30 months, while that of patients with residual nodal disease was 10 months ($P = 0.0005$).

On the basis of the results from that study, the NCI had launched a phase III multicenter trial for patients with biopsy-proven N2 disease and potentially resectable NSCLC (NCI Protocol INT 139). Patients were stratified by performance and T statuses and were randomized to receive induction chemoradiotherapy (45 Gy) followed by surgery or concurrent chemotherapy and definitive radiotherapy (61 Gy). All patients received an additional two courses of chemotherapy (20). The data showed a significantly greater progression-free survival rate for the trimodality arm. Survival curves were superimposed through year 2 and then separated. By year 5, an absolute survival benefit of 7% favored the surgery arm [odds ratio = 0.63 (0.36, 1.10), $P = 0.10$]. Subgroup analysis revealed better survival for patients who underwent a lobectomy than patients who underwent definitive chemoradiotherapy ($P = 0.002$). However, trimodality therapy was not optimal when a pneumonectomy was required because of the high risk of death associated with pneumonectomy. Finally, N0 status at surgery significantly predicted a higher 5-year survival rate than patient had positive lymph node. The authors suggested that surgical resection after chemoradiotherapy can be considered for fit patients when lobectomy is feasible (20).

The optimal regimen for induction treatment for N2 disease remains investigational. The Radiation Therapy Oncology Group (RTOG) is conducting a phase III study to compare induction chemotherapy with induction chemoradiotherapy followed by surgical resection in pathologically proven N2 NSCLC.

ADJUVANT THERAPY

Postoperative Radiotherapy

In general, postoperative radiotherapy (PORT) is indicated in incomplete resections (close or positive margins) or positive mediastinal metastases (N2). PORT is currently contraindicated in patients with stage I completely resected disease, concluded a recent PORT meta-analysis (21). Data for stage II and higher disease neither support nor refute the use of PORT (because the hazard ratio error bars include 1.0), although PORT clearly improves regional control.

The Lung Cancer Study Group conducted a randomized study (22) to evaluate PORT in patients with completely resected stages II and IIIA squamous cell carcinoma of the lung. Only patients with hilar (N1) or mediastinal (N2) lymph node metastasis were included in the study. Patients in the adjuvant radiation arm were treated to 50 Gy in 5 weeks. No difference in overall survival was detected. However, patients who received radiation had reduced local recurrence rates (3% vs. 41%), especially patients with N2 disease.

Adjuvant chemotherapy

A meta-analysis in 1995 compared surgery alone with surgery followed by cisplatin-based chemotherapy. This study included eight trials and 1394 patients, and showed a 13% reduction in the risk of death in the chemotherapy group, suggesting that adjuvant chemotherapy afforded an absolute survival benefit of 5% at 5 years ($P = 0.08$). This was not affected by patient gender, performance status, age, or tumor histologic subtype (23). The International Adjuvant Lung Trial (24) included 1867 patients who underwent randomization either to receive three or four cycles of adjuvant cisplatin-based chemotherapy or to undergo observation. The investigators concluded that cisplatin-based adjuvant chemotherapy prolonged survival in patients with completely resected NSCLC (24). The National Cancer Institute of Canada's JBR10 study (25) reported a survival benefit of 15% at 5 years, and the Cancer and Leukemia Group B (CALGB) 9633 study (26) reported a benefit of 12% at 4 years. With longer follow-up, the CALGB trial no longer shows a benefit for adjuvant chemotherapy although there is a significant difference in favor of adjuvant chemotherapy in disease-free survival. In the Adjuvant Navelbine International Trialist Association trial (27), an 8% survival benefit was observed in the adjuvant chemotherapy arm. Furthermore, a Japanese meta-analysis (28) of 2003 patients randomized in six trials of uracil-tegafur showed a 5% survival benefit at 7 years, confirming the results of the Japanese Lung Cancer Research Group study (29). Supplementing surgery for NSCLC with chemotherapy (either adjuvant or neoadjuvant) is becoming the standard of care, and standardization, optimization, and individualization of this approach is expected soon (30,31). However, with the reanalysis of the CALGB trial, none of the studies show benefit for stage IB patients, so this remains an area for further investigation.

DEFINITIVE RADIOTHERAPY FOR INOPERABLE NSCLC

Stage I/II NSCLC

Patients with stage I or II NSCLC who cannot undergo surgery because of their lung function, cardiac

function, bleeding tendency, or other comorbid conditions or who refuse surgery should be considered for definitive radiotherapy. Results of retrospective studies suggest better results in patients with tumors smaller than 3 cm, in patients with excellent performance status, and in those given radiation doses of 60 Gy or more. Dosoretz and colleagues (32) reported that rates of distant metastasis were correlated to the size of the primary tumor. Incidences of metastasis in 3 years were 8% for cases with tumors smaller than 3 cm, 27% for tumors measuring 3–5 cm, and 50% for tumors larger than 5 cm. They reported that the local control rates at 3 years were 77% for 4-cm lesions and 48% for those larger than 4 cm (32). As would be expected, the intercurrent death rates in patients with inoperable stage I or II NSCLC are quite high. Cause-specific survival was more descriptive of tumor control in the medically inoperable population but was poorly documented because of a lack of systematic image follow-up (32).

In most previous studies, conventional fractionated radiotherapy (60–66 Gy in 1.8- or 2-Gy fractions) was used, with reported 5-year local control and overall survival rates ranging from 30–50% and 10–30%, respectively (32,33). Several studies (32–35) have reported a benefit from dose escalation, suggesting a dose–response relationship in both survival and local control in these patients. Because early stage NSCLC is not inherently a systemic disease from diagnosis and because local control is poor after conventional radiotherapy, research measures to improve survival should put significant emphasis on improving local tumor obliteration. To make sure the target volume is adequately covered, tumor motion during and between radiotherapy treatments should also be taken into consideration (see Chapter 4 for details). Image-guided hypofractionated stereotactic body radiotherapy (SBRT) with an escalated biological effective dose has been shown recently to achieve higher than 90% local control rates and improved survival. SBRT may become a standard of treatment for medically inoperable stage I NSCLC (see Chapter 6 for details).

Stage III NSCLC

Definitive radiotherapy alone

Most patients registered for radiotherapy have locoregionally advanced lung cancer (stage IIIA or IIIB) that is inoperable. Combined modality treatment including definitive radiotherapy and chemotherapy has been considered standard for this group of patients. Definitive radiotherapy consists of a minimum dose of 60–75 Gy to the gross disease and 50 Gy to microscopic disease with standard fractionation (1.8 or 2 Gy/fraction). A minimal tumor dose of 60 Gy has

been considered standard for the past 20 years. However, the optimal dose and regimen remain unclear. We know that the local control rate when 60 Gy is used in stage III NSCLC is only about 30%, and a higher dose is required to improve local control and survival. However, dose escalation is limited by its toxic effect. Image-guided three-dimensional conformal radiotherapy (3DCRT) and the recently developed intensity-modulated radiotherapy (IMRT) and proton therapy for lung cancer may allow further dose escalation with tolerable toxic effects (see Chapter 7 for details).

Conventional dose and fractionation

Current radiotherapy doses (60 Gy given in single daily fractions of 2 Gy) for patients with unresectable, locally advanced NSCLC (stages IIIA and IIIB) were established by RTOG 73-01 (36). In that study, 375 patients with inoperable or unresectable stage III (T1 N2, T2 N2, T3 N0, T3 N1, or T3 N2) NSCLC (squamous cell carcinoma, adenocarcinoma, or large-cell undifferentiated carcinoma) were randomized to receive a dose of 40-Gy split-course dose of radiation or a 40-, 50-, or 60-Gy dose in a continuous course with daily doses of 2 Gy. At 2–3 years, survival rates were 15% and 20% for patients treated with 50 and 60 Gy, respectively, compared with 10% for patients in the 40-Gy groups ($P = 0.10$). After 4 years, survival was comparable in all groups (4–6%). In patients treated with 40 Gy, the rates of intrathoracic failure were 44% and 52% compared with 33–45% in those treated with 50 or 60 Gy. The incidences of distant metastasis as detected by clinical or radiographic examination were 75–80% in all groups (37). In patients surviving 6–12 months, a statistically significant increase in survival was noted when the intrathoracic tumor was controlled. Patients treated with 50–60 Gy and showing tumor control had a 3-year survival rate of 22% versus 10% if they had intrathoracic tumor failure ($P = 0.05$) (38).

Radiation dose escalation and acceleration

From basic principles advocated by Fletcher (39), doses in the range of 80–100 Gy are required to sterilize the tumors frequently treated in patients with bronchogenic carcinoma. There are two fundamental problems with the delivery of such doses in lung cancer: the high rate of distant metastases (the major contributor to tumor-related mortality) and the toxic effects to normal thoracic organs. To improve survival rates for this population, the RTOG set out in 1983 to reduce local failures by administering intensified radiotherapy regimens in a second dose-escalation trial (40,41). Hyperfractionation regimens (1.2 Gy twice daily) were used to decrease toxic effects

to normal tissue. Five radiation doses were tested: 60, 64.8, 69.6, 74.4, and 79 Gy. The best results were seen in a cohort of patients with good performance (Karnofsky performance status score ≥70 and weight loss ≤50%) who received 69.6 Gy; the 1-year survival rate was 58%, and the 3-year survival rate was 20% (40,41).

Saunders et al. (42) reported the results of a multicenter European trial in which continuous, hyperfractionated, accelerated radiotherapy was compared with standard radiotherapy for NSCLC. Patients randomized to the experimental arm received 36 fractions of 1.5 Gy/fraction given as three fractions per day for 12 consecutive days, for a total dose of 54 Gy. The control arm received 2 Gy/fraction to 60 Gy over 6 weeks. Both 1- and 2-year survival rates were improved with the intensive radiotherapy course. There was no difference reported in acute and late toxic effects between the groups (43).

In an Eastern Cooperative Oncology Group (ECOG 4593) phase-II hyperfractionated, accelerated, radiotherapy trial (44), 30 patients were treated with 1.5- to 1.8-Gy fractions three times per day for 16 days, for a total dose of 57.6 Gy. This protocol called for no treatments to be given on weekends. At the 19-month analysis, the median survival time was 13 months and the 1-year survival rate was 57% (44). This regimen is being compared with standard radiotherapy (60 Gy over 6–7 weeks) by ECOG in a phase III trial.

A trial from the Netherlands (45) intensified the radiation delivered by using a concomitant-boost technique. Thirty-three patients with inoperable NSCLC were treated with 60 Gy in 20 fractions in 25 days. Fifteen patients received 40 Gy in 2-Gy fractions to the primary tumor and a part of the mediastinum, and 18 patients received the same dose to the primary tumor and the whole mediastinum. During each session, a simultaneous boost of 1 Gy was administered to the primary tumor. Moderate acute toxic effects to the esophagus were observed in seven of 33 patients (21%) and severe late toxic effects were seen in one patient (3%). After a mean follow-up of 14 months, 17 patients (52%) had local tumor control, 13 (39%) developed a confirmed local recurrence within the treated area, and three (9%) had suspected tumor regrowth (45).

The RTOG recently completed a phase II dose-escalation study (RTOG 9311) (46). Patients were treated with either radiation alone or radiation following neoadjuvant chemotherapy. 3DCRT was planned with target volumes limited to the gross tumor volume plus a margin. Because the study was designed to find the maximum tolerated radiation dose, the total volume of normal lung treated determined the dose. Patients with smaller lung volumes irradiated were treated to higher doses according to the escalation schema. Total doses ranged from 70.9 to 90.3 Gy for the small-volume group and 70.9–77.4 Gy for the large-volume group. The daily fraction size was 2.15 Gy. RTOG 9311 showed that acute toxic effect rates were acceptable for the dose up to 90.3 Gy (rate less than 15% for grade 3 and above pneumonitis and no esophagitis). However, late toxic effects were more pronounced. Late grade 3 and above radiation pneumonitis occurred at a rate of 15% for patients with a V20 <25% treated to dose levels of 77.4 Gy or above with a fraction size of 2.15 Gy. For patients with a V20 of 25–37%, grade 3 and above late pneumonitis occurred at a rate of 15% for the doses of 70.9 Gy or higher. The late grade 3 and above esophagitis occurred in less than 7% of the patients. The rate of late esophagitis was not directly correlated with doses, but it may have been related to the volume of esophagus treated (46).

University of Michigan investigators performed a dose-escalation trial that included 106 patients with stages I–III NSCLC treated with 63–103 Gy in 2.1-Gy fractions using 3DCRT (47). Targets included only the primary tumor and any lymph nodes ≥1 cm. Eighty-one percent of the patients received no chemotherapy. The median survival was 19 months. Multivariate analysis revealed that weight loss ($P = 0.011$) and radiation dose ($P = 0.0006$) were significant predictors of overall survival. The 5-year overall survival rates were 4%, 22%, and 28% for patients receiving 63–69 Gy, 74–84 Gy, and 92–103 Gy, respectively. Radiation dose was the only significant predictor when multiple variables were included ($P = 0.015$). They concluded that higher-dose radiation is associated with improved outcomes in patients treated within the range of 63–103 Gy.

Altered fractionation and/or dose escalation remain investigational for stage III NSCLC. Because lung cancer has a high occurrence of distant metastasis (>50%) and is particularly affected by tumor motion during radiotherapy (>50% of tumors move more than 5 mm), chemotherapy and image-guided radiotherapy play an important role in the management of NSCLC.

Definitive chemoradiotherapy
Conventional radiotherapy alone resulted in a median survival time of 10 months and a 5-year survival rate of 5%. To improve the outcome of treatment, chemotherapy was added to radiotherapy. Chemotherapy and radiotherapy can be delivered sequentially or concurrently. The most well-known trial, reported by the CALGB (48), compared standard radiotherapy to 60 Gy to sequential cisplatin and vinblastine chemotherapy for two cycles followed by

radiotherapy to 60 Gy. Median survival times and 5-year survival rates were superior for the chemoradiotherapy arm (13.8 vs. 9.7 months, 19% vs. 7%, respectively) (48).

These results led the RTOG to conduct a three-arm trial (RTOG 88-08) comparing standard radiotherapy, sequential chemoradiotherapy (CALGB regimen), and 69.6-Gy hyperfractionated radiotherapy (40,49). Sequential chemoradiotherapy was statistically superior to standard and hyperfractionated radiotherapy.

Dillman et al. (50) later reported that a retrospective quality-control review of the CALGB trial identified 23% of cases in which portal films failed to completely encompass the tumor. Two-dimensional radiotherapy, not modern IGRT, was used for radiotherapy planning in all these trials. Further efforts to improve local control and decrease distant metastasis has led investigators to pursue additional strategies, including concurrent cisplatin-based chemotherapy with radiotherapy, combined chemotherapy and hyperfractionated radiotherapy, and new chemotherapeutic agents combined with radiotherapy.

Schaake-Koning et al. (51) compared radiotherapy alone with radiotherapy plus daily cisplatin or weekly cisplatin. There was no difference in distant failure rates between the groups with or without cisplatin. However, the survival rate in the radiotherapy-plus-cisplatin group was 54% at 1 year, 26% at 2 years, and 16% at 3 years, compared with 46%, 13%, and 2% in the radiotherapy-alone group ($P = 0.009$). Therefore, this study showed that a gain in local tumor control seems to have translated into increased survival time.

Furuse et al. (52) compared patients receiving two cycles of mitomycin, vindesine, and cisplatin given every 28 days concurrent with split-course radiotherapy (total dose of 56 Gy) with patients receiving two cycles of mitomycin, vindesine, and cisplatin followed by continuous radiotherapy (total dose of 56 Gy). The concurrent treatment yielded an improved 5-year survival rate compared with the sequential treatment. A subsequent report demonstrated that the difference in survival was attributed to better intrathoracic tumor control in the patients receiving concurrent treatment (53).

The RTOG (RTOG 9410) (54) conducted a three-arm randomized trial to analyze whether the concurrent delivery of cisplatin-based chemotherapy with TRT improves survival compared with the sequential delivery of these therapies for patients with locally advanced, unresected stages II–III NSCLC. The sequential therapy consisted of cisplatin (P, 100 mg/m^2) and Vib (5 mg/m^2) followed by 60 Gy of radiation. The concurrent treatment used the same chemotherapy with 60 Gy of radiation beginning on day 1 of chemotherapy (CON-QD RT). The third treatment was concurrent P (50 mg/m^2) and oral etoposide (50 mg) with 69.6 Gy of radiation in 1.2-Gy BID fractions beginning on day 1 (CON-BID RT). For the 595 analyzable patients, the acute grade 3–5 nonhematologic toxic effect rates were higher with concurrent therapy than sequential therapy, but late toxic effect rates were similar (18–27%). With minimum and median follow-up times of 4.0 and 6.0 years, the median survival times and 4-year survival rates were 14.6 months and 12% for patients receiving sequential treatment, 17.1 months and 21% for patients receiving CON-QD RT, and 15.2 months and 17% for patients receiving CON-BID RT. The CON-QD RT group had better survival times and rates than the sequential group ($P = 0.046$).

That trial (54) demonstrated that the concurrent delivery of cisplatin-based chemotherapy with TRT conferred a greater long-term survival benefit than did the sequential delivery of these therapies. The locoregional failure rates were 50% for patients receiving sequential treatment, 43% for patients receiving CON-QD RT, and 34% for patients receiving CON-BID RT. The rate of acute toxic effects were higher in the CON-BID RT group (68% grade 3 and above) than in the CON-QD RT group (48% grade 3 and above). There was no significant difference in late toxic effects and survival between these two groups. However, the rate of radiotherapy in-field failure was lower in the CON-BID RT group than in the CON-QD RT group. The higher rate of toxic effects in the CON-BID RT group may explain its lack of a survival benefit. In RTOG 9410 (54), radiotherapy was based on two-dimensional planning, which is usually associated with higher toxic effect rates.

A third trial (55) comparing concurrent with sequential chemoradiotherapy reported in 2001 and updated in 2005 also explored the use of consolidation chemotherapy. In this phase III trial from France, 205 patients were assigned to receive two cycles of cisplatin plus vinorelbine followed by 66 Gy of radiation or cisplatin/etoposide and concurrent radiation to 66 Gy followed by two cycles of consolidation chemotherapy with cisplatin and vinorelbine. Local control rates were improved with the concurrent regimen (40% vs. 24%), and the median survival times and 4-year survival rates were numerically superior (but not statistically superior) in the concurrent arm of the trial (16.3 vs. 14.5 months and 21% vs. 14%, respectively). However, the incidence of grade 3 esophagitis was significantly higher in the concurrent arm (32% vs. 3%), and the toxic effects-related death rates were high in both arms (9.5% in the concurrent arm and 5.6% in the sequential arm).

These three phase III trials consistently demonstrated longer survival times for patients receiving

Table 4   Concurrent and Sequential Chemoradiotherapy for Inoperable Stage III NSCLC

Trial	Number of patients	Median survival time (months)		Survival rate, % (years)		Esophagitis, % (Gr. 3–4)	
		S	C	S	C	S	C
Furuse et al. (52)	314	13.3	16.5	8	16 (5)	4	23
Curran et al. (54)	400	14.6	17.1	12	21 (4)	5	26
Fournel et al. (55)	205	14.5	16.3	14	21 (4)	3	32

Abbreviations: C, concurrent; S, sequential.

concurrent chemoradiotherapy, and this difference was significant in two of the three trials (Table 4). On the basis of these results, concurrent chemoradiotherapy has been the standard of care since 2001. It is important to note that toxic effects are significantly more common with concurrent chemoradiotherapy than with sequential chemoradiotherapy.

In RTOG 9410 (54), the locoregional failure rate after concurrent chemoradiotherapy was still around 34–43%. To improve the local control rate, three groups (RTOG, NCCTG, and the University of North Carolina) (56–58) have separately performed radiation dose-escalation trials for patients with inoperable stage III NSCLC and reported results supporting the safety of 74 Gy. University of North Carolina (58) conducted a phase I/II dose-escalation clinical trial using high-dose 3DCRT (60–74 Gy) for inoperable stage IIIA/IIIB NSCLC with induction chemotherapy followed by concurrent chemoradiotherapy. They reported a 3-year survival rate of 36% and a 13% locoregional relapse rate as the only site of failure. For patients who finished radiotherapy, the 3-year survival rate was 45%. No grade 3 or higher toxic effects to the lung were reported; 8% of the patients developed grade 3/4 esophagitis.

The same group is conducting a higher dose-escalation study using up to 90 Gy of radiation (58,59). At 90 Gy of radiation, cases of broncho-esophageal fistula, bronchial stenosis, and fatal pulmonary hemoptysis have been reported, although the incidence still has been very low. One hundred twelve patients have been accrued; the median follow-up time is 4.9 years for surviving patients. The median survival was 24 months (range, 18–31 months). The 1-, 3-, and 5-year overall survival rates were 69% (range 60–77%), 36% (range 27–45%), and 24% (range 16–33%), respectively. Distant metastasis was still the major failure.

Because of the promising local control, good survival data, and acceptable toxic effects obtained using 3DCRT to doses of 74 Gy with concurrent chemotherapy, RTOG is planning a phase III study to compare conventional radiotherapy to 64-Gy with 3DCRT to 74 Gy, both administered concurrently with weekly paclitaxel and carboplatin in patients with stage IIIA/B NSCLC. IGRT will be strongly recommended for the study. IMRT will be allowed if tumor motion is taken into consideration. Consolidation chemotherapy will be required.

Newer chemoradiotherapy regimens
The most commonly used chemoradiotherapy combination consists of carboplatin and paclitaxel (Taxol) or cisplatin and etoposide (VP-16). Selected phase II trials (60,61) using paclitaxel, an inhibitor of normal microtubule function, and carboplatin have reported encouraging results. Paclitaxel has been shown to arrest cells in G2/M phase, the most radiosensitive phase of the cell cycle. The early response rates and survival rates appear promising in patients with unresectable stage III NSCLC. The reported grade 3 or 4 esophagitis and pneumonitis rates approach 26–46% and 17–22%, respectively, when chemotherapy is used concurrently with radiotherapy (60,61).

Other systemic therapies being tested in clinical trials include docetaxel (Taxotere®), vinorelbine (Navelbine®), gemcitabine (Gemzar®), and irinotecan (Camptosar®). In 2001, the CALGB (60) completed a three-arm randomized phase II study testing combinations of gemcitabine/cisplatin, paclitaxel/cisplatin, and vinorelbine/cisplatin with concurrent radiotherapy to 66 Gy. The results indicated the feasibility of administering chemotherapy concurrently with these newer chemotherapeutic agents. However, caution is advised when gemcitabine is delivered concurrently with radiation because it enhances tissue radiosensitivity.

The concept of administering a possibly non–cross-resistant chemotherapeutic agent following the completion of concurrent chemoradiotherapy was examined in a recent SWOG study (63). In this multi-institutional single-arm phase II study, 71 patients with unresectable stage IIIB NSCLC were treated with cisplatin and etoposide concurrently with TRT followed by three cycles of docetaxel (75–100 mg/m^2 given every 3 weeks) (63). The median survival time was an impressive 27 months, and the projected 3-year survival rate was 47%. On the basis of these promising results, SWOG investigators now are conducting a phase III study comparing this regimen

(cisplatin, etoposide, and radiation followed by three cycles of docetaxel) with an identical regimen followed by maintenance therapy with ZD 1839 (Iressa), a specific inhibitor of epidermal growth factor receptor (EGFR) tyrosine kinase.

The role of induction chemotherapy followed by concurrent chemoradiotherapy or concurrent chemoradiotherapy followed by consolidation chemotherapy remains investigational. Belani et al. (64) reported a multi-institutional randomized phase II study for locally advanced NSCLC. Patients were randomized to receive two cycles of induction paclitaxel (200 mg/m^2) and carboplatin (AUC = 6) followed by 63 Gy of radiation (arm 1), two cycles of induction paclitaxel (200 mg/m^2)/carboplatin (AUC = 6) followed by weekly paclitaxel (45 mg/m^2)/carboplatin (AUC = 2) with concurrent TRT (63.0 Gy) (arm 2, induction/concurrent) or weekly paclitaxel (45 mg/m^2)/carboplatin (AUC = 2)/TRT (63.0 Gy) followed by two cycles of paclitaxel (200 mg/m^2)/carboplatin (AUC = 6; arm 3, concurrent/consolidation). The data indicated that concurrent weekly paclitaxel, carboplatin, and TRT followed by consolidation chemotherapy seemed to be conferred the best outcome, although this schedule was associated with more toxic effects than the other schedule.

Molecular targeting and molecular markers
Several targeted therapies or biologic agents are undergoing extensive evaluation in patients with NSCLC. Some of these agents are administered orally and have a very favorable toxicity profile. If proven to be active, these agents alone or in combination with chemotherapy and/or radiotherapy could significantly affect the outcome of patients with NSCLC. Several new agents that target specific receptors or receptor tyrosine kinases now have become available for clinical research. The most promising among them is a class of compounds that target the EGFR or receptor tyrosine kinases. Agents that target EGFR or receptor tyrosine kinases have been studied recently in metastatic NSCLC. Randomized phase II/III studies have been completed recently with ZD 1839 (Iressa) and erlotinib (Tarceva). The preliminary data showed that erlotinib was associated with a trend toward improved progression-free and overall survival. Cetuximab (C225), an antibody against EGFR, has been recently investigated for its role in concurrent chemoradiotherapy by RTOG. Bevacizumab (Avastin) is a recombinant monoclonal antibody that blocks vascular endothelial growth factor. On the basis of phase II/III clinical trials, the ECOG (ECOG 4599) recommends bevacizumab in combination with paclitaxel and carboplatin as a new treatment for patients with stage IV nonsquamous NSCLC.

Biological markers particularly for apoptosis pathway (such as p53 polymorphisms), EGF receptor mutation and DNA repairing function have been shown to predict clinical outcome in lung patients treated with concurrent chemoradiotherapy and/or molecular therapy (65–67). Recently, correlation study of International Adjuvant Lung Cancer Trial showed that Patients with completely resected NSCLC and excision repair cross complementation group 1 (ERCC1) negative tumors appear to benefit from adjuvant cisplatin-based chemotherapy, whereas patients with ERCC1-positive tumors do not (68). We predict that molecular markers will guide our future combined modality treatment of NSCLC and will also identify patients who need radiation dose escalation for tumor control due to radiation resistance or need radiation dose reduction to normal tissues due to intrinsic radiation sensitivity. Combination of IGRT and molecular markers will help us to individualize patient management and further improve therapeutic ratio of combined modality treatment in NSCLC.

SUMMARY

Image-guided lung cancer screening (such as spiral CT) has the potential to detect curable early-stage lung cancer. PET/CT imaging has improved the accuracy for lung cancer staging, treatment triage, radiotherapy target delineation, and therapeutic evaluation. It has not only changed the management of lung cancer, but has also provided an imaging tool to predict clinical response and possible survival.

For operable stage I/II NSCLC, lobectomy and mediastinal lymph node dissection/sampling have been considered standard treatment. For stage III operable NSCLC, combined modality therapy including neoadjuvant or adjuvant chemotherapy and/or radiotherapy should be considered. Recent studies have confirmed a survival benefit from adjuvant chemotherapy in NSCLC after surgical resection, and such a regimen has become standard treatment for resected stage II/III NSCLC. PORT is indicated for patients with close or positive margins and/or resected N2 disease. The role of neoadjuvant chemotherapy or chemoradiotherapy in stage III NSCLC is being actively investigated.

Medically inoperable stage I/II NSCLC should be treated with definitive radiotherapy with or without adjuvant chemotherapy. The conventional dose of 60–66 Gy is too low to achieve higher than 50% local control, so dose escalation is required. SBRT with a high biological effective dose may become standard treatment and improve local control and overall survival for this group of patients. Combined modality treatment is needed for locally advanced stage III

NSCLC. Concurrent chemoradiotherapy has been considered standard therapy for this group of patients. The role of neoadjuvant or adjuvant chemotherapy in this setting remains controversial. For the past decades, the standard radiation dose for treating stage III NSCLC has been about 60 Gy. However, the median survival time associated with that dose is 10–17 months even with concurrent chemoradiotherapy. The optimal dose for stage III NSCLC is being actively investigated.

IGRT allows potential dose escalation with tolerable toxicity for both stages I and III NSCLC by improved targeting that could be translated into better local control and survival.

REFERENCES

1. Parkin D, Bray F, Ferlay J, et al. Global Cancer Statistics, 2002. CA Cancer J Clin 2005; 55(2):74–108.

2. Jemal A, Siegel R, Ward E, et al. Cancer statistics. CA Cancer J Clin 2006; 56(2): 106–30.

3. Henschke C, Naidich D, Yankelevitz D, et al. Early lung cancer action project. Cancer 2001; 92(1):153–9.

4. Flehinger B, Melamed M, Zaman M, et al. Early lung cancer detection: results of the initial (prevalence) radiologic and cytologic screening in the Memorial Sloan-Kettering study. Am Rev Respir Dis 1984; 130:555.

5. The International Early Lung Cancer Action Program Investigators. Survival of Patients with Stage I Lung Cancer Detected on CT Screening. N Eng J Med 2006; 355(17):1763–71.

6. Gohagan J, Marcus P, Fagerstrom R, et al. Baseline findings of a randomized feasibility trial of lung cancer screening with spiral CT scan vs chest radiograph: the lung screening study of the national cancer institute. Chest 2004; 126(1):114–21.

7. Pieterman R, van Putten J, Meuzelaar J, et al. Preoperative staging of non-small-cell lung cancer with positron-emission tomography. N Eng J Med 2000; 343(4): 254–61.

8. Vansteenkiste J, Fischer B, Dooms C, et al. Positron-emission tomography in prognostic and therapeutic assessment of lung cancer: systematic review. Lancet Oncol 2004; 5(9):531–40.

9. Sasaki R, Komaki R, Macapinlac H, et al. Fluorode-oxyglucose uptake by positron emission tomography predicts outcome of non-small-cell lung cancer. J Clin Oncol 2005; 23(6):1136–43.

10. Lardinois D, Weder W, Hany T, et al. Staging of non-small-cell lung cancer with integrated positron-emission tomography and computed tomography. N Engl J Med 2003; 348(25):2500–7.

11. Mountain C, Carr D, Anderson W. A system for the clinical staging of lung cancer. Am J Roentgenol Radium Ther Nucl Med 1974; 120:130.

12. Mountain C. The international system for staging lung cancer. Semin Surg Oncol 2000; 18(2):106–15.

13. Mountain C, Dresler C. Regional lymph node classification for lung cancer staging. Chest 1997; 111(6):1718–23.

14. Stanley K. Prognostic factors for survival in patients with inoperable lung cancer. J Natl Cancer Inst 1980; 65:25–32.

15. Ginsberg R, Rubinstein L. Randomized trial of lobectomy versus limited resection for T1 N0 non-small cell lung cancer. Lung Cancer Study Group. Ann Thorac Surg 1995; 60:615–22.

16. Mountain C. Prognostic implications of the Inter-national Staging System for Lung Cancer. Semin Oncol 1988; 3:236–41.

17. Roth J, Fossella F, Komaki R, et al. A randomized trial comparing perioperative chemotherapy and surgery with surgery alone in resectable stage IIIA non-small-cell lung cancer. J Natl Cancer Inst 1994; 86:673–80.

18. Rosell R, Gomez-Codina J, Camps C, et al. A randomized trial comparing preoperative chemotherapy plus surgery with surgery alone in patients with non-small-cell lung cancer. N Engl J Med 1994; 330(3):153–8.

19. Rusch V, Albain K, Crowley J, et al. Neoadjuvant therapy: a novel and effective treatment for stage IIIb non-small cell lung cancer. Southwest Oncology Group. Ann Thorac Surg 1994; 58:290–5.

20. Albain K, Swann S, Rusch V, et al. Phase III study of concurrent chemotherapy and radiotherapy (CT/RT) vs CT/RT followed by surgical resection for stage IIIA (PN2) non-small-cell lung cancer (NSCLC): outcomes update of North America Intergroup 0139 (RTOG 9309). J Clin Oncol 2005; 23(16):624.

21. Port Meta-analysis Trialists Group. Postoperative radiotherapy in nonsmall cell lung cancer: systematic review and meta-analysis of individual patient data from nine randomised clinical trials. Lancet 1998; 352:257–63.

22. Lung Cancer Study Group. Effects of postoperative mediastinal radiation on completely resected Stage II and Stage III epidermoid cancer of the lung. N Eng J Med 1986; 315:1377–81.

23. Non–Small-Cell Lung Cancer Collaborative Group. Chemotherapy in non-small cell lung cancer: a meta-analysis using updated data on individual patients from 52 randomised clinical trials. BMJ 1995; 311(7010):899–909.

24. Arriagada R, Bergman B, Dunant A, et al. Cisplatin-based adjuvant chemotherapy in patients with completely resected non-small-cell lung cancer. N Eng J Med 2004; 350(4):351–60.

25. Winton T, Livingston R, Johnson D, et al. Vinorelbine plus cisplatin vs. observation in resected non-small-cell lung cancer. N Engl J Med 2005; 352(25):2589–97.

26. Strauss G, Herndon J, Maddaus M, et al. Random-ized clinical trial of adjuvant chemotherapy with paclitaxel and carboplatin following resection in Stage IB non-small cell lung cancer (NSCLC): Report of cancer and leukemia group B (CALGB) protocol 9633. J Clin Oncol 2004; 22(14):7019.

27. Douillard JY, Rosell R, Delena M, et al. Phase III adjuvant vinorelbine (N) and cisplatin (P) versus observation (OBS) in completely resected (stage I-III)non-small cell lung cnacer (NSCLC) patients (pts): Final results after 70-month median follow-up. J Clin Oncol 2005; 23:16.

28. Hamada C, Ohta M, Wada H, et al. Survival benefit of oral UFT for adjuvant chemotherapy after completely resected non-small lung cancer. J Clin Oncol 2004; 22(14):7002.

29. Kato H, Ichinose Y, Ohta M, et al. A randomized trial of adjuvant chemotherapy with uracil-tegafur for adeno-carcinoma of the lung. N Engl J Med 2004; 350(17): 1713–21.

30. Pisters K. Adjuvant chemotherapy for non-small-cell lung cancer- the smoke clears. N Engl J Med 2005; 352:2640–2.

31. Le Chevalier T, Arriagada R, Pignon J, et al. Should adjuvant chemotherapy become standard treatment in all patients with resected non-small-cell lung cancer. Lancet Oncol 2005; 6:182–4.

32. Dosoretz D, Galmarini D, Rubenstein J, et al. Local control in medically inoperable lung cancer: an analysis of its importance in outcome and factors determining the probability of tumor eradication. Int J Radiat Oncol Biol Phys 1993; 27:507–16.

33. Kaskowitz L, Graham M, Emami B, et al. Radiation therapy alone for stage I non-small cell lung cancer. Int J Radiat Oncol Biol Phys 1993; 27:517–23.

34. Dosoretz D, Katin M, Blitzer P, et al. Medically inoperable lung carcinoma: The role of radiation therapy. Semin Radiat Oncol 1996; 6:98–104.

35. Sibley G, Jamieson T, Marks L, et al. Radiotherapy alone for medically inoperable stage I non-small-cell lung cancer: the duke experience. Int J Radiat Oncol Biol Phys 1998; 40(1):149–54.

36. Perez C, Stanley K, Rubin P, et al. A prospective randomized study of various irradiation doses and fractionation schedules in the treatment of inoperable non-oat-cell carcinoma of the lung. Preliminary report by the Radiation Therapy Oncology Group. Cancer 1980; 45:2744–53.

37. Perez C, Pajak T, Rubin P, et al. Long-term observations of the patterns of failure in patients with unresectable non-oat cell carcinoma of the lung treated with definitive radiotherapy. Report by the Radiation Therapy Oncology Group. Cancer 1987; 59:1874–81.

38. Perez C, Bauer M, Edelstein S, et al. Impact of tumor control on survival in carcinoma of the lung treated with irradiation. Int J Radiat Oncol Biol Phys 1986; 12:539–47.

39. Fletcher G. Clinical dose response curves of human malignant epithelial tumours. Br J Cancer 1973; 46:1–12.

40. Sause W, Scott C, Taylor S, et al. Radiation Therapy Oncology Group (RTOG) 88-08 and Eastern Co-operative Oncology Group (ECOG) 4588: preliminary results of a phase III trial in regionally advanced, unresectable non-small-cell lung cancer. J Natl Cancer Inst 1995; 87(3): 198–205.

41. Cox J, Azarnia N, Byhardt R, et al. N2 (clinical) non-small cell carcinoma of the lung: prospective trials of radiation therapy with total doses 60 Gy by the Radiation Therapy Oncology Group. Int J Radiat Oncol Biol Phys 1991; 20:7–12.

42. Saunders M, Dische S, Barrett A, et al. Continu-ous, hyperfractionated, accelerated radiotherapy (CHART) versus conventional radiotherapy in non-small cell lung cancer: mature data from the randomised multicentre trial. Radiother Oncol 1999; 52(2):137–48.

43. Bailey A, Parmar M, Stephens R. Patient-reported short-term and long-term physical and psychologic symptoms: results of the continuous hyperfractionated accelerated radiotherapy (CHART) randomized trial in non-small-cell lung cancer. CHART Steering Committee. J Clin Oncol 1998; 16(9):3082–93.

44. Mehta MP, Tannehill SP, Adak S, et al. Phase II trial of hyperfractionated accelerated radiation therapy for nonresectable non-small-cell lung cancer: results of Eastern Cooperative Oncology Group 4593. J Clin Oncol 1998; 16(11):3518–23.

45. Schuster-Uitterhoeve A, Hulshof M, Gonzalez G, et al. Feasibility of curative radiotherapy with a concomitant boost technique in 33 patients with non-small cell lung cancer (NSCLC). Radiother Oncol 1993; 28:247–51.

46. Bradley J, Graham M, Winter K, et al. Toxicity and outcome results of RTOG 9311: A phase I–II dose-escalation study using three-dimensional conformal radio-therapy in patients with inoperable non-small-cell lung carcinoma. Int J Radiat Oncol Biol Phys 2005; 61(2):318–28.

47. Kong F, Ten Haken R, Schipper M, et al. High-dose radiation improved local tumor control and overall survival in patients with inoperable/unresectable non-small-cell lung cancer: Long-term results of a radiation dose escalation study. Int J Radiat Oncol Biol Phys 2005; 63(2):324–33.

48. Dillman R, Seagren S, Propert K, et al. A randomized trial of induction chemotherapy plus high-dose radiation versus radiation alone in stage III non-small-cell lung cancer. N Eng J Med 1990; 323:940–5.

49. Dillman RO, Herndon J, Seagren SL, et al. Improved survival in stage III non-small-cell lung cancer: seven year follow-up of Cancer and Leukemia Group B (CALGB) 8433 trial. J Natl Cancer Inst 1996; 88:1210–15.

50. Sause W, Kolesar P, Taylor SIV, et al. Final Results of Phase III Trial in Regionally Advanced Unresectable Non-Small Cell Lung Cancer: Radiation Therapy Oncology Group, Eastern Cooperative Oncology Group, and Southwest Oncology Group. Chest 2000; 117(2):358–64.

51. Schaake-Koning C, van den Bogaert W, Dalesio O, et al. Effects of concomitant cisplatin and radiotherapy on inoperable non-small-cell lung cancer. N Eng J Med 1992; 326:524–30.

52. Furuse K, Fukuoka M, Kawahara M, et al. Phase III study of concurrent versus sequential thoracic radiotherapy in combination with mitomycin, vindesine, and cisplatin in unresectable stage III non-small-cell lung cancer. J Clin Oncol 1999; 17 (9):2692.

53. Furuse K, Hosoe S, Masuda T, et al. Impact of tumor control on survival in unresectable stage III non-small lung cancer (NSCLC) treated with concurrent thoracic radiotherapy (TRT) and chemotherapy (CT). Proc Am Soc Clin Oncol 2000; 19:1893a.

54. Curran W, Scott C, Langer C, et al. Long term benefit is observed in a phase III comparison of sequential vs concurrent chemo-radiation for patients with unresectable NSCLC:RTOG 9410. In: Proc Am Soc Clin Oncol; 2003; 2003. p. 621a.

55. Fournel P, Robinet G, Thomas P, et al. Randomized phase III trial of sequential chemoradiotherapy compared with concurrent chemoradiotherapy in locally advanced non-small-cell lung cancer: Groupe Lyon-Saint-Etienne d'Oncologie Thoracique-Groupe Francais de Pneumo-Cancerologie NPC 95-01 Study. J Clin Oncol 2005; 23(25):5910–7.

56. Bradley J, Graham M, Suzanne S, et al. Phase I results of RTOG L-0117; a Phase I/ II dose intensification study using 3DCRT and concurrent chemotherapy for patients with inoperable NSCLC. Proc Am Soc Clin Oncol 2005; 23(7063A):16S.

57. Schild S, McGinnis W, Graham D, et al. Results of a phase I trial of concurrent chemotherapy and escalating doses of radiation for unresectable non-small-cell lung cancer. Int J Radiat Oncol Biol Phys 2006; 65(4):1106–11.

58. Socinski M, Rosenman J, Halle J, et al. Dose-escalating conformal thoracic radiation therapy with induction and concurrent carboplatin/paclitaxel in unresectable stage IIIA/B non-small-cell lung carcinoma. Cancer 2001; 92(5):1213–23.

59. Lee C, Socinski M, Lin L, et al. High-dose 3D chemoradiotherapy trials in stage III non-small cell lung cancer (NSCLC) at the University of North Carolina: Long-term follow up and late complications. Proc Am Soc Clin Oncol 2006; 24(7145A):18S.

60. Choy H, Akerley W, Safran H, et al. Multiinstitut-ional phase II trial of paclitaxel, carboplatin, and concurrent radiation therapy for locally advanced non-small-cell lung cancer. J Clin Oncol 1998; 16(10):3316–22.

61. Lau D, Leigh B, Gandara D, et al. Twice-Weekly paclitaxel and weekly carboplatin with concurrent Thoracic Radiation Followed by carboplatin/paclitaxel consol-idation for stage III non-small-cell lung cancer: A california cancer consortium phase II trial. J Clin Oncol 2001; 19(2):442–7.

62. Vokes E, Herndon J-I, Crawford J, et al. Randomized Phase II Study of Cisplatin With Gemcitabine or Paclitaxel or Vinorelbine as Induction Chemotherapy Followed by Concomitant Chemoradiotherapy for Stage IIIB Non-Small-Cell Lung Cancer: Cancer and Leukemia Group B Study 9431. J Clin Oncol 2002; 20(20):4191–8.

63. Laurie G, Chansky J, Albain K, et al. Consolidation dcetaxel following concurrent chemoradiotherapy in pathologic stage IIIB non-small cell lung cancer (NSCLC) (SWOG9504): Patterns of failure and updated survival. Proc Am Soc Clin Oncol 2001; 1225a.

64. Belani C, Choy H, Bonomi P, et al. Combined chemo-radiotherapy regimens of Paclitaxel and Carboplatin for Locally Advanced Non-Small-Cell Lung Cancer: A Randomized Phase II Locally Advanced Multi-Modality Protocol. J Clin Oncol 2005; 23(25):5883–91.

65. Rohatgi P, Chang J, Spitz M, et al. Polymorphisms predict poor clinical outcome in non-small-cell lung cancer patients treated with radiotherapy/chemotherapy. Int J Radiat Oncol Biol Phys2006; 66(3, Supplement 1):S156–S.

66. Kobayashi S, Boggon T, Dayaram T, et al. EGFR mutation and resistance of non-small-cell lung cancer to gefitinib. N Eng J Med 2005; 352(8):786–92.

67. Chang J, Komaki R, Sasaki R, et al. High mutagen sensitivity in peripheral blood lymphocytes predicts poor overall and disease-specific survival in patients with stage III non-small cell lung cancer treated with radiotherapy and chemotherapy. Clin Cancer Res 2005; 11(8):2894–8.

68. Olaussen K, Dunant A, Fouret P, et al. DNA repair by ERCC1 in non-small-cell lung cancer and cisplatin-based adjuvant chemotherapy. N Eng J Med 2006; 355(10):983–91.

69. American Joint Committee on Cancer. *AJCC cancer staging manual*, Sixth Edition. New York: Spring-Verlag, Chapter 19, Lung 2002; 191–203.

70. Brambilla E, Travis WD, Colby TV, et al. The new World Health Organization classification of lung tumours. Eur Respir J 2001; 18:1059–68.

Guidelines and Techniques for Image-Guided Radiotherapy for Non–Small Cell Lung Cancer

Joe Y. Chang
Department of Radiation Oncology, University of Texas M.D. Anderson Cancer Center, Houston, Texas, U.S.A.

Lung cancer is the leading cause of cancer death in both men and women in the United States and the world (1), with non–small cell lung cancer (NSCLC) accounting for nearly 80% of all cases. Of patients who present with stage I/II disease, 25% have tumors that could be completely resected surgically; some of these patients, however, cannot tolerate a surgical procedure because of medical comorbidities and require definitive radiotherapy. About 50% of patients with NSCLC present with locally advanced (stage III) disease and require multimodality treatment, including radiotherapy. Even with concurrent chemotherapy and radiotherapy, however, the median survival time for such patients is low. For example, the survival duration for patients with locally advanced stage III disease who were enrolled in the Radiation Therapy Oncology Group (RTOG) 94-10 trial was only 15–17 months, with 5-year survival rates of 13–16%; 43% of those patients developed regional failure, and 45% developed distant metastases (2). Patients with stage IV disease may need palliative radiotherapy.

Radiotherapy for lung cancer has evolved from two-dimensional (2D) treatment (RTOG 94-10) to three-dimensional conformal radiotherapy (3D-CRT), and then to image-guided four-dimensional (4D) radiotherapy, which takes into consideration the motion of organs during treatment. The challenge of these rapidly changing technologies is designing radiotherapy to achieve the maximal therapeutic ratio.

It is well known that radiation oncologists' preferences in doses, targeting delineation, treatment margin determination, and radiation delivery vary substantially. It is also recognized that using poor treatment techniques results in high levels of toxicity and/or missed target areas or underdosing. This wide variation in techniques and the serious adverse effects that can result explain the very poor clinical outcome seen frequently in patients with NSCLC who undergo radiotherapy.

However, a "standard" radiotherapy for patients with NSCLC has been evolving. At The University of Texas M.D. Anderson Cancer Center, we developed guidelines and techniques for using image-guided radiotherapy that were based on the findings from our recent research studies and from those of other studies in the literature. This chapter discusses the role of radiotherapy in NSCLC and current guidelines and techniques for the determination of doses and fraction sizes and treatment design, particularly in target volume delineation and tumor motion consideration.

3D AND 4D RADIOTHERAPY

With the advent of 3D-CRT, the traditional 2D portals, target volumes, and beam arrangements have been questioned. Because of high local failure rates reported for patients with NSCLC, one goal of 3D-CRT is to increase the dose delivered to the gross tumor and/or to minimize the dose to normal tissues. 3D-CRT has important advantages over 2D treatment in tumor and normal tissue delineation, image segmentation and display, accurate dose calculation, and the ability to manipulate beam geometry and weighting through the forward planning process.

The importance of improved target delineation cannot be overemphasized. Once patients are immobilized and undergo computed tomography (CT) in the treatment position, the radiation oncologist can delineate the tumor and adjacent tissues in three dimensions, choose beam angles to maximize tumor coverage and/or minimize doses to normal tissues, alter beam weighting, and perhaps alter couch angles for noncoplanar beam delivery. 3D-CRT also enables the fusion of complementary imaging modalities such as positron emission tomography (PET) for delineating tumors or single-photon emission CT (3) for choosing beam angles. Clinical data have indicated that compared with 2D radiotherapy, 3D-CRT improves local control and survival in patients with early-stage NSCLC (4).

One major obstacle to target delineation has been respiration-induced target motion, or intrafractional tumor motion, which can add considerable geometrical uncertainty to the radiation treatment (5,6). Such motion requires enlargement of the treatment field

portals to cover the excursion of the tumor during treatment. With the development of multislice detectors and faster imaging reconstruction, it is now possible to image patients as they breathe in real time and to assess organ motion using 4D-CT (7).

4D-CT rapidly scans patients in a single couch position for the whole breathing cycle (usually 5–6 sec in each position) and then moves to the next couch position. After scanning is completed in all couch positions, a computer re-sorts all the images and reconstructs the tumor positions for the whole breathing cycle, that is, it provides a motion picture of the tumor. The radiotherapy is then based on the path of the tumor motion or on the inspiration and expiration breath-holds so that the irradiation is gated at certain phases of the breathing cycle.

Attention should be paid to irregular breathing and variation in the breathing pattern over the course of treatment. Even with 4D-CT, the free-breathing simulation is only a snapshot and a single stochastic sampling of the patient's breathing. The uncertainty of the patient's breathing during the course of treatment should also be considered (see Chapter 10 for details) (8,9).

ELECTIVE NODAL IRRADIATION

For many years, the standard radiotherapy for NSCLC in the United States, with recent exception (10–14), was to first deliver 40–50 Gy to the regional lymph nodes (in ipsilateral, contralateral, hilar, mediastinal, and occasionally supraclavicular areas) that showed no evidence of tumor involvement and to then deliver 20 Gy to the primary tumor through reduced fields. This regimen was based on pathologic information about the high incidence of hilar and mediastinal lymph node metastases in patients with bronchogenic carcinoma. Perez et al. (15), in an analysis of protocol compliance among 316 patients in the RTOG 73-01 trial, reported that in patients with radiographically negative lymph nodes, survival rates were higher in the group with no protocol variations who had adequate coverage of the hilar and mediastinal lymph nodes. However, the difference was not statistically significant ($P = 0.35$).

The rationale against the use of elective nodal irradiation is the high rate of local disease recurrence within the previously irradiated tumor and the high risk of distant metastasis and toxicity associated with a large radiation volume. Furthermore, if the gross disease cannot be controlled, there is no point to enlarging the irradiated volumes to include areas that may harbor microscopic disease.

Three major factors have changes since the RTOG 73-01 trial established the standard radiotherapy for NSCLC: the use of chemotherapy, the advent of 3D-CRT, and better staging and target delineation with PET. Emerging clinical data show that omitting prophylactic lymph node irradiation does not reduce the local control rate in patients receiving definitive radiotherapy. In these patients, the local recurrence rates in the isolated outside-field (field of radiotherapy) have been <8%, particularly in patients with stage I disease and in those who had undergone PET scanning for staging (10,12–14,16,17). We recently reported a series of 118 patients treated definitively with 3D-CRT to involved field volumes and without elective nodal irradiation. Although 21% of these patients developed local recurrence within the radiation field and 50% developed distant metastases (16), only 4% experienced failure in lymph nodes that had shown no evidence of tumor involvement. This 4% failure rate was lower than expected, and there are two possible explanations. First, incidental doses to the ipsilateral hilum, paratracheal, and subcarinal nodes approach 40–50 Gy when these regions are not intentionally irradiated (18). Second, patients with lung cancer experience competing causes of mortality, for example, their cancer and underlying comorbid illness. Such patients may die of local failure, distant failure, or intercurrent illness before failure is detected in the lymph nodes that had shown no evidence of tumor involvement.

The addition of PET to CT has substantially enhanced the clinical mediastinal staging of regional lymph nodes, resulting in improvements in sensitivity and specificity to about 90% compared with CT alone which was around 70–80% (19). More accurate clinical staging with PET may allow the radiation oncologist to include involved hilar and mediastinal lymph nodes that were not appreciated on CT alone and thereby reduce the probability of failure in electively treated lymph nodes. As the number of facilities with dedicated PET with fluorodeoxyglucose F 18 (FDG-PET) scanners and specifically combined PET-CT units increases, these technologies will help radiation oncologists design planning target volumes (PTVs) (see the "Target Volume Delineation" section) (17).

Thus, in patients with NSCLC, it is important to deliver adequate doses of radiation to involved nodal or mediastinal areas. Irradiation of other electively treated lymph nodes may not be necessary, particularly in patients staged with both CT and PET.

GENERAL GUIDELINES FOR IMAGE-GUIDED TARGET VOLUME DELINEATION IN NSCLC

A 4D-CT simulation is desirable for evaluating tumor motion and individualizing the target volume and margin. Spiral CT or extended-time CT (slow CT) simulation can be used if 4D-CT is not available (see details below).

Several commercial devices are available for immobilizing patients for lung cancer treatment. At M.D. Anderson Cancer Center, we use a Vac-Loc bag and T-bar that have a daily setup uncertainty of about 7 mm. Each device should be evaluated for setup uncertainty in each facility.

Patients should be evaluated for regularity of breathing, responsiveness to feedback guidance, breath-holding capability, and suitability for implantation of fiducial markers. On the basis of this evaluation, one of the following treatment-delivery techniques should be selected:

1. breath-hold (with or without feedback guidance),
2. respiratory gating, or
3. free breath (with or without feedback guidance).

The breath-hold treatment-delivery method is the most accurate for patients who are able to comply (Fig. 1A). Active breathing control and deep inspiration breath-hold are two techniques that have been pioneered to help patients hold their breaths at reproducible points in the respiratory cycle (20,21). The radiation beam is then initiated. These two techniques limit patient respiratory excursion to fixed volumes and limit diaphragm excursion to about 5 mm instead of 10–15 mm. These techniques require very cooperative patients who are able to hold their breath for at least 15 sec. Unfortunately, patients with poor pulmonary function (who would most benefit from reduction in irradiated lung volumes) are the patients least able to comply with breath-hold techniques. Their breathing also tends to be irregular during radiotherapy.
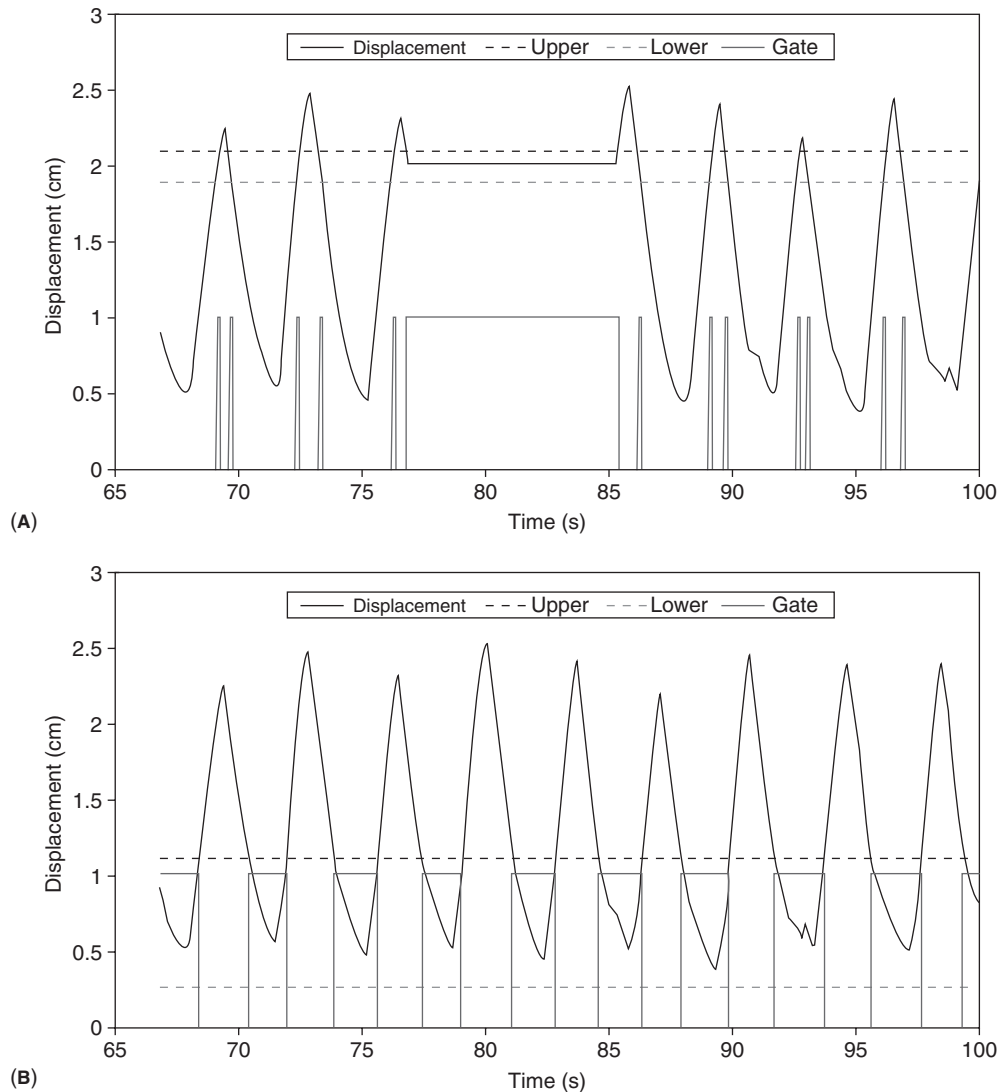

(A)

(B)

Figure 1 (**A**) The optimal approach to reducing tumor motion is for the patient to hold his or her breath at the end of inspiration during radiotherapy if he or she is able to comply. (**B**) Respiratory-gated radiotherapy is used at the end of expiration for a patient who can breathe regularly and reproducibly but cannot comply with the breath-hold technique.

Patients who do not qualify for the breath-hold treatment delivery but are able to breathe regularly and reproducibly should be treated with the respiratory-gating method when it is available (Fig. 1B). If patients do not qualify for the breath-hold delivery or do not have regular reproducible breathing or if respiratory-gating is not available, they should be treated with the free-breath technique. Visual and/or audio feedback guidance should be used for all patients who respond well to training with the feedback devices.

Target Volume Delineation

The International Commission on Radiation Units (ICRU) Report No. 50 guidelines (22) for defining targets have been applied to the treatment of lung cancer. The gross tumor volume (GTV) is the tumor that is visible by any imaging modality (the primary tumor) along with any grossly involved lymph nodes. The clinical target volume (CTV) is the anatomically defined area (the hilar or mediastinal lymph nodes or a margin around the grossly visible disease) believed to harbor micrometastasis. The PTV accounts for physiologic organ motion during treatment and the inaccuracies of daily setup in fractionated therapy (Fig. 2).

GTV

The pulmonary extent of lung tumors should be delineated on pulmonary windows, and the mediastinal extent of tumors should be delineated using mediastinal windows. In general, a lymph node >1 cm in its shortest dimension on CT is considered positive because of >15% involvement. The FDG-PET image is quite important for radiation treatment volume planning in stage III disease. In particular, FDG-PET can help to categorize suspected mediastinal and hilar lymph node adenopathy and differentiate benign collapsed lung tissue from tumor (Fig. 3A and 3B). Higher standard uptake values are predictive of metastatic disease and possible radiation resistance that may need aggressive treatment with stronger chemotherapy and higher doses of radiation (23,24). However, false-positive PET scans can be caused by inflammation, and a biopsy is recommended if there is any question (Fig. 3C).

CTV

In lung paranchymal disease, a radiographic-histopathologic study (25) demonstrated that GTV to CTV expansions of 6 mm for squamous cancers and 8 mm for adenocarcinomas are required to cover the gross tumor and microscopic disease with 95% accuracy. Expansions for other histologic types have not been determined, but a conservative approach would be to
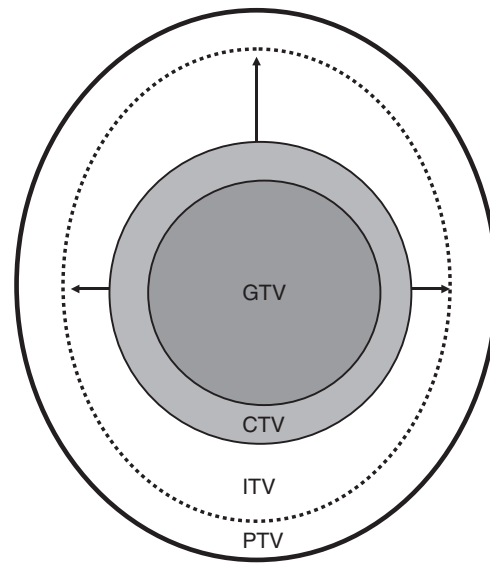

Figure 2   Graphic representation of the ICRU definition GTV, CTV, ITV, and PTV. Arrows indicate CTV motion. *Abbreviations*: CTV, clinical tumor volume; GTV, gross tumor volume; ICRU, International Commission on Radiation Units; ITV, internatl target volume; PTV, planning target volume.

use 8 mm. An appropriate CTV for mediastinal involvement has not been rigorously determined. An abstract in the American Society for Therapeutic Radiology and Oncology 2006 proceedings indicated that the maximal microscopic extension of involved lymph node was between 0.5 and 8.9 mm (average, 3.2 mm) (26). We empirically use 8-mm expansions around involved nodes (either gross involvement or FDG-PET positivity). Obviously, these expansions should not necessarily be applied uniformly along all axes and should always be individualized on the basis of the location of the primary tumor and involved lymph node. In the absence of radiographic proof of invasion, the CTV of the primary lesion should not extend into the chest wall or mediastinum. CTV expansions of lymph node disease should not extend into the major airways or lung, chest wall, or vertebral body without evidence of invasion on CT and/or magnetic resonance imaging.

PTV

It is defined as the CTV with a margin to account for daily setup error and target motion. M.D. Anderson have shown that when patients are immobilized with a Vac-Loc bag and T-bar, expansion along all axes of 7 mm accounts for 95% of the day-to-day setup uncertainty. Setup uncertainty is likely both technique dependent and institution dependent and should be measured individually for each technique. If a daily kV image is used, the setup uncertainty can be reduced to 5 mm. If a daily onboard image such as CT on-rail or cone-beam CT is used before each
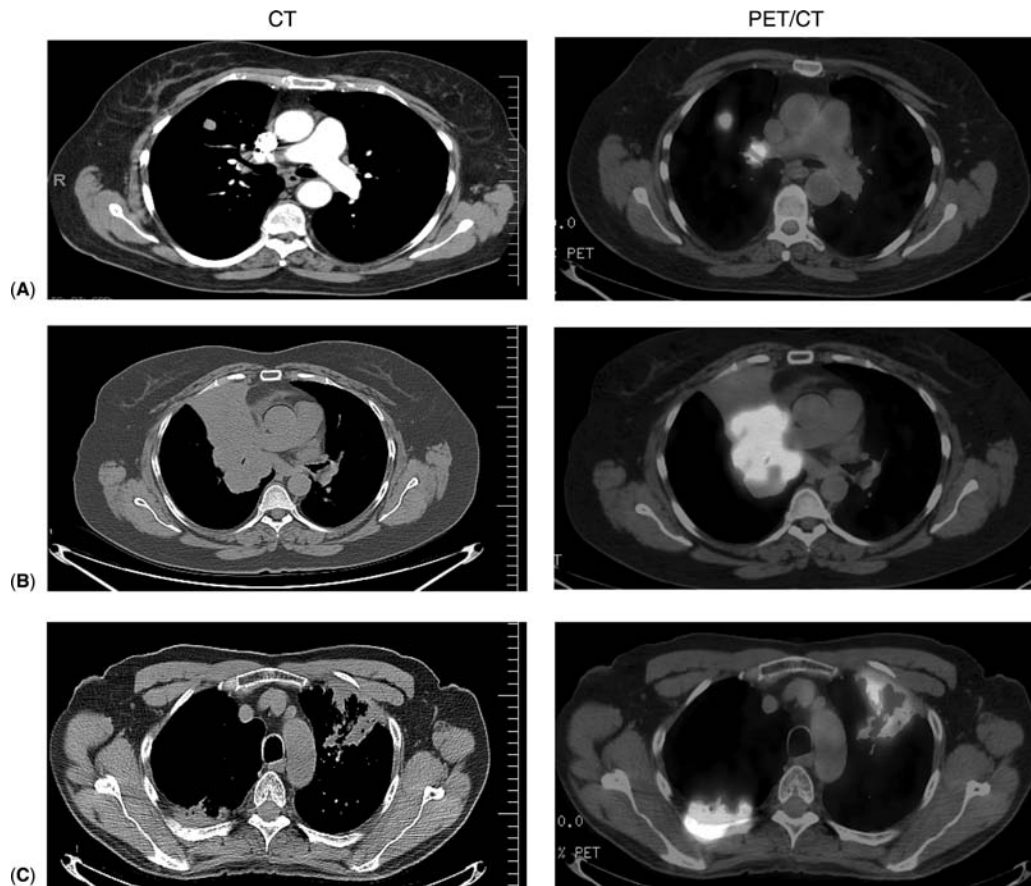
Figure 3 (*See color insert.*) PET-CT guided target volume delineation. (**A**) A PET-CT image indicates right hilar lymph node involvement that was not clearly evident on CT alone. (**B**) A PET/CT image differentiates gross tumor from collapsed lung tissue. (**C**) False-positive PET-CT scans can be caused by inflammation associated with infection or pneumonitis following radiotherapy. The right upper lobe lesion was squamous cell carcinoma; the left upper lobe lesion, however, was shown on biopsy to be inflammation. *Abbreviations*: CT, computed tomography; PET, positron emission tomography.

fraction of radiotherapy, day-to-day setup uncertainty can be reduced to 3 mm.

Tumor Motion

Tumor motion consideration is critical for lung cancer radiotherapy. Our 4D-CT study showed that >50% of the tumor moves >5 mm during treatment and that 13% moves >1 cm (possibly as much as 3–4 cm), particularly for a lesion close to the diaphragm. Thus, a new concept called the internal target volume (ITV) was introduced by the ICRU in 1999; the ITV combines the respiratory or other intrafractional target motion margin and the CTV (Fig. 1).

Tumor motion is best assessed individually for each patient. For patients with tumor motion of <5 mm, simple expansion for the GTV margin is adequate. However, for patients with substantial tumor motion, particularly >1 cm, an individualized tumor motion margin should be considered. The treatment machine can be gated with the patient's respiration, the patient can use an assisted breath-hold

technique, or an ITV-based approach can possibly be used (see below). A commercially available system can be used to gate the linac (27). This technique uses an externally placed fiducial marker that is tracked as the patient breathes. The beam can be triggered at a chosen point in the respiratory cycle, typically at end-expiration because this is the longest and most reproducible portion of the respiratory cycle. This technique requires patients to breathe slowly in a regular pattern (see Chapter 5 for details).

ITV is an expansion of CTV in which target motion is explicitly measured and taken into account as defined by ICRU62. Using new technologies such as multislice detectors and faster imaging reconstruction, it is now possible to image patients during real-time breathing and assess organ motion using 4D-CT. When 4D-CT is available for treatment planning, we propose a new concept called internal gross tumor volume (IGTV, Fig. 4), which is the volume containing the GTV throughout its motion during respiration. To delineate IGTV from 4D-CT images, the tumor volume that is

Figure 4 (*See color insert.*) Breath evaluation and tumor-motion consideration using 4D-CT. (**A**) Evaluation of the tumor location during 10 breath cycles shows a left lobe lesion that moved >2 cm. If the patient breathes regularly, this tumor should be treated at the end of expiration (red line) using respiratory-gated radiotherapy. However, if the patient cannot breathe regularly, the ITV approach should be used. (**B**) Maximal intensity projection image covers the envelope of the tumor motion path as the IGTV (red line). *Abbreviations*: 4D-CT, four-dimensional computed tomography; IGTV, internal gross tumor volume; ITV, internatl target volume.

outlined on the expiratory phase of the 4D images is registered on other phases of the images to create a union of target contours enclosing all possible positions of the target. Another method is to create an image of maximal intensity projection by combining the data from the multiple CT data sets with that from the whole breath cycle. In this case, the ITV should consist of the IGTV plus a margin to allow for microscopic disease (8 mm). The same principle can be applied to the images acquired with inspiration and expiration breath-holds. Attention should be paid to irregular breathing and variation in the breathing pattern over the course of the treatment and to the effects of these irregularities on the ITV margin.

If 4D-CT is not available, alternative approaches, such as those that follow, should be used so that tumor motion is taken into consideration.

ITV based on breath-hold spiral CT
When ITV is based on breath-hold spiral CT, images are acquired with use of the standard extended temporal (ET) thoracic CT protocol. This imaging protocol requires the patient to breathe normally. The ET-CT images should be acquired at the beginning of the simulation; the isocenter is then set. Subsequently, patients should be imaged using a fast CT simulation protocol while at 100% tidal volume (end of inspiration) and 0% tidal volume (end of expiration). The traces from the RPM system should be recorded. Separated GTVs and CTVs should be delineated by a

physician on both the 100% tidal volume CT image set and the 0% tidal volume image set. An ITV is then generated by combining these two CTVs on the ET CT scan and by forming an enveloped ITV that includes the entire path of the CTV as it moves from inspiration to expiration. A 3-mm margin should be added for the uncertainty of tumor motion and image registration. Normal tissues should be contoured in the ET CT images. The IVT should be superimposed on the slow CT images, which will serve as the basis for treatment planning.

Respiratory gating
We use the RPM system (end of expiration, Fig. 1B) to gate respiration. Our study showed that respiratory-gated therapy was the most beneficial for patients with a tumor volume of <100 cm^3 (usually <5 cm in diameter if the tumor is almost round) and a tumor motion of >1 cm. In general, tumors in the lower lobes of the lung move more than those in other locations during breathing. A 5-mm margin is recommended to allow for the uncertainty of day-to-day tumor localization from gating (28–30).

Slow CT simulation (single-slice helical scanner)
If a patient is not treated with either the respiratory-gating or ITV technique, slow CT simulation is recommended. Our recent study of tumors of different sizes and locations (31) revealed that 95% of tumors moved <6 mm from left to right (L to R) and

anteriorly to posteriorly (A to P); 95% moved <6 mm superiorly to inferiorly (S to I) if the tumor was located in the highest quadrant of lung. For tumor located in the two middle quadrant of lung, 95% moves <13 mm with tumor diameter <50 and <7 mm with tumor diameter >50 mm. However, 95% of tumors that were <50 mm and located in the lowest quadrant of lung moved ≤18 mm S to I. We therefore recommend 6-mm tumor-motion margins from L to R and A to P in all cases and from S to I for tumor located in the highest quadrant of lung regardless tumor size or middle two quadrant of lung with tumor diameter >50 mm. For tumor with diameter <50 mm and located in the middle two quadrant of lung, or tumor with diameter 50–80 mm located in the lowest quadrant of lung, we recommend 13 mm tumor-motion margin. We further recommend a 18-mm margin for lowest quadrant of lung lesion with diameter <50 mm.

Summary of Recommended Margins for Target Delineation Using Different Techniques

GTV: Based on image information using CT or PET-CT.

IGTV: Envelope of GTV throughout the entire 4D-CT data set or a specified part of the data set (when gated treatments are delivered). The IGTV is obtained from the GTV either by manually delineating the GTV in all the data sets that make up the respiratory cycle, or by automatically propagating the GTV through all the data sets that make up the respiratory cycle, or from the GTV as imaged on a maximal intensity projection reconstruction. If 4D-CT is not available, the GTV that combines volumes from the end of inspiration and the end of expiration using fast spiral CT with breath-hold should be used.

CTV: GTV + 8-mm margin (to account for microscopic disease). CTV margins may be manually reduced if there is confidence that microscopic disease does not exist in a specified region.

ITV: IGTV + 8-mm margin (for microscopic disease), or CTV + location/size-specific tumor-motion margin (see above) when explicit motion is not demonstrated.

PTV: ITV + 3-mm margin (for motion uncertainty) + 7-mm margin (for setup uncertainty). If daily image-guidance techniques are used, setup uncertainty can be reduced to 3 mm for CT on-rail or cone-beam CT and to 5 mm for kV image-guided setup. If the ITV approach is not used, the patient can be treated with respiratory-gated therapy or with slow CT simulation with a location/size-specific tumor-motion margin.

Respiratory gating for PTV: CTV + 12-mm margin (7-mm setup uncertainty + 5-mm gating margin for residual motion or other uncertainty).

Slow CT simulation for PTV: CTV + 7-mm setup uncertainty + location/size-specific tumor-motion margin.

As discussed above, for 4D-CT simulation, PTV = IGTV + 18-mm margin (8 mm + 7 mm + 3 mm); for respiratory-gated treatment, PTV = GTV at the end of expiration + 20-mm margin (8 mm + 5 mm + 7 mm); for slow CT simulation, PTV = GTV + 15 mm (8 mm + 7 mm) + location/size-specific tumor-motion margin.

Several important points need to be noted in defining target volume:

1. If the tumor moves >1 cm and the GTV is <100 cm^3, respiratory-gated radiotherapy may spare substantial amounts of normal structures.
2. Compared with slow CT, the 4D-CT–based approach spares more normal structures and reduces the chance of missing the target.
3. If dose escalation is intended for gross disease but not for microscopic disease, we may prescribe a higher dose to an IGTV plus setup uncertainty margin. We propose a new concept of the planning IGTV (PIGTV). The PIGTV = IGTV + 3-mm margin (for motion uncertainty) + 7-mm margin (for setup uncertainty). Appropriate reductions may be made in setup uncertainty if the daily image guidance is used. In this case, the final PTV should be covered by at least 50 Gy for microscopic disease.
4. In clinical practice, if the patient has very poor pulmonary function or a very large GTV, we need to consider radiation toxicity in addition to optimal tumor coverage. Clinical judgment should be applied to balance these two issues. In addition, biologic cytoprotectors such as amifostine may be considered if the lung V20 (the volume of total lung that received at least 20 Gy) is >40% or the patient exhibits poor pulmonary function (32).

At this time, several techniques for the planning and delivery of radiation are being investigated for their possible future use in the treatment of lung cancer. These include explicitly incorporating motion and setup uncertainty into the calculation of radiation doses and tracking the motion of a moving target for the delivery of radiation.

RADIOTHERAPY GUIDELINES AND TECHNIQUES FOR PATIENTS WITH STAGE I OR II NSCLC

Surgical resection by lobectomy with mediastinal lymph node dissection or sampling is considered the standard treatment for early-stage NSCLC, with 65–70% (stage I, T1-2 N0 M0) and 35–50% (stage II; T1-2 N1 M0, T3 N0 M0) 5-year overall survival rates. Adjuvant platin-based chemotherapy has been recently reported to prolong overall survival rates in patients with stage II disease (33–35). Adjuvant radiotherapy decreases local recurrence but not length of survival. In addition, it is indicated only for close or positive margins or positive multiple hilar lymph nodes (see "Postoperative Radiotherapy" section).

Definitive Radiotherapy for Stage I/II NSCLC

Indications for definitive radiotherapy include patient refusal of surgery and/or a patient who is medically unable to undergo surgery because of a condition such as poor pulmonary function, recent myocardial infarction, or bleeding tendency.

Radiotherapy strategy and design

A dose of 60–66 Gy delivered in 30–33 fractions is considered the standard according to RTOG 73–11. However, this regimen provides a biologically effective dose (BED) of 70.2 Gy, resulting in 3 years of 30–50% local control (36) and a 5-year cause-specific survival rate of 13–31% in patients with medically inoperable stage I NSCLC (Tl-2 N0 M0) (12,36); this local control rate was worse than the >70% rate seen in patients with stage I disease who underwent surgical resection. However, significant understaging occurs because of the lack of adequate imaging such as PET, mediastinal lymph node dissection, or sampling, particularly for T2 and higher lesions. Tumor motion during breathing also results in inadequate treatment of the tumor. Finally, 60–66 Gy may not be a high enough dose to kill all the cancer cells. An uncontrolled locoregional tumor is a major source of continuous seeding to distant organs and causes eventual treatment failure. A 30–40% distant failure rate was also noted. Thus, eradication of the locoregional tumor is an essential step for cure.

A dose-response relationship for disease-free survival in stage I NSCLC has been reported. Dosoretz et al. (10,11) showed that the actuarial disease–free survival rates at 2 years were 50%, 33%, 22%, and <20% with 70 Gy ($n = 4$), 60–69 Gy ($n = 116$), 50–59 Gy ($n = 26$), and <50 Gy ($n = 6$), respectively. In a dose-response relationship for local tumor control, the actuarial risks for local failure at 3 years were 33%, 60%, and 58% for >70 Gy ($n = 4$), 60–69 Gy ($n = 91$), and 50–59 Gy ($n = 19$), respectively.

Recommendations

PET or PET-CT should be used for stage work-up to rule out distant metastasis and hilar/mediastinal lymph node involvement (see "Specific Guidelines and Techniques for Patients with Stage III NSCLC" section).

1. If there is any doubt about hilar/mediastinal lymph node involvement, medianoscopy or another diagnostic procedure should be considered. However, PET should be used only for staging; PET should not be used for target delineation for stage I disease because of a possible mismatch of the PET image except if average CT is used for the PET-CT attenuation correction (37). The GTV contour should be based on the CT image.
2. The tumor motion, particularly for lesions close to the diaphragm, should be considered to individualize treatment. If the tumor moves >1 cm and the patient breathes regularly, respiratory-gated radiotherapy is preferred.
3. Without more clinical data, a dose of approximately 70 Gy delivered as 2 Gy/fraction should be considered for patients with stage I/II NSCLC. Adjuvant chemotherapy may be considered for stages Ib and II disease if the patient can tolerate it.

Stereotactic Body Radiation Therapy in Selected Patients with Stage I or II NSCLC

The conventional radiotherapy dose (60–66 Gy) for patients with early-stage NSCLC is associated with a >50% local recurrence rate. Our and others' recent research has shown that hypofractionated stereotactic body radiotherapy (SBRT) provided promising local control (>85%) and survival rates with minimal toxicity in selected patients with stage I (T1-2 N0 M0) or stage II (T3 N0 M0) NSCLC because of higher BEDs and accurate targeting (38–41). According to Onishi et al. (39), BEDs of ≥100 Gy are associated with better local control (91.9% vs. 73.6%) and survival rates (88.4% vs. 69.4%) than are BEDs of <100 Gy.

Our preliminary clinical experience supports the efficacy and safety of SBRT. The optimal dose regimen for SBRT, however, is controversial. In general, a BED of >100 Gy is required. Peripheral lesions tolerate higher BEDs, but centrally located lesions may develop considerable long-term toxicity if SBRT with a very high BED is delivered. At M.D. Anderson, patients with stage I or T3 (chest wall involvement) N0 M0 NSCLC receive SBRT as a total dose of 50 Gy delivered as 12.5 Gy/fraction to the PTV for four contiguous treatments. Daily onboard imaging using on-rail or cone-beam CT is required before each fraction (see Chapter 6 for details).

Radiotherapy Guidelines and Techniques for Patients with Locally Advanced Stage IIIA or IIIB NSCLC

Concurrent chemotherapy and radiotherapy has been considered the standard treatment for patients with a good performance status and inoperable stage IIIA (T3 N1 M0, T1-3 N2 M0) or IIIB (TX N3 M0, T4 NX M0) NSCLC. RTOG 94-10 and other studies (2,42,43) using 2D radiotherapy have shown that concurrent chemotherapy and radiotherapy provides better locoregional control and overall survival rates than do sequential chemotherapy and radiotherapy. However, levels of toxicity associated with chemoradiotherapy have been significantly higher than levels seen with sequential chemotherapy and radiotherapy (50% vs. 30% grade ≥3 toxicity levels). It has been reported that 3D-CRT reduces toxicity levels and allows a dose escalation from 60 Gy (in RTOG 94-10) to 74 Gy (44–46). Our preliminary data showed that intensity-modulated radiation therapy (IMRT) may further reduce lung and esophageal toxicity levels by decreasing V20, V10, and the total mean dose to the lungs and spare more esophageal and heart tissues (47,48). Although radiation doses of approximately 60 Gy have been considered standard for decades for patients with stage III NSCLC, this dose has been associated with 40–50% locoregional failure and the need for dose escalation. Several studies has shown the potential benefit in local control and survival rates with image-guided 3D-CRT dose-escalated radiotherapy (44–46).

Induction chemotherapy followed by chemoradiotherapy or chemoradiotherapy followed by adjuvant chemotherapy?

Full-dose induction chemotherapy may improve clinical outcome by decreasing distant metastasis, whereas concurrent radiotherapy with a dose of a radiation-sensitizing chemotherapeutic agent may further improve clinical outcome by increasing locoregional control. A recent phase II randomized study (the LAMP study) (49) compared induction chemotherapy followed by radiotherapy, concurrent chemotherapy and radiotherapy followed by adjuvant chemotherapy, or induction chemotherapy followed by concurrent chemotherapy and radiotherapy. The preliminary data showed that patients who received concurrent weekly paclitaxel, carboplatin, and thoracic radiotherapy followed by consolidation chemotherapy experienced the best outcome, although this schedule was associated with greater toxicity.

If patients have already undergone induction chemotherapy, we usually give concurrent chemotherapy and radiotherapy. If patients cannot tolerate these therapies concurrently, we give 2 or 3 cycles of induction chemotherapy followed by radiotherapy alone. If the patient can tolerate no chemotherapy, radiotherapy alone may be considered.

For patients with pathologically proven stage III N2 NSCLC, induction chemotherapy followed by surgery has resulted in better overall survival rates than has surgical resection alone (50,51). Induction chemoradiotherapy followed by surgery has also yielded better disease-free survival rates than has definitive chemoradiotherapy (52). These approaches have been actively investigated by the RTOG. The principle and radiation target volume delineation for induction therapy followed the same guidelines with definitive treatment except that the dose was 45–50 Gy.

Specific Guidelines and Techniques for Patients with Stage III NSCLC

Radiation doses in combined modality treatment

In RTOG 94-10, the locoregional failure rate after the concurrent use of chemotherapy and a standard radiation dose of approximately 60 Gy was about 34–43%. To improve the local control rate, three groups (RTOG, the North Central Cancer Treatment Group, and the University of North Carolina) separately performed radiation dose–escalation trials for this population, and their results supported the safety and efficacy of using 74 Gy concurrently with chemotherapy in patients with stage III NSCLC (44–46). In a recent dose-escalation study, Schild et al. (45) reported that the maximal tolerated dose was 74 Gy when used with weekly carboplatin and paclitaxel in patients with stage III NSCLC.

On the basis of promising local control rates and survival data and an acceptable toxicity level obtained using 3D-CRT to a dose of 74 Gy with concurrent chemotherapy, RTOG is planning to conduct a phase III study to compare the conventional 60-Gy dose of radiotherapy with 3D-CRT to a dose of 74 Gy used concurrently with weekly paclitaxel and carboplatin in patients with stage IIIA or IIIB NSCLC. Image-guided radiotherapy is strongly recommended for the study. IMRT will be allowed if tumor motion has been taken into consideration, and consolidation chemotherapy is required.

Recommendations

1. For patients with stage III NSCLC, radiotherapy at doses of 60–70 Gy delivered as 1.8–2 Gy/fraction with concurrent chemotherapy should be considered off protocol. This regimen should be followed by 2–4 cycles of adjuvant chemotherapy if the patient can tolerate it.
2. Induction chemotherapy followed by concurrent chemotherapy and radiotherapy is another

option, particularly for a very bulky lesion. If the patient cannot tolerate chemotherapy or chemoradiotherapy, 66–74 Gy delivered in 33–35 fractions (1 fraction/day) may be considered.

3. For a superior sulcus tumor, 69.6 Gy delivered as 1.2 Gy/fraction twice a day with concurrent chemotherapy is recommended to spare the spinal cord and bronchial plexus.

Specific Points for Target Volume Delineation in Patients with Stage III NSCLC

The GTV includes the primary tumor and all nodal disease documented in image studies, including CT and/or PET scans. The pulmonary extent of a lung tumor should be delineated on lung windows, and the mediastinal extent of the lung tumor should be delineated using mediastinal windows. PET-CT in a simulated position is strongly encouraged. The GTV should be delineated on the basis of 4D-CT images, and a PET scan should be used as a guide. If the results on PET are positive but there is no CT correlation, the physician should consult with a diagnostic radiologist. However, if a CT image meets the criteria of pathologic change in a lymph node (1 cm in the shortest axis) but the results on PET are negative, the physician may include the lesions as a GTV on the basis of his or her clinical judgment.

For patients who have obstructive atelectasis, PET-CT should be considered to exclude the atelectasis from the GTV. Both CT and PET imaging can be considered as guides to exclude the atelectasis (Fig. 2). Re-simulation should be considered 3–4 weeks after treatment in case the lung has expanded.

Contralateral mediastinal, contralateral hilar, or superior clavicular lymph nodes should be included as GTV only when they are positive for disease in PET and/or CT images. According to a surgical analysis (53), if subcarinal lymph nodes or mediastinal lymph nodes are involved, a plan should be considered for delivering a 45–50 Gy dose for microscopic disease to the ipsilateral hilum. For the right mid lobe or right lower lobe, left lingular, or left lower lobe lesion, if a mediastinal lymph node is involved, the ipsilateral hilar and subcarinal lymph nodes should be evaluated to receive 45–50 Gy. For a left upper lobe lesion, the anterior–posterior window lymph node should be evaluated to receive 45–50 Gy if there is mediastinal lymph node involvement, including subcarinal lymph nodes.

For patients who receive induction chemotherapy followed by chemoradiotherapy, the GTV should include the lung extent of the GTV after chemotherapy, abnormal lymph node stations before chemotherapy. If the patient has a complete response after chemotherapy, the areas of the lymph node station and of lung parenchymal disease before chemotherapy should be included as CTV and treated with at least 50 Gy. If disease progresses during chemotherapy, the GTV should cover the area of progressed disease.

Postoperative radiotherapy

Postoperative radiotherapy (PORT) is indicated for patients with close or positive margins and/or resected N2 disease. If results from the resection margin are negative and those from the mediastinal nodes are positive, 2–4 cycles of adjuvant chemotherapy should be given, followed by radiotherapy. If results from the resection margin are positive, PORT should be given first, followed by adjuvant chemotherapy. The role of PORT in positive N1 disease remains controversial. Because of the potential long-term survival of the patients, chronic toxicity associated with PORT should be considered. For positive or close margins with no N1 or N2 involvement, the target volume should be limited to only the site of the positive margin. The dose should be 60–66 Gy. For gross positive margins (subtotal resection), patients should receive definitive therapy with chemoradiotherapy. For patients with N2 disease that has been surgically resected, the target volume should be limited to the positive lymph node station plus or minus the ipsilateral hilar and subcarinal lymph nodes, depending on the location of the primary cancer and whether a full lymph node dissection was performed during surgery. The dose should be limited to about 50 Gy delivered in standard fraction sizes.

Indications for PORT

- any positive N2 node,
- any T4 disease except for separate nodules in the same lobes or malignant pleural effusion,
- close or positive microscopic surgical margins,
- gross residual disease,
- positive hilar node (debatable).

A patient treated with induction chemotherapy followed by surgery has the same indications for postoperative treatment. PORT improves local control and possibly disease-free survival duration for patients with pathologic N2 disease (54). Adjuvant chemotherapy has been shown to improve survival duration in patients with stages Ib to III NSCLC and should be considered standard therapy (33–35). Interestingly, a secondary analysis of Adjuvant Navelbine International Trialist Association randomized study showed improved overall survival using PORT in patients with N2 disease (Douillard, ASTRO 2006 plenary presentation).

Technique for PORT

Dose: Complete the resection with negative margins and then deliver 50 Gy in 25 fractions of 2 Gy/fraction every day, off protocol.
Positive extra-capsule extension: 54 Gy/fraction.
Margin positive for microscopic disease: 60 Gy delivered in 30 fractions.
Gross residual disease: 66 Gy delivered in 33 fractions or 63–70 Gy delivered in 35 fractions with concurrent chemotherapy.

Target volumes

GTV: Usually, there is no GTV in the adjuvant setting except in some clinical situations such as uncompleted resection with either gross positive margins or even gross residual disease as indicated by CT, PET, operative note, or pathologic report.

CTV: GTV plus 8-mm margin. For patients who receive induction chemotherapy, the 8-mm margin should also be considered. In most cases, the CTV includes just the involved lymph node stations as described below. The margins that are positive for microscopic disease or a very close margin in the surgical stump should also be considered to be in the CTV. It is very important to discuss the high-risk areas with surgeons. Ideally, we should ask the surgeon to review target volumes at the treatment-planning workstation.

The Ipsilateral hilum should be included in the CTV if the subcarinal or mediastinal lymph nodes are involved. For the right mid lobe or right lower lobe or for a left lingular left lower lobe lesion, if the mediastinal lymph nodes are involved, the subcarinal lymph nodes should be included in the CTV. For a left upper lobe lesion, the anterior-posterior window nodes should be included in the CTV if there is mediastinal lymph node involvement, including the subcarinal lymph nodes.

If the patient has only a pathologically positive hilar lymph node, the CTV should cover the ipsilateral hilum. If the patient has only positive surgical margins with no nodal involvement, the CTV should cover the site of the positive margin. However, if there is no mediastinal lymph node dissection or adequate mapping, the ipsilateral hilar and ipsilateral mediastinal lymph nodes should be considered as in the CTV.

PTV: CTV + 7-mm margin for setup uncertainty and 3-mm margin for tumor motion. If the patient has gross residual disease in the mediastinum, the treatment technique should follow the recommendations as described for the definitive cases.

Intensity-Modulated Radiation Therapy

The use of IMRT in patients with lung cancer has been delayed because of general concerns and the assumption that IMRT may deliver low yet damaging doses to a larger volume of normal lung tissue. Moreover, the possible movement of a tumor due to respiration introduces another level of complexity to both the IMRT dosimetry and the technique used.

We investigated dosimetric improvement with respect to target dose, tumor conformity, and normal tissue sparing, comparing IMRT with 3D-CRT for patients with early-stage and locally advanced NSCLC (47,48). We found that IMRT may be more suitable than 3D-CRT treatment planning for patients with advanced-stage disease with a larger GTV and thus a greater volume of normal lung involvement. Using IMRT, the median absolute reductions in the percentage of lung volume irradiated at >10 and >20 Gy were 7% and 10%, respectively. This corresponded to decreases of >2 Gy in the mean total lung dose and of 10% in the risk of radiation pneumonitis. The volumes of the heart and esophagus irradiated to about 50 Gy and of normal thoracic tissue irradiated to >10–40 Gy were reduced using the IMRT plans. In contrast to common belief, the integral dose delivered to the patient was also reduced with IMRT in certain cases. There was a marginal increase in the spinal cord maximal dose and lung volume of >5 Gy in the IMRT plans in half the patients, which could have been caused by the substantial increase in monitoring units and thus leakage dose in IMRT for the sliding window delivery technique used in these studies.

Although IMRT may be effective in reducing normal tissue toxicity and improving tumor coverage, its high-dose gradient and conformity require a high level of precision in dose delivery and tumor localization. In the meantime, the complexity introduced by tumor motion must be recognized when using IMRT. Unlike 3D-CRT, IMRT treats only a portion of the target volume at a particular time. There is a great deal of concern as to whether target motion and collimator motion during IMRT delivery have substantial interplay, thus degrading the planned dose distributions. For IMRT to be feasible and more effective in treating NSCLC, motion-reduction techniques should be explored further, such as breath holding and tumor tracking. Our preliminary clinical data indicated that IMRT may reduce toxic effects in
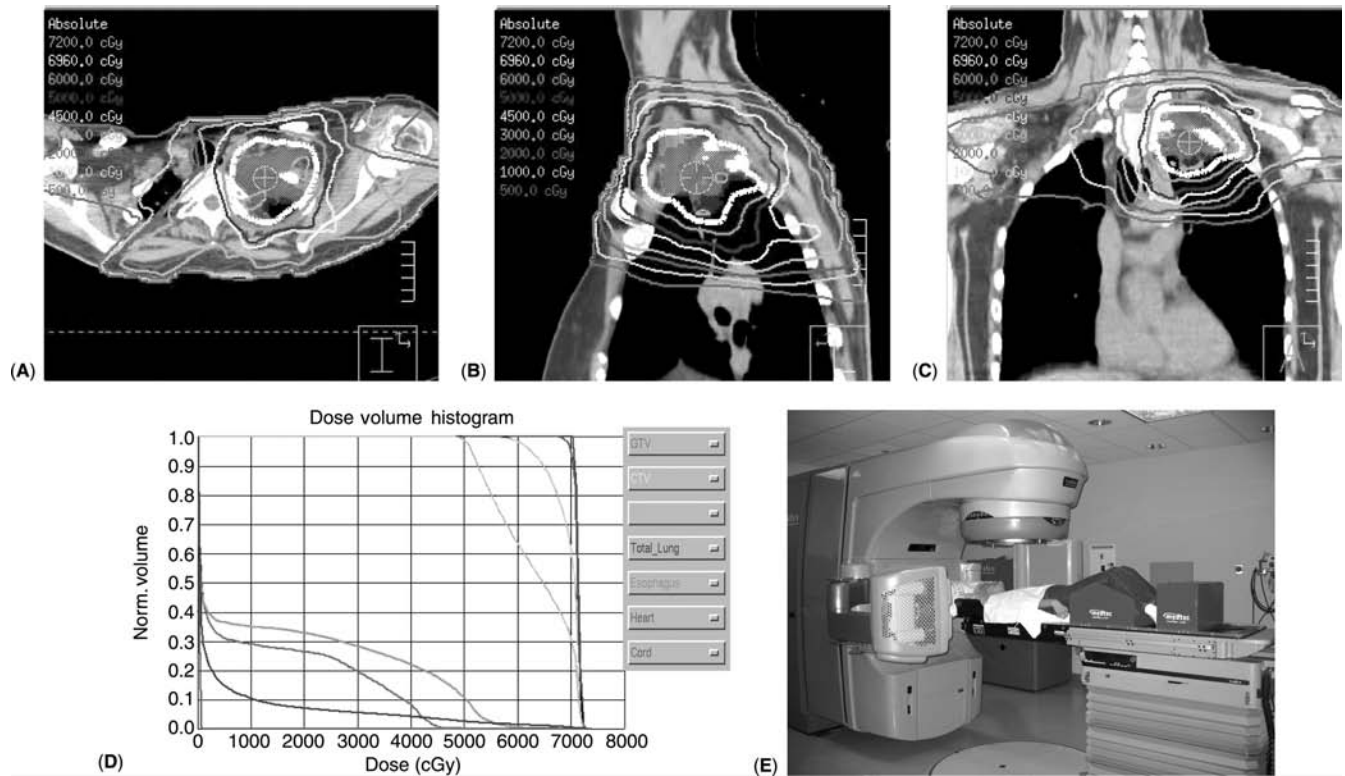
Figure 5 (*See color insert.*) Onboard image-guided IMRT for superior sulcus cancer treated with concurrent chemotherapy; 69.6 Gy was prescribed and delivered as 1.2 Gy/fraction twice a day. Because of the proximity of the tumor to the spinal cord and brachial plexus, only the GTV plus the setup uncertainty margin (3 mm using daily onboard cone-beam CT) received 69.6 Gy, whereas the spinal cord dose was kept to <45 Gy and the brachial plexus dose to <66 Gy. The clinical tumor volume received a minimal dose of about 60 Gy, and the PTV received a minimal dose of about 50 Gy. Isodose distribution of transverse (**A**) sagital (**B**) and coronal (**C**) images; Dose volume histogram (**D**) and on-board cone beam CT (**E**) before each fraction of radiotherapy. *Abbreviations:* CT, computed tomography; GTV, gross tumor volume; IMRT, intensity-modulated radiation therapy; PTV, planning target volume.

normal tissue in selected patients, particularly for tumors that move <10 mm, and may allow further dose escalation (55). We have recently developed IMRT guidelines for patients with NSCLC using image-guided radiotherapy (56).

4D planning is more important for IMRT than conventional 3D planning because of the high degree of dose shaping and conformity created in the IMRT plans. The logical extension of 4D planning is to incorporate interfractional change of the anatomy into the planning process so that we can estimate the actual delivered dose for the entire course of treatment and can adjust the treatment if the patient's anatomy changes significantly during the course. Such anatomic changes can be caused by physiologic fluctuation and tissue response to the radiation or chemoradiation. Frequent imaging may be needed to guide the treatment planning and delivery. The scope of 4D planning should thus include both interfractional and intrafractional uncertainties and address such changes appropriately for the improvement of the treatment outcome.

Guidelines for Lung Cancer IMRT Treatment

IMRT for lung cancer treatment may have the potential to reduce the normal tissue toxicity levels and allow dose escalation in high-risk regions. However, more data, particularly a long-term clinical study, are needed before IMRT can be used routinely in the community hospital. On the basis of our research and reports published by others, we recommend the following guidelines for IMRT lung cancer treatment.

Patient selection and immobilization

Not every patient will benefit from IMRT treatment. On the basis of published data, patients with a tumor located in the superior sulcus or close to the esophagus or spinal cord or those with positive lymph nodes may benefit more than other patients from IMRT treatment (Figs. 5 and 6). Earlier-stage
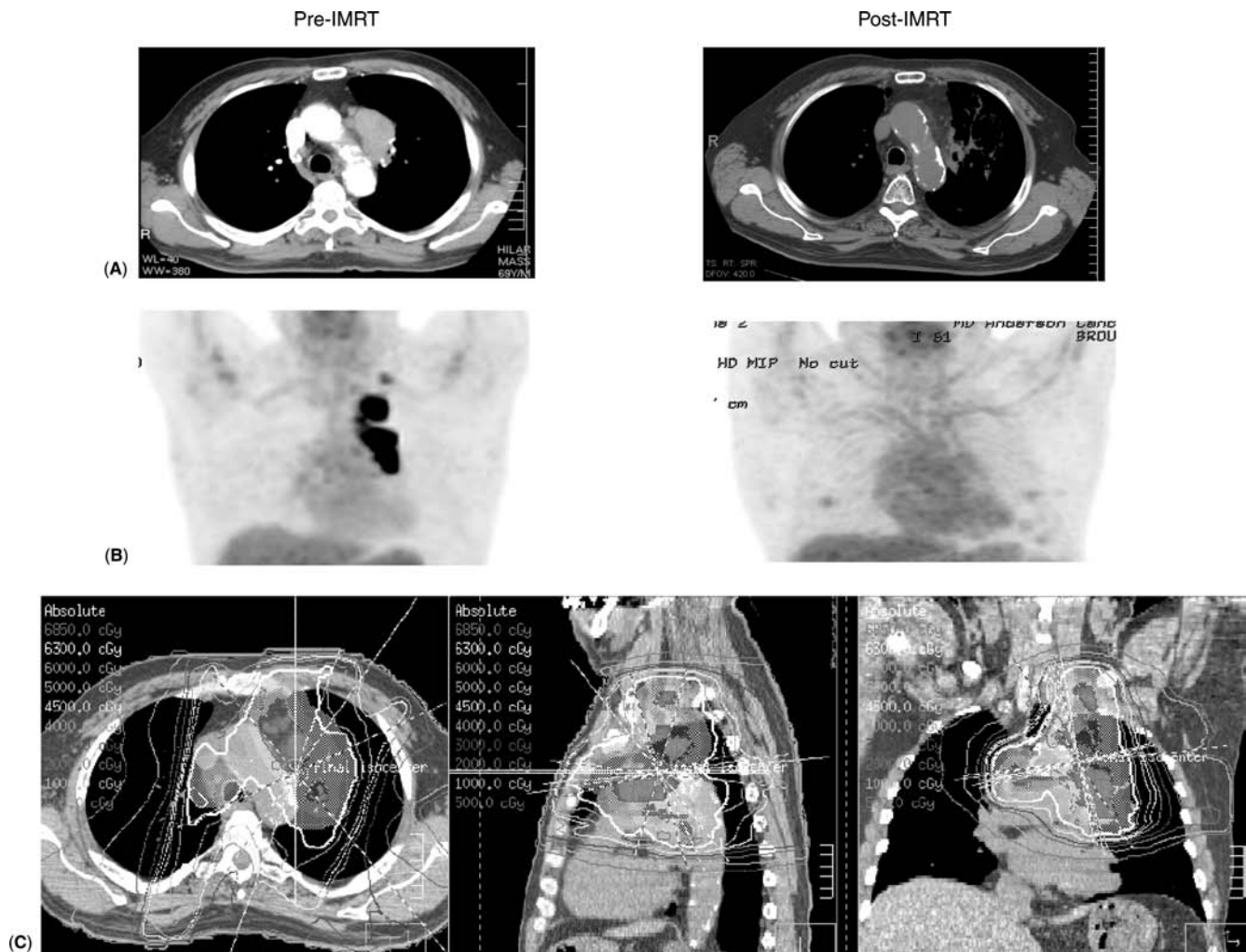
Pre-IMRT   Post-IMRT

Figure 6 (*See color insert.*) Image-guided therapeutic efficacy evaluation for stage III NSCLC treated with IMRT. (**A**) Before and after IMRT computed tomographic scans. (**B**) Before and after IMRT positron emission tomographic scans. At 3 months after IMRT, a complete clinical response was seen in this patient, who had bulky disease in the left upper lobe lesion and contralateral mediastinal and superior clavicular lymph node involvement. (**C**) IMRT isodose distribution. The white line indicates the prescription line at 63 Gy. The patient was treated with concurrent chemotherapy and radiotherapy and achieved a clinical complete response with grade II esophagitis. *Abbreviations*: IMRT, intensity-modulated radiation therapy; NSCLC, non–small cell lung cancer.

small mobile tumors may not be good candidates for IMRT treatment unless motion-mitigation techniques are involved. In addition, the conformal dose distribution and high-dose gradients in IMRT mandate improved patient immobilization.

Target volume and tumor motion consideration
IMRT for lung cancer requires a detailed understanding of chest radiographic anatomy, including both tumor volume and critical structures such as normal lung, esophagus, heart, and spinal cord. PET-CT is recommended for target delineation.

Organ motion during treatment must be considered and addressed individually. Patients should be evaluated for regularity of breathing, responsiveness

to feedback guidance, and breath-holding capability. On the basis of this evaluation, a treatment-delivery technique should be selected from free-breath, breath-hold, or other alternatives. A 4D-CT study is recommended for treatment-planning purposes. At a minimum, tumor motion should be assessed with fluoroscopy.

If the tumor moves <10 mm, the patient can be treated with free-breath IMRT using the ITV technique with an adequate margin. However, if considerable tumor motion is anticipated, the patient should be treated with breath-hold, respiratory-gated therapy or other means of tumor tracking if such techniques can be used to freeze the tumor position at reproducible positions.

Tissue heterogeneity consideration

Because heterogeneity affects some beamlets more than others, resulting in substantial differences in dose distribution, heterogeneity should be corrected for in all IMRT lung cancer treatment plans.

Plan evaluation and quality assurance

IMRT may cause cold spots or hot spots in unexpected locations that may not be reflected by dose volume distribution. Therefore, the isodose distribution should be inspected on every image slide. To reduce the potential for low-dose (<10 Gy) delivery to the normal lung, the use of fewer beams (5–7) is recommended, in particular to reduce the beam-delivery time and improve patient comfort. Experienced IMRT planning and delivery are necessary, which means that physicians need to balance dose inhomogeneity and lung tissue sparing; in addition, strict quality assurance is required for both mechanical and dosimetric accuracy.

TOXICITY OF NORMAL TISSUE AND DOSE VOLUME CONSTRAINTS

It is extremely important to not exceed the maximal doses tolerated by sensitive intrathoracic structures such as the lung, bronchus, esophagus, spinal cord, and heart. Radiation-induced toxic effects in normal tissue are related to both dose and volume. In addition, the spatial arrangement of the functional subunits (FSU) in normal tissue is critical. In those tissues in which the FSUs are arranged in series, such as spinal cord, esophagus, trachea, bronchus, vessels, and nerves, the integrity of each FSU is important for organ function, and the elimination of any FSU may result in serious toxicity. In this case, we should minimize the hot spots, particularly those caused by very high doses, to these organs, even for a small volume. In contrast, in tissues in which the FSUs are arranged in parallel, not serially, such as in the lung, the integrity of each FSU is less important; instead, the volume irradiated or spared plays a major role in complications in these tissues.

Emami et al. (57) published partial-volume irradiation parameters for various organs derived from a National Cancer Institute-designated task force. The parameters were derived from a review of the literature and from clinical opinions of experienced radiation oncologists. These data have served us for the past decade by defining partial-organ tolerances. Toxicity end points are a 5% complication rate at 5 years (TD 5/5) and a 50% complication rate at 5 years (TD 50/5) for different volumes irradiated. However, these toxicity parameters are incomplete and were based on clinical data from patients who received 2D radiotherapy alone without chemotherapy. The most important complication from radiotherapy in lung cancer is toxicity of the lung and esophagus. The current clinical data concerning this toxicity, based on 3D-CRT with dose-volume histographic analysis, is discussed in the following section.

Lung Toxicity

Radiation-induced pneumonitis, when it occurs, usually appears after completion of radiotherapy, peaks at 2 months, and stabilizes or resolves within 6–12 months. It can be treated with corticosteroids, such as prednisone, at 20–60 mg/day. Pulmonary fibrosis can occur a few months after radiation and can become chronic. Emerging clinical data based on 3D-CRT in lung cancer have shown that the mean lung dose (MLD), V5, V13, V20, and V30 are correlated with pulmonary radiation injury. Graham et al. (22) recommended a cutoff point of V20 Gy at 40% with radiotherapy alone, at which point 36% of patients developed grade ≥2 pneumonitis. They also reported that a total MLD of ≥20 Gy is associated with a 24% occurrence rate of grade ≥2 pneumonitis. Yorke et al. (58) reported that grade ≥3 pneumonitis correlated well with the MLD and V20. At an MLD of 20 Gy, about 28% of patients developed grade ≥3 pneumonitis. In addition, Yorke et al. reported strong correlations in the lower portion of the lungs and the ipsilateral lung. In a further analysis using a 3D-CRT dose-escalation study (from 70.2 to 90 Gy), they found a significant correlation between grade ≥3 pneumonitis and total, ipsilateral, and lower lung V5 to V40. When using a 20% rate of grade ≥3 pneumonitis as a cutoff, the V5, V10, and V20 of the total lung were estimated to be 58%, 48%, and 36%, respectively. Our data from M.D. Anderson support these estimations (59,60). Currently, we recommend an MLD of <20 Gy and V5, V10, and V20 (GTV is excluded from lung volume calculation) of <65%, <45%, and <35%, respectively, as our cutoff threshold for lung cancer radiotherapy when concurrent chemotherapy is given (Table 1). These cutoffs are based on currently available information, and further modification may be needed when more mature data are available. Based on our experience in mesothelioma treated with extraplural pneumonectomy, we recommend an MLD of <8.8 Gy and V20 <10% for patients who have undergone pneumonectomy (61).

Esophageal Toxicity

The radiotherapeutic management of thoracic malignancies often exposes the esophagus to high levels of ionizing radiation. After 2–3 weeks of conventionally fractionated radiotherapy, patients often experience dysphagia and/or odynophagia that usually worsens toward the end of radiotherapy and peaks at the first week after completion of radiotherapy. This acute

Table 1 Dose–Volume Constraints for Normal Tissues Using Standard Fractionation to Target Volume

	RT alone	Chemo and RT	Chemo and RT before surgery
Spinal cord[a]	50 Gy	45 Gy	45 Gy
Lung[b]	MLD <20 Gy	MLD <20 Gy	MLD <20 Gy
	V20 <40%	V20 <35%	V20 <20%
		V10 <45%	V10 <40%
		V5 <65%	V5 <55%
Heart	V40 <50%	V40 <50%	V40 <50%
Esophagus	Dmax <75 Gy	Dmax <75 Gy	Dmax <75 Gy
	V60 <50%	V55 <50%	V55 <50%
Kidney[c]	20 Gy (<50% of combined both kidneys or <75% of one side of kidney if other kidney is not functional)	Same as RT alone	Same as RT alone
Liver	30 Gy (<40%)	Same as RT alone	Same as RT alone

[a] The treated volume size of the spinal cord should be considered. The chance of spinal cord damage is increased as the treated volume is increased. Physicians should consider off the cord earlier if a substantial amount of spinal cord has received a constrained dose. In general, the spinal cord should not receive >60 Gy, even in a very limited volume. A higher fraction size of radiation or a higher daily dose decreases the tolerance. If the patient is treated with 3 Gy/fraction, the constrained dose to the cord should be approximately 40 Gy (based on the BED calculation).
[b] V20 = the effective lung volume (total lung volume – gross tumor volume) that received ≥20 Gy. If the patient undergoes pneumonectomy before radiotherapy, we recommend an MLD of <8.5 Gy and a V20 of <10%.
[c] Consider a kidney scan if a large volume of one kidney will be treated with a high dose.
Abbreviations: chemo, chemotherapy; MLD, mean lung dose; Dmax, maximal dose; RT, radiotherapy.

reaction to radiation can cause considerable morbidity from dehydration and weight loss and can lead to treatment interruptions. The late reactions of the esophagus to radiation generally involve fibrosis of the organ that can lead to strictures. Patients may experience various degrees of dysphagia and may require endoscopic dilation. As with the acute reaction, rare cases may involve perforation or fistula formation.

The clinical and dosimetric predictors of acute and late esophagitis have become particularly important in the era of radiation-dose escalation and concurrent chemotherapy and radiotherapy. Emami and colleagues (57) reported that TD 5/5 and TD 50/5 values in 2D radiotherapy for stricture and perforation of the esophagus are 60 and 72 Gy in one third of the volume, respectively. Emerging clinical data based on 3D-CRT indicated that in general, the tolerance of the esophagus is approximately 60 Gy; however, the volume (particularly the length of the circumference involvement) is very crucial. Singh et al. (57) reported that the threshold maximal esophageal point dose for grade 3–5 esophagitis was 58 Gy when concurrent chemotherapy was given. The esophageal surface area

receiving ≥55 Gy, the esophageal volume receiving ≥60 Gy (V60), and the use of concurrent chemotherapy were the most statistically significant predictive factors for acute esophagitis (62). For all grades of late toxicity, the length of 100% of the circumference receiving ≥50 Gy, the V50, the percentage of surface area treated with ≥50 Gy, and the maximal percentage of circumference receiving ≥60 Gy are predictive (63, 64). About 32% of patients developed late esophageal toxicity if the V50 was >32% or the length of 100% of the circumference was >3.2 cm. Patients who received >80 Gy to any portion of the esophageal circumference have an approximately 50% risk for late toxicity. Of note, acute esophagitis (grade 2–3) is correlated significantly with V40–V70 (65). In clinical practice, it is difficult to avoid esophagitis totally when the target volume is close to the esophagus. Attention should be paid to minimize grade ≥3 toxicity. On the basis of available dose–volume histographic data, to avoid severe acute and chronic toxicity, we suggest thresholds of V55 <50% and a maximal dose of <75 Gy if concurrent chemotherapy is given (Table 1).

REFERENCES

1. Jemal A, Siegel R, Ward E, et al. Cancer statistics. CA Cancer J Clin 2006; 56(2): 106–30.

2. Curran W, Scott C, Langer C, et al. Long term benefit is observed in a phase III comparison of sequential vs concurrent chemo-radiation for patients with unresectable NSCLC:RTOG 9410. In: Proceedings of the American Society of Clinical Oncology, 2003, p. 621a.

3. Shioyama Y, Jang S, Liu H, et al. Preserving perfused functioning lung using intensity-modulated radiotherapy for advanced-stage non-small-cell lung cancer (2486a). Int J Radiat Oncol Biol Phys 2006; 66(3):481.

4. Fang L, Komaki R, Allen P, et al. Comparison of out-comes for patients with medically inoperable Stage I non-small-cell lung cancer treated with two-dimensional vs. three-dimensional radiotherapy. Int J Radiat Oncol Biol Phys 2006; 66(1):108–16.

5. Liu H, Koch N, Starkschall G, et al. Evaluation of internal lung motion for respiratory-gated radiotherapy using MRI: Part II–margin reduction of internal target volume. Int J Radiat Oncol Biol Phys 2004; 60(5): 1473–83.

6. Koch N, Liu H, Starkschall G, et al. Evaluation of internal lung motion for respiratory-gated radiotherapy using MRI: Part I–correlating internal lung motion with skin fiducial motion. Int J Radiat Oncol Biol Phys 2004; 60(5):1459–72.

7. Nehmeh S, Erdi Y, Pan T, et al. Four-dimensional (4D) PET/CT imaging of the thorax. Med Phys 2004; 31:3179–86.

8. Vedam S, Dong L, Zhang J, et al. Impact of respiration-induced tumor motion uncertainties on adaptive treatment delivery stratergies: A comparison through repeat 4D CT imaging. Int J Radiat Oncol Biol Phys 2006; 66(3):614.

9. Britton K, Starkschall G, Pan T, et al. Time trends in mobility and size of target volumes for locally advanced stage III non-small-cell lung cancer patients using serial our-dimensional computed tomography (4-DCT). Int J Radiat Oncol Biol Phys 2006; 66(3):468.

10. Dosoretz D, Galmarini D, Rubenstein J, et al. Local control in medically inoperable lung cancer: an analysis of its importance in outcome and factors determining the probability of tumor eradication. Int J Radiat Oncol Biol Phys 1993; 27:507–16.

11. Dosoretz D, Katin M, Blitzer P, et al. Medically inoperable lung carcinoma: The role of radiation therapy. Semin Radiat Oncol 1996; 6:98–104.

12. Krol A, Aussems P, Noordijk E, et al. Local irradiation alone for peripheral Stage I lung cancer: Could we omit the elective regional nodal irradiation? Int J Radiat Oncol Biol Phys1996; 34(2):297–302.

13. Rosenzweig KE, Sim SE, Mychalczak B, et al. Elective nodal irradiation in the treatment of non-small-cell lung cancer with three-dimensional conformal radiation therapy. Int J Radiat Oncol Biol Phys 2001; 50(3):681–5.

14. Senan S, Burgers J, Samson M, et al. Can elective nodal irradiation be omitted in Stage III non-small-cell lung cancer? An analysis of recurrences after sequential chemotherapy and "involved-field" radiotherapy to 70 Gy. Int J Radiat Oncol Biol Phys 2001; 51:21.

15. Perez C, Stanley K, Grundy G, et al. Impact of irradiation technique and tumor extent in tumor control and survival of patients with unresectable non-oat cell carcinoma of the lung: report by the Radiation Therapy Oncology Group. Cancer 1982; 50:1091–9.

16. Sulman E, Chang J, Liao Z, et al. Exclusion of elective nodal irradiation does not decrease local regional control of non-small-cell lung cancer. Int J Radiat Oncol Biol Phys2005; 63(Supplement 1):S226–7.

17. Bradley J, Thorstad W, Mutic S, et al. Impact of FDG-PET on radiation therapy volume delineation in non-small-cell lung cancer. Int J Radiat Oncol Biol Phys 2004; 59(1):78–86.

18. Martel M, SahijdakW, Hayman J, et al. Incidental dose to clinically negative nodes from conformal treatment fields for non-small-cell lung cancer. Int J Radiat Oncol Biol Phys 1997; 45:244.

19. Pieterman R, van Putten J, Meuzelaar J, et al. Pre-operative staging of non-small-cell lung cancer with positron-emission tomography. N Eng J Med 2000; 343(4):254–61.

20. Rosenzweig K, Hanley J, Mah D, et al. The deep inspiration breath-hold technique in the treatment of inoperable non-small-cell lung cancer. Int J Radiat Oncol Biol Phys 2000; 48(1):81–7.

21. Sixel K, Aznar M, Ung Y. Deep inspiration breath hold to reduce irradiated heart volume in breast cancer patients. Int J Radiat Oncol Biol Phys 2001; 49(1):199–204.

22. International Commission on Radiation Units and Measurements. Prescribing, recording, and reporting photon beam therapy. Bethesda, MD, 1993: Report No.: 50.

23. Sasaki R, Komaki R, Macapinlac H, et al. Fluoro-deoxyglucose uptake by positron emission tomography predicts outcome of non-small-cell lung cancer. J Clin Oncol 2005; 23(6):1136–43.

24. Klopp A, Chang J, Liu H, et al. Intra-thoracic pat-terns of failure for non-small-cell lung cancer (NSCLC) with PET/CT-defined target delineation (2463a). Int J Radiat Oncol Biol Phys 2006; 66(3, Supplement 1):S467.

25. Giraud P, Antoine M, Larrouy A, et al. Evaluation of microscopic tumor extension in non-small-cell lung cancer for three-dimensional conformal radiotherapy planning. Int J Radiat Oncol Biol Phys 2000; 48(4):1015–24.

26. Yu J, Meng X, Xing L, et al. The study on correlation between F-18 FDG PET/CT standard uptake value and clinical target volume definition in radiotherapy for non-small-cell lung cancer (2484a). Int J Radiat Oncol Biol Phys 2006; 66(3, Supplement 1):S480.

27. Ramsey C, Scaperoth D, Arwood D, et al. Clinical efficacy of respiratory gated conformal radiation therapy. Med Dosim 1999; 24(2):115–9.

28. Starkschall G, Nelson C, Morice R, et al. Use of portal imaging and implanted fiducial to assess respiratory motion in gated radiotherapy. In: 9th International Workshop Electronic Portal Imaging,2006:146–7.

29. Nelson C, Starkschall G, Morice R, et al. Estimation of lung tumor setup uncertainties using bony landmarks and implanted fiducials. Med Phys 2006; 33 (6):2297.

30. Nelson C, Starkschall G, Chang J. Dose escalation resulting from reduced margins used to generate the planning target volume. Med Phys 2005; 32(6):1946.

31. Liu H, Balter P, Tutt T, et al. Assessing respiration-induced tumor motion and internal target volume using 4cdt for radiation therapy of lung cancer. Int J Radiat Oncol Biol Phys 2007; 68(2):531–40.

32. Komaki R, Lee J, Milas L, et al. Effects of amifostine on acute toxicity from concurrent chemotherapy and radiotherapy for inoperable non-small-cell lung cancer: report of a randomized comparative trial. Int J Radiat Oncol Biol Phys 2004; 58(5):1369–77.

33. Strauss G, Herndon J, Maddaus M, et al. Randomized clinical trial of adjuvant chemotherapy with paclitaxel and carboplatin following resection in Stage IB non-small cell lung cancer (NSCLC): Report of cancer and leukemia group B (CALGB) protocol 9633. J Clin Oncol 2004; 22(14):7019.

34. Douillard JY, Rosell R, Delena M, et al. Phase III adjuvant vinorelbine (N) and cisplatin (P) versus observation (OBS) in completely resected (stage I-III) non-small cell lung cnacer (NSCLC) patients (pts): Final results after 70-month median follow-up. J Clin Oncol 2005; 23:16.

35. Arriagada R, Bergman B, Dunant A, et al. Cisplatin-based adjuvant chemotherapy in patients with completely resected non-small-cell lung cancer. N Eng J Med 2004; 350(4):351–60.

36. Kaskowitz L, Graham M, Emami B, et al. Radiation therapy alone for stage I non-small cell lung cancer. Int J Radiat Oncol Biol Phys 1993; 27:517–23.

37. Pan T, Luo D, Liu H, et al. Improving tumor localization and standard uptake value quantitation of non-small cell lung cancer and esophageal cancer patients by new respiration-averaged CT in PET/CT imaging (2466a). Int J Radiat Oncol Biol Phys 2006; 66(3):S468–9.

38. Xia T, Li H, Sun Q, et al. Promising clinical outcome of stereotactic body radiation therapy for patients with inoperable Stage I/II non-small-cell lung cancer. Int J Radiat Oncol Biol Phys 2006; 66:117–25.

39. Onishi H, Araki T, Shirato H, et al. Stereotactic hypofractionated high-dose irradiation for stage I non-small cell lung carcinoma clinical outcome in 245 subjects in a Japanese multi-institutional study. Cancer 2004; 101(7):1623–31.

40. Nagata Y, Takayama K, Matsuo Y, et al. Clinical outcomes of a phase I/II study of 48 Gy of stereotactic body radiotherapy in 4 fractions for primary lung cancer using a stereotactic body frame. Int J Radiat Oncol Biol Phys 2005; 63(5):1427–31.

41. Chang J, Balter P, Liao Z, et al. Preliminary report of image-guided hypofractionated sterotactic body radiotherapy to treat patients with medically inoperable stage I or isolated peripheral lung recurrent non-small-cell lung cancer. Int J Radiat Oncol Biol Phys 2006; 66(3):S480.

42. Furuse K, Fukuoka M, Kawahara M, et al. Phase III study of concurrent versus sequential thoracic radiotherapy in combination with mitomycin, vindesine, and cisplatin in unresectable stage III non-small-cell lung cancer. J Clin Oncol 1999; 17 (9):2692.

43. Fournel P, Robinet G, Thomas P, et al. Randomized phase III trial of sequential chemoradiotherapy compared with concurrent chemoradiotherapy in locally advanced non-small-cell lung cancer: Groupe Lyon-Saint-Etienne d'Oncologie Thoracique-Groupe Francais de Pneumo-Cancerologie NPC 95-01 Study. J Clin Oncol 2005; 23(25):5910–7.

44. Socinski M, Rosenman J, Halle J, et al. Dose-escalating conformal thoracic radiation therapy with induction and concurrent carboplatin/paclitaxel in unresectable stage IIIA/B non-small-cell lung carcinoma. Cancer 2001; 92(5):1213–23.

45. Schild S, McGinnis W, Graham D, et al. Results of a phase I trial of concurrent chemotherapy and escalating doses of radiation for unresectable non-small-cell lung cancer. Int J Radiat Oncol Biol Phys 2006; 65(4):1106–11.

46. Bradley J, Graham M, Suzanne S, et al. Phase I results of RTOG L-0117; a Phase I/II dose intensification study using 3DCRT and concurrent chemotherapy for patients with inoperable NSCLC. Proc Am Soc Clin Oncol 2005; 23(7063A):16S.

47. Murshed H, Liu H, Liao Z, et al. Dose and volume reduction for normal lung using intensity-modulated radiotherapy for advanced-stage non-small-cell lung cancer. Int J Radiat Oncol Biol Phys2004; 58(4):1258–67.

48. Liu H, Wang X, Dong L, et al. Feasibility of sparing lung and other thoracic structures with intensity-modulated radiotherapy for non-small-cell lung cancer. Int J Radiat Oncol Biol Phys 2004; 58(4):1268–79.

49. Belani C, Choy H, Bonomi P, et al. Combined chemo-radiotherapy regimens of Paclitaxel and Carboplatin for Locally Advanced Non-Small-Cell Lung Cancer:

A Randomized Phase II Locally Advanced Multi-Modality Protocol. J Clin Oncol 2005; 23(25):5883–91.

50. Roth J, Fossella F, Komaki R, et al. A randomized trial comparing perioperative chemotherapy and surgery with surgery alone in resectable stage IIIA non-small-cell lung cancer. J Natl Cancer Inst 1994; 86:673–80.

51. Rosell R, Gomez-Codina J, Camps C, et al. A ran-domized trial comparing preoperative chemotherapy plus surgery with surgery alone in patients with non-small-cell lung cancer. N Engl J Med 1994; 330(3):153–8.

52. Albain K, Swann S, Rusch V, et al. Phase III study of concurrent chemotherapy and radiotherapy (CT/RT) vs CT/RT followed by surgical resection for stage IIIA (PN2) non-small-cell lung cancer (NSCLC): outcomes update of North America Intergroup 0139 (RTOG 9309). J Clin Oncol 2005; 23(16):624.

53. Asamura H, Nakayama H, Kondo H, et al. Lobe-specific extent of systematic lymph node dissection for non-small-cell lung carcinomas according to a retrospective study of metastasis and prognosis. J Thorac Cardiovasc Surg 1999; 117(6):1102–11.

54. Lung Cancer Study Group. Effects of postoperative mediastinal radiation on completely resected Stage II and Stage III epidermoid cancer of the lung. N Eng J Med 1986; 315:1377–81.

55. Yom S, Liao Z, Liu H, et al. Analysis of acute toxicity results of intensity modulated radiationtherapy (IMRT) in the treatment of non-small cell lung cancer (NSCLC) (O-152a). Lung Cancer 2005; 49(Supplement 2):S52.

56. Chang J, Liu H, Komaki R. Intensity modulated radiation therapy and proton radiotherapy for non-small-cell lung cancer. Curr Oncol Rep 2005; 7:255–9.

57. Emami B, Lyman J, Brown A, et al. Tolerance of normal tissue to therapeutic irradiation. Int J Radiat Oncol Biol Phys 1991; 21(1):109–22.

58. Yorke E, Jackson A, Rosenzweig K, et al. Dose-volume factors contributing to the incidence of radiation pneumonitis in non-small-cell lung cancer patients treated with three-dimensional conformal radiation therapy. Int J Radiat Oncol Biol Phys 2002; 54(2):329–39.

59. Liao Z, Wang S, Wei X, et al. Analysis of clinical and dosimetric factors associated with radiation pneumonitis (RP) in patients with non-small-cell lung cancer (NSCLC) treated with concurrent chemotherapy (ConChT) and three dimensional conformal radiotherapy (3D-CRT) (68a). Int J Radiat Oncol Biol Phys 2005; 63(Supplement 1):S41.

60. Liao Z, Liu H, Tucker S, et al. The volume of lung receiving low radiation doses is associated with treatment related lung toxicity when irradiating tumors in the thorax. Int J Radiat Oncol Biol Phys 2006; 66(3, Supplement 1):S472.

61. Rice D, Liao Z, Vaporciyan A, et al. V20 predicts fatal pulmonary toxicity after extrapleural pneumonectomy and intensity modulated radiation therapy (111a). Int J Radiat Oncol Biol Phys2006; 66(3, Supplement 1):S63.

62. Bradley J, Leumwananonthachai N, Purdy J, et al. Gross tumor volume, critical prognostic factor in patients treated with three-dimensional conformal radiation therapy for non-small-cell lung carcinoma. Int J Radiat Oncol Biol Phys 2002; 52(1):49–57.

63. Ahn S, Kahn D, Zhou S, et al. Dosimetric and clinical predictors for radiation-induced esophageal injury. Int J Radiat Oncol Biol Phys 2005; 61(2):335–47.

64. Maguire P, Sibley G, Zhou S, et al. Clinical and dosimetric predictors of radiation-induced esophageal toxicity. Int J Radiat Oncol Biol Phys 1999; 45(1):97–103.

65. Chapet O, Kong F, Lee J, et al. Normal tissue complication probability modeling for acute esophagitis in patients treated with conformal radiation therapy for non-small cell lung cancer. Radiother Oncol 2005; 77(2):176–81.

Radiotherapy Guidelines in Small Cell Lung Cancer

Ritsuko Komaki
Department of Radiation Oncology, University of Texas M.D. Anderson Cancer Center, Houston, Texas, U.S.A.

INTRODUCTION

In the United States, approximately 40,000 persons were expected to receive a diagnosis of small cell lung cancer (SCLC) during 2006, accounting for 20–25% of all lung cancer cases (1,2). Among those patients with SCLC, only one-fourth of them will be expected to have limited disease in the thorax because the majority already has disseminated disease in the thorax or extrathorax.

One important aspect of the management of SCLC is distinguishing its cytology or histology from that of non–small cell lung cancer (NSCLC) (Table 1). SCLC and adenocarcinoma of the lung are characterized by positive transcription thyroid factor-1 (TTF-1). On the other hand, squamous cancer does not express TTF-1. Cytokeratins 5/6 are highly positive in squamous carcinoma, but not in SCLC (Table 1). Table 2 shows markers that distinguish SCLC and NSCLC based on endothelial growth factor receptor, chromosome 3 deletion, Leu-7 antigen, radiation sensitivity, blc-c/C-myc status, inactive rhabdomyosarcoma, p53 mutation, and other related markers, including a related peptide hormone and neuron-secreting elase.

Physical examination of patients with SCLC aims to identify prognostic indicators and clinical manifestations, such as paraneoplastic syndromes, to distinguish them from patients with NSCLC (Table 3). Patients with SCLC often manifest inappropriate antidiuretic hormone secretion, ectopic adrenocorticotropic hormone-producing syndrome, gynecomastia, or Eaton-Lambert hormone syndrome. Yet neither hypercalcemia nor osteoarthropathy is a common manifestation among patients with SCLC. Hyper-coagulaopathy is common to any type of lung cancer (Table 3). This is essential for determination of the type of treatment modality, aggressiveness of treatment, and other supportive management. When combined thoracic radiation therapy (TRT) and chemotherapy are given, conformal radiation therapy is used to reduce such normal tissue toxicities as esophagitis, pneumonitis, pericarditis, and myelitis. This is essential for patients with limited-stage SCLC (LSCLC) and good performance status who will need to tolerate acute toxicities during TRT/chemotherapy without break of TRT or modification of the dose of chemotherapy and/or TRT. Prophylactic cranial irradiation (PCI) has become a part of the standard management for patients with LSCLC who have achieved complete response.

PATHOLOGY

The World Health Organization classification subdivides SCLC into three cell types (pure or classic, variant cell, and mixed), although there is no significant difference in outcome by subtype. Pure SCLC is more sensitive to chemotherapy and radiation therapy than is the variant cell type, although there is some controversy about whether the variant cell type significantly affects patient outcome. Aisner et al. (3) reviewed a series of 577 patients with LSCLC treated by chemotherapy and radiation therapy on an Eastern Cooperative Oncology Group (ECOG) protocol. There were 24 cases (4.4%) with the variant cell type. Complete response rates were 27% for patients

Table 1 Poorly Differentiated Adenocarcinomas Compared with Other Types of NSCLC and SCLC and Related Biomarkers

Immunohistochemistry marker	Adenocarcinoma (%)	Squamous carcinoma (%)	SCLC/large cell neuroendocrine carcinoma (%)
TTF-1	96	0–6	87
Cytokeratin 7	98	~20	70 (LCNEC)
Cytokeratins 5/6	Negative	100	10
Surfactant apoprotein A	46	Negative	Negative

Note: Data were not available for all patients from all participating institutions for all characteristics.
Abbreviations: SCLC, small cell lung cancer; NSCLC, non–small cell lung cancer.

Table 2 Markers for Identifying SCLC

| Marker/characteristics | SCLC | | NSCLC |
	Classic	Variant	
Endothelial growth factor receptors	−	−	+
Chromosome 3 deletion	+	+	−
Leu-7 antigen	+	+	−
Radiation sensitive	Sensitive	Resistant	Resistant
B-lymphoid cell-2 (blc-2)/C-*myc* oncogene	−	+	±
Inactive retinoblastoma p53 mutation	+	+	−
Boombesin-like immunoreactivity/gastrin receptor peptide	++	−	−
Neuron-specific enolase	++	+	-
Creatinine kinase BB	++	++	−
Neurotensin	++	−	−
Peptide hormone	++	±	−
Bombesin-like receptors	+	−	−

Abbreviation: SCLC, small cell lung cancer.

with the variant cell type and 19% for patients with classic cell type ($P = 0.45$). The mixed-cell type should be treated as NSCLC rather than SCLC because its chemotherapeutic sensitivity and radiosensitivity are similar to those for NSCLC rather than SCLC.

PROGNOSTIC FACTORS

The most important prognostic factor for SCLC is stage (limited vs. extensive). Limited disease (LSCLC) is confined to the hemithorax, although the presence of malignant pleural effusion will affect the outcome adversely. Patients who present with pleural effusion have poorer outcomes than those without pleural effusion. However, the patients who have negative cytology of the pleural effusion do have better outcomes than those with positive cytology. Extensive SCLC extends beyond the hemithorax, such as disease in both lungs or extrathoracic extension often to the brain, leptomeninges, spinal cord, bone, bone marrow, adrenal gland, liver, pancreas, kidneys,

small bowel, or pelvis. Patient factors influencing outcome are performance status and sex. Age is not a significant prognostic variable in patients with LSCLC (4). However, patients older than 80 years old will have limitations on the aggressive systemic treatment. Continuation of smoking will adversely affect the outcome. Other prognostic factors indicating an adverse effect on outcome are elevated lactic dehydrogenase and alkaline phosphatase levels, low sodium level, and possibly the presence of paraneoplastic syndromes, which include the syndrome of inappropriate antidiuretic hormone, adrenocorticotropic hormone-producing syndrome, and Eaton–Lambert syndrome.

STAGING

The workup to define SCLC is similar to that of NSCLC. The history and physical examination need to include any signs and symptoms related to one or more paraneoplastic syndromes. It is also important

Table 3 Lung Cancer: Paraneoplastic Syndromes by Cell Type

Syndrome	Small cell	Large cell	Squamous	Adenocarcinoma
Inappropriate antidiuretic hormone secretion	+++			
Ectopic adrenocorticotropic hormone production	+++			
Gynecomastia	++	+		
Eaton-Lambert	++			
Hypercalcemia (nonmetastatic)		+++	+++	
Hypertrophic osteoarthropathy		+++		+++
Thrombocytosis	++	++	++	++
Hypercoagulable stage	++	++	++	++

Note: Data were not available for all patients from all participating institutions for all characteristics.
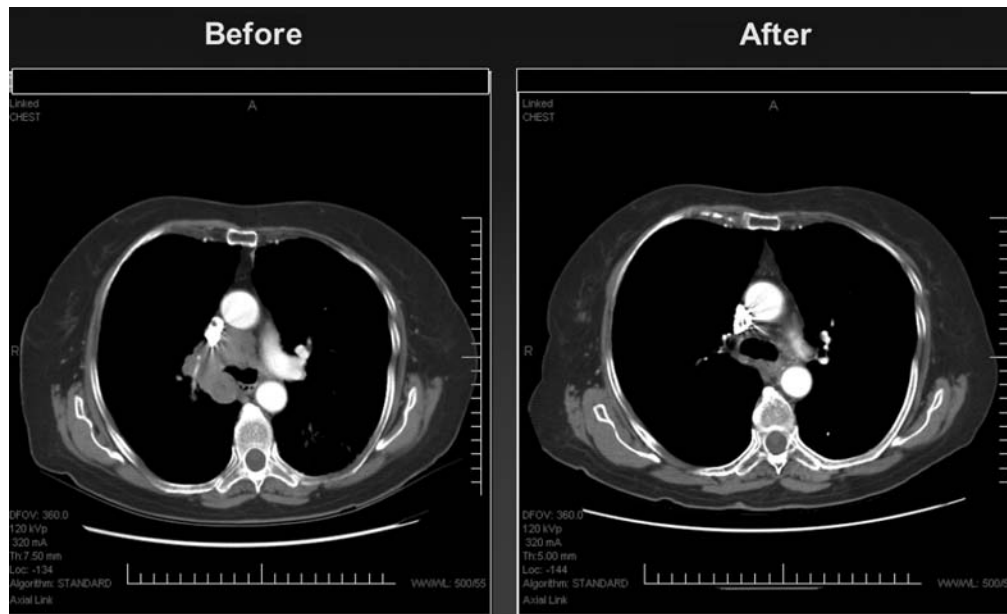
Figure 1 In these CT scans of the chest of a 71-year-old woman who presented with syndrome of inappropriate antidiuretic hormone, bulky and extensive lymph node involvement is evident pretreatment *(left)* and an excellent response to chemoradiotherapy is evident posttreatment *(right). Abbreviation*: CT, computerized tomography.

for all patients to undergo magnetic resonance imaging to rule out metastatic disease. Patients who achieve a complete response to the chemotherapy and radiotherapy are candidates for PCI. For patients with limited-stage disease, bone scan and bone marrow aspiration or biopsy are indicated if the lactic dehydrogenase level is elevated, and thoracentesis is indicated if pleural effusion is present. Follow-up imaging studies and other work-up should be ordered as suggested by the Oncology Practice Guidelines of the National Comprehensive Cancer Network (5). Positron-emission tomography scanning to evaluate the extent of lung cancer, including mediastinal nodal involvement, has become fairly accurate with the assistance of computerized tomography (CT) in NSCLC and may help in SCLC (6).

STAGE-BASED TREATMENT GUIDELINES

Early-stage SCLC is diagnosed in less than 5% of patients with SCLC. For patients with clinical stage I (T1-2, N0), complete resection with a lobectomy with mediastinal nodal dissection or sampling may be considered. However, mediastinoscopy should be performed to rule out occult nodal disease prior to resection. Postoperative chemotherapy should be considered even if surgical pathology shows no lymph node involvement. For patients with positive lymph node involvement after surgical resection, postoperative chemotherapy and radiotherapy should be considered. In all cases, PCI should be considered.

Most patients with SCLC present with bulky and extensive lymph node involvement (Fig. 1). Management of this group of SCLC cases has evolved from employing single chemotherapeutic agents in the 1940s and 1950s to using multichemotherapeutic agents with TRT and PCI for LSCLC in the 1990s (7). Feld et al. (8) reviewed eight series published between 1979 and 1987 and reported a rise in 2-year survival rates from a range of 10–15% to a range of 25–30%. Most if not all of the improvement in outcome was attributed to more effective combination chemotherapy regimens. Locoregional therapy alone, achieved with either surgery or radiation therapy, improved the short-term survival only slightly, primarily for a subset of patients with limited-stage disease with very rare 5-year survival. In a landmark trial conducted by the Medical Research Council in the 1960s, patients who were considered candidates for surgical resection by the standards of the time were randomized to thoracotomy with the intent of tumor removal or to definitive irradiation of the primary tumor and regional lymphatics (9). Radiation therapy resulted in slightly better mean survival duration (6.5 vs. 10 months, $P = 0.04$) with 1-, 2-, and 5-year survival rates of 22%, 10%, and 4%, respectively, compared with 21%, 4%, and 1% for the surgery arm (Table 4). Of interest, the one 5-year survivor in the surgery arm was unable to undergo surgery and was given radiation therapy. These studies led to the abandonment of surgery as a primary modality of treatment of SCLC with the possible exception of patients with

Table 4 LSCLC Surgery Compared with Radiotherapy

		Patients alive (%)			Median
Treatment	N	1 year	2 years	5 years	survival (days)
Radical surgery	71	15 (21%)	3 (4%)	1 (1%)	199
Radiotherapy	73	16 (22%)	7 (10%)	3 (4%)	300

Abbreviation: LSCLC, limited small cell lung cancer.

solitary pulmonary nodules (10). A more recent approach is concurrent chemotherapy and TRT followed by aggressive systemic chemotherapy supported by granulocyte colony-stimulating factor, antibiotics, management of electrolytes, and erythropoietin-stimulating agent.

CHEMOTHERAPY FOR SCLC

Standard Chemotherapy

A major step in the systemic treatment of SCLC was reported in 1969 when alkylating agents were compared to an inert compound in about 2000 lung cancer patients at a group of Veterans Administration hospitals (11). Antitumor effects of chemotherapy were analyzed according to cell type, and improvement in survival was the sole criterion of drug activity. Although the 4-month median survival for patients with SCLC on alkylating agents was only slightly better than the 1.5-month median survival of patients treated with inert compound ($P = 0.0005$), the trial was the first to show a statistically significant survival benefit of chemotherapy in lung cancer. Cyclophosphamide became a cornerstone in successful SCLC treatment, just as the nitrogen mustard in mechlorethamine, vincristine (Oncovin®), procarbazine, and prednisone chemotherapy was in Hodgkin's disease.

Although the magic combination never emerged, the power of chemotherapy was clearly improved with multi-agent chemotherapy. Many permutations and variations of protocols containing five drugs (cyclophosphamide, doxorubicin, vincristine, etoposide, and cisplatin) or their analogues have been reported, and a number of regimens have been used in phase III studies. In 1975, Einhorn et al. (12) combined cyclophosphamide, doxorubicin, and vincristine (CAV) and produced not only high response rates but also complete responses in 20% of cases. It is notable and somewhat disconcerting that the CAV regimen and cyclophosphamide, doxorubicin, and etoposide regimen have persisted as standard combinations for thirty years. Interest in the combination of etoposide and cisplatin (EP) (13) was stimulated after it was shown to produce tumor regression in patients whose cancers had progressed following initial drug treatment with a cyclophosphamide-based regimen (14). The consistent performance of EP or carboplatin and etoposide in clinical trials plus the bonus of its compatibility with radiotherapy has made it a standard of such durability that it persists as the treatment of choice (15).

Investigational Chemotherapy

Extensive-stage SCLC (ESCLC) remains impervious to chemotherapy innovations. At the most basic level, it was easily demonstrated that monotherapy was inferior to combination chemotherapy (16,17). However, beyond that, it has not been shown conclusively that any innovation of chemotherapy has been associated with a consistent improvement in survival. Major areas of research have been chemotherapy diversity, quantity of drugs administered (dose, dose intensity, duration of chemotherapy), and introduction of new agents. New drug development has included testing in previously untreated extensive disease without apparent detriment to survival, but the need is for agents that cause response in disease resistant to standard therapy. Unfortunately, no such agents loom on the horizon.

Drug diversity is a fundamental principle governing the use of combination chemotherapy that attempts to avoid or minimize the development of resistant clones (18). Models of drug diversity acquisition include altering the standard regimen by adding drugs, substituting drugs, alternating combinations, and creating complex weekly regimens. An informative study by the Southeastern Cancer Study Group that compared sequential CAV, sequential EP, and alternating CAV and EP showed no statistically significant differences in response rates or survival for ESCLC (19). Additionally, this trial demonstrated that an iso-effective result could be generated with four cycles of EP compared with six cycles of CAV or CAV/EP. The CODE (cisplatin, vincristine, doxorubicin, and etoposide) regimen incorporated both drug diversity and a doubling of dose intensity but failed to improve survival for ESCLC when compared with CAV/EP (19).

Occasional examples exist of an incremental but statistically significant benefit of adding a third drug to a two-drug protocol in ESCLC, such as adding ifosfamide to the EP regimen (20), but the small

survival gain weighed against the toxicity/logistical cost has not changed practice. Other drug addition regimens, such as the addition of paclitaxel and granulocyte colony-stimulating factor to EP (TEP), which has been compared with EP, have clearly had no impact on survival in ESCLC (21). The addition of paclitaxel to EP did result in added toxicity. Renal toxicity, motor-sensory neuropathy, and hearing loss were more common in the arm undergoing positron-emission tomography. The toxic death rate was three times as high in patients receiving the triplet combination (6.5% vs. 2.4%). The Greek Lung Cancer Cooperative Group also conducted a prospective randomized trial of TEP versus EP (22). The trial was closed early because of unacceptable toxicity in the three-drug arm.

In a different type of drug addition study, ECOG randomized ESCLC patients who were stable or responding to four induction courses of EP to four cycles of maintenance or consolidation chemotherapy with topotecan or a control group (23). Progression-free survival was trivially better for the topotecan arm than the observation arm (3.6 vs. 2.3 months). However, there was no difference in median survival (8.9 vs. 9.3 months, $P = 0.43$), and topotecan added substantial toxicity. In this study, it is poignant that even when patients with ESCLC are selected for chemotherapy-responsive biology (patients with progressive disease were not randomized), maintenance treatment beyond four cycles of EP with putatively non–cross-resistant properties failed to improve survival.

Randomized trials (24–28) of dose intensification have consistently been negative in ESCLC, as was a meta-analysis of dose intensity (29). Although trials of high-dose chemotherapy with stem cell support for SCLC are still under way in Europe, the failure of this approach to overcome drug resistance in epithelial cancers in general has marginalized this difficult line of investigation to enthusiasts.

With respect to the introduction of new chemotherapy agents, a phase III trial from Japan (30) was stopped early when the combination of irinotecan and cisplatin demonstrated survival superiority to the EP combination in ESCLC. Median survival was typical in the EP arm at 9.4 months versus 12.8 months for the irinotecan-treated arm ($P = 0.002$). At 2 years, the percentage of patients surviving was 19.5% versus 5.2%. At the 2005 meeting of the American Society of Clinical Oncology, a phase III trial of a different schedule (days 1, 8) of irinotecan and cisplatin generated identical outcomes compared with the EP regimen (31). A confirmatory phase III trial by the Southwest Oncology Group (S0124) has been designed to reproduce the clinical data of the Japanese trial in a larger population (620 patients) and also

investigate pharmacogenomic end points predictive of toxicity or efficacy of irinotecan and cisplatin. Additionally, this study will examine polymorphisms of genes associated with drug metabolism (UGT1A1) and excision repair genes for platinum (ERCC-1, XRCC-1). In the largest phase III trial ever conducted for SCLC, Eckardt et al. (32) randomized 859 patients to EP versus cisplatin with oral topotecan. Response rates, median time to progression, and overall survival were not statistically significantly different. The negative results of the two North American trials (31,32) testing the utility of the substitution of topoisomerase I inhibitors for etoposide in a platinum protocol have generated a pall of pessimism that combinations with this drug class are capable of displacing EP as standard therapy for ESCLC.

Other new drugs such as pemetrexed (33) and amrubicin (34) are active and undergoing testing in combination with a platinum agent in ESCLC. However, like advanced NSCLC, it is increasingly unlikely that the plateau in the power of treatment for ESCLC will be changed with the introduction of new cytotoxic agents.

Impact of Chemotherapy Innovations

While chemotherapy alone cures a small proportion of patients with LSCLC (35), long-term survivors in the ESCLC population are uncommon (1%). This difference makes LSCLC a model of a curable neoplasm in which incremental improvements in chemotherapy efficacy can be more easily detected than in palliative ESCLC patients. This effect has been shown in several clinical trials using several chemotherapy variations.

The most notable example comes from Norway where Sundstrom et al. (36) randomized 436 patients with SCLC to either cyclophosphamide, epirubicin, and vincristine or EP for five cycles. Two hundred eighteen patients with LSCLC were to receive thoracic irradiation (TI) between the third and fourth course of chemotherapy to a dose of 42 Gy. For ESCLC patients, there was no significant survival difference between the treatment arms. However, for LSCLC, the median survival time was 14.5 versus 9.7 months in the EP and CEV arms, respectively ($P = 0.001$). The 2- and 5-year survival rates of 25% and 19% in the EP arm compared with 8% and 3% in the CEV arm ($P = 0.001$). This trial provides compelling evidence that cyclophosphamide/anthracycline regimens are inappropriate frontline regimens for LSCLC.

In a drug substitution trial, Reck et al. (37) compared CEV to paclitaxel, etoposide, and carboplatin (TEC)—the experimental arm. The 608-patient study included 302 patients with LSCLC, and randomization was stratified by stage. Patients with LSCLC received TI after 6 cycles of chemotherapy. Median survival for patients in the TEC arm was

superior to that achieved by patients in the CEV arm (12.7 vs. 11.7 months), and the hazard ratio of death was statistically significantly higher in the CEV arm (hazard ratio = 1.22; $P = 0.02$) than in the TEC arm. When analyzed by stage, the median survival advantage of TEC over CEV was confined to LSCLC patients (17.6 vs. 16.6 months); the difference in 3-year survival appears more impressive but was not cited in the paper. There was no difference in outcome for ESCLC, for which the median survival rate was 9.8 months in one arm and 10.0 months in the other.

In a trial of dose intensification, Thatcher et al. (38) randomized 403 patients to a standard six cycles of doxorubicin, cyclophosphamide, and etoposide (ACE) at 3-week intervals versus the same regimen given every 2 weeks with granulocyte colony-stimulating factor support. The patient population had predominantly limited stage disease (77%), and all patients had good prognostic factors as defined by this group. Survival was longer in the group receiving intensified therapy (hazard ratio = 0.80; 95% confidence interval [CI], 0.65–0.99; $P = 0.04$). At 24 months survival was 13% versus 8% in favor of the more intensive regimen. The same group examined a patient population with a higher proportion of LSCLC patients (87%) and favorable prognostic factors with a randomization between ICE-V (ifosfamide, carboplatin, etoposide, and vincristine) versus standard chemotherapy (mainly CAV) (39). Consolidation TI and PCI was recommended after chemotherapy was complete. The median survival was 15.6 months in the ICE-V group and 11.6 months in the control group, and the 2-year survival rates were 20% and 11% respectively ($P = 0.0049$).

These randomized trials of LSCLC patients with good prognostic factors suggest that small but statistically significant survival gains can be achieved from chemotherapy innovations for this group. However, there is a problem. Unless profound differences exist in prognostic factors or staging methods that make these patients incomparable to other recently published LSCLC results, the median and long-term survival outcomes of all these trials are clearly inferior to what would be expected from early concurrent EP and TI. With initial concurrent chemoradiation, the median survival times exceed 20 months: 2-year survival is more than 40% and actual 5-year survival rates of more than 20% are fairly consistently reported (40–42).

Concurrent administration of full doses of EP and TI can be accomplished with manageable toxicity without reduction of either modality. However, when chemotherapy is manipulated by dose intensification or addition of drugs that are less compatible with TI, the fidelity of both modalities of treatment is impaired by increased hematological and nonhematological toxicity. As an example, a recently reported Radiation Therapy Oncology Group (RTOG) phase II study that incorporated paclitaxel with EP and twice-daily TI (45 Gy in 3 weeks) showed a favorable median survival of 24.7 months and a 2-year survival rate of 54% (43). Four- and five-year survival was about 20%. Grades 3 and 4 esophagitis was 32% and 4%, respectively, and 6% of patients died of toxicity. After due consideration, the authors concluded that this three-drug protocol was unlikely to improve the results in LSCLC compared with the standard EP chemotherapy regimen and that this line of investigation would be pursued no further.

The demographic patterns of patients diagnosed with LSCLC are not conducive to increasingly toxic combined modality protocols. Gaspar et al. (44) examined a National Cancer Data Base including four patient cohorts diagnosed with LSCLC in 1985 ($N = 2123$), 1990 ($N = 279$), 1995 ($N = 7815$), and 2000 ($N = 2123$). The proportion of older patients (age >70 years) increased significantly over time, from 31.6% in 1985 to 44.9% in 2000 ($P < 0.001$). Moreover, SCLC patients are generally physiologically aged beyond their chronological age at least in part because of heavy smoking. This analysis identified the continued need for the evaluation of new treatments in this group of patients, but more aggressive chemotherapy in combined modality protocols is unlikely to enhance the therapeutic index.

COMBINED MODALITY THERAPY

Thirteen randomized studies, including 2140 patients, have investigated the role of thoracic radiotherapy in LSCLC. Two meta-analyses (35,45) have been published that examine these trials. Both show a modest improvement in survival rates in those patients given thoracic radiotherapy in addition to chemotherapy. Survival benefit becomes evident at about 15 months after the start of treatment and persists beyond 5 years. At 3 years, 8.9% of the chemotherapy-only group is alive compared with 14.3% of the combined-modality group. The relative risk of death in the combined modality group as compared with the chemotherapy group was 0.86 (95% CI, 0.78–0.95; $P = 0.001$), corresponding to a 14% reduction in the mortality rate. The analysis of local control showed a 2-year local failure rate of 23% for irradiated patients versus 48% for nonirradiated patients ($P = 0.0001$). These benefits were obtained at the cost of an increase in treatment-related deaths of 1%.

The meta-analyses (35,45) have been a valuable addition to the oncology literature, and the principal conclusion that chemotherapy combined with TI is superior to chemotherapy alone is undoubtedly

correct. However, the meta-analyses underestimate the absolute long-term survival contribution of state-of-the-art integrated chemoradiation. Most studies in the meta-analyses commenced before 1981, and none delivered cisplatin and etoposide, either as initial treatment or concurrently with TI. Investigators reported relative risk of death rather than the proportion of long-term survivors, which masked the contribution of radiotherapy. Even the survival curve is initially better for chemotherapy alone, but at about one year the curves cross, showing a clear benefit of combined modality therapy on long-term survival. Chemotherapy prescriptions from a previous era that administer concurrent chemoradiation with cyclophosphamide, doxorubicin, and nitrosoureas are associated with problematic hematological and non-hematologic toxicity. Reliable delivery of both chemotherapy and radiotherapy is uncertain. The negative impact of chemoradiation using incompatible chemotherapy regimens can be seen in two subgroups reported in the meta-analysis of Pignon (35).

Subgroup analysis on the basis of age indicated that the benefit from radiotherapy on mortality was greatest for patients younger than 55 years of age ($P = 0.01$). The relative risk of death in favor of combined modality therapy was 0.72 (95% CI, 0.56–0.93) for patients younger than 55 years and 1.07 (95% CI, 0.70–1.64) for patients older than 70 years of age. This adverse effect of age on the benefit of combined modality therapy has been contradicted by two recent studies (4,46) that examined treatment effects in older patients (≥70 years of age) versus younger patients (<70 years of age) in studies that administered early EP with TI. The two groups were similar for baseline patient characteristics; treatment field sizes, toxicity, response rates, and overall survival. These analyses conclude that age does not appear to have an impact on the delivery, tolerance, or efficacy of radiotherapy when used with platinum and etoposide in patients with LSCLC. A plausible explanation of the discrepancy would be that toxicity of concurrent chemoradiation as used in the trials examined in the meta-analysis had a disproportionate effect on elderly patients. Clearly, fit elderly patients should not be denied the benefit from chemoradiation for LSCLC based on the meta-analysis (35). The same meta-analysis examined the question of the timing of TI (sequential, alternation, and concurrent), and no statistically significant differences were found among the various treatment schedules (35). However, 3 of the 4 trials that showed a significant survival advantage for combined modality therapy employed a concurrent or alternating scheme, whereas seven of the nine trials that did not demonstrate a survival advantage employed a sequential plan. Comparisons between sequential and concurrent therapy depend on compatibility of chemotherapy and radiotherapy; in fact, the alternating methodology was employed as a way to get around the excess toxicity of concurrent therapy with an anthracycline. The use of anthracyclines and alternating therapy has faded into the past, but rises with each evidence-based assessment and review of these studies. The survival advantage of TI becomes important 2–5 years postdiagnosis in LSCLC when the proportion of cured patients becomes manifest (40).

Sequencing and Timing of Thoracic Radiotherapy

Although investigation of TI timing is reported in seven randomized trials (41,42,47–51) of varying structure, size, and vintage, sequence and timing continue to generate controversy. Recently, a meta-analysis performed according to the Cochrane Collaboration Guidelines examined randomized controlled clinical trials comparing different timing of chest radiotherapy in patients with LSCLC (52). Early chest irradiation was defined as beginning within 30 days after the start of chemotherapy. Seven randomized trials were eligible (41,42,47–51). A weighted estimate of the typical treatment effect across studies was computed for 2-year survival data as well as the 5-year survival data, local control, and toxicities. The odds ratio (OR) was used as the effect measure. Taking all seven studies into account, the overall survival at 2 years (OR, 0.84; 95% CI, 0.56–1.28) or at 5 years (OR, 0.80; 95% CI, 0.47–1.38) was not significantly different between early and late chest radiotherapy. When the one trial that delivered nonplatinum chemotherapy concurrently with chest radiation (49) was excluded, the OR at 5 years was significantly in favor of early chest radiotherapy (OR, 0.64; 95% CI, 0.44–0.92, $P = 0.02$). When studies with an overall treatment time of chest radiation of less than 30 days were considered (41,42,47,48,50), the 5-year survival was even better (OR, 0.56; 95% CI, 0.37–0.85; $P = 0.006$). As expected, esophageal and pulmonary toxicity was worse with initial concurrent chemoradiation, but severe leukopenia was more frequent in patients receiving late chest radiotherapy ($P = 0.0004$).

Although a conclusion in favor of early concurrent chemoradiation for LSCLC is not definitive, analysis of relevant subsets of the data is rational. Exclusion of nonplatinum chemotherapy is supported by a meta-analysis showing superiority of SCLC regimens containing cisplatin (53) and a conclusive phase III trial showing better survival of patients on the EP regimen than that of those on a cyclophosphamide/anthracycline-based regimen (36). Early TI cannot be expected to perform well unless it is coupled with a chemotherapy regimen compatible with concurrent radiotherapy and efficacious
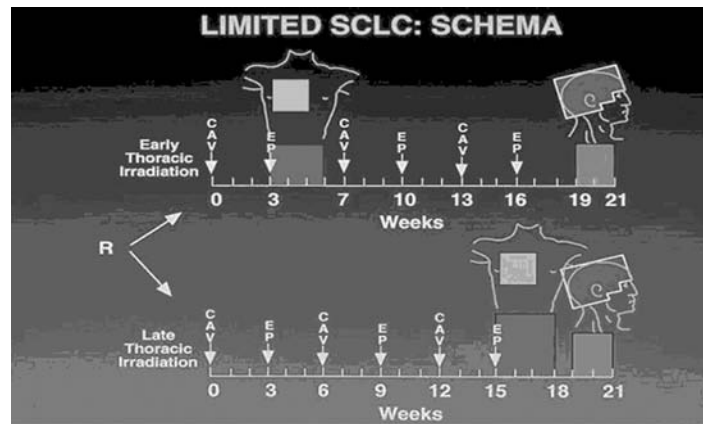
Figure 2   In a study of LSCLC, Murray et al. (42) compared early TI at week 3 with late TI at week 15. After completion of all chemotherapy, including CAV and EP, and thoracic radiotherapy, complete responders received prophylactic cranial radiotherapy of 25 Gy in 10 fractions over 2 weeks beginning at week 19. *Abbreviations*: CAV, Cyclophosphamide, doxorubicin, and vincristine; EP, etoposide and cisplatin; LSCLC, limited-stage small cell lung cancer. *Source*: From Ref. 42.

enough to improve control of micrometastases outside the TI volume. Parenthetically, it is important to note that the odds ratios adduced in favor of early concurrent TI versus delayed TI (0.80, 0.64, 0.56) in the meta-analysis by Pijls (52) are more favorable than the OR of 0.86 calculated in favor of combined modality therapy versus chemotherapy alone (35).

Another factor that influenced the less-than-robust statistics of the meta-analysis on the timing of TI is that the prognostic factors of the patients in the trials appear different. If a poor prognosis LSCLC population (as evidenced by a short median survival) is studied, the proportion of patients who can have their prognosis improved by better integration of chemoradiation will be low and the benefit of early TI timing will be diluted by having a majority of incurable cases. That the study populations in the Perry (49,54), Work (51), and James(47) trials, which failed to show superiority of early chemoradiation, contained more patients with a poorer prognosis is strongly suggested by the short median survival times reported. The average median survival of all patients (both arms) in these trials was 13.75 months for the Perry trial, 11.25 months for the Work trial, and 14.3 months for the James study. In the trials that support early concurrent chemoradiation, the average median survival of all trial patients was 18.6 months for the Murray study (42), 23.5 months for the Takada trial (41), and 30 months for the Jeremic trial (48). These are rather large differences (range of factors, 1.3–2.6).

The National Cancer Institute of Canada clinical trial group (42) compared early against late TRT in a randomized trial. Three hundred eight patients were randomized to receive early TRT (40 Gy in 15 fractions over 3 weeks) to the primary site with concurrent alternating EP and CAV or to receive late TI at week 15 with the same radiation therapy dose and same concurrent chemotherapy. After completion of all chemotherapy and TRT, complete responders received PCI (25 Gy in 10 fractions over 2 weeks) (Fig. 2). Although complete response rates did not significantly differ between the early and late TRT groups, progression-free survival ($P = 0.036$) and overall survival ($P = 0.008$) (Fig. 3) were significantly better in the early thoracic group. Patients in the late thoracic radiation group had significantly higher rates of brain metastases ($P = 0.006$). Results indicated that the early administration of TRT with concurrent chemotherapy improved survival, possibly by reducing the last clonogens in the primary.

Selection of patients for combined modality trials of stage III NSCLC requires that the patient population be carefully staged and has favorable prognostic factors. Similarly in LSCLC, patients who benefit from early concurrent chemoradiation are those with good prognostic factors and a reasonable chance of being cured.

The Chemoradiation Package: Optimally Integrating Modalities

Peters and Withers addressed the concept of the "chemoradiation package" in discussion of the treatment of head and neck cancers (55). Most sequential combined modality protocols emerged as pragmatic grafting of chemotherapy onto a course of radiotherapy. The failure of induction chemotherapy to improve results in the combined modality treatment
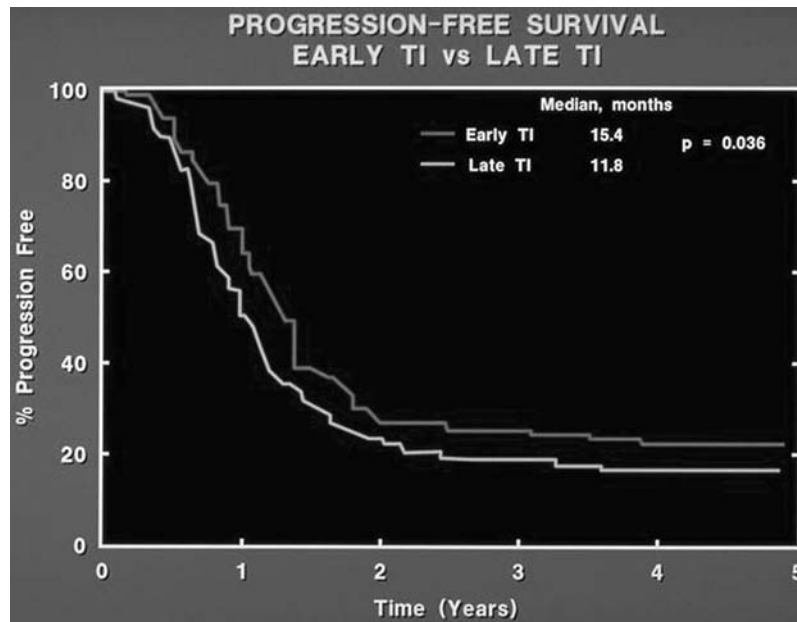
Figure 3 In their comparison of early and late TI with chemotherapy, Murray et al. found that complete response rates did not significantly differ between the groups, but progression-free survival ($P = 0.036$) and overall survival ($P = 0.008$) were significantly better in the group undergoing early TI. *Abbreviation*: TI, thoracic irradiation. *Source*: From Ref. 42.

of head and neck cancer can be explained by the hypothesis that the cell kill produced by induction chemotherapy is offset by tumor cell regeneration occurring during the prolonged overall course of treatment (56).

Duration of the Chemoradiotherapy

The duration of the chemoradiation package for LSCLC may be defined as the time elapsed from the first therapeutic intervention until the completion of the radiotherapy treatment. The use of this definition does not presume that additional chemotherapy cycles after completion of radiotherapy are unimportant, but that the rapid tumor destruction caused by combined modality therapy is crucial and markedly influences the probability that treatment will eventually eliminate the last tumor clonagen. That initial concurrent chemoradiation is the most efficient way to rapidly destroy cancer cells is self-evident. Based on data from in vitro assays of radiosensitivity of human SCLC lines (57), numerically, more cancer clonagens are eliminated locally by the first 2-Gy fraction (surviving fraction at 2 Gy, or SF2) than by the entire remainder of the radiotherapy course. When initial concurrent systemic chemotherapy is added to the radiotherapy effect, inhibition of tumor repopulation and metastatic events by rapid tumor destruction will be greater than when radiotherapy is delayed during protracted induction chemotherapy. The theoretical basis of the superiority of initial chemoradiation is discussed in detail elsewhere (58). This

concept has been recently been statistically evaluated by De Ruysscher et al.(59) from the Netherlands. The hypothesis was that the overall treatment time available for accelerated proliferation of tumor cells could be a major determinant of tumor outcome in LSCLC. They performed a systematic overview and identified six published phase III trials (40–42,48, 51,60) combining chest irradiation and platinum-based chemotherapy in the primary management of LSCLC and reporting 5-year survival. The following parameters and their influence on local tumor control, survival, esophagitis, and pneumonitis were analyzed: the total radiotherapy dose, the overall treatment time of chest radiotherapy, and the day of the start of radiotherapy as an indicator of early versus late radiation, the SER (start of any treatment till the end of radiotherapy), concurrent versus sequential radiotherapy and chemotherapy, the study period measured by the year the trial was initiated, and the equivalent radiation dose in 2-Gy fractions, corrected for the overall treatment time of chest radiotherapy (EQD_2,T). The definition of *SER* and the chemoradiation package are the same.

Using meta-analysis methodology, the SER was the most important predictor of outcome. There was a significantly higher 5-year survival rate in the shorter SER arms (OR, 0.60; 95%CI, 0.45–0.80; $P = 0.0006$), which was more than 20% when SER was less than 30 days. Although no significant relation between the SER and local tumor control was found (OR, 0.73; 95% CI, 0.46–1.14; $P = 0.16$), local tumor control was higher

with increasing EQD_2,T radiation doses ($P = 0.02$). This suggests that for local tumor control, both time and radiation dose are important factors. A lower SER was associated with a higher incidence of severe esophagitis (OR, 0.47; 95% CI, 0.33–0.66; $P < 0.001$). SER was not statistically associated with pneumonitis (too few events), severe leukopenia, or thrombocytopenia.

The authors concluded that a short SER (less than 30 days) results in improved survival for patients with LSCLC. This novel parameter, taking into account accelerated proliferation of tumor during both radiotherapy and chemotherapy, may facilitate a more rational design of combined modality treatment in rapidly proliferating tumors.

Thoracic Radiotherapy Target Volume

Selection of target to treat has evolved because of CT and treatment planning systems that allow more accurate definition of structures that warrant treatment and distinguish them from normal tissue. Global mediastinal and supraclavicular irradiation dominated thoracic radiotherapy ports through the trials of the 1980s, including the Intergroup trial (40), in which regional nodal irradiation encompassed the entire mediastinum. Relapse patterns rarely report regional nodal failure as first or ultimate site of relapse, and this is especially true of supraclavicular nodal regions. As with other occult positive disease, managing sites with systemic chemotherapy is feasible, treating uninvolved nodes with radiotherapy may not be necessary, and exposing radiographically normal nodal stations to radiation beams may add to toxicity. Diminishing mediastinal irradiation only to areas of bulky nodes reduces exposure to the esophagus, the lung, and other sensitive normal tissues and reduces esophagitis and pneumonitis.

Target size can be challenging with initial concurrent therapy if a tumor's initial bulk is too large for a reasonable radiotherapy port. This fact may influence sequence of therapy. A cycle or two of chemotherapy may reduce volume sufficiently to more facilely apply radiation without excessive irradiation to lungs. The target can then become the residual mass after reduction by chemotherapy. The volume of TRT to encompass prechemotherapy or postchemotherapy fields has been controversial. In the 1980s, there were significantly different survival rates if the prechemotherapy volumes had not been encompassed. More recently, however, studies by Arriagada et al. (61), Kies et al. (62) (Table 5), and the Mayo Clinic (63) have not shown any significant difference in survival when patients received postchemotherapy volume encompassed by TRT compared with prechemotherapy volume irradiated. However, prechemotherapy CT scan should be

Table 5 Volume of TRT

Reference	Patients (N)	Intrathoracic Recurrence (%)	P
Mantyla et al. (1985) (89)			
Original tumor volume	28	18	0.003
Reduced tumor volume	24	58	
Perez et al. (1981) (90)			
Adequate portals	40	33	0.02
Inadequate portals	13	69	
White et al. (1982) (91)			
Fully evaluable or minor variations	38	34	0.04
Major variations	16	69	
Kies et al. (1987)			
Wide volume radiotherapy	93	32	NS
Reduced volume Radiotherapy	98	28	
Image-guided radiotherapy			
Adequate coverage	12	33	0.86
Inadequate coverage	50	36	

Abbreviation: TRT, target radiotherapy.
Source: From Ref. 61.

reviewed to include the originally involved lymph node regions in the target volume. Three-dimensional conformal radiotherapy (3D-CRT) should be used to reduce normal tissue toxicity yet offer an adequate dose to the target volume.

Data supporting this approach are limited, but an analysis from the Mayo Clinic (63) shows support for the tactic of targeting postchemotherapy residual disease or at least indicates no clear hazard is posed by not encompassing the initial bulk. This issue has not drawn sufficient attention to prompt construction of a prospective clinical trial to test volume-related issues.

Nodal structures that measure 1 cm or larger on CT scan, clinically palpable nodes in the supraclavicular fossa, and disease found by bronchoscopy constitute an appropriate target. Elective treatment of uninvolved nodes does not have a good rationale, and the risk of normal tissue exposure with toxicity of esophagitis and reduction in lung function militates strongly against expansive volumes. Since SCLC is a chemoradiosensitive tumor, after a couple weeks of treatment, boost fields can be applied to avoid normal tissue toxicities. Such an approach produced a remarkable response to chemoradiotherapy after 14 1.8-Gy fractions: the gross target volume was reduced, which reduced the volume of V20 to the total lung from 24% to 18% and the maximum spinal cord dose from 46 to 42 Gy. V40 of the esophagus was reduced from 50% to 40% (Fig. 4).
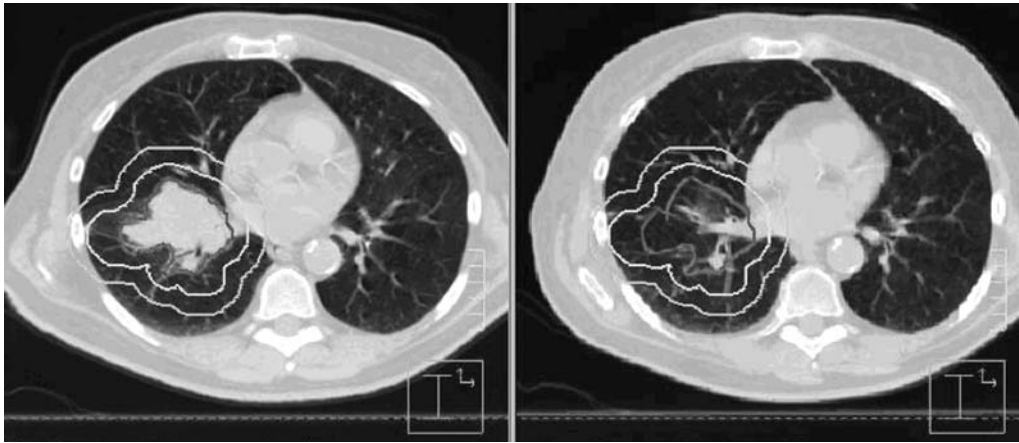
Figure 4 This pretreatment *(left)* and posttreatment *(right)* chest CR scan is that of a 56-year-old woman who was treated on RTOG 0239. Post-treatment view shows results after 2.5 weeks of radiotherapy, indicating almost complete resolution of the gross tumor. Patients underwent concurrent therapy, 61.2 Gy in 5 weeks and three courses of chemotherapy. Therefore, resimulation was performed to reduce radiotherapy fields. *Abbreviation*: RTOG, radiation therapy oncology group.

Concurrent Thoracic Radiotherapy and Chemotherapy

The potential advantages from concurrent chemotherapy and radiation therapy are early use of both modalities, patient expectation and acceptance of greater toxicity, ability to plan radiation therapy more accurately, short overall treatment time (high-dose intensity), and possible sensitization of the tumor. The disadvantages are enhanced normal tissue toxicity (potentially moderated by dose modification and/or treatment breaks) and an inability to assess response to either modality separately. In the 1970s, concurrent chemotherapy (CAV) and TRT was tried at the National Cancer Institute, which successfully treated patients with LSCLC, although the mortality rate from the treatment was 20% (64). Because of this high mortality, the use of concurrent TRT and doxorubicin was abandoned.

Other strategies of concurrent radiation therapy and chemotherapy have been tried. McCracken et al. (65) reported results from a Southwest Oncology Group phase II trial in which two courses of cisplatin, etoposide, and vincristine were given with concurrent radiation therapy using one fraction of 1.8 Gy per day, 5 days per week, to a total dose of 45 Gy. Additional chemotherapy with vincristine, methotrexate, and etoposide, alternating with doxorubicin and cyclophosphamide for 12 weeks, followed the concurrent therapy. They evaluated 154 patients, and with a minimum period of observation of 3 years, the 2-year survival rate was 42% and the 4-year rate was 30%. Updated, this study showed a 5-year survival of 26% (66). Johnson et al. (67,68) and Turrisi and associates (69) reported a small series of patients treated with concurrent cisplatin and etoposide with accelerated fractionation: a dose of 1.5 Gy twice daily, 5 days per week, was given for 3 weeks for a total dose

of 45 Gy. Two-year survival rates were 57% and 65% for the Turrisi (69) and Johnson (64,68) studies, respectively. Updated 4-year survival rates by Turrisi (40) were 36%.

The Japanese Clinical Oncology Group (70) reported a prospective randomized study for patients with LSCLC treated by sequential or concurrent chemotherapy. Two hundred thirty-one patients younger than 75 years of age with LSCLC and good performance status were enrolled. Chemotherapy consisted of paclitaxel (80 mg/m^2 on day 1) and etoposide (100 mg/m^2 on days 1–3) every 3 weeks. Radiation therapy consisted of 45 Gy given in 1.5-Gy fractions twice daily, 5 days per week. The concurrent arm started chemotherapy and TRT on day 1, and the sequential arm started TRT after two cycles of chemotherapy. Chemotherapy was given for a total of four cycles. The group's data showed significant improvement of survival with concurrent chemoradiotherapy compared with sequential chemotherapy and radiotherapy (Table 6).

Fractionation

According to several phase II trials that have used TI twice daily with concurrent chemotherapy, median survival ranged from 18 to 27 months and 2-year survival rates ranged from 19% to 60% with local control from 32% to 91% (68,69). Intergroup Trial 0096 was conducted through ECOG and RTOG to investigate whether accelerated hyperfractionated radiation therapy could outperform daily fractionation of radiation therapy with concurrent cisplatin and etoposide in LSCLC (Fig. 5) (40). The total dose for TRT was 45 Gy, with concurrent cisplatin and etoposide for four cycles. The cisplatin dose was 60 mg/m^2 on day 1, and etoposide was given intravenously at a dose of 120 mg/m^2 on days 1, 3, and 5. This course was

Table 6 Concurrent Radiotherapy Compared with Sequential Radiotherapy for LSCLC

Characteristic	Sequential radiotherapy	Concurrent radiotherapy
Patients	114	114
Complete response	33 (29%)	42 (37%)
Partial response	71 (62%)	70 (61%)
Median survival (months)	20.8	31.3

Note: Data were not available for all patients from all participating institutions for all characteristics.
Abbreviation: LSCLC, limited small cell lung cancer.
Source: From Ref. 70.

Table 7 End Point Intergroup Trial 0096: ECOG Trial 3588/RTOG Trial 88-15

Treatment, outcomes, and side effects	Arm 1	Arm 2	RTOG trial 0239 goals
Total radiotherapy	45 Gy	45 Gy	61.2 Gy
Duration (weeks)	5	3	5
Median survival (months)	19	23	30
Survival			
1 year	63%	67%	74%
2 years	44%	47%	60%
5 years	16%	26%[a]	36%
LF	53%	36%[b]	20%
Grade 3 esophagitis	11%	27%[c]	20%

Note: Data were not available for all patients from all participating institutions for all characteristics.
[a] $P = 0.04$.
[b] $P = 0.07$.
[c] $P = 0.01$.
Abbreviations: ECOG, RTOG, radiation therapy oncology group.
Source: From Ref. 40.

repeated every 21 days for four cycles. The daily fractionation group (arm 1) received a single 1.8-Gy fraction daily, with a total tumor dose of 45 Gy over 5 weeks compared with accelerated hyperfractionated radiation therapy (1.5-Gy fractions twice daily with a 4- to 6-hour interfractional interval (arm 2). Total tumor dose was 45 Gy in 30 fractions in 3 weeks. Those patients who achieved complete response were considered eligible to receive PCI (2.5 Gy in 10 fractions). Overall, median survival for the group receiving hyperfractionation was 23 months with a 2-year progression-free survival of 47% compared with the daily fractionation group showing 19 months and 44%, respectively, without a significant difference (Table 7). Overall, concurrent chemotherapy and radiotherapy can be tolerated and efficacious, according to this study, which shows a 2-year survival rate of 40% by a large

cooperative group, which is a rate twice as good as that of a decade ago. After 5 years, survival rates of the two groups were statistically significantly different (Fig. 6) (Table 7), with accelerated hyperfractionation (26%) outperforming daily fractionation (16%) by 10 percentage points ($P = 0.043$) (40) demonstrating remarkable improvement in 5-year survival rates in this nationwide randomized study.

Toxicities in the two arms were identical with the exception of acute grade 3 esophagitis, seen in 27% of the patients treated by accelerated treatment and in 11% of the daily fraction group (Table 7). There has not been a significant difference in late toxicity of the esophagus. The treatment-related death rate was 2%.
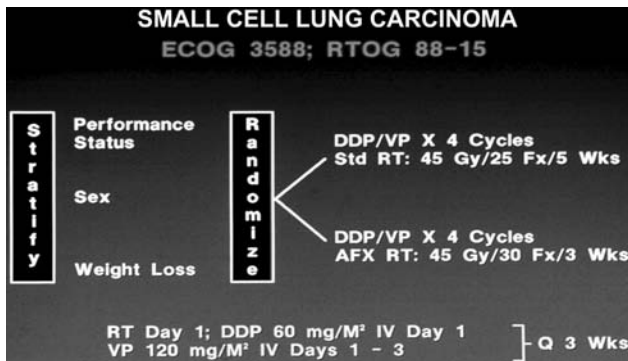
Figure 5 Selection of target to treat has evolved because of CT and treatment planning systems that allow more accurate definition of structures that warrant treatment, limiting the exposure of other anatomy to radiation. The EGOG and the RTOG conducted an Intergroup study comparing accelerated fractionation (Fx) of radiotherapy (AFX RT) over 3 weeks (Wks) with standard fractionation of radiotherapy (Std RT) over 5 weeks. Patients also received concurrent cisplatin (DDP) and etoposide (VP) every (Q) 3 weeks. *Abbreviations*: AFX-RT, accelerated fractionation of radiotherapy; EGOG, Eastern Cooperative Oncology Group; RTOG, Radiation Therapy Oncology Group. *Source*: From Ref. 40.
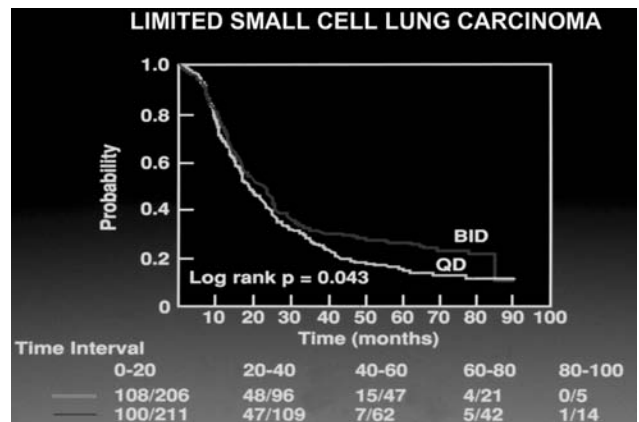
Figure 6 In Turisi et al.'s Intergroup study, 5-year survival was 26% in the group undergoing radiotherapy twice daily (BID) in a hyperfractionated schedule and 16% in the group undergoing daily (QD) standard fractionation, and the difference was statistically significant ($P = 0.043$).

Dose of Thoracic Radiation

The radiation dose to the thorax is another controversial area (71,72). The duration of overlapping chemotherapy and thoracic radiotherapy may influence tolerability and survival as well as toxicity. In the 1980s, the issue for thoracic radiotherapy was whether it was needed at all, and the responsiveness of SCLC to either radiotherapy or chemotherapy was so great that higher doses were not contemplated. Doses commonly recommended were in the range of 40–50 Gy. Because of concern for spinal cord tolerance, simple techniques, such as a posterior shield, were used to ensure spinal cord tolerance. The fact that the spinal cord shield also blocked tumor centrally was considered a necessary problem. Since that time treatment planning techniques allow delivery of dose to targets defined by radiation oncologists without concern for spinal cord tolerance. Toxicity to the lung and esophagus are more practical concerns. Modern planning allows delivery of doses higher than ever considered 25 years ago either by once- or twice-daily treatment.

The National Cancer Institute of Canada reported an important study to show a dose-response relationship in the thorax (73). These researchers found a clear dose–response relationship with increased thoracic progression-free survival by giving 37.5 Gy in 15 fractions in 3 weeks and comparing that schedule with 25 Gy in 10 fractions in 2 weeks, which was used as a consolidation therapy after completion of EP and CAV alternating or sequential chemotherapy. In Canada, 40 Gy in 3 weeks is still widely used (42). We really do not know that longer treatments or higher doses are better for local control or survival, but we are now able to deliver doses up to 70 Gy in 7 weeks (74) without a clear signal that higher doses are superior.

Arriagada and associates at the Institute of Gustave-Roussy published a report of 173 patients with LSCLC treated in three consecutive trials (61). The total dose of thoracic radiotherapy increased from 45 Gy (15-15-15) to 55 Gy (20-20-15) to 65 Gy (20-20-25), which was given by split courses interdigitating with chemotherapy. Their 3-year local control rates were 66%, 70%, and 70%, respectively, and 5-year survival rates were 16%, 16%, and 20%, respectively. There was a 10% rate of lethal toxicity without a significant difference, depending on the dose. The authors concluded that there was no significant difference in local tumor control or survival with treatment between 45 and 65 Gy when effective chemotherapy was given.

By evidence, the standard dose and treatment for LSCLC is 45 Gy delivered in 3 weeks in 30 fractions of 1.5 Gy, administered concurrently with cisplatin plus etoposide (40). The North Central Cancer Treatment Group Study (75), which also studied twice-daily treatment, failed to show differences between the twice-daily treatment and once-daily treatment. However, both arms had delayed initiation of chemoradiotherapy after induction chemotherapy, and the duration of radiotherapy was not different despite a twice-daily scheme. The trial intentionally interrupted treatment midcourse on the twice-daily arm, but that resulted in a reduction of toxicity. There was no significant difference in survival. The interruption muted any effect of twice daily treatment. While some cast doubt that twice-daily treatment is superior because of this trial, the interruption of and protraction of treatment diminished the intensity of the radiotherapy. Thus, the midcourse interruptions and course extension of the twice-daily schedule may blunt esophagitis, but they also blunt any effect on survival as well.

The Massachusetts General Hospital group (76) has consistently endorsed a policy of higher doses of once-daily treatment, and have slowly escalated the dose in successive cohorts of patients to 70 Gy. Survival plots of patients treated at higher doses show no inferiority and possibly a slight benefit for protracted, high-dose treatment. Both Cancer and Leukemia Group B and Massachusetts General Hospital data sets use induction chemotherapy and postchemotherapy target volumes. American cooperative groups have escalated LSCLC thoracic radiotherapy doses to doses of 61–63 Gy paralleling doses used for stage III NSCLC. However, none of these doses appears superior to 40–45 Gy in 3 weeks, and lengthy, high-dose treatments over 6–7 weeks are associated with a long SER. Additionally, protracted TI overlaps with more chemotherapy cycles, leading to more dose reductions and delays. There is no evidence from controlled trials that demonstrates benefit to higher dose TI, and no such study has been approved.

It is difficult to go to a higher dose by accelerated hyperfractionation without increasing acute esophagitis. Although local failure was almost 60% with 45 Gy in 5 weeks, it fell to 40% with the hyperfractionated and accelerated TRT from the Intergroup study, but a high esophagitis rate—27% of patients had severe grade 3 esophagitis—prevented attempting a higher dose of TRT with concurrent chemotherapy. Therefore, Komaki et al. developed a phase I study (RTOG 97-12) to increase TRT dose during boost treatment by reducing the treatment field for the second daily fraction (Fig. 7) (77). The dose was escalated from 50 to 64.8 Gy with concurrent oral etoposide and intravenous cisplatin. According to this study maximum tolerated dose (MTD) was 61.2 Gy in 5 weeks. Therefore, a phase II study (RTOG 0239) was opened in June 2003 and closed in May 2006, accruing
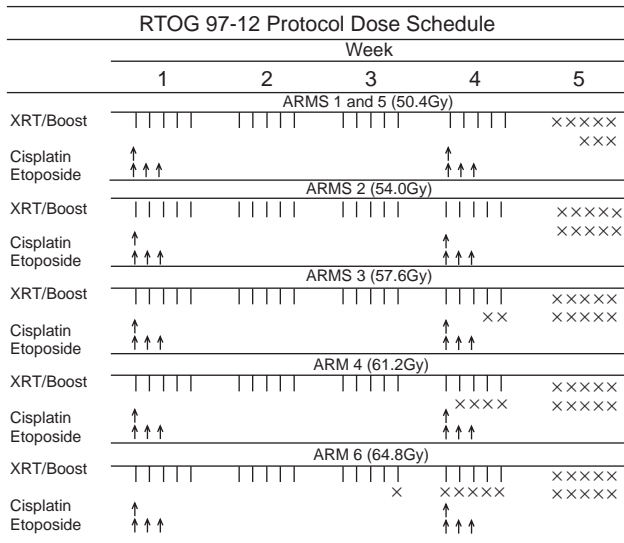
Figure 7 In order to increase dose without increasing toxicity, Komaki et al. (77) undertook a six-arm phase I study (RTOG study 97-12) in which the thoracic radiotherapy (XRT) dose (1.8 Gy) was hyperfractionated (*vertical bar*, large field; ×, boost), and the second daily fraction (1.8 Gy) was delivered to a reduced lung treatment field that did not include the spinal cord. Patients also received chemotherapy *(upright arrow)* of cisplatin and etoposide and PCI after completion of radiotherapy and chemotherapy (not shown). Cisplatin was administered at 60 mg/m2 on day 1, and etoposide was given intravenously at 120 mg/m2 on day 1 and by mouth at 240 mg/m2 on days 2 and 3. Chemotherapy was administered every 22 days for four cycles. Maximum tolerated dose was 61.2 Gy in 5 weeks. *Abbreviations*: PCI, Prophylactic cranial irradiation; RTOG, Radiation Therapy Oncology Group. *Source*: From Ref. 77.

a total of 72 patients (Fig. 8). Radiation was given once daily (1.8 Gy to large fields in 16 fractions followed by large fields in the morning and off-cord boost fields (1.8 Gy) in the afternoon with a 5- to 6-hour interval on days 17–20, and then off cords in twice a day 1.8 Gy for the last 5 days (Fig. 9). Figure 7 shows the chemotherapy (EP) dose starting on day 1, which was repeated every 3 weeks for 4 cycles. There were four grade 5 toxicities, including two cases of hematological complications (neutropenic fever and low platelet count), one case of pulmonary complications, and one case of dehydration), but response was noteworthy in its scope and rapidity (Fig. 4). We are still waiting for the analysis of efficacy.

A Cancer and Leukemia Group B study also showed promising results: 36% of patients had 3-year survival with 70 with 2 Gy per fraction of radiotherapy with concurrent chemotherapy. To this point, the optimal dose of radiotherapy in SCLC using modern 3DCRT with concurrent chemotherapy remains controversial. Off protocol, 45 Gy with 1.5 Gy per fraction given as a twice-a-day regimen is considered standard (78).

RADIATION THERAPY ONCOLOGY GROUP
0239 Phase II Schema

Radiation
- **Large field 28.8 Gy: 1.8 Gy/fx/5 days × 16 fx**
- **Boost with second treatment (bid) just in pm @ 1.8 Gy/fx on days 17–20 (use anterior-posterior/posterior-anterior fields in am @ 1.8 Gy/fax)**
  - **Then boost with 1.8 Gy bid × last 5 days**
  Total dose: 61.2 Gy in 5 weeks

Chemotherapy
Chemotherapy will be started on day 1 of thoracic radiotherapy (± 24 hr)
- **Cisplatin: 60 mg/m^2 intravenously day 1**
- **Etoposide: 120 mg/m^2 intravenously day 1**
- **Etoposide: 240 mg/m^2 by mouth/day on days 2 and 3**
  Repeat cycle every 3 weeks × 4 cycles

Figure 8 A phase II study, the RTOG 0239 trial evaluated the effectiveness of hyperfractionated radiotherapy in a total dose of 61.2 Gy paired with a concurrent 3-week chemotherapy course repeated for four cycles. *Abbreviation*: RTOG, radiation therapy oncology group.

In RTOG 0241, a phase I dose escalation study, Langer et al. tested 45 Gy in 30 fractions (twice daily) (arm A) against 70 Gy in daily fractions for 7 weeks (arm B) with dose escalation of irinotecan from 40 to 60 mg/m^2 (79). Dose of cisplatin was constant at 60 mg/m^2. The chemotherapy was initiated on day 1 and repeated every 3 weeks, and a total of four cycles were given (Fig. 10). Thirty-six patients were accrued to this study: 21 patients in arm A and 15 patients in arm B. Acute toxicities attributable to reaching MTD were not seen in arm A; however, MTD was reached at 50 mg/m^2 in arm B. Three out of the three developed grade 3 or higher nonhematologic acute toxicities.

Figure 9 The RTOG 0239 study, which enrolled 72 patients between June 2003 and May 2006, administered total doses of 61.2 Gy over 5 weeks. Standard large (L) field and boost (B) radiotherapy (XRT) fractions were 1.8 Gy each, and patients received cisplatin (C) and etoposide (E) as indicated. During boost phase, fractions were delivered twice daily (B, or BID), avoiding the spinal cord (off cord). *Abbreviation*: RTOG, radiation therapy oncology group.

RTOG 0241

SCHEMA (1/12/04)

This is a non-randomized dose escalation study in which patients are assigned in a sequential fashion, alternating between treatment sequences. Treatment assignment will begin with Sequence A, Level 1 and after enrollment of 6 patients, will progress to Sequence B, Level 1. Dose escalation will follow this pattern to the next level until the MTD in both treatment sequences is reached

*Sequence A (Arm 1)

Level	Irinotecan mg/m^2	Cis mg/m^2	# of Pts.
1	40	60	6
2	50	60	6
3	60	60	6

Irinotecan: day 1, day 8 for 1 cycle
Cis: 60 mg/m^2 day 1 for 1 cycle
**Concurrent RT: 1.5 Gy, BID, M-F, in 30 fractions for a total of 45 Gy

*Sequence B (Arm 2)

Level	Irinotecan mg/m^2	Cis mg/m^2	# of Pts.
1	40	60	6
2	50	60	6
3	60	60	6

Irinotecan: day 1, day 8 q3 wks for 2 cycles
Cis: 60mg/m^2 d1 q3 wks for 2 cycles
**Concurrent RT: 2.0 Gy, once daily, M-F, in 35 fractions for a total of 70 Gy

*Post-RT Chemotherapy: for 3 cycles
Irinotecan: 60 mg/m^2 d 1, 8 q3 wk
Cisplatin: 60 mg/m^2 d 1 q3 wk

*Post-RT Chemotherapy: for 2 cycles
Irinotecan: 60 mg/m^2 d 1, 8 q3 wk
Cisplatin: 60 mg/m^2 d 1 q3 wk

Restage → Prophylactic cranial XRT

Figure 10 The RTOG study 0241, a phase I, dose escalation study to determine MTD, was intended to enroll 18 patients (Pts) in each arm, but enrolled 21 in arm A and 12 patients in arm B. Therapy included cisplatin (Cis), irinotecan, and radiotherapy (RT) twice daily (BID) Monday through Friday (M–F). Chemotherapy was initiated on day 1 (d1), and in arm 2 patients were treated with drugs every 3 weeks (q3 wk) for two cycles. After restaging, patients underwent prophylactic cranial radiotherapy (XRT). *Abbreviations*: MTD, maximum tolerated dose; RTOG, radiation therapy oncology group.

When we consider altering dose fractionation and duration of the TRT, biological effective dose (BED) needs to be considered. The alpha–beta ratio for the esophagus or tumor response to radiation is 10. Potential tumor doubling time is 3 or 7 days for SCLC, since tumor cells are not homogeneous. Five-year survival based on BED assuming a 3-day tumor doubling time (Fig. 11) and 7-day doubling time (Fig. 12) is shown. Does the probability of the 5-year survival rate increase beyond 45 Gy at BED (3-day tumor doubling time) or beyond 60 Gy at BED (7-day tumor doubling time)? This is unknown because of concurrent chemotherapy, which might increase normal tissue toxicities, compromising 5-year curability.

PROPHYLACTIC CRANIAL IRRADIATION

The role of PCI has been controversial because of the lack of definitive input for improvement of overall survival and previously reported late neurotoxicities. However, the risk of brain metastasis from SCLC is correlated to the length of survival, and as more effective treatment extends life, a higher risk of brain

metastasis has been observed (80). An autopsy series by Nugent et al. found that 80% of patients who died 2 years after completion of treatment had metastases in the central nervous system (CNS), including the
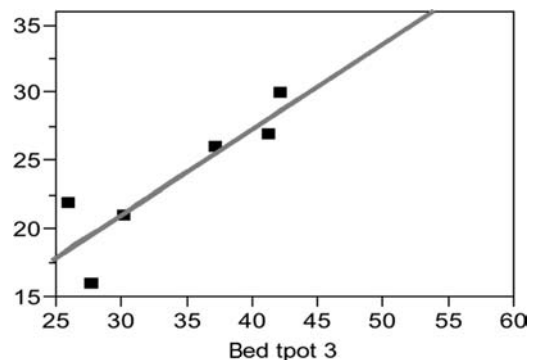
Figure 11 The 5-year survival rate is plotted against the corrected BED based on 12 fractionation schedules and a potential tumor doubling time of 3 days. Because of the possibility of concurrent chemotherapy increasing normal tissue toxicity, it is unknown whether the 5-year survival rate would increase with doses greater than 45 Gy. *Abbreviation*: BED, biological effective dose.
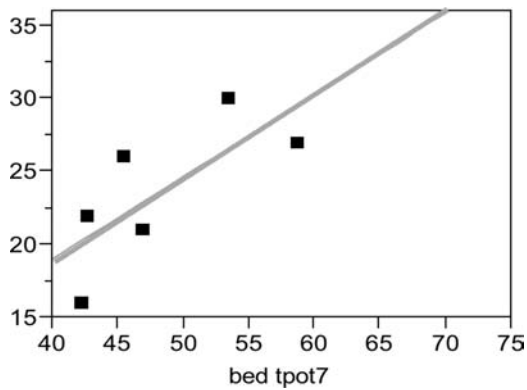
Figure 12 The 5-year survival rate is plotted against the corrected BED based on 12 fractionation schedules and a potential tumor doubling time of 7 days. Because of the possibility of concurrent chemotherapy increasing normal tissue toxicity, it is unknown whether the 5-year survival rate would increase with doses greater than 60 Gy. *Abbreviation*: BED, biological effective dose.

brain parenchyma, base of the skull, leptomeninges, or spinal cord (Fig. 13) (81). Better and less toxic treatment has been sought. Factors contributing to decreased late neurotoxicities include a lower total dose (24–30 Gy), smaller fraction size (2.0–2.5 Gy), timing of PCI, no concurrent chemotherapy, and less neurotoxic chemotherapy (82). Clinical brain metastasis occurs in up to 50% in 24 months after completion of treatment for LSCLC with the increment of 3% in every month after completion. PCI has reduced intracranial recurrence of SCLC down to 10%; however, extracranial central nerve system recurrence became more obvious (detected in up to 20% of patients) once intracranial metastasis had been

controlled (Fig. 14) (83). Baseline and follow-up neuropsychological tests showed that 83% (25/30) of patients with LSCLC had evidence of cognitive dysfunction before PCI, and no significant differences were found from pretreatment tests after PCI (84).

PCI has reduced brain tumor recurrence significantly among the long-term survivors without obvious neurotoxicities, although the majority of studies have been done retrospectively (85,86).

Recently, the NCI reported excellent results when 38 patients with LSCLC were treated with EP with concurrent hyperfractionated radiation therapy (1.5 Gy twice daily with a total dose of 45 Gy over 3 weeks) (67). The 1-year actuarial survival was 83%, and the 2-year survival was 43%. The 5-year survival rate and median survival were 19% and 21.3 months, respectively. However, the CNS was the only site of initial relapse in 34% (13/38) of the patients, and all of these patients died of CNS metastasis. This study concluded that combined chemotherapy and radiation therapy for LSCLC resulted in a 2-year survival of 43%. However, the main cause of death among the patients was relapse of the original cancer, and isolated CNS metastasis caused more than 30% of the cancer deaths.

A meta-analysis reported in 1999 of seven prospective, randomized clinical trials found a disease-free survival and overall survival advantage in those patients who underwent PCI compared with those not receiving PCI (Tables 8 and 9) (87). Several problems with that report include the fact that four of the seven trials analyzed had fewer than 100 total patients, which may undercut the validity of the statistical analyses. Also, approximately 14% of all 987
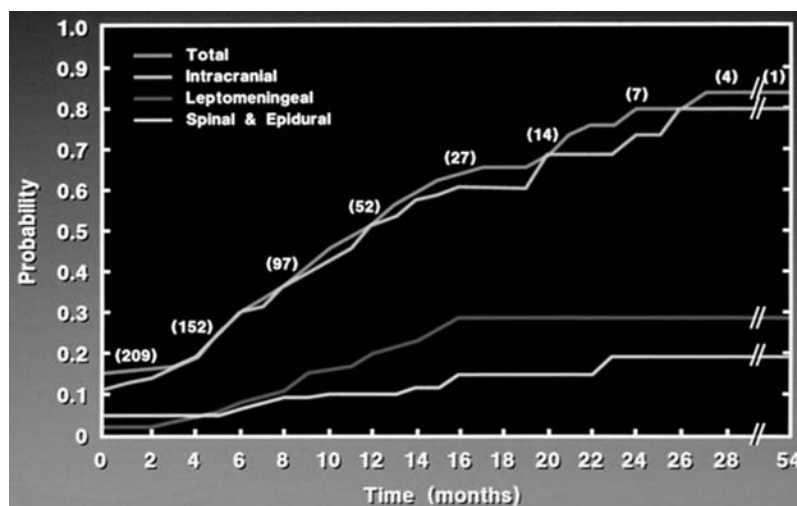
Figure 13   (*See color insert.*) Nugent et al. (81) analyzed an autopsy series and found that 80% of patients who died 2 years after completion of treatment for small cell carcinoma of the lung (SCCL) had metastasis in the CNS, including the brain parenchyma, base of the skull, leptomeninges, or spinal cord. *Abbreviations*: CNS, entral nervous system; SSLC, small cell lung cancer. *Source*: From Ref. 81.
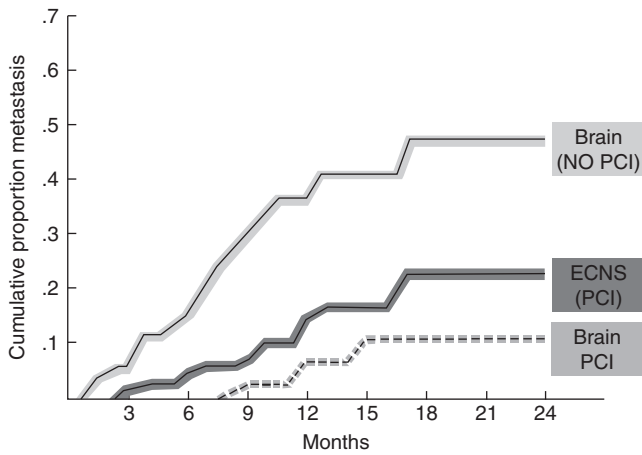
Figure 14 Once PCI helped control intracranial metastasis, extracranial nervous system metastasis was recognized as representing 20% of cases in metastatic SCLC. *Abbreviations*: PCI, prophylactic cranial irradiation; SCLC, small cell lung cancer. *Source*: From Ref. 80.

patients had extensive rather than limited disease. In addition, the dose fractionation of those patients who received PCI was not uniform. There was, however, a trend in the reduction of brain relapses in the subset of

Table 8 Characteristics of 987 Patients with Complete SCLC in Remission

Characteristic	Group treated with PCI (N = 526)	Control group (N = 461)
Male sex—no. (%)	403 (77)	352 (76)
Age		
Median—yr	59	59
Range—yr	26–80	21–79
<55 yr—no. (%)	147 (28)	158 (34)
55–64 yr—no. (%)	250 (48)	185 (40%)
≥65 yr—no. (%)	129 (25)	118 (26)
Performance status—no. (%)[a]		
0	212 (67)	215 (66)
1	96 (30)	105 (32)
2–3	7 (2)	6 (2)
Extensive initial disease—no. (%)	62 (12)	78 (17)
Induction treatment with chemotherapy plus thoracic radiotherapy—no. (%)	314 (77)	248 (74)

Note: Data were not available for all patients from all participating institutions for all characteristics.
[a] 0 denotes asymptomatic, 1, symptomatic and fully ambulatory, 2 symptomatic and in bed less than 50% of the day, and 3 symptomatic and in bed 50% or more of the day.
Abbreviation: PCI, prophylactic cranial irradiation.
Source: From Ref. 87.

PCI patients who were treated with at least 36 Gy of total radiation dose at the conventional 2-Gy fraction. The short-term neurotoxicities were not increased by PCI. Finally, this meta-analysis made no attempt to determine the risk of long-term neurotoxicity in those receiving and not receiving PCI. The optimal dose for PCI remains unclear. RTOG is conducting a phase II/III randomized study to compare different regimens of PCI—25 Gy in 10 fractions, 36 Gy in 18 fractions, and 36 Gy in 24 fractions given as twice a day (1.5 Gy twice daily) for patients with LSCLC who have achieved complete clinical response.

To investigate which patients receive more benefit from PCI without high risk of neurotoxicity, we developed a decision-analytic model to compare quality-adjusted life expectancy (QALE) in a cohort of SCLC patients who did or did not receive PCI by varying survival rates and the frequency and severity of PCI-related neurotoxicity (88). Sensitivity analyses were applied to examine the robustness of the optimal decision. At current published survival rates (26% 5-year survival rate with PCI and 22% without PCI) and a low neurotoxicity rate, undergoing PCI offered a benefit over not undergoing PCI (QALE = 4.31 and 3.70 for mild neurotoxicity severity; QALE = 4.09 and 3.70 for substantial neurotoxicity severity, respectively).

With a moderate neurotoxicity rate, undergoing PCI was still preferred. If the PCI survival rate increased to 40%, PCI outperformed not undergoing PCI with a mildly severe neurotoxicity. However, not undergoing PCI was preferred over undergoing PCI (QALE = 5.72 vs. 5.47) when the severity of the neurotoxicity was substantial. Two-way sensitivity analyses showed that having PCI was preferred for low neurotoxicity rates, mild neurotoxicity severity, and low long-term survival rates. No PCI was preferred otherwise (Fig. 14).

We concluded that the current data suggest undergoing PCI offers better QALE than not undergoing PCI in patients with LSCLC who have achieved complete response. As the survival rate for SCLC patients continues to improve, the neurotoxicity rate and neurotoxicity severity must be controlled to maintain a favorable benefit-risk ratio for recommending PCI.

SUMMARY

For LSCLC, concurrent chemoradiotherapy should be considered. Radiotherapy should be delivered to 45 Gy, (given in 1.5-Gy fractions twice a day) with concurrent cisplatin and etoposide chemotherapy. Patients should be encouraged to participate in research protocols using newer chemotherapy and/or dose escalation/escalation radiotherapy. PCI should be considered for complete clinical responders with a dose of 25–36 Gy.

Table 9 Results of PCI in Patients with SCLC in Complete Remission

	Patients			Rate in the control group over a 3-year period	Absolute benefit at 3 years
End point	Treatment group	Control group	p		
Overall survival	526	461	0.01	15.3	+5.4
Disease-free survival	526	461	<0.001	13.5	+8.8
Cumulative incidence of brain metastasis	524	457	<0.001	58.6	−25.3
Cumulative incidence of other metastases	325	332	0.37	45.6	−3.8
Cumulative incidence of local or regional recurrence	323	334	0.84	45.1	−1.0

Note: Data were not available for all patients from all participating institutions for all characteristics.
Abbreviations: PCI, prophylactic cranial irradiation.
Source: From Ref. 87.

Some evidence exists that incremental survival gains may be seen when dose-intensive or more complex regimens are administered before delayed TI. However, the best reported results for LSCLC are achieved with initial concurrent EP chemotherapy and TI. More intensive protocols or regimens that add another chemotherapeutic agent to the EP motif have not prospered in investigations of LSCLC because of safety concerns and fidelity of chemotherapy and radiotherapy delivery.

REFERENCES

1. American Cancer Society. Cranial irradiation and small cell lung cancer: Radiation improves survival for some lung cancer patients. Available on the World Wide Web: http://www.cancer.org/docroot/NWS/content/NWS_1_1x_ Cranial_Irradiation_and_Small_Cell_Lung_Cancer.asp (accessed January 2007).

2. American Lung Association. Facts about lung cancer. Available on the World Wide Web: http://www.lungusa.org/site/pp.asp?c=dvLUK9O0E&b=35427 (accessed January 2007).

3. Aisner S, Finkelstein D, Ettinger D, Abeloff M, Ruckdeschel J, Eggleston J. The clinical significance of variant-morphology small-cell carcinoma of the lung. J Clin Oncol 1990; 8(3): 402–8.

4. Siu LL, Shepherd FA, Murray N, Feld R, Pater J, Zee B. Influence of age on the treatment of limited-stage small-cell lung cancer. J Clin Oncol 1996; 14(3): 821–8.

5. National Comprehensive Cancer Network. Oncology practice guideline. Small cell lung cancer. Oncology 1996; 10:179–94.

6. Pieterman R, van Putten J, Meuzelaar J, et al. Preoperative staging of non-small-cell lung cancer with positron-emission tomography. N Engl J Med 2000; 343(4): 254–61.

7. Bunn P, Ihde D. Small cell bronchogenic carcinoma: A review of therapeutic results. In: Livingston R, ed., Lung Cancer, Vol. 1. The Hague: Marinus Nijhoff, 1981; 169–208.

8. Feld R, Ginsberg R, Payne D. Treatment of a small cell lung cancer. In: Roth J, Ruckdeschel J, Weisenburger T, eds., Thoracic Oncology. Philadelphia: W. B. Saunders, 1993; 229–262.

9. Fox W, Scadding J. Treatment of oat-celled carcinoma of the bronchus. Lancet 1973; 2:63–5.

10. Higgins G, Shields T, Keehn R. The solitary pulmonary nodule. Ten-year follow-up of veterans administration-armed forces cooperative study. Arch Surg 1975; 110:570–7.

11. Green R, Humphrey E, Close H, Patno M. Alkylating agents in bronchogenic carcinoma. Am J Med 1969; 46(4):516–25.

12. Einhorn L, Fee W, Farber M, Livingston R, Gottlieb J. Improved chemotherapy for small-cell undifferentiated lung cancer. JAMA 1976; 253:1225–9.

13. Sierocki J, Hilaris B, Hopfan S, et al. Cis-dichlorodiammineplatinum(ii) and VP-16-213: An active induction regimen for small cell carcinoma of the lung. Cancer Treat Rep 1979; 63:1593–7.

14. Evans W, Shepherd F, Feld R, Osoba D, Dang P, Deboer G. VP-16 and cisplatin as first-line therapy for small-cell lung cancer. J Clin Oncol 1985; 3(11):1471–7.

15. Spira A, Ettinger D. Multidisciplinary management of lung cancer. N Engl J Med 2004; 350:379–92.

16. Souhami R, Spiro S, Rudd R, et al. Five-day oral etoposide treatment for advanced small-cell lung cancer: Randomized comparison with intravenous chemotherapy. J Natl Cancer Inst 1997; 89:577–80.

17. Girling D. Comparison of oral etoposide and standard intravenous multidrug chemotherapy for small-cell lung cancer: A stopped multicentre randomised trial. Lancet 1996; 348:563–6.

18. DeVita V, Young R, Canellos G. Combination versus single agent chemotherapy: A review of the basis for selection of drug treatment of cancer. Cancer 1975; 35: 98–110.

19. Roth B, Johnson D, Einhorn L, et al. Randomized study of cyclophosphamide, doxorubicin, and vincristine versus etoposide and cisplatin versus alternation of these two regimens in extensive small-cell lung cancer: A phase iii trial of the southeastern cancer study group. J Clin Oncol 1992; 10:282–91.

20. Loehrer P, Ansari R, Gonin R, et al. Cisplatin plus etoposide with and without ifosfamide in extensive small- cell lung cancer: A hoosier oncology group study. J Clin Oncol 1995; 13:2594–9.

21. Niell H, Herndon J, Miller A, et al. Randomized phase iii intergroup trial of etoposide and cisplatin with or without paclitaxel and granulocyte colony-stimulating factor in patients with extensive-stage small-cell lung cancer: Cancer and Leukemia Group B trial 9732. J Clin Oncol 2005; 23:3752–9.

22. Mavroudis D, Papadakis E, Veslemes M, et al. A multicenter randomized clinical trial comparing paclitaxel-cisplatin-etoposide versus cisplatin-etoposide as first-line treatment in patients with small-cell lung cancer. Ann Oncol 2001; 12:463–70.

23. Schiller J, Adak S, Cella D, DeVore R, Johnson D. Topotecan versus observation after cisplatin plus etoposide in extensive-stage small-cell lung cancer: E7593–A phase III trial of the Eastern Cooperative Oncology Group. J Clin Oncol 2001; 19: 2114–22.

24. Sculier J, Paesmans M, Lecomte J, et al. A three-arm phase III randomised trial assessing, in patients with extensive-disease small-cell lung cancer, accelerated chemotherapy with support of haematological growth factor or oral antibiotics. Br J Cancer 2001; 85:1444–51.

25. Schild S, McGinnis W, Graham D, et al. Results of a phase i trial of concurrent chemotherapy and escalating doses of radiation for unresectable non-small-cell lung cancer. Int J Radiat Oncol Biol Phys 2006; 65(4):1106–11.

26. Johnson D, Einhorn L, Birch R, et al. A randomized comparison of high-dose versus conventional-dose cyclophosphamide, doxorubicin, and vincristine for extensive-stage small-cell lung cancer: A phase III trial of the Southeastern Cancer Study Group. J Clin Oncol 1987; 5:1731–8.

27. Ihde D, Mulshine J, Kramer B, et al. Prospective randomized comparison of high-dose and standard-dose etoposide and cisplatin chemotherapy in patients with extensive-stage small-cell lung cancer. J Clin Oncol 1994; 12:2022–34.

28. Ardizzoni A, Hansen H, Dombernowsky P, et al. Topotecan, a new active drug in the second-line treatment of small-cell lung cancer: A phase II study in patients with refractory and sensitive disease. The European Organization for Research and Treatment of Cancer Early Clinical Studies Group and New Drug Development Office, and the Lung Cancer Cooperative Group. J Clin Oncol 1997; 15:2090–6.

29. Klasa R, Murray N, Coldman A. Dose-intensity meta-analysis of chemotherapy regimens in small-cell carcinoma of the lung. J Clin Oncol 1991; 9:499–508.

30. Noda K, Nishiwaki Y, Kawahara M, et al. Irinotecan plus cisplatin compared with etoposide plus cisplatin for extensive small-cell lung cancer. N Engl J Med 2002; 346:85–91.

31. Hanna N, Einhorn L, Sandler A, et al. Randomized, phase III trial comparing irinotecan/cisplatin (IP) with etoposide/cisplatin (EP) in patients (pts) with previously untreated, extensive-stage (ES) small cell lung cancer (SCLC). J Clin Oncol 2005; 23:7004.

32. Eckardt J, von Pawel J, Manikhas G, et al. Comparable activity with oral topotecan/cisplatin (TC) and iv etoposide/cisplatin (PE) as treatment for chemotherapy-naive patients (pts) with extensive disease small cell lung cancer (ED-SCLC): Final results of a randomized phase III trial (389). J Clin Oncol 2005; 23:7003.

33. Socinski M, Weissman C, Hart L, et al. A randomized phase II trial of pemetrexed (P) plus cisplatin (Cis) or carboplatin (Carbo) in extensive stage small cell lung cancer (ES-SCLC). J Clin Oncol 2005; 23:7165.

34. Ohe Y, Negoro S, Matsui K, et al. Phase I-II study of amrubicin and cisplatin in previously untreated patients with extensive-stage small-cell lung cancer. Ann Oncol 2005; 16:430–6.

35. Pignon J, Arriagada R, Ihde D, et al. A meta-analysis of thoracic radiotherapy for small-cell lung cancer. N Engl J Med 1992; 327:1618–1624.

36. Sundstrom S, Bremnes R, Kaasa S, et al. Cisplatin and etoposide regimen is superior to cyclophosphamide, epirubicin, and vincristine regimen in small-cell lung cancer: Results from a randomized phase iii trial with 5 years' follow-up. J Clin Oncol 2002; 20:4665–72.

37. Reck M, von Pawel J, Macha H, et al. Randomized phase iii trial of paclitaxel, etoposide, and carboplatin versus carboplatin, etoposide, and vincristine in patients with small-cell lung cancer. J Natl Cancer Inst 2003; 95:1118–27.

38. Thatcher N, Girling D, Hopwood P, Sambrook R, Qian W, Stephens R. Improving survival without reducing quality of life in small-cell lung cancer patients by increasing the dose-intensity of chemotherapy with granulocyte colony-stimulating factor support: Results of a British Medical Research Council multicenter randomized trial. J Clin Oncol 2000; 18:395–404.

39. Thatcher N, Qian W, Clark P, et al. Ifosfamide, carboplatin, and etoposide with midcycle vincristine versus standard chemotherapy in patients with small-cell lung cancer and good performance status: Clinical and quality-of-life results of the British Medical Research Council multicenter randomized LU21 trial. J Clin Oncol 2005; 23:8371–9.

40. Turrisi AT, Kim K, Blum R, et al. Twice-daily compared with once-daily thoracic radiotherapy in limited small-cell lung cancer treated concurrently with cisplatin and etoposide. N Engl J Med 1999; 340(4):265–71.

41. Takada M, Fukuoka M, Kawahara M, et al. Phase III study of concurrent versus sequential thoracic radiotherapy in combination with cisplatin and etoposide for limited-stage small-cell lung cancer: Results of the Japan Clinical Oncology Group study 9104. J Clin Oncol 2002; 20:3054–60.

42. Murray N, Coy P, Pater JL, et al. Importance of timing for thoracic irradiation in the combined modality treatment of limited-stage small-cell lung cancer. J Clin Oncol 1993; 11(2):336–44.

43. Ettinger D, Berkey B, Abrams R, et al. Study of paclitaxel, etoposide, and cisplatin chemotherapy combined with twice-daily thoracic radiotherapy for patients with limited-stage small-cell lung cancer: A radiation therapy oncology group 9609 phase II study. J Clin Oncol 2005; 23:4991–8.

44. Gaspar L, Greer G, Crawford J, Putnam J, Herbst R, Bonner J. Limited-stage small-cell lung cancer (stages i–iii): Observations from the national cancer data base. Clin Lung Cancer 2005; 6:355–60.

45. Warde P, Payne D. Does thoracic irradiation improve survival and local control in limited- stage small-cell carcinoma of the lung? A meta-analysis. J Clin Oncol 1992; 10(6):890–5.

46. Yuen A, Zou G, Turrisi A, et al. Similar outcome of elderly patients in Intergroup trial 0096. Cancer 2000; 89:1953–60.

47. James L, Spiro S, O'Donnell K, et al. A randomized study of timing of thoracic irradiation in small cell lung cancer (SCLC)–study 8. Lung Cancer 2003; 41:S23.

48. Jeremic B, Shibamoto Y, Acimovic L, Milisavljevic S. Initial versus delayed accelerated hyperfractionated radiation therapy and concurrent chemotherapy in limited small-cell lung cancer: A randomized study. J Clin Oncol 1997; 15:893–900.

49. Perry M, Eaton W, Propert K, et al. Chemotherapy with or without radiation therapy in limited small-cell carcinoma of the lung. N Engl J Med 1987; 316: 912–18.

50. Skarlos D, Samantas E, Briassoulis E, et al. Randomized comparison of early versus late hyperfractionated thoracic irradiation concurrently with chemotherapy in limited disease small-cell lung cancer: A randomized phase II study of the Hellenic Cooperative Oncology Group (HECOG). Ann Oncol 2001; 12:1231–8.

51. Work E, Nielsen O, Bentzen S, Fode K, Palshof T. Randomized study of initial versus late chest irradiation combined with chemotherapy in limited-stage small-cell lung cancer. Aarhus Lung Cancer Group. J Clin Oncol 1997; 15:3030–7.

52. Pijls M, De Ruysscher D, Rutten I, Lambin P, Vansteenkiste J. Pd-116 early versus late chest radiotherapy for limited stage small cell lung cancer: A systematic review and meta-analysis. Lung Cancer 2005; 49:S101.

53. Pujol J, Carestia L, Daurès J. Is there a case for cisplatin in the treatment of small-cell lung cancer? A meta-analysis of randomized trials of a cisplatin-containing regimen versus a regimen without this alkylating agent. Br J Cancer 2000; 83:8–15.

54. Percy RF, Perryman RA, Amornmarn R, et al. Prolonged survival in a patient with primary angiosarcoma of the heart. Am Heart J 1987, 113 (5), 1228–1230.

55. Peters L, Withers H. Applying radiobiological principles to combined modality treatment of head and neck cancer–the time factor. Int J Radiat Oncol Biol Phys 1997; 39:831–6.

56. Pignon JP, Bourhis J, Domenge C, Designe L, MACH-NC Collaborative Group. Chemotherapy added to locoregional treatment for head and neck squamous-cell carcinoma: Three meta-analyses of updated individual data. Lancet 2000; 355: 949–55.

57. Carmichael J, Degraff W, Gamson J, et al. Radiation sensitivity of human lung cancer cell lines. Eur J Cancer Clin Oncol 1989; 25:527–34.

58. Erridge S, Murray N. Thoracic radiotherapy for limited-stage small cell lung cancer: Issues of timing, volumes, dose, and fractionation. Semin Oncol 2003; 30:26–37.

59. De Ruysscher D, Pijls M, Bentzen S, et al. P-758 ser, a novel time factor predictive for long-term survival in patients with limited disease small cell lung cancer after combined chest radiotherapy and chemotherapy. Lung Cancer 2005; 49:S318.

60. Gregor A, Drings P, Burghouts J, et al. Randomized trial of alternating versus sequential radiotherapy/chemotherapy in limited-disease patients with small-cell lung cancer: A European Organization for Research and Treatment of Cancer Lung Cancer Cooperative Group study. J Clin Oncol 1997; 15:2840–9.

61. Arriagada R, Pellae-Cosset B, Ladron de Guevara J, et al. Alternating radiotherapy and chemotherapy schedules in limited small cell lung cancer: Analysis of local chest recurrences. Radiother Oncol 1991; 20(2):91–8.

62. Kies M, Mira J, Crowley J, et al. Multimodal therapy for limited small-cell lung cancer: A randomized study of induction combination chemotherapy with or without thoracic radiation in complete responders; and with wide-field versus reduced- field radiation in partial responders: A southwest oncology group study. J Clin Oncol 1987; 5(4):592–600.

63. Liengswangwong V, Bonner JA, Shaw EG, et al. Limited-stage small-cell lung cancer: Patterns of intrathoracic recurrence and the implications for thoracic radiotherapy. J Clin Oncol 1994; 12(3):496–502.

64. Johnson R, Brereton H, Kent C. Small-cell carcinoma of the lung: Attempt to remedy causes of past therapeutic failure. Lancet 1976; 2:289–91.

65. McCracken JD, Janaki LM, Crowley JJ, et al. Concurrent chemotherapy/ radiotherapy for limited small-cell lung carcinoma: A Southwest Oncology Group study. J Clin Oncol 1990; 8 (5):892–8.

66. Ishida T, Yano T, Maeda K, Kaneko S, Tateishi M, Sugimachi K. Strategy for lymphadenectomy in lung cancer three centimeters or less in diameter. Ann Thoracic Surg 1990; 50:708–13.

67. Johnson B, Bridges J, Sobczeck M, et al. Patients with limited-stage small-cell lung cancer treated with concurrent twice-daily chest radiotherapy and etoposide/cisplatin followed by cyclophosphamide, doxorubicin, and vincristine. J Clin Oncol 1996; 14(3): 806–13.

68. Johnson B, Salem C, Nesbitt J. Limited stage small cell lung cancer treated with concurrent hyperfractionated chest radiotherapy and etoside/cisplatin. Lung Cancer 1993; 3:21–26.

69. Turrisi A, Glover D, Mason B. Long-term results of platinum, etoposide and twice daily thoracic radiotherapy for limited small cell lung cancer: Results on 32 patients with 48 month minimum follow-up. Proc Am Soc Clin Oncol 1992; 11:292a.

70. Goto K, Nishiwaki Y, Takasa M. Final results of a phase III study of concurrent versus sequential thoracic radiotherapy (TRT) in combination with cisplatin (P) and etopside (E) for limited-stage small-cell lung cancer (LD-SCLC): The Japan Clincial Oncology Group (JCOG) study. Proc Am Soc Clin Oncol 1999; 18:468a.

71. Ariyoshi Y, Fukuoka M, Furuse K, et al. Concurrent cisplatin-etoposide chemotherapy plus thoracic radiotherapy for limited-stage small cell lung cancer. Japanese Lung Cancer Chemotherapy Group in Japanese Clinical Oncology Group. Japanese J Clin Oncol 1994; 24:275–81.

72. Cox J. Dose-response in small cell carcinoma. Int J Radiat Oncol Biol Phys 1988; 14(2): 393–4.

73. Coy P, Hodson I, Payne D, et al. The effect of dose of thoracic irradiation on recurrence in patients with limited stage small cell lung cancer: Initial results of a Canadian multicenter randomized trial. Int J Radiat Oncol Biol Phys 1988; 14: 219–26.

74. Bogart J, Herndon J, Lyss A, et al. 70 Gy thoracic radiotherapy is feasible concurrent with chemotherapy for limited-stage small-cell lung cancer: Analysis of Cancer and Leukemia Group B study 39808. Int J Radiat Oncol Biol Phys 2004; 59:460–8.

75. Schild S, Bonner J, Shanahan T, et al. Long-term results of a phase iii trial comparing once-daily radiotherapy with twice-daily radiotherapy in limited-stage small-cell lung cancer. Int J Radiat Oncol Biol Phys 2004; 59:943–51.

76. Roof K, Fidias P, Lynch T, Choi N. Radiation dose intensification in limited-stage small-cell lung cancer. Clin Lung Cancer 2003; 4:339–46.

77. Komaki R, Swann R, Ettinger D, et al. Phase I study of thoracic radiation dose escalation with concurrent chemotherapy for patients with limited small-cell lung cancer: Report of radiation therapy oncology group (RTOG) protocol 97–12. Int J Radiat Oncol Biol Phys 2005; 62:342–50.

78. Choi N, Herndon J, Rosenman J, et al. Long-term survival data from CALGB 8837: Radiation dose escalation and concurrent chemotherapy (ct) in limited stage small cell lung cancer (LD-SCLC). Possible radiation dose-survival relationship. Proc Am Soc Clin Oncol 2002; 21:298a (abstract 1190).

79. Langer C, Swann S, Werner-Wasik M, et al. Phase I study of irinotecan (IR) and cisplatin (DDP) in combination with thoracic radiotherapy (RT), either twice daily (45 Gy) or once daily (70 Gy), in patients with limited (ltd) small cell lung carcinoma (SCLC): Early analysis of RTOG 0241. Proc Am Soc Clin Oncol 2006; 24 (18S):7058.

80. Komaki R, Cox J, Whitson W. Risk of brain metastasis from small cell carcinoma of the lung related to length of survival and prophylactic irradiation. Cancer Treat Rep 1981; 65:811.

81. Nugent J, Bunn PJ, Matthews M, et al. CNS metastases in small cell bronchogenic carcinoma: Increasing frequency and changing pattern with lengthening survival. Cancer 1979; 44:1885–93.

82. Komaki R, Byhardt R, Anderson T, et al. What is the lowest effective biologic dose for prophylactic cranial irradiation. Am J Clin Oncol 1985; 8:523.

83. Komaki R, Roh J, Cox J, Lopes da Conceicao A. Superior sulcus tumors: Results of irradiation of 36 patients. Cancer 1981; 48:1563–8.

84. Komaki R, Meyers C, Shin D, et al. Evaluation of cognitive function in patients with limited small cell lung cancer prior to and shortly following prophylactic cranial irradiation. Int J Radiat Oncol Biol Phys 1995; 33(1):179–82.

85. Cull A, Gregor A, Hopwood P, et al. Neurological and cognitive impairment in long-term survivors of small cell lung cancer. Eur J Cancer 1994; 30A:1067–74.

86. Shaw E, Su J, Eagan R. Analysis of long-term survival and impact of prophylactic cranial irradiation in complete responsders with small cell lung cancer: Analysis of the Mayo Clinic and North Central Cancer Treatment Group databases. Proc Am Soc Clin Oncol, 1993; 12:328a.

87. Auperin A, Arriagada R, Pignon J, et al. Prophylactic cranial irradiation for patients with small-cell lung cancer in complete remission. N Engl J Med 1999; 341(7):476–84.

88. Lee JJ, Bekele BN, Zhou X, Cantor SB, Komaki R, Lee JS. Decision analysis for prophylactic cranial irradiation for patients with small-cell lung cancer. J Clin Oncol 2006; 24(22):3597–603.

89. Mantyla M, Nurranen A. The treatment volume in radiation therapy of small cell lung cancer (abstract 473). IV world conference of lung cancer, Toronto, 1985:34.

90. Perez CA, Krauss S, Bartolucci AA, et al., and the Southeastern Cancer Study Group. Thoracic and elective brain irradiation with concomitant or delayed multiagent chemotherapy in the treatment of localized small cell carcinoma of the lung: A randomized prospective study by the Southeastern cancer Study Group. Cancer 1981; 47:2407–13.

91. White JE, Chen T, McCracken J, et al. The influence of radiation therapy quality control on survival, response and sites of relapse in oat cell carcinoma of the lung. Preliminary report of a Southwest Oncology Group Study Cancer 1982; 50: 1084–1090.

Image Guidance to Account for Interfractional and Intrafractional Variations: From a Clinical and Physics Perspective

Keith R. Britton, Lei Dong, and Radhe Mohan
Department of Radiation Physics, University of Texas M.D. Anderson Cancer Center, Houston, Texas, U.S.A.

INTRODUCTION

It is increasingly being recognized that treatment targets and the intervening and surrounding normal tissues are subject to substantial inter- and intrafractional variations in shape, volume, and position. The causes of such variations include respiratory motion, non-rigidity of the body, weight loss, and radiation-induced changes such as tumor shrinkage. These variations can significantly affect the outcome of treatment.

It is assumed implicitly that the treatment targets and anatomy identified by initial imaging remain static during a radiotherapy (RT) treatment fraction and throughout the course of RT. State-of-the-art planning and delivery of RT are based on the use of computed tomography (CT) images (often supplemented with information derived from positron emission tomography and magnetic resonance images) acquired before the course of treatment. In the current practice, treatment fields with large margins, derived from population-based studies, are used to ensure coverage of the disease, exposing excessive volumes of normal tissues to unwanted radiation. The use of large margins also limits the opportunity for RT dose escalation, particularly when concurrent chemotherapy is given. This limitation is important because the current standard dose of 60–66 Gy is not considered to be adequate. Furthermore, even with such large margins, marginal misses of moving and shifting target volumes is likely. These factors may, in part, be responsible for the poor outcome of RT for lung cancers. Thus, techniques to accurately target lung cancer, to reduce margins, and to allow radiation dose escalation to higher levels may be vital to achieve optimal outcomes.

The goal of image-guided radiotherapy (IGRT) for lung cancer is to mitigate the detrimental effects of inter- and intrafractional variations in anatomy. Generally, image-guided interventions (IGIs) in RT are based on types of images. (1) Four-dimensional CT (4D-CT) images may be used to choose the appropriate IGI strategy, to design the initial treatment plan, and to establish treatment parameters. A 4D-CT image is a sequence of 3D-CT images spanning the phases of the breathing cycle. Repeat 4D-CT images, acquired on different days, may then be used to adapt treatment plans to interfractional anatomic changes occurring during the course of RT. (2) Gated static X-ray images may be used for accurate daily setup of the patient's anatomy. A gated image is obtained by triggering the image acquisition at a certain point in the breathing cycle, for example, at the end of exhalation. (3) Fluoroscopic images (or appropriately correlated_surrogates) may be used for real-time tracking and targeting of moving tumors.

Numerous preclinical imaging and treatment simulation (treatment planning) studies are being conducted to evaluate the current practices and potential of IGRT, and limited implementation of essential IGRT is now taking place. Eventually, IGRT strategies based on the patient's specific anatomy and tumor characteristics will be used. For a typical lung cancer IGRT process, a 4D-CT image and a breath-hold CT image will be acquired for each patient, and then an appropriate IGI strategy and treatment plan will be designed to match/account for the characteristics of the patient and the tumor. For example, if the tumor motion assessed by 4D-CT is significant, then during each RT fraction, the data from 4D and/or breath-hold images would be correlated with the 2D fluoroscopic or gated static X-rays to set up the patient. The fluoroscopic images (or those from an appropriately correlated surrogate) may be used to automatically track and target the tumor in real time. The irradiation may be gated as appropriate. To account for interfractional changes in anatomy, repeat 4D and breath-hold images may be acquired (e.g. once a week) over the entire course of RT. Depending on the nature and the magnitude of the interfractional changes, the treatment plan may be modified periodically. Ideally, the modified plan should take into consideration the cumulative biologically effective dose already delivered.

Investigators have conducted preliminary studies (1–10) demonstrating that interfractional and respiration-induced anatomic variations and their dosimetric effects may be clinically significant (11–13). Over the last 5 years, 4D-CT and positron emission tomography-CT (PET-CT) imaging technologies have been introduced, and they are evolving rapidly. These technologies are beginning to be used to quantify respiratory motion-induced anatomic variations. Studies to establish the dosimetric effects of anatomic variations determined from 4D imaging are at a preliminary stage. Suboptimal image accuracy and quality due to variability and inconsistencies in patient breathing are some of the obstacles to be overcome through research and development. Furthermore, sophisticated image-processing tools, including those for deformable registration and auto-segmentation, are evolving and are current topics of intense research and development at The University of Texas M.D. Anderson Cancer Center and other institutions (14–17).

We expect that continuing preclinical imaging and computerized treatment simulation studies will fill numerous gaps in the knowledge of IGRT of lung cancers. They will reveal the clinical benefits of IGRT and form the basis for subsequent clinical trials. The methods currently under development will also be used to translate IGRT into clinical practice soon. Implementing these methods will increase the precision and accuracy of radiation dose distributions, reduce marginal misses of tumors, and spare larger volumes of normal tissues and, therefore, improve local control and reduce morbidity. In addition, in the long run, improving the accuracy of the dose actually delivered should improve the quality of dose–response data, which in turn, could improve treatment designs.

In the treatment of highly conformal RT for lung tumors, high precision technologies and strategies are called for not only at the time of simulation but also during the course of treatment due to uncertainties related to patient positioning, organ motion, among others.

This chapter summarizes the rationale for IGRT for lung cancer, discusses several relevant aspects of infrastructure, new approaches and their clinical implementation as well as evaluates the usefulness of extending imaging in 4D-CT into treatment planning and during treatment to mitigate the consequences of inter- and intrafractional variations.

TECHNOLOGY AND METHODOLOGY

4D-CT Imaging

Respiratory-correlated 4D and breath-hold CT image data sets, and those of standard free-breathing CT, are required to quantify the extent of intrafractional motion and to design treatment plans for various respiration-correlated treatment techniques. CT image data acquired synchronously with respiration signals are used to reconstruct a 4D-CT image composed of a set of 3D-CT scans representing the 3D anatomy at a sequence of respiratory phases. This collection of 3D-CT data sets describes the snapshots of a patient's 3D anatomy over a periodic respiratory signal. The snapshots are acquired using one of the various multislice CT scanners equipped with appropriate respiratory monitoring and control equipment. Radiopaque markers, if required, may be implanted in or near the tumor.

Respiration-induced motion may be monitored using one of several commercially available systems, for example, a real-time position management (RPM) respiratory monitoring system (Varian Medical Systems, Palo Alto, CA), strain gauge, or fluoroscopically detected internal implanted markers. Figure 1 shows the Varian system.

The respiratory signal may vary from cycle to cycle and over the course of RT. However, it is implicitly assumed in the reconstruction of 4D-CT imaging that the motion is periodic and regular. Deviations from the regular periodic motion can affect the quality of 4D-CT images and the accuracy of the anatomy discerned from these images. For instance, irregular breathing may cause image artifacts. Also, irregular breathing during an imaging and treatment session and from one session to another may cause the dose distribution actually delivered to be different from the intended dose. Thus, a minimal degree of regularity and reproducibility of breathing or breath hold may be required for undergoing various lung IGRT strategies. Respiratory training could help patients meet that requirement and improve the quality of images.

Therefore, before the respiratory-correlated CT imaging is performed, patients may be trained with video-feedback guidance to breathe in a manner conducive to quality 4D or breath-hold imaging. Audio prompting and video feedback during imaging (and subsequent respiratory-correlated treatment) is then provided to guide the patient on breathing in a regular and reproducible manner.

Another important aspect of respiration-correlated imaging and treatments is the degree of correlation between the marker serving as a surrogate for breathing and the position and motion of the anatomic structures and the intra- and interfractional reproducibility of such correlation. Since images of the marker or markers are used to guide the setup of the patient and to trigger the radiation beam on and off, it is important for this correlation to be reproducible from one breathing cycle to the next and from one
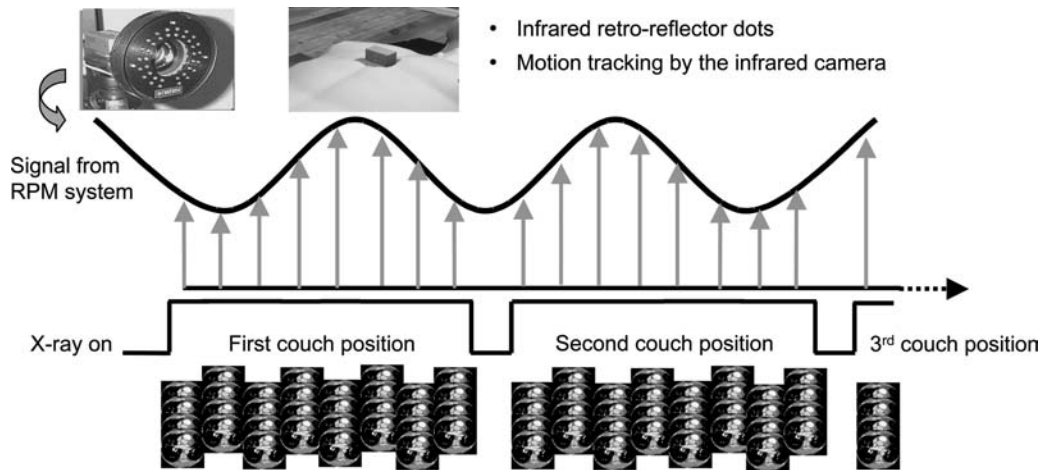
Figure 1   Illustration of 4D-CT data acquisition (cine mode CT scanning), with signals from the RPM using a commercial 8-slice PET-CT scanner. Multiple high-quality images are acquired in synchrony with respiration by combining respiratory sensor information with CT images (4D-CT). A small plastic block with infrared retro-reflector dots is placed at a specified fixed location on the patient's abdomen, and its motion is tracked by an infrared camera. The camera images are processed in real time to generate the respiration signal, which is correlated with the free-breathing CT data acquired. The same device and its signal are also used during irradiation for the delivery of gated or breath-hold radiation treatments. *Abbreviations*: 4D-CT, four-dimensional computed tomography; PET-CT, positron emission tomography computed tomography; RPM, real-time position management.

fraction to another. The correlation of an external marker with internal anatomy, however, may not be reproducible from fraction to fraction. For such cases, correlation will need to be reestablished online on the treatment machine fluoroscopically for each treatment fraction.

The 4D-CT data may be acquired in helical mode, as described by Keall et al. (9,10), or in the axial cine scanning mode, as described by Pan et al. (18). In helical CT, the patient couch moves slowly and continuously to allow acquisition of data in closely spaced slices. In axial cine scanning, the patient table is fixed to acquired data for a set of 4–16 slices and the scanner scans the same region repeatedly (approximately every 0.5 sec) to acquire data over more than the time of a complete breathing cycle. Both methods have their advantages and disadvantages.

Real-Time Tracking

Real-time tracking of tumors is feasible when the tumor can be easily identified fluoroscopically on a projection X-ray or indirectly from the images of fiducial markers implanted in or near the tumor.

Fluoroscopic tumor tracking systems are either ceiling mounted, linac gantry mounted, or robotic. An interesting ceiling-mounted system for real-time tracking has been developed by Shirato et al., at the University of Hokkaido, in collaboration with Mitsubishi (19,20). It uses a pair of X-ray tubes that rotate on a circular track embedded in the floor (Fig. 2A). Each tube has a corresponding X-ray detector that rotates synchronously on a ceiling-mounted track.

This configuration allows avoidance of obstruction of the patient by the treatment gantry for imaging. A previous version of this technology employed four fixed pairs of tubes and detectors. These X-ray tubes have a higher capacity than the ones used for conventional imaging to allow pulsed imaging interlaced with linac pulses to treat the patient. The primary use of the system is to set up the patient and deliver gated treatments based on tracking the radiopaque markers implanted in the small bronchial tubes around the lung tumor (19). The marker images are tracked with pulsed fluoroscopy before the beginning of treatment, and the patient is repositioned so that the end of the track corresponding to the least mobile portion of the motion is within a predefined gating window. During irradiation, fluoroscopy continues and the beam is automatically switched on only while the detected image of the fiducial is within the window.

An example of a ceiling-mounted system is the Novalis Body system developed by BrainLab AG (Heimstetten, Germany) (Fig. 2B). The Novalis Body system is an integrated IGRT system for target localization, setup correction, and delivery of high-precision stereotactic radiosurgery and stereotactic RT. Image guidance uses two distinct imaging subsystems: real-time infrared tracking and kilovoltage stereoscopic X-ray imaging. Two ceiling-mounted infrared cameras are used to monitor the movement of infrared-reflecting markers placed on the patient's skin or on the reference frame mounted on the treatment couch. The marker images are automatically compared to stored reference information and generate the initial

Figure 2 Real-time tumor tracking systems for RT. Three-dimensional imaging and patient positioning for high-precision dose delivery has been introduced by ceiling-mounted (**A**), linac gantry-mounted (**B**,**C**) and robotic systems (**D**). *Abbreviation*: RT, radiotherapy.

couch shift instruction to set up the patient. A video camera provides additional visual feedback on the patient's position. The X-ray imaging guidance system then takes over and performs further internal target alignment based on either bony landmarks or implanted fiducial markers. The reference digitally reconstructed radiographs are provided by the treatment planning system. During treatment delivery, the infrared optical tracking system and the fluoroscopic X-ray imaging system can work together to monitor target position and perform treatment interventions. Research and clinical experience with this system have been reported by various groups (21–23).

A dual fluoroscopy and flat panel system on the gantry of a medical linear accelerator (Clinac 23 EX, Varian Medical Systems) consisting of high-frequency (32 kW) dual X-ray generators (RAD II simulator, Haynes Radiation Ltd.) and paired a-Si flat-panel

imagers (PaxScan 2520, Varian Medical Systems) are shown in Figure 2C. The active area of the detector comprises 1408×1888 pixels, providing an imaging area of 17.9×23.8 cm. It can intrinsically recognize the coordinates, in 3D, of the center of the implanted gold seeds as the pixel positions in the a-Si flat panels through computer-controlled steps. The flat panels operate at a frame time of 33 msec; further imaging is processed through digital video signals and video graphic array monitors. Views are always taken from $0°$ of the gantry. The values are quantified as the geographical coordinates of the markers and expressed as digital figures. This system's accuracy, stability, and clinical use have been reported (24–26).

Onboard fluoroscopic X-ray imaging can be used for tracking implanted fiducials and, possibly, tumors in high-contrast regions. However, there are technological challenges to be overcome for

fluoroscopic imaging performed during state-of-the-art irradiation. For instance, imaging and irradiation must be pulsed and sequenced so that scattering from the treatment beam does not affect the quality of the kilovoltage image. Alternatively, the image detectors must be located far enough away from the source of scattering, which is not practical for gantry-mounted systems.

Another example is the CyberKnife system (Accuray Inc., Sunnyvale, CA), which is an X-ray stereoscopic guidance system designed primarily for radiosurgery applications (Fig. 2D). It is an intelligent robotic application in RT. The radiation source is a small X-band linear accelerator mounted on a robotic arm, and a ceiling-mounted stereoscopic X-ray imaging system is used for patient setup and tracking target movement during treatment. The robotic arm can move several centimeters per second, allowing it to keep up with breathing-induced tumor motion. The CyberKnife was the first clinical RT system to use real-time motion compensation, and a wealth of data has been accumulated on its performance in tracking moving targets in many treatment scenarios (27). Also, its use in frameless image-guided cranial (28), spinal (26,29–32), pancreatic (33), and lung radio-surgery (34) has been reported.

Image-Guidance Infrastructure

Development, evaluation, and implementation of IGRT into routine clinical practice requires certain image-processing tools. These include deformable image registration, auto-segmentation, and high-speed algorithms and systems for treatment planning and optimization of 3D conformal RT and intensity-modulated RT (IMRT).

Image registration is an essential step in all image-guided procedures. In general, rigid-body registration is necessary for simple geometric guidance, such as couch translation to correct a patient setup error. To quantify and track the shape, spatial, and temporal variations in a patient's anatomy, deformable image registration is necessary to map the position of each subvolume (voxel) to a reference image. The reference image may be the original planning CT for which the original treatment plan was designed or a reference-phase CT image (e.g. the end-of-expiration-phase CT) in a 4D-CT data set. Deformable image registration can be used to map and track radiation doses deposited in a deformed organ over the course of fractionated treatment, which enables adaptive planning of IGRT (35). Deformable image registration is being extensively investigated by various research groups (15,17,36–38). For example, Yan et al. (35) used a finite element method to calculate the organ deformation based on a set of predetermined boundary points. Schaly et al. (39) used a contour-based, thin-plate-spline technique for mapping dose distributions from one day to another. Lu et al. (23) proposed a deformable image registration method based on the variational principle (15), and Wang et al. (40) proposed a modified Thirion's demons algorithm (41) to register a pair of CT images.

Deformable image registration may also be used to map contours drawn on the reference CT image to other CT images in the 4D-CT data sets or to the 4D-CT images on subsequent days. However, other auto-segmentation techniques that do not depend on such prior knowledge have also been developed (36,42,43).

To adapt a treatment plan to the changed anatomy, it may be necessary to design a new plan or to modify the original one. The frequency of adaptive replanning will undoubtedly depend on the degree of interfractional changes as discerned from repeat 4D-CT imaging. Making replanning affordable requires fast treatment planning and optimization techniques. Numerous such techniques are under development. They range from those in which new leaf positions for multiple segments of an IMRT plan are computed directly to full-fledged reoptimization of IMRT plans.

CLINICAL IMPLEMENTATION OF IGRT

Currently, neither control nor monitoring of motion is widely done during routine CT imaging or daily treatments. Previous reports have stated that the magnitude of tumor motion during treatment cannot be predicted before treatment and must be explicitly measured to be ascertained (6,7). Consequently, 4D-CT has been used to explicitly measure intrafractional motion and to determine internal target volumes (ITVs) (10,18). This technique can obtain images demonstrating both spatial and temporal anatomic changes at planning and delivery of RT (44,45) and thus improve the characterization of target mobility (46).

In order to enhance the accuracy of IGRT, patients are trained to breathe or to hold their breath in a regular and reproducible manner. A 4D-CT image and a breath-hold CT image are acquired for each patient. The patient can receive video-feedback guidance to control his or her breathing by being shown his or her respiratory trace on a liquid crystal display in virtual reality video goggles. The respiratory trace is acquired with the aid of a respiratory monitoring device, such as Varian's RPM system. Figure 3 shows a patient in position for acquiring a respiration-correlated CT image.

Respiration and RT may cause tumor motion and size changes; so far, no conclusive data exist on
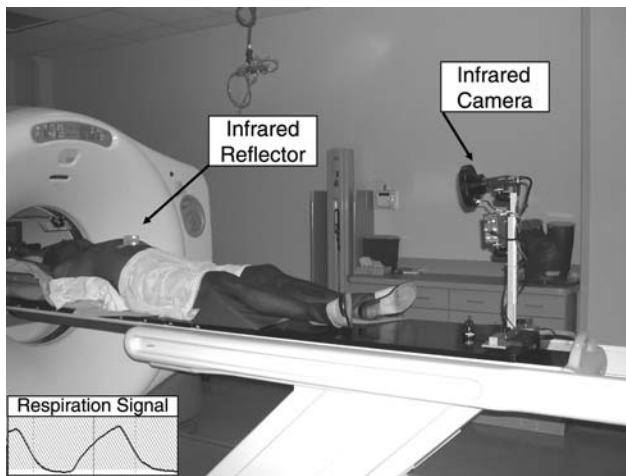
Figure 3 A view of the RPM system. The infrared camera tracks the position of an abdominal fiducial (infrared reflector) visible on an optical monitor. Correlation is made with the acquired CT images over complete respiratory cycles. Left lower graph shows an example from the respiration signal acquired from the system. *Abbreviations*: CT, computed tomography; RPM, real-time position management.

the nature of the intrafractional motion, interfractional changes in the intrafractional motion, or the time at which these changes may occur. Treatment delivery parameters need to reflect motion and shape changes through the entire course of treatment, or overirradiation of normal tissues or respiration-induced target miss could occur and may negatively affect clinical outcomes (35,47). In addition, because of the possibility that as a result of the irradiation the tumor shrinks, it may be possible to reduce the treatment portal.

Depending on the patient and tumor characteristics (e.g. breathing performance and reproducibility and tumor size, location, and extent of motion), a suitable IGI strategy may be selected. A treatment plan appropriate for the particular IGI strategy is then designed.

Because of these changes and the high degree of conformality in the beam configuration, beam configurations based on the initial 4D-CT data set may not adequately irradiate the target during the entire course of treatment and it may be necessary to acquire repeat CT scans or replan the patient's treatment.

INTER- AND INTRAFRACTIONAL VARIATIONS IN THE MOBILITY, SIZE, AND SHAPE OF LUNG TUMORS

Knowing the tumor position before and during treatment is essential (48,49) because tumor position can be affected not only by respiration but also by body motion, extremity positions, immobilization (50), and other factors. A number of studies have

provided evidence of image-based determination of the excursion of lung tumors. The studies have more recently included the use of fluoroscopy (51), serial CT scans (52), dynamic magnetic resonance imaging (53), real-time tumor tracking (19,48), and respiration-correlated 4D-CT (10,18,54,55). Recent reports on the clinical implementation of single or serial imaging approaches during treatment have suggested that different techniques may confer benefits in assessing changes in the size and mobility of target volumes (10,18,56). It is, however, impossible to either predict or eliminate all potential sources of uncertainty during the whole course of treatment.

Respiration-correlated image acquisition for treatment planning has been increasingly used in most of the major oncology centers, and tools for rapid data management have also been developed. Once the target volumes and other structures have been delineated, quantification of volume and position variations is a relatively straightforward task. However, quantification of shape variation is more complex. Research is in progress to use Fourier descriptors, wavelet descriptors, and the moments of various orders as quantitative indices of shape. Shape, volume, and position changes will eventually be correlated with changes in dose–volume and dose–response indices. Such correlations could ultimately be used to make decisions regarding the choice of the IGI strategy and the associated margins based on imaging.

Time Trends in Tumor Mobility

Early experience at M.D. Anderson Cancer Center suggests that typically patients fall into 1 of the following 3 categories: (1) Patients for whom tumor motion is small and image-guided setup for treatments can reduce the positioning uncertainty to less than 3 mm and the total margin to 4–6 mm. These tend to be patients with tumors in the upper lobe and those with large tumors (Fig. 4). Such patients may require minimal or no intrafractional IGIs. (2) Patients for whom the tumor position variation and residual motion with image guidance are substantial. (3) Patients who are unable to breathe regularly and reproducibly. For this last group, the image guidance strategies use customized ITV that integrates the full extent of target motion. Typically for this group of patients, the total margin for positioning and motion may be in the range of 10–20 mm. Previous reports involving 25 patients with lung cancer (6,7,57) who underwent end-inhale and end-exhale CT imaging before the course of RT and at the end of the course, we found the following: (1) Respiration-induced intrafractional tumor motion may be significant (as much as 2–3 cm). (2) Tumor motion magnitude and direction, tumor shape, and size may change over the course of RT. Superior–inferior (SI) motion for one
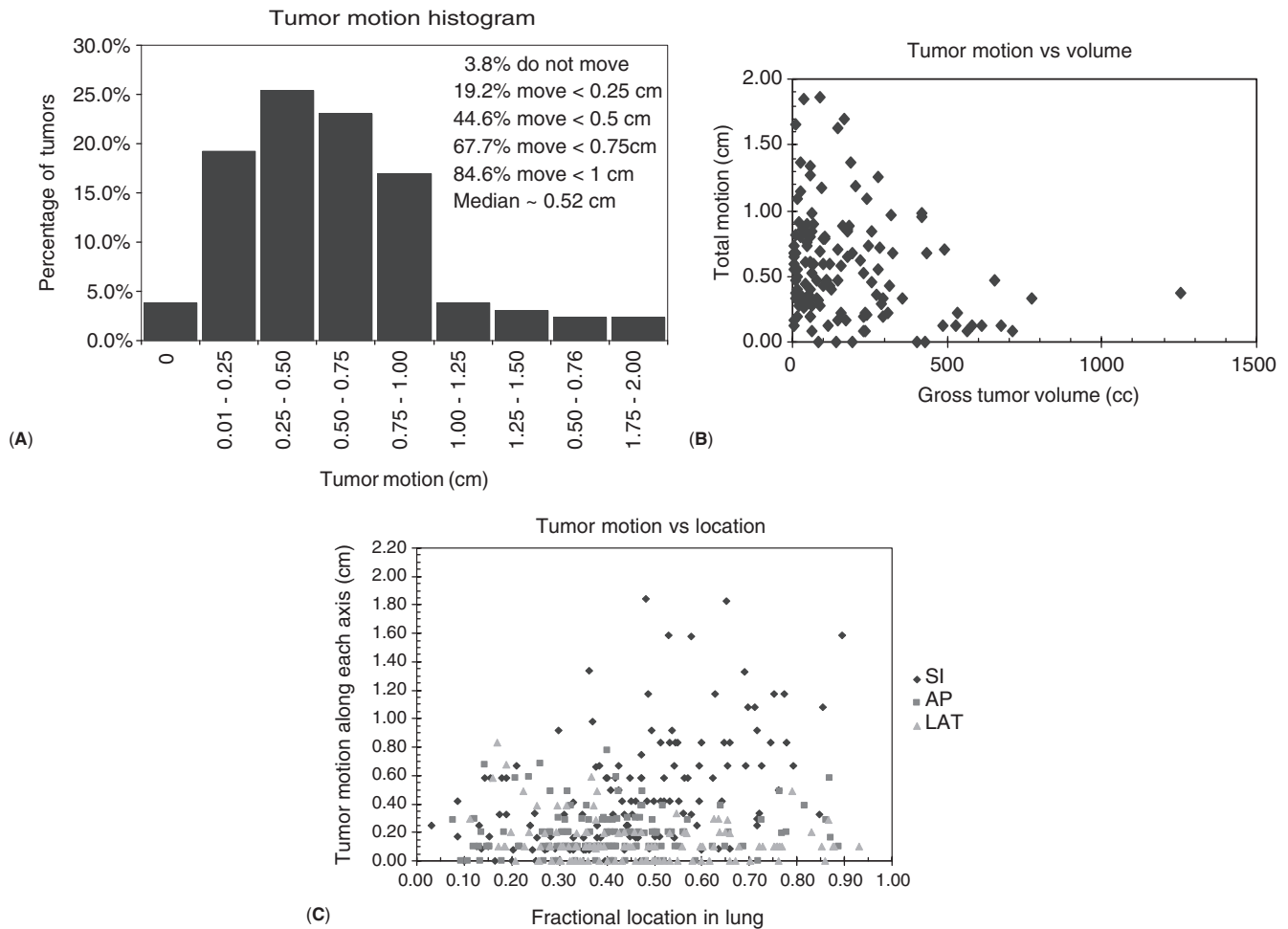
Figure 4 Preliminary analyses of 4D-CT data for 130 patients. (**A**) Histogram shows that the extent of tumor motion is less than 0.25 cm for about 20% of the patients and less than 0.5 cm for 45% of the patients. (**B**) Scatter plot shows that small tumors tend to move more than larger tumors. (**C**) Scatter plot shows that there is a correlation between SI tumor motion and relative distance from the apex ($P = 0.0001$), but that there is no correlation between AP location and motion ($P = 0.207$) or between lateral location and lateral motion ($P = 0.346$). *Abbreviations*: 4D-CT, four-dimensional computed tomography; AP, anterior–posterior.

patient changed from 9 mm in the inferior direction, based on pre-RT CT, to 4 mm in the superior direction, for post-RT CT (3). No factor predicted tumor motion in this small data set. (4) Synchronizing beam gating with respiration could significantly reduce the mass of normal lung exposed to damaging levels of radiation.

The use of 4D-CT scans, acquired before RT, has become the standard of practice at M.D. Anderson Cancer Center for delineating the motion-integrated ITV that encompasses the entire range of motion during free breathing. A recent report from van der Geld et al. (58) showed the advantages of deriving ITV margins based on 4D-CT images as opposed to conventional fluoroscopy. Mean ITVs derived using fluoroscopy were 52% larger than those derived using 4D-CT contours.

More recently, at M.D. Anderson Cancer Center, a protocol was implemented to assess tumor motion

on a weekly basis by 4D-CT imaging (26). Magnitudes of primary tumor excursion in the lateral direction remained fairly stable during treatment. However, a tendency incremental was observed in the anterior–posterior (AP) and SI directions (Fig. 5). Within this 10-patient group analysis (83 4D datasets), motion was significantly greater for those lesions in the lower lobes (5 lesions) than for those in the upper lobes (5 lesions; $P < 0.001$). This result is consistent with those of previous reports (50,58–60).

This study also assessed the interfractional tumor positional variations during irradiation. The bony anatomy of the spine was used to co-register all scans because this structure is relatively insensitive respiratory and cardiac motion. Tumor centroid positions showed mean overall displacements of 0.30 ± 0.23 cm in the right–left (RL) direction, 0.45 ± 0.27 cm in the AP direction, and 0.54 ± 0.32 cm
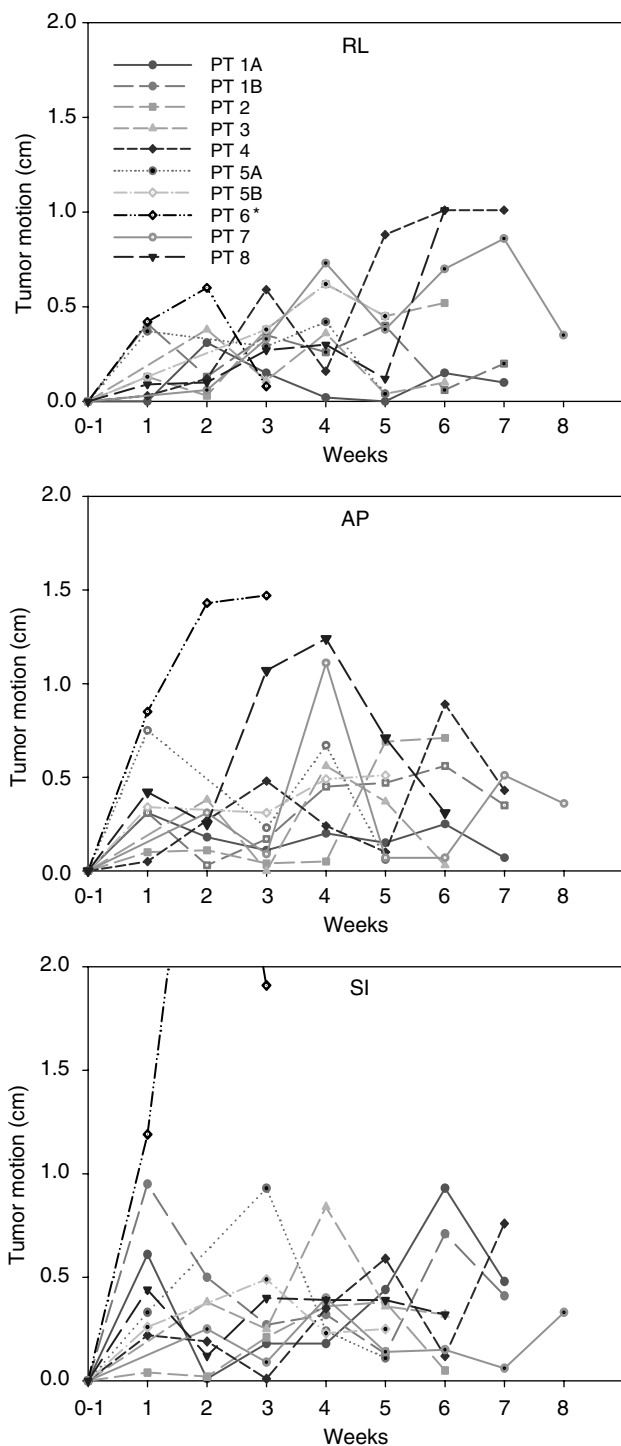
Figure 5 Interfractional magnitude of variations in the position of the GTV centroid during treatment in the RL, AP, and SI directions, as derived from 4D-CT scans. Although slight progressive changes occurred in all directions between treatment weeks, no significant trend was identified. *Patient with progressive pleural effusion. Patients 1 and 5 had two separate lesion denoted as A, B. *Abbreviations*: 4D-CT, four-dimensional computed tomography; AP, anterior–posterior; GTV, gross tumor volume; RL, right–left; SI, superior–inferior.

in the SI direction. Each treatment week, a marginally significant ($P = 0.049$) increase in the 3D motion of the gross tumor volume (GTV) centroid was observed; the average increase was 6.3 mm per week. This trend was caused primarily by an increase in the magnitude of tumor motion in the RL direction ($P = 0.006$) rather than the AP and SI directions ($P = 0.308$ and $P = 0.651$, respectively). However, patients with upper-lobe tumors had slightly greater motion amplitudes in the AP direction than in the RL and SI directions, and lower-lobe tumors showed significantly greater motion than upper-lobe tumors. This analysis was extended to the weekly spatial position variations of the ITV centroid relative to the initial planned position for each 4D scan.

Figure 6 displays an example of the week-to-week variations in 3D paths of tumor centroids for two studied patients with stage III non–small cell lung cancer (NSCLC) in their right lower lobe. These data were extracted from weekly 4D-CT scans acquired as a part of our studies to quantify inter- and intrafractional anatomic variations. Although weekly scans were acquired, for better visualization, Figure 6 shows only scans for weeks 0–1 (simulation), 2, 4, and 6. CT scans were aligned using bony anatomy (vertebral bodies). Significant variations in tumor centroid position from week to week are seen, indicating the need for daily image-guided setup in addition to IGI to account for respiration-induced motion.

Another example of the interfractional variations of an internal fiducial placed near the tumor during irradiation with gated beams around the exhale phase is shown in Figure 7. Systematic and random uncertainties in patient setup and tumor motion could cause deleterious target miscoverage and poor outcomes, making IGIs a necessity for some patients under gated or non gated RT. Image-guided approaches for conventional and hypofractionated lung irradiation have mitigated tumor motion and improved normal tissue sparing, specially in gated modalities(61–63).

Positional Variation of the ITV

Positional variation of the ITV (based on target centroid) could result from motion of the GTV. These changes could be quantified with repeat 4D-CT imaging and tracking their 3D position relative to initial (at simulation) positions. Initial data for patients with NSCLC treated in the Department of Radiation Oncology at M.D. Anderson Cancer Center showed an overall average ITV positional variation of 0.81 ± 0.26 cm (26). The positional variations of the 3D GTV and ITV centroids did not differ significantly ($P = 0.605$), and there was not a significant time-trend
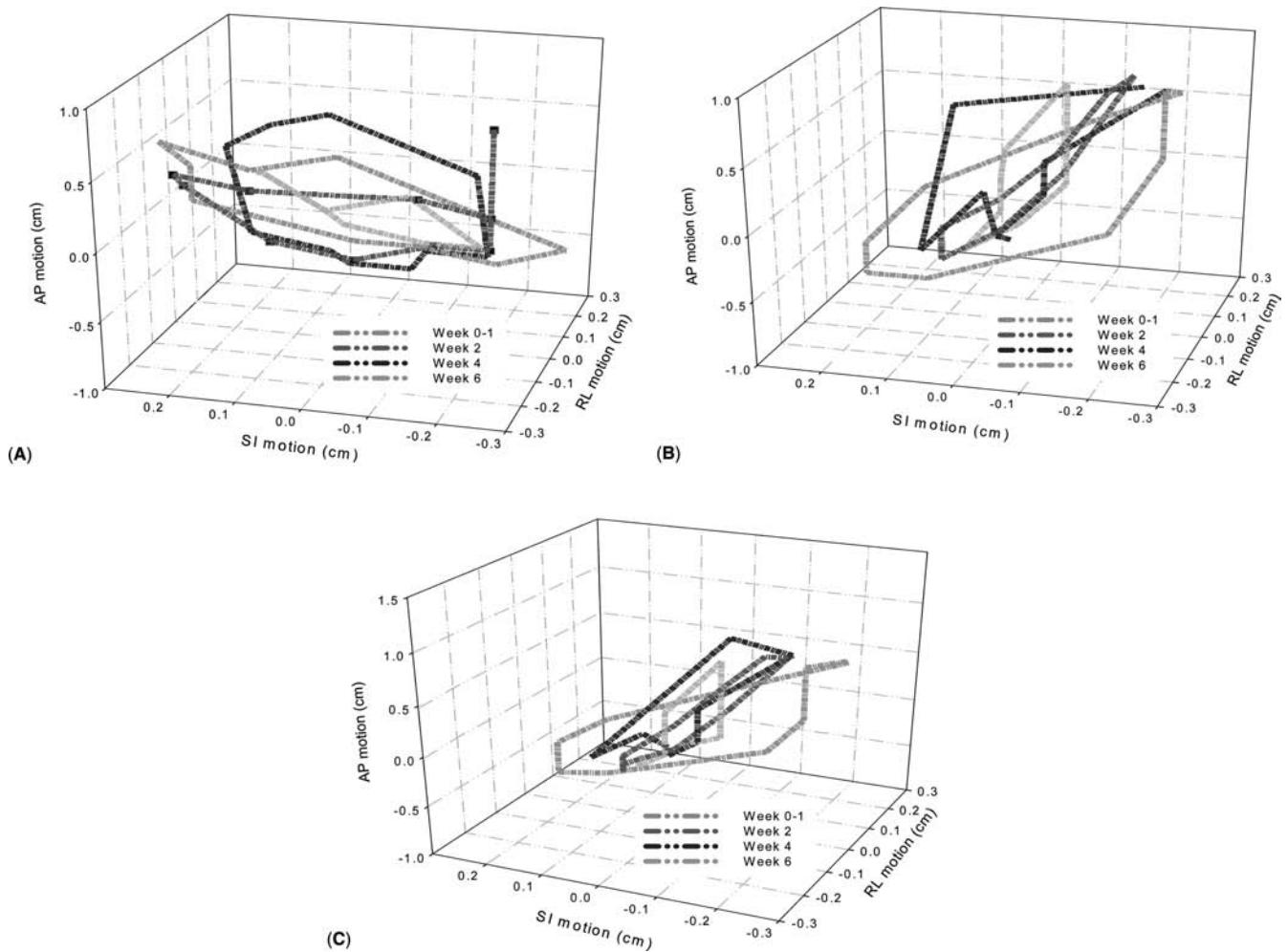
Figure 6 (*See color insert.*) Three-dimensional paths of GTV centroid motion (at 50% phase) during inhale to exhale respiratory phases at weeks 0–1 (simulation), 2, 4, and 6 for two selected patients (**A,B**) with a similar tumor volume, location, and clinical stage and the same prescribed radiation dose. The paths for weeks 2, 4, and 6 show greater progressive changes in motion amplitudes as compared to paths at simulation. Also, there is evidence of hysteresis (differences in paths between inhale and exhale phases) and changes in the spatial position of the tumors. After spinal-body registration was performed, (**C**) improvements in the interfractional tumor reproducibility (IGRT effect) could be obtained. *Abbreviations*: AP, anterior–posterior; GTV, gross tumor volume; IGRT, image-guided radiotherapy; SI, superior–inferior; RL, right–left.

difference between these two quantities ($P = 0.516$). A higher incidence in ITV centroid positional variation was observed during mid-treatment. A total of 4 of the 10 patients had shifts larger than 1 cm at week 3, 2 at week 4, and none at week 5. Similarly to ours, a study conducted by Underberg et al. (56) using weekly 4D-CT datasets for patients with stage I NSCLC reported that similar trends were observed for the ITV and GTV and that in 5% (2 of the 40) of the patients, the spatial position of the ITV was greater than 10 mm.

IGIs by repeat CT images, cone-beam CT, or real-time tumor tracking may aid in the adaptation of dose to target more precisely, especially in patients presenting greater target volume mobility.

Time Trends in GTV Volumes

Recent data suggest that we may have to consider the use of IGIs (adaptation) during treatment to update treatment plans that fail to encompass the entire target volume because of treatment-related or motion-induced tumor displacement. An analysis of serial 4D datasets in a cohort of 10 patients was done, observing slight increments in tumor motion with treatment weeks as well as anisotropic tumor volume loss in all patients (26). Although no trends were identified, most changes occurred from the mid to the last weeks of treatment.

A progressive decrease in the size of the GTV was observed for all patients. Mean volumes were similar for drawn tumor contours at end of inspiration (56 cm^3;
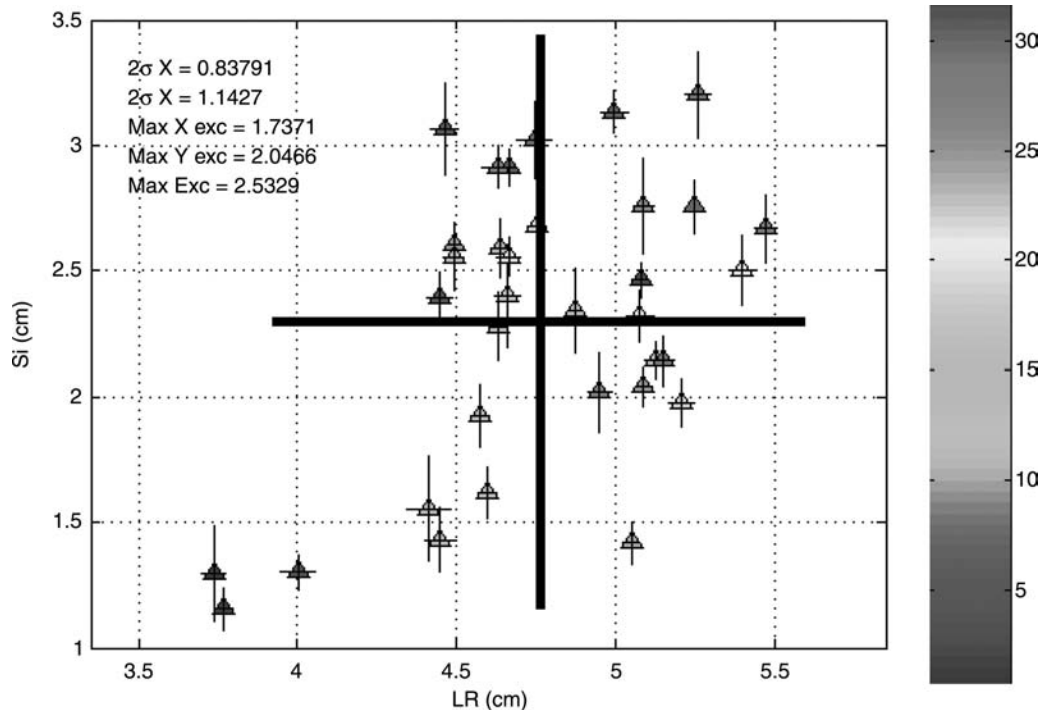
Figure 7 For this patient, radiopaque markers (fiducials) were implanted in and around the lung tumor. The tumor was estimated to move approximately 0.9–1.3 cm based on weekly 4D-CT scans acquired over the course of RT. For daily treatments, the patient was immobilized and set up using skin marks (tattoos) and lasers. Irradiation beams were gated around the end exhale. For each treatment session, a gated electronic portal image of each beam was acquired. The error bars show the range of residual motion of the fiducial within the gate. Each point on the graph represents a fraction and shows that, even with careful alignment, the mean position of the moving tumor may shift significantly (~2 cm for this patient) over the course of RT. *Abbreviations*: 4D-CT, four-dimensional computed tomography; RT, radiotherapy.

range, 1–176 cm^3) and at end of expiration (53 cm^3; range, 1–151 cm^3). Figure 8 illustrates such changes at end of inspiration and end of expiration with treatment weeks for a single patient.

Tumor volume shrinkage over the course of treatment can be addressed with tools in the treatment planning system. Tumor volume assessment during RT is valuable and has been looked at in a non-3D context using CT or X-rays (64) and more recently in a 3D context for lung tumors (65–67). Some of the previous studies used portal imaging (66). Erridge et al. (66), showed that in 25 patients with stages I–IIIb disease treated with conventional doses over 6–7 weeks, tumor shrinkage of at least 20% occurred in 40% of the patients. In our study, a volume loss of at least 40% occurred in 50% of the patients treated over the same period for mainly stage III disease. Kupelian et al. (67), studies tumor volumes in 3D with the use of serial megavoltage imaging at the beginning and end of treatment for stage I lung tumors treated with conventional fractionated schedules.

Similarly, Underberg et al. (56) used 4D scans to evaluate trends in GTV and ITV for patients with stage I disease undergoing stereotactic RT for up to 5 weeks. They observed an initial increase in tumor

volume of 10 cm^3 in at least 2 of the 40 patients, which is consistent with findings in our study. Also, volume changes were observed after the fourth week of stereotactic RT and 3 months after treatment. Our serial 4D imaging study showed total volume losses of 41% at end of inspiration and 38% at end of expiration. A report from Bosmans et al. (68), using respiration-correlated CT scans limited to weeks 1 and 2 of conventional treatment, showed no significant changes in either average tumor motion or tumor volume.

CONSEQUENCES OF INTER- AND INTRAFRACTIONAL VARIATIONS IN THE CURRENT PRACTICE

In the current practice of treating lung cancer with RT at M.D. Anderson Cancer Center, we determine the motion-integrated customized ITV on the basis of the extent of the movement of the target discerned from a 4D-CT scan acquired before the course of RT. This ITV is used to design radiation beam apertures for treatment planning. It is assumed that the treatment plan represents the real dose distribution in all phases of a breathing cycle and throughout the course of RT,
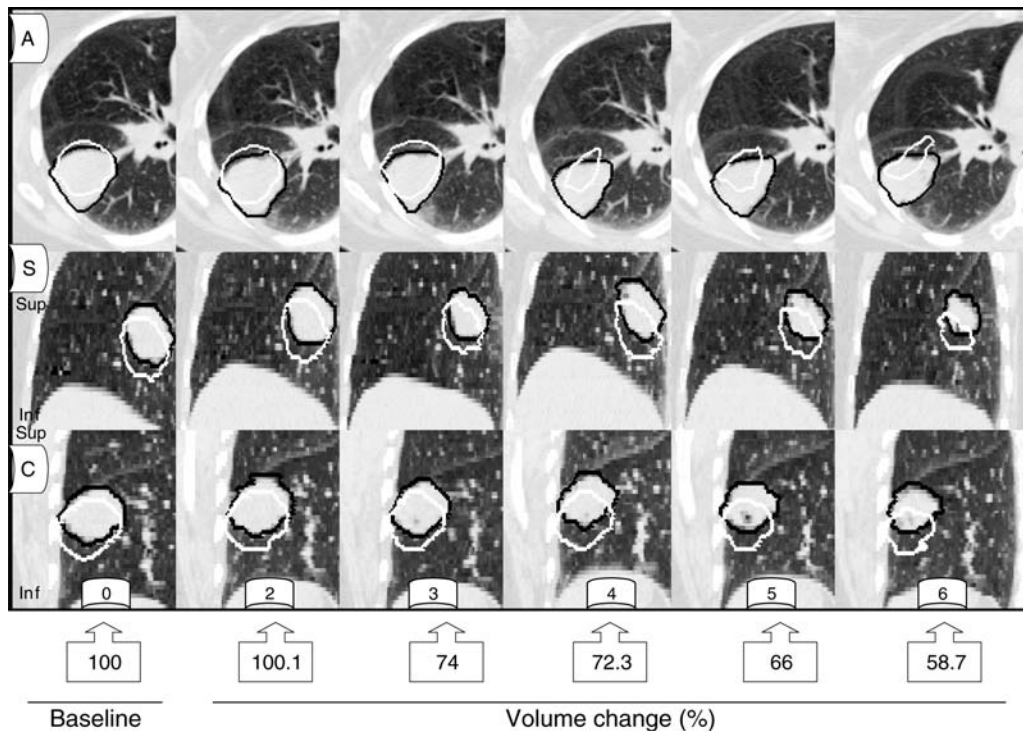
Figure 8 4D-CT scan of axial (A), sagittal (S), and coronal (C) sections depicting the primary GTV contours from the initial simulation scan to the last treatment week. Primary tumor volumes at end of inspiration (white contours) and expiration (black contours) throughout treatment show intra-/interfractional size changes. Column labeled 0 refers to the reference scan acquired prior to the beginning of the RT course for treatment planning, and columns labeled 2–6 represent the subsequent treatment weeks and respective volume changes. Total volume loss at week 6 of treatment was 41.3% of the initial volume. In 10 prospectively treated patients at M.D. Anderson Cancer Center, a progressive reduction of tumor size was observed for all patients. Images shown correspond to the exhale (50%) phase of the breathing cycle. *Abbreviations*: A, axial; C, coronal; GTV, gross tumor volume; Inf, inferior; RT, radiotherapy; S, sagittal; Sup, superior.

regardless of intra- and interfractional anatomic variations.

At most other institutions, treatment planning is based on a fast free-breathing 3D-CT scan. For such a practice, the location of the tumor, or the portions thereof, as captured on the image could be anywhere over the extent of motion.

Treatment plans to simulate free-breathing treatments may be designed by using the target margins of the current standard of practice. These plans depict what we call the perceived dose distributions. Computation of real dose distributions, which may actually be delivered, is a two-step process. In the first step, the radiation beam configuration is applied to each 3D component of the 4D-CT, and the dose distribution for each phase will be calculated. Three-dimensional components of the 4D image are deformably mapped to one of the components chosen as a reference (typically the one for the end-exhale phase). The same deformation transformation is used to map all dose distributions to the reference component. The time-average of all dose distributions, called the 4D dose distribution, yields the real dose distribution expected to be delivered for that fraction.

In the second step, the cumulative dose distribution expected to be delivered over the entire course of RT is computed. The reference component image of each fraction is deformably mapped to the reference component of a 4D image chosen to be the overall reference for the RT course. The overall reference image is normally the one acquired before the course of RT for planning purposes. The deformation transformation matrices derived from the interfractional deformable registration process are used to map the corresponding dose distributions to the overall reference image. Ideally, to account for the fact that each voxel would, in general, receive different doses for different fractions, the transformed dose distributions should be converted to biologically equivalent dose distributions (BEDDs) using the linear-quadratic model and the currently accepted alpha/beta values for lung tumors and relevant normal critical structures. The resulting dose values would then be added together to produce the cumulative BEDD. We define the cumulative biologically equivalent dose in a voxel as the equivalent physical dose that the voxel would have received if it had received the same dose for every fraction.
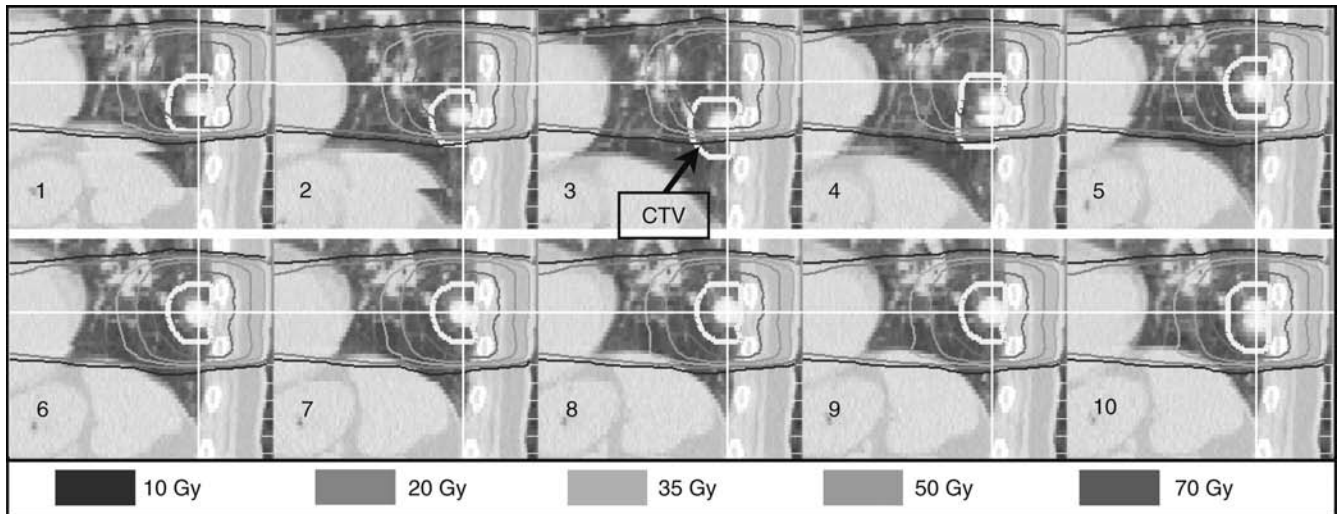
Figure 9 (*See color insert.*) 4D-CT scans showing the intrafractional effects of tumor motion on the dose distributed by IMRT. A 10-phase (respiratory cycle) isodose distribution is shown for the CTV. In phases 2, 3, and 4, the clinical target volume (shown by the thick yellow line) is not adequately covered by the 70-Gy prescription dose (line in red). *Abbreviations*: 4D-CT, four-dimensional computed tomography; CTV, clinical target volume; IMRT, intensity-modulated radiotherapy.

Figure 9 shows the sagittal radiation dose distribution resulting from an IMRT treatment plan (with an 8-mm margin to accommodate tumor motion) applied to each of the 10 breathing phases for a patient with lung cancer. The real dose distribution may not be the same once the effect of internal motion had been taken into consideration. The inferior portion of the clinical target volume receives a lower dose, which could affect the probability of tumor control. Figure 10 shows similar data for protons.

Previous studies have addressed the effect of respiration and setup uncertainties on dose-to-target
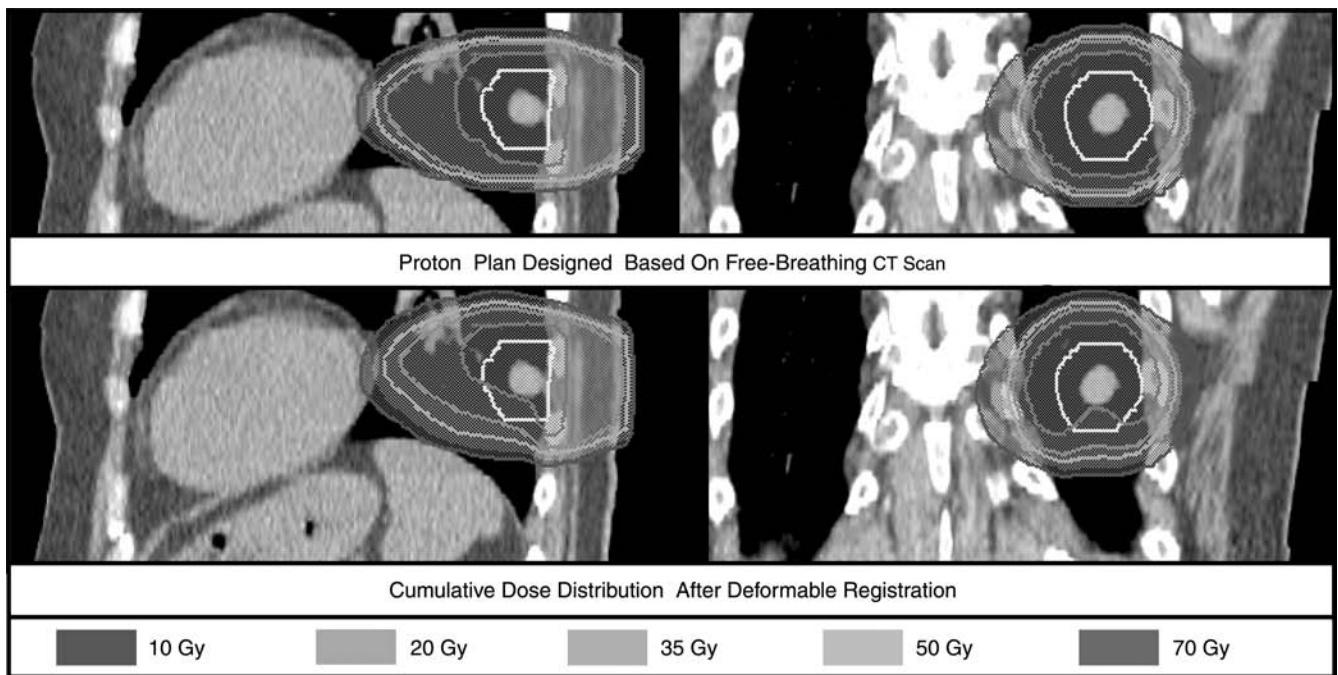
Figure 10 (*See color insert.*) 4D-CT scans showing a comparison of dose distributions of an IMRT plan for a patient with NSCLC. Top row shows plan without consideration of internal organ motion, and the bottom row shows the time-integrated cumulative dose distribution computed using M.D. Anderson Cancer Center's deformable image registration algorithm. *Abbreviations*: 4D-CT, four-dimensional computed tomography; IMRT, intensity-modulated radiotherapy; NSCLC, non–small cell lung cancer.

volumes and normal tissues. Mechalakos et al. (69) analyzed dosimetric (D95, V95) and parameters for 12 patients with lung cancer treated with planning target volume (PTV) margins ranging from 1 to 2 cm. Setup errors (with a systematic component) and breathing motion (diaphragmatic fluoroscopy movies) parameters were incorporated. They showed that the combination of both uncertainties could result in a 30–40% probability of a greater than 10% reduction in the studied parameters (worst-case scenario). However, without taking into account the intrafractional breathing motion, this probability was reduced to less than 10%, and for the normal breathing cases, the probability was less than 4%. A recent planning study for lung tumors by Schwarz et al. (70) also addressed the effect of geometric uncertainties on dose distribution. In general, their current margins of 10 mm used for GTV-PTV were considered adequate for their 3D conformal RT and IMRT plans when respiratory amplitudes were less than 10 mm. Variation in the respiratory patterns could be seen along the course of treatment, which could hinder the delivery of ideal prescribed doses.

IGI STRATEGIES

Image-Guided Determination of Motion-Integrated Custom ITV

As noted above, the use of customized motion-integrated ITV, which is determined by the range of tumor motion using 4D-CT, became the standard of practice at M.D. Anderson Cancer Center in 2004. Previously, the margins for motion were typically chosen with the provision that they cover the entire target in >95–98% of the time for the patient population. With customized ITV, margins can be smaller if the respiration-induced motion is small, and on average, a substantial reduction in normal tissues exposed to damaging levels of radiation should be expected. The margin width must be increased to account for daily setup uncertainty, and treatments may be planned and delivered as usual.

Image-Guided Target Localization

Image guidance may also be used for positioning patients for each fraction of RT to ensure that the target is covered fully by the radiation beam. If breath-hold was used, IGI would involve repositioning the patient on the basis of the correlation between breath-held static X-ray images acquired on the treatment machine and the digitally reconstructed radiographs derived from the breath-held CT scan. Imaging at the treatment machine is carried out using video feedback guidance in a manner identical to that used during initial imaging for treatment

planning. This is to ensure that the breathing pattern or the breath hold during treatment is reproduced from day to day and corresponds to that for initial imaging.

For gated or free-breathing treatments, alignment is based on the correlation of fluoroscopic images with digitally reconstructed "fluorographs" (DRFs) derived from the 4D-CT scans. For gated treatments, the beam is typically on within a 20–30% window of the respiratory cycle near end exhale. Repositioning for a gated treatment may use just the end-exhale frames of the DRF and the fluoroscopic image. Alternatively, a gated static X-ray image at end exhale may be used. Repositioning for a free-breathing treatment may be based on the midpoint of the range of motions seen on the DRF and on the fluoroscopic image.

The unpredictability of respiration-driven lung tumor motion makes treatment planning and adaptation a great challenge. Several clinically implemented techniques to accommodate the whole range of tumor excursion during the course of treatment have been described in this chapter. The bony-spine alignment method is used to reduce systematic setup uncertainties during treatment. We analyzed the geometric correlation of the PTV margins to ITV margins in the presence of a tumor with an average motion (SI) of 1.01 cm (Fig. 11). Serial imaging may help limit the potential geometric target miss due to organ motion and, therefore, facilitate the most appropriate image guidance strategy.

The choice of gated, breath-hold, or free-breathing modes depends on tumor and patient characteristics (e.g. the patient's ability to hold breath or the volume of normal lung exposed to damaging levels of radiation).

Real-Time Monitoring and Tracking for Intrafractional Variation

Because respiratory-correlated CT imaging is not feasible during irradiation, the following IGI strategies for real-time monitoring and tracking of tumors during irradiation should be used. Such a process involves localizing the target using fluoroscopic guidance (as described above) and tracking the target or the radiopaque markers implanted in and around the tumor volume. Just before the start of the treatment, the respiratory monitoring system (e.g. real-time position monitoring system) signal is correlated with fluoroscopic images and with the patient immobilized and positioned on the treatment table. This strategy may be necessary if fluoroscopy cannot be used during irradiation because of technical obstacles related to the interference between irradiation and imaging. Currently, this is the case for most,
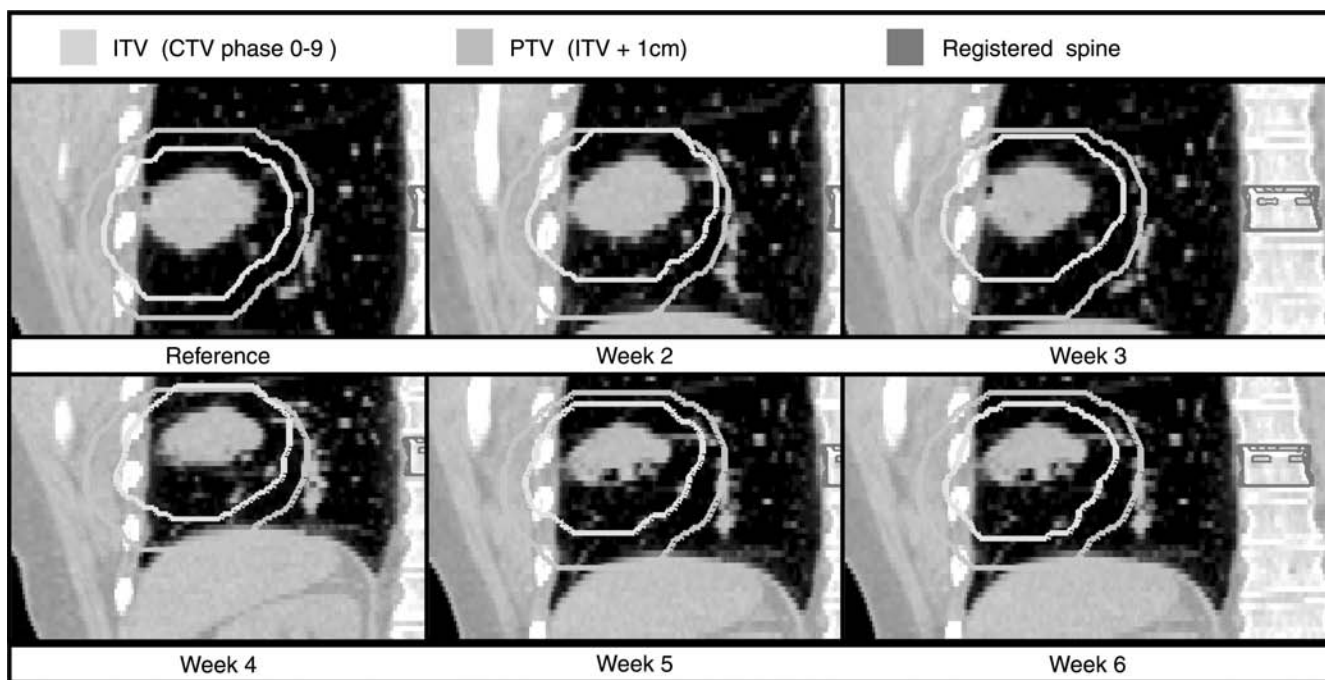
Figure 11 (*See color insert*.) Serial 4D-CT scan (coronal view) of a non–small cell primary lung tumor with the reference planning target volume (PTV in cyan) geometrically correlated with the internal target volume (ITV in khaki). The PTV is the internal tumor volume plus 1 cm. The average SI magnitude of tumor displacement was 1.01 cm. Weeks 2 and 4 showed a slight compromise in the PTV-to-ITV coverage when datasets were registered by bony spine structures (image-guided technique for alignment). Failure to use image guidance-based techniques before or during treatment could cause greater geographic target miss. *Abbreviations*: 4D-CT, four-dimensional computed tomography; ITV, internal target volume; PTV, planning target volume.

if not all, photon and proton treatment machines. Even if this obstacle were overcome, the proposed strategy would be preferable to reduce the radiation dose caused by fluoroscopy.

Modification of the Treatment Plan in Response to Interfractional Variations (Adaptive IGRT)

In addition to image-guided setup and real-time tracking of the target, the treatment plan may be modified on the basis of the images acquired during the course of RT to account for interfractional variations. If the changes are below a threshold of clinical significance, no modification of the treatment plan would be necessary. Otherwise, the plan may be modified off-line. Automated and rapid methods of modifying IMRT and proton plans based on images acquired online in the treatment position are necessary and are being developed.

For photon and proton 3D conformal RT of lung tumors, modifying the treatment plan may involve only modifying the beam apertures to conform to the new shape of the target, followed by recomputation of the dose distribution. For IMRT and intensity-modulated proton therapy plans, however, reoptimization of intensities and recomputation of treatment delivery parameters, such as dynamic multileaf collimator leaf positions, would be required.

Current limitations exist for the regular application of replanning during treatment and for the acquisition of multiple image datasets over the course of treatment. Although the replanning and acquisition just mentioned is crucial for some patients, it is vital to not underestimate the cost of such procedures. The procedures require substantial staff involvement (i.e. physicians, physicists, dosimetrists, therapists, and associated personnel) and incur extra expenses for additional imaging and planning. Also, the interobserver uncertainties in contouring of tumor volumes may be another factor (23).

Appropriateness of IGI Strategies

It is not clear a priori whether a given strategy would yield clinically significant improvements compared to simpler ones for a given patient or for a given class of patients. Treatment simulation studies need to be conducted to determine the appropriateness of IGI strategies based on the criteria of clinical benefits defined in terms of significant change in dose-volume and dose-response indices. For each IGI strategy, the degree of statistical correlation of dose–volume and dose–response indices with the patient and tumor characteristics will determine the appropriateness of the strategy.

CONCLUSIONS

IGRT for lung tumors offers improvements in the setup and treatment processes in the settings of highly conformal radiation techniques. It is increasingly been recognized the substantial influence of inter- and intrafractional uncertainties related to patient positioning, respiration-driven organ motion, tumor volume changes, among others, on treatment targets and the intervening surrounding normal tissues.

The goal of IGRT for lung cancer is to mitigate the detrimental effects of inter- and intrafractional variations in anatomy. New approaches and techniques are been implemented to accurately target lung cancer as well as to reduce margins, and to allow radiation dose escalation to higher levels; this is vital to achieve optimal outcomes.

Currently, the implementation of new and existing imaging technologies (like 4D-CT) is the topic of ongoing preclinical and clinical research. The aim is to determine the dependence of respiration and treatment-related uncertainties on tumor and patient characteristics (e.g. tumor size and location, lung function, breathing regularity and reproducibility, and chemotherapy) and to establish which IGI strategy is most appropriate for specific extents and patterns of variation, tumor and patient characteristics.

Implementing these and other methods will increase the precision and accuracy of radiation dose distributions, reduce marginal misses of tumors, spare larger volumes of normal tissues and, therefore, improve local control and reduce morbidity.

We expect that continuing imaging and computerized treatment simulation studies will fill numerous gaps in the knowledge of IGRT of lung cancers. They will reveal the clinical benefits of IGRT and form the basis for subsequent clinical trials. Furthermore, sophisticated image-processing tools, including those for deformable registration and auto-segmentation, are evolving and are current topics of intense research and development at The University of Texas M.D. Anderson Cancer Center and other institutions. Critical appraisal of all image-based adaptive technologies will soon establish their role in patient care.

REFERENCES

1. Wong JW, Sharpe MB, Jaffray DA, et al. The use of active breathing control (ABC) to reduce margin for breathing motion. Int J Radiat Oncol Biol Phys 1999; 44(4):911–19.

2. Shimizu S, Shirato H, Ogura S, et al. Detection of lung tumor movement in real-time tumor-tracking radiotherapy. Int J Radiat Oncol Biol Phys 2001; 51(2):304–10.

3. Sixel KE, Ruschin M, Tirona R, Cheung PC. Digital fluoroscopy to quantify lung tumor motion: potential for patient-specific planning target volumes. Int J Radiat Oncol Biol Phys 2003; 57(3):717–23.

4. Plathow C, Fink C, Ley S, et al. Measurement of tumor diameter-dependent mobility of lung tumors by dynamic MRI. Radiother Oncol 2004; 73(3):349–54.

5. Shih HA, Jiang SB, Aljarrah KM, Doppke KP, Choi NC. Internal target volume determined with expansion margins beyond composite gross tumor volume in three-dimensional conformal radiotherapy for lung cancer. Int J Radiat Oncol Biol Phys 2004; 60(2):613–22.

6. Stevens CW, Munden RF, Forster KM, et al. Respiratory-driven lung tumor motion is independent of tumor size, tumor location, and pulmonary function. Int J Radiat Oncol Biol Phys 2001; 51(1):62–8.

7. Starkschall G, Forster KM, Kitamura K, Cardenas A, Tucker SL, Stevens CW. Correlation of gross tumor volume excursion with potential benefits of respiratory gating. Int J Radiat Oncol Biol Phys 2004; 60(4):1291–7.

8. Liu HH, Koch N, Starkschall G, et al. Evaluation of internal lung motion for respiratory-gated radiotherapy using MRI: Part II-margin reduction of internal target volume. Int J Radiat Oncol Biol Phys 2004; 60(5):1473–83.

9. Keall P. 4-dimensional computed tomography imaging and treatment planning. Semin Radiat Oncol 2004; 14(1):81–90.

10. Keall PJ, Starkschall G, Shukla H, et al. Acquiring 4D thoracic CT scans using a multislice helical method. Phys Med Biol 2004; 49(10):2053–67.

11. Engelsman M, Damen EM, De Jaeger K, van Ingen KM, Mijnheer BJ. The effect of breathing and set-up errors on the cumulative dose to a lung tumor. Radiother Oncol 2001; 60(1):95–105.

12. Kung JH, Zygmanski P, Choi N, Chen GT. A method of calculating a lung clinical target volume DVH for IMRT with intrafractional motion. Med Phys 2003; 30(6):1103–9.

13. Chui CS, Yorke E, Hong L. The effects of intra-fraction organ motion on the delivery of intensity-modulated field with a multileaf collimator. Med Phys 2003; 30(7):1736–46.

14. Zhang T, Jeraj R, Keller H, et al. Treatment plan optimization incorporating respiratory motion. Med Phys 2004; 31(6):1576–86.

15. Lu W, Chen ML, Olivera GH, Ruchala KJ, Mackie TR. Fast free-form deformable registration via calculus of variations. Phys Med Biol 2004; 49(14):3067–87.

16. Keall PJ, Siebers JV, Joshi S, Mohan R. Monte Carlo as a four-dimensional radiotherapy treatment-planning tool to account for respiratory motion. Phys Med Biol 2004; 49(16):3639–48.

17. Wang H, Dong L, Lii MF, et al. Implementation and validation of a three-dimensional deformable registration algorithm for targeted prostate cancer radiotherapy. Int J Radiat Oncol Biol Phys 2005; 61(3):725–35.

18. Pan T, Lee TY, Rietzel E, Chen GT. 4D-CT imaging of a volume influenced by respiratory motion on multi-slice CT. Med Phys 2004; 31(2):333–40.

19. Shirato H, Suzuki K, Sharp GC, et al. Speed and amplitude of lung tumor motion precisely detected in four-dimensional setup and in real-time tumor-tracking radiotherapy. Int J Radiat Oncol Biol Phys 2006; 64(4):1229–36.

20. Kitamura K, Shirato H, Shimizu S, et al. Registrat-ion accuracy and possible migration of internal fiducial gold marker implanted in prostate and liver treated with real-time tumor-tracking radiation therapy (RTRT). Radiother Oncol 2002; 62 (3):275–81.

21. Wulf J, Hadinger U, Oppitz U, Thiele W, Flentje M. Impact of target reproducibility on tumor dose in stereotactic radiotherapy of targets in the lung and liver. Radiother Oncol 2003; 66(2):141–50.

22. Vedam SS, Kini VR, Keall PJ, Ramakrishnan V, Mostafavi H, Mohan R. Quantifying the predictability of diaphragm motion during respiration with a noninvasive external marker. Med Phys 2003; 30(4):505–13.

23. Verellen D, Soete G, Linthout N, et al. Quality assurance of a system for improved target localization and patient set-up that combines real-time infrared tracking and stereoscopic X-ray imaging. Radiother Oncol 2003; 67(1):129–41.

24. Takai Y, Mitsuya M, Nemoto K. Development of a Real-time tumor tracking system with dmlc with dual X-ray fluoroscopy and amorphous silicon flat planel on the gantry of the linear accelerator. Int J Radiat Oncol Biol Phys 2002; 54 (Suppl.):193–4.

25. Wong J. Methods to manage respiratory motion in radiation treatment. In: Palta JR, Mackie TR, eds. Medical physics publishing. Madison WI: American Association of Physics in Medicine (AAPM), 2003.

26. Britton KR, Takai Y, Mitsuya M, Nemoto K, Ogawa Y, Yamada S. Evaluation of inter- and intrafraction organ motion during intensity modulated radiation therapy (IMRT) for localized prostate cancer measured by a newly developed on-board image-guided system. Radiat Med 2005; 23(1):14–24.

27. Joseph J, Adler JR, Cox R. Linear accelerator-based stereotactic radiosurgery for brain metastases: The influence of number of lesions on survival. J Clin Oncol 1996; 14:1085–92.

28. Gwak HS, Yoo HJ, Youn SM, et al. Hypofractionated stereotactic radiation therapy for skull base and upper cervical chordoma and chondrosarcoma: preliminary results. Stereotact Funct Neurosurg 2005; 83(5–6):233–43.

29. Bradley J, Graham MV, Winter K, et al. Toxicity and outcome results of RTOG 9311: a phase I-II dose-escalation study using three-dimensional conformal radiotherapy in patients with inoperable non-small-cell lung carcinoma. Int J Radiat Oncol Biol Phys 2005; 61(2):318–28.

30. Gerszten PC, Ozhasoglu C, Burton SA, et al. Evaluation of CyberKnife frameless real-time image-guided stereotactic radiosurgery for spinal lesions. Stereotact Funct Neurosurg 2003; 81(1–4):84–9.

31. Degen JW, Gagnon GJ, Voyadzis JM, et al. CyberKnife stereotactic radiosurgical treatment of spinal tumors for pain control and quality of life. J Neurosurg Spine 2005; 2(5):540–9.

32. Chang SD. The CyberKnife®: Potential in patients with cranial and spinal tumors. Amer J Cancer 2005; 4(6):383–93.

33. Murphy MJ, Adler JR, Jr., Bodduluri M, et al. Image-guided radiosurgery for the spine and pancreas. Comput Aided Surg 2000; 5(4):278–88.

34. Whyte RI, Crownover R, Murphy MJ, et al. Stereotactic radiosurgery for lung tumors: preliminary report of a phase I trial. Ann Thorac Surg 2003; 75(4): 1097–101.

35. Yan D, Jaffray DA, Wong JW. A model to accumulate fractionated dose in a deforming organ. Int J Radiat Oncol Biol Phys 1999; 44(3):665–75.

36. Dawson LA, Brock KK, Kazanjian S, et al. The reproducibility of organ position using active breathing control (ABC) during liver radiotherapy. Int J Radiat Oncol Biol Phys 2001; 51(5):1410–21.

37. Wang H, Dong L, O'Daniel J, et al. Validation of an accelerated 'demons' algorithm for deformable image registration in radiation therapy. Phys Med Biol 2005; 50(12):2887–905.

38. Keall PJ, Joshi S, Vedam SS, Siebers JV, Kini VR, Mohan R. Four-dimensional radiotherapy planning for DMLC-based respiratory motion tracking. Med Phys 2005; 32(4):942–51.

39. Schaly B, Bauman GS, Battista JJ, Van Dyk J. Validation of contour-driven thin-plate splines for tracking fraction-to-fraction changes in anatomy and radiation therapy dose mapping. Phys Med Biol 2005; 50(3):459–75.

40. Wang H, Dong L, O'Daniel J, et al. Validation of an accelerated 'demons' algorithm for deformable image registration in radiation therapy. Phys Med Biol 2005; 50(12):2887–905.

41. Thirion JP. Image matching as a diffusion process: an analogy with Maxwell's demons. Med Image Anal 1998; 2(3):243–60.

42. Lu J, Zhu XR, Munro P, Chi P-cM, Mohan R, Pan T. Amplitude correlated 4-dimensional cone beam CT. In: Flynn MJ, Hsieh J, eds. Medical Imaging 2006: Physics of Medical Imaging;2006: SPIE, 2006:61422I.

43. Wang H, O'Daniel J, Ahamad A, Garden A, Mohan R, Dong L. Automatic contour delineation on subsequent CT images using deformable registration: TU-C-J-6B-09. Med Phys 2005; 32(6):2084.

44. Vedam SS, Keall PJ, Kini VR, Mostafavi H, Shukla HP, Mohan R. Acquiring a four-dimensional computed tomography dataset using an external respiratory signal. Phys Med Biol 2003; 48(1):45–62.

45. Keall P. 4-dimensional computed tomography imaging and treatment planning. Semin Radiat Oncol 2004; 1:81–90.

46. Underberg RW, Lagerwaard FJ, Cuijpers JP, Slotman BJ, van Sornsen de Koste JR, Senan S. Four-dimensional CT scans for treatment planning in stereotactic radiotherapy for stage I lung cancer. Int J Radiat Oncol Biol Phys 2004; 60(4): 1283–90.

47. Yan D, Wong J, Vicini F, et al. Adaptive modification of treatment planning to minimize the deleterious effects of treatment setup errors. Int J Radiat Oncol Biol Phys 1997; 38(1):197–206.

48. Kitamura K, Shirato H, Seppenwoolde Y, et al. Three-dimensional intrafractional movement of prostate measured during real-time tumor-tracking radiotherapy in supine and prone treatment positions. Int J Radiat Oncol Biol Phys 2002; 53(5): 1117–23.

49. Timmerman R, Papiez L, McGarry R, et al. Extracranial stereotactic radioablation: results of a phase I study in medically inoperable stage I non-small cell lung cancer. Chest 2003; 124(5):1946–55.

50. Giraud P, De Rycke Y, Dubray B, et al. Conformal radiotherapy (CRT) planning for lung cancer: analysis of intrathoracic organ motion during extreme phases of breathing. Int J Radiat Oncol Biol Phys 2001; 51(4):1081–92.

51. Ekberg L, Holmberg O, Wittgren L, Bjelkengren G, Landberg T. What margins should be added to the clinical target volume in radiotherapy treatment planning for lung cancer? Radiother Oncol 1998; 48(1):71–7.

52. van Sornsen de Koste JR, Lagerwaard FJ, Nijssen-Visser MR, Graveland WJ, Senan S. Tumor location cannot predict the mobility of lung tumors: a 3D analysis of data generated from multiple CT scans. Int J Radiat Oncol Biol Phys 2003; 56(2): 348–54.

53. Plathow C, Ley S, Fink C, et al. Analysis of intrathoracic tumor mobility during whole breathing cycle by dynamic MRI. Int J Radiat Oncol Biol Phys 2004; 59(4): 952–9.

54. Kini VR, Vedam SS, Keall PJ, Patil S, Chen C, Mohan R. Patient training in respiratory-gated radiotherapy. Med Dosim 2003; 28(1):7–11.

55. Mageras GS, Pevsner A, Yorke ED, et al. Measurement of lung tumor motion using respiration-correlated CT. Int J Radiat Oncol Biol Phys 2004; 60(3):933–41.

56. Underberg RW, Lagerwaard FJ, van Tinteren H, Cuijpers JP, Slotman BJ, Senan S. Time trends in target volumes for stage I non-small-cell lung cancer after stereotactic radiotherapy. Int J Radiat Oncol Biol Phys 2006; 64(4):1221–8.

57. Butler LE, Forster KM, Stevens CW, et al. Dosimetric benefits of respiratory gating: a preliminary study. J Appl Clin Med Phys 2004; 5(1):16–24.

58. van der Geld YG, Senan S, van Sornsen de Koste JR, et al. Evaluating mobility for radiotherapy planning of lung tumors: a comparison of virtual fluoroscopy and 4DCT. Lung Cancer 2006; 53(1):31–7.

59. Ross CS, Hussey DH, Pennington EC, Stanford W, Doornbos JF. Analysis of movement of intrathoracic neoplasms using ultrafast computerized tomography. Int J Radiat Oncol Biol Phys 1990; 18(3):671–7.

60. Shirato H, Seppenwoolde Y, Kitamura K, Onimura R, Shimizu S. Intrafractional tumor motion: lung and liver. Semin Radiat Oncol 2004; 14(1):10–18.

61. Cover KS, Lagerwaard FJ, Senan S. Color intensity projections: a rapid approach for evaluating four-dimensional CT scans in treatment planning. Int J Radiat Oncol Biol Phys 2006; 64(3):954–61.

62. Underberg RW, Lagerwaard FJ, Slotman BJ, Cuijpers JP, Senan S. Benefit of respiration-gated stereotactic radiotherapy for stage I lung cancer: an analysis of 4DCT datasets. Int J Radiat Oncol Biol Phys 2005; 62(2):554–60.

63. George R, Chung TD, Vedam SS, et al. Audio-visual biofeedback for respiratory-gated radiotherapy: impact of audio instruction and audio-visual biofeedback on respiratory-gated radiotherapy. Int J Radiat Oncol Biol Phys 2006; 65(3):924–33.

64. Kupelian PA, Komaki R, Allen P. Prognostic factors in the treatment of node-negative nonsmall cell lung carcinoma with radiotherapy alone. Int J Radiat Oncol Biol Phys 1996; 36(3):607–13.

65. Werner-Wasik M, Xiao Y, Pequignot E, Curran WJ, Hauck W. Assessment of lung cancer response after nonoperative therapy: tumor diameter, bidimensional product, and volume. A serial CT scan-based study. Int J Radiat Oncol Biol Phys 2001; 51(1):56–61.

66. Erridge SC, Seppenwoolde Y, Muller SH, et al. Portal imaging to assess set-up errors, tumor motion and tumor shrinkage during conformal radiotherapy of non-small cell lung cancer. Radiother Oncol 2003; 66(1):75–85.

67. Kupelian PA, Ramsey C, Meeks SL, et al. Serial megavoltage CT imaging during external beam radiotherapy for non-small-cell lung cancer: Observations on tumor regression during treatment. Int J Radiat Oncol Biol Phys 2005; 63(4):1024–8.

68. Bosmans G, van Baardwijk A, Dekker A, et al. Intra-patient variability of tumor volume and tumor motion during conventionally fractionated radiotherapy for locally advanced non-small-cell lung cancer: a prospective clinical study. Int J Radiat Oncol Biol Phys 2006; 66(3):748–53.

69. Mechalakos JG, Mageras GS, Zelefsky MJ, et al. Time trends in organ position and volume in patients receiving prostate three-dimensional conformal radiotherapy. Radiother Oncol 2002; 62(3):261–5.

70. Schwarz M, Van der Geer J, Van Herk M, Lebesque JV, Mijnheer BJ, Damen EM. Impact of geometrical uncertainties on 3D CRT and IMRT dose distributions for lung cancer treatment. Int J Radiat Oncol Biol Phys 2006; 65(4):1260–9.

Respiratory-Gated Radiation Therapy

George Starkschall
Department of Radiation Physics, University of Texas M.D. Anderson Cancer Center, Houston, Texas, U.S.A.

INTRODUCTION

Conventional radiation treatment planning is based on the assumption that a single computed tomography (CT) image data set, acquired up to several days before the initiation of radiation treatment, will accurately reflect the patient geometry during the entire course of the radiation treatment. That is, conventional planning techniques assume that nothing about the patient or tumor will move, either during a single treatment or from treatment to treatment.

In reality, this is not the case. Indeed, several types of motion occur in patients during radiation treatment. The first type is interfractional motion, or interfractional variation. This type of motion reflects the daily changes that occur in patient anatomy, such as weight gain or loss, tumor regression, and bladder and rectal filling and emptying (1,2). Such motion can be assessed by a variety of methods, including B-mode ultrasonography, in-room CT, kilovoltage imaging, and cone-beam CT. The effects of interfractional variation and how various modalities can be used to account for them are addressed elsewhere in this book.

The second type of motion is intrafractional motion, or physiologic motion that occurs during the actual delivery of a single radiation treatment. Intrafractional motion includes such movements as those induced by respiration, cardiac rhythms, or peristalsis.

Respiratory motion is a particularly challenging clinical problem, and in the past few years, many clinical approaches have been introduced to either account for its effects or mitigate its magnitude. One such approach is the use of respiratory-gated radiation therapy. In this chapter, we attempt to provide answers to the following questions about this approach:

1. What is respiratory-gated radiation therapy?
2. Why might we need respiratory-gated radiation therapy?
3. How do we plan for respiratory-gated radiation therapy?
4. How do we deliver respiratory-gated radiation therapy?
5. Does respiratory-gated radiation therapy have the potential to improve the quality of radiation treatment?
6. Does respiratory-gated radiation therapy actually improve the quality of radiation treatment?
7. How can we improve the quality of respiratory-gated radiation therapy?

WHAT IS RESPIRATORY-GATED RADIATION THERAPY?

Respiratory gating is a technique used to mitigate the effects of respiratory motion. It works by synchronizing the delivery of radiation with a specified condition of the respiratory cycle (3). The two types of respiratory gating are amplitude (or displacement) gating, in which the delivery of radiation is gated based on the position of either the actual tumor or a surrogate for the tumor, and phase gating, in which the delivery of radiation is gated based on the phase of the respiratory cycle. Figure 1 is an illustration of a respiratory signal gated according to the position of an external fiducial surrogate. The horizontal lines in the lower graph indicate amplitude-based gates. When the motion of the external fiducial indicates that the respiratory cycle lies within the gate, a signal is sent to the linear accelerator, initiating beam delivery. Similarly, when the fiducial marker moves outside the gate, another signal is sent to the accelerator, terminating beam delivery.

It is important to differentiate between two terms in common use, respiratory gating and respiratory correlation, because they are not synonymous and are sometimes incorrectly interchanged. Respiratory gating is the act of synchronizing some action, typically beam delivery, to a point or portion of the respiratory cycle, while respiratory correlation is the act of associating some component of imaging or treatment with the respiratory cycle. Thus, respiratory gating is a subset of respiratory correlation, but respiratory gating and respiratory correlation are not the same.
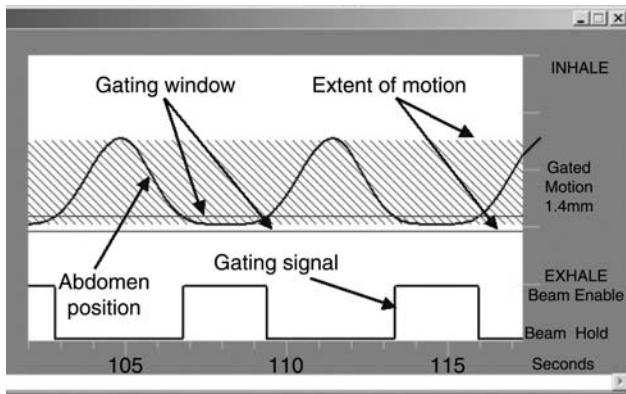
Figure 1 A gated respiratory signal as indicated by an external fiducial surrogate. The horizontal lines indicate amplitude-based gates, and the vertical lines indicate times for opening and closing the gates.

WHY MIGHT WE NEED RESPIRATORY-GATED RADIATION THERAPY?

The impetus for gating the delivery of radiation is based on the fact that lung tumors move. The extent of motion can be marked, even exceeding 2 cm in some cases (4–6). However, predicting the extent of this motion is not straightforward. Recent four-dimensional CT (4D-CT) studies of tumor motion have indicated wide variability in its magnitude, with an average vector displacement in the range of 0.5–1 cm (7). Moreover, it has been shown that neither the magnitude nor the direction of motion can be predicted based on tumor stage, tumor location, or pulmonary function test results (8). Although in general small tumors move more than large tumors and tumors in the lower lobes move more than those in the upper lobes, the extent and trajectory of motion must be determined for each patient. Figure 2 illustrates a coronal image of a thorax reconstructed using binned data from a single phase in a 4D-CT image data set. Superimposed on this image are two outlines of a lung tumor, one drawn on an end-inspiration data set and the other on an end-expiration data set. The shift in the outline indicates the how far a lung tumor may move during respiration.

To account for respiratory motion, the standard of practice has been to surround the clinical target volume (CTV) with a large, isotropic margin that is sufficient to account for both respiratory motion and setup uncertainty. This margin has been the same value for each patient. However, tumor motion differs between patients. Thus, the use of a single margin value means that for some patients with a large magnitude of tumor motion, the radiation field may be insufficient, resulting in inadequate tumor coverage, while for other patients with little or no tumor motion, the field is likely to be too large, resulting in

irradiation of an unacceptable amount of uninvolved lung tissue. Furthermore, since respiration-induced tumor motion is approximately linear, isotropic expansion of the CTV will result in the unnecessary irradiation of even more lung tissue.

Recently, 4D-CT images, which explicitly account for respiratory motion, have been used to calculate internal target volumes (ITV) and thereby decrease the size of treatment portals (Balter et al. Manuscript in progress). By gating the delivery of radiation, it may be possible to decrease the size of the treatment portal even more, possibly improving lung sparing (9,10). Conversely, if the treatment portal can be reduced, then it might be possible to escalate the dose to the tumor while keeping the dose to normal tissue the same as that in ungated treatments (11). Moreover, it has been hypothesized that even if the size of the treatment portal cannot be reduced, gating the delivery of radiation may allow the volume of lung moving into and out of the treatment portal to be reduced, thus reducing the dose to normal lung.

While the potential benefits of gating for conventional photon radiation therapy are great, the potential benefits of gating for proton radiation therapy are even greater due to the finite penetration of the proton beam. Respiration may affect the radiologic depth of the distal edge of the target volume, with consequential effects on the range of the proton beam. Proton radiation gating may be designed to ensure dose administration according to the location of dose fall-off along the central axis of the proton beam, thus ensuring precise delivery of the radiation.

HOW DO WE PLAN FOR RESPIRATORY-GATED RADIATION THERAPY?

The first step in planning for respiratory-gated radiation therapy is to acquire information about the tumor's motion by generating a CT image data set. The state-of-the-art method for creating that set is 4D-CT. This method is preferred to gated CT acquisition because it is able to provide more reliable and detailed data about the patient's respiratory cycle, which is related to the method by which the scanned images are obtained. In gated CT image acquisition, a respiratory signal triggers the acquisition of a CT image in a single gantry rotation at a specified point in the respiratory cycle. The CT scanner operates in axial mode. When the desired phase is reached in a subsequent respiratory cycle, projections are obtained in another single gantry rotation and reconstructed. This process continues until the entire desired region has been scanned. Thus in gated CT, information is

Figure 2   Coronal reconstruction of a 4D thoracic CT data set at end inspiration. The red area is the GTV at end inspiration, while the green area is the GTV contoured on the end expiration data set and transferred onto the end inspiration data set. *Abbreviations*: 4D, four-dimensional; CT, computed tomography; GTV, gross tumor volume.

obtained at a single phase. If information about multiple phases of the respiratory cycle is desired, then the image acquisition process is repeated with the gate set to a different phase.

Because this process is cumbersome and yields information about only one phase at a time, gated CT image acquisition has largely been replaced by 4D-CT image acquisition. In 4D-CT phase-dependent CT image data sets are obtained based on periodic patient motion, such as respiratory motion. Because the "fourth dimension" in 4D-CT is the phase of the respiratory cycle rather than time, the images are phase-dependent rather than time-dependent. A 4D-CT data set, then, consists of a set of multiple 3D data sets, each of which will cover a specific phase in the respiratory cycle (8–10 phases are typically imaged).

The general approach to 4D image acquisition involves the acquisition of a limited set of image data at specific phases in each of several respiratory cycles. CT information is acquired over a region limited by the width of the CT detector. For many multislice helical CT scanners, this width is in the range 2.5–4.0 cm. Image data obtained at the same phase but during different respiratory cycles are eventually combined to generate the full 4D image data set.

Two approaches to 4D-CT imaging have been developed. The first approach uses image binning (IB) (12), and the second approach uses projection binning (PB) (13). While it is possible to acquire 4D-CT images using a single-slice scanner, that technique is difficult; thus, both IB and PB require a multislice CT scanner. Both these 4D imaging techniques also require a device that can monitor the respiratory cycle, as discussed in the following section.

In the IB approach, the CT scanner is operated in cine mode. Projections are acquired for a period

of time at least equal to that of one respiratory cycle plus a gantry rotation. After this period, the table is indexed and the next set of projections is acquired. At each table position, images are reconstructed at specified time intervals, which usually are set to equal approximately half the gantry rotation time, thus a typical interval is ~0.25 sec. Typically, ~2000–2500 images are acquired in all. However, adjustments may be called for. For example, the time interval may have to be increased because of limits on the number of CT images that can be acquired. After image acquisition, the image acquisition times are correlated to the respiratory signal and the images are binned according to the phase of the respiratory cycle.

In the PB approach, the CT scanner is operated in helical mode at a very low pitch. The low pitch is required to ensure that the table moves sufficiently slowly that the entire width of the CT detector will be present to image a transverse region of the patient during an entire respiratory cycle. The relationship between pitch and respiratory rate is given by the following equation:

$$\text{pitch} \leq \frac{\text{gantry rotation time (sec)} \times \text{respiratory rate } (\text{min}^{-1})}{60 \text{ sec/min}}$$

Because of the low pitch, many projections are acquired, resulting in a data file of several GBytes. The projections are tagged at the same phase point in each respiratory cycle, typically at end-inspiration (0% phase). After the projections have been acquired, phases for reconstruction (typically at 10% intervals) are determined. The projections acquired near each phase interval are binned together, and the images are then reconstructed.
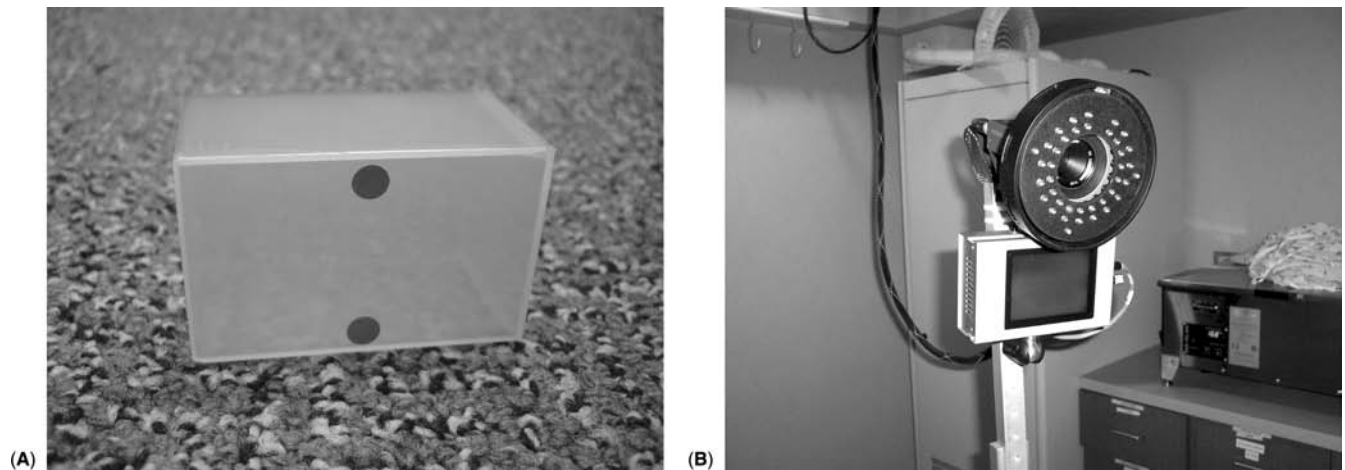
Figure 3 A respiratory monitor that uses external fiducials to track respiratory motion. (**A**) A plastic box containing two reflectors 3 cm apart is attached to the patient's anterior abdominal or thoracic surface. (**B**) An infrared light source and a CCD camera are used to track the reflectors. *Abbreviation*: CCD, charge-coupled device.

To summarize, the IP approach first reconstructs the images and then bins them, while the PB approach first bins the projections and then reconstructs them.

The ideal next step would be to perform a 4D dose calculation on an appropriate subset of the CT scans to mimic the gated beam delivery. The 4D dose calculation would calculate the dose on each phase of the CT data set, take the dose calculation points from a reference phase, and then recalculate the doses to those points on the other phases based on an appropriate form of deformable image registration (14). Doses accumulated on each phase would then be summed to obtain the composite 4D dose calculation.

This technique has not yet been implemented in commercial radiation treatment planning systems, however, so the 4D image data set is presently used primarily for tumor targeting. The 4D image data set is acquired, and an ITV is determined based on the extent of motion of the gross tumor volume (GTV) as demonstrated in the 4D data set (15). The ITV is expanded by a specified amount to account for uncertainties in setup and gating position to generate a planning target volume (PTV). The PTV is then transferred to a composite average CT image for treatment planning and dose calculation.

HOW DO WE DELIVER RESPIRATORY-GATED RADIOTHERAPY?

The technology that enables gated delivery of radiation is a respiratory monitor. The most commonly used respiratory monitor tracks motion of the anterior abdominal surface as a surrogate for respiratory motion. One such device (RPM, Varian Oncology Systems, Palo Alto, California) tracks the motion of a

plastic box with two reflective markers (Fig. 3A) placed on the anterior surface of the patient's chest or abdomen. The reflectors' position is tracked by an infrared light source and charge-coupled device (CCD) camera mounted in the treatment room (Fig. 3B). The position of one reflector is displayed on a monitor at the treatment console, allowing the operator to set the respiratory gate. When the position of this reflector passes the gate threshold, a signal is sent to the linear accelerator, initiating beam delivery; when the reflector moves out of the gate, another signal is sent, terminating beam delivery. The respiratory trace in Figure 1 is labeled to show how the respiratory gate is set and when the signal initiating beam delivery is sent.

Other types of respiratory monitors are also used. A spirometer (Fig. 4) monitors respiration by measuring airflow. With appropriate calibration, it can be used to measure respiratory volume and, hence, position in the respiratory cycle. Lu et al. (16) have suggested that a spirometer more accurately depicts

Figure 4 A spirometer used to track respiratory motion.

the respiratory cycle than an external fiducial marker, although the spirometer is subject to signal drift (17). A bellows device or a strain gauge placed around the patient's abdomen measures abdominal motion, which can then serve as a surrogate for respiratory phase. All these methods are surrogates for tumor position, and so their accuracy must be validated (18).

More direct tracking of tumor position for gating the delivery of radiation has been accomplished by radiographic imaging of small gold fiducials implanted near tumors (19). A new technology that uses electromagnetic tracking of implanted fiducials (20) may have an application in tracking the motion of lung tumors during respiration. The advantage of electromagnetic tracking over radiographic tracking is that the former confers no radiation dose. Limiting the use of electromagnetic devices, however, is the fact that current implantable transponders are substantially larger (at ~1 cm long) than current implantable gold fiducial markers (at ~3 mm long).

DOES RESPIRATORY-GATED RADIOTHERAPY HAVE THE POTENTIAL TO IMPROVE THE QUALITY OF RADIATION TREATMENT?

Several studies have been undertaken to determine whether respiratory-gated radiation therapy actually improves the quality of radiation treatment. Barnes et al. (21) and Butler et al. (9) compared free-breathing treatment plans with those for which GTV values were determined from breath-hold CT scans. Barnes et al. compared free-breathing and deep-inspiration breath-hold plans, while Butler et al. compared free-breathing plans to plans using breath-hold at normal end expiration, normal end inspiration, and deep inspiration. In both studies, the PTVs for the free-breathing plans were generated by assuming isotropic expansion of the CTV to allow for both setup uncertainty and intrafractional motion. Both investigations found that the breath-hold plans reduced the amount of irradiated normal lung. Figure 5, taken from the work of Butler et al. (9), shows that gating at appropriate points in the respiratory cycle could reduce the amount of irradiated lung by 30% in some cases.

With the introduction of 4D-CT imaging into the radiation oncology clinic, it became possible to track tumor motion during the respiratory cycle and explicitly account for respiratory motion in the delineation of the ITV. Starkschall et al. (10) compared treatment plans for which the treatment portals were based on ITVs obtained from explicit delineation of tumor excursion with plans for which treatment portals were based on breath-hold GTVs. Using V20 (the volume of lung receiving 20 Gy or more) as a measure of lung toxicity (22), they found a reduction in V20 by at least 10% only in patients with small
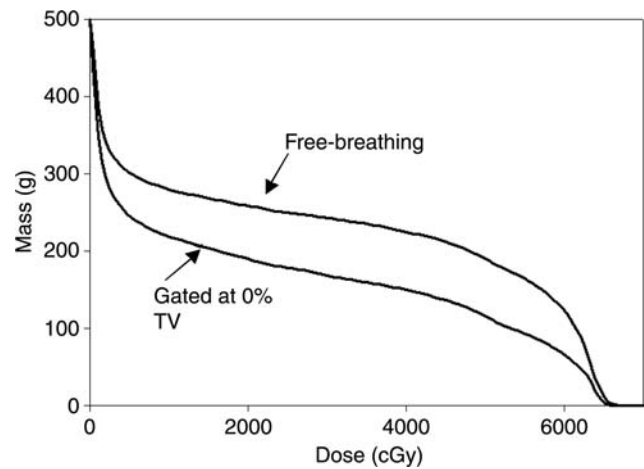
Figure 5 Dose-mass histograms for a treatment plan based on isotropic expansion of the CTV to generate a PTV (line labeled "free-breathing") and a treatment plan based on explicit delineation of the CTV at specific phase of the respiratory cycle (line labeled "gated at 0% TV"); the area between the lines represents the potential reduction in the mass of lung irradiated if gating is used. *Abbreviations*: CTV, clinical target volume; PTV, planning target volume; TV, target volume.

tumors (GTV $<100\,cm^3$) that moved with respiration (excursion >1 cm), provided that the residual motion during gating was kept small.

Recently, Lai and Starkschall (23) tested the hypothesis that even if margins were not reduced for gated delivery (24), the decrease in volume of lung moving into and out of the high-dose region would improve lung sparing. In this study, the authors analyzed a cohort of 25 patients whose original treatment plans had been created using 4D-CT imaging; the investigators repeated the dose calculations using the original beam configuration on the 10 phases that comprised the 4D-CT data set using a beta version of the treatment planning software that supported dose calculations across multiple phases of a 4D data set (Pinnacle^3, v7.9u, Philips Medical Systems, Milpitas, CA). The same beam configuration was then used to calculate the radiation dose on three phases (40%, 50%, and 60%) that simulated radiation treatment gated at end-expiration, and the radiation doses to the lung were then compared. Typical reductions in V20, indicating improved lung sparing, were in the range of 1% to 2%, certainly not a clinically significant value.

DOES RESPIRATORY-GATED RADIOTHERAPY ACTUALLY IMPROVE THE QUALITY OF RADIATION TREATMENT?

The question that needs to be asked, then, is whether or not gating actually improves the quality of

radiation treatment. To determine the answer to this question, Nelson et al (24) undertook a study in which small gold fiducials (NMPE, Inc., Lynnwood, WA) were implanted near the tumor. Fiducials were imaged weekly during 4D-CT image acquisition and daily during gated delivery using an electronic portal imaging device operating in cine mode, with images acquired in 2-sec intervals.

Nelson et al. (24) showed that residual motion under respiratory gating could be significant (up to 0.5 cm) but that setup uncertainties were at least as large as, if not greater than, residual motion under gating. Setup uncertainties required margins of at least 0.7–1.0 cm surrounding the measured ITV to ensure adequate tumor coverage. Consequently, efforts to reduce setup uncertainty are likely to have a markedly greater impact on reducing margins than respiratory gating.

It is also unclear how accurately surrogates for respiratory motion actually represent the extent of motion. For example, the motion of the anterior abdominal surface is approximately linear, so external fiducial markers that reflect this motion may not accurately reflect the three-dimensional motion of a tumor. On one hand, such inaccuracy may not be a problem, especially regarding the control of gating beam delivery at an endpoint of the respiratory cycle. On the other hand, there may be a time difference between the motions of the external patient surface and the internal tumor. Although both these motions are driven by the single motion of the diaphragm, the elasticity of lung tissue may cause a tumor in the upper lobe to move later than the diaphragm and the fiducial marker. Ongoing work is seeking to understand the temporal aspects of tumor and marker motion, and planning systems soon will be able to account for any time lags by incorporating correction algorithms based on tumor position, patient factors, and possibly other features.

HOW CAN WE IMPROVE THE QUALITY OF RESPIRATORY-GATED RADIATION THERAPY?

Margins placed around the CTV to generate the PTV arise from two major sources of uncertainty of tumor location: uncertainty resulting from patient setup and uncertainty resulting from residual motion. Thus, to improve the quality of respiratory-gated radiation therapy, both setup uncertainty and residual motion must be reduced.

As shown by Nelson et al. (24), setup uncertainty is the primary contribution to the need for margins surrounding the CTV; consequently, methods for reducing setup uncertainty should be applied before residual motion is addressed. Setup uncertainty can be reduced by improving patient immobilization and incorporating image guidance into the patient setup. Immobilization can be improved by using an extended vacuum bag indexed to the table (Fig. 6A) or by incorporating leg immobilization along with upper body immobilization (Fig. 6A). Image guidance can also be used, through the use of either on-board kilovoltage imaging (Fig. 7A) or some sort of in-room CT scanning; the latter option may consist of a conventional CT scanner placed on rails (25) (Fig. 7B) or a kilovoltage imaging system capable of cone-beam CT scanning. Improvements in immobilization can reduce margins that account for setup uncertainty to ~3 mm.

Once setup uncertainty has been reduced, the problem of residual tumor motion can be addressed. One possible approach is the use of a breath-hold maneuver, and several breath-hold techniques have been attempted in the effort to reduce tumor motion.
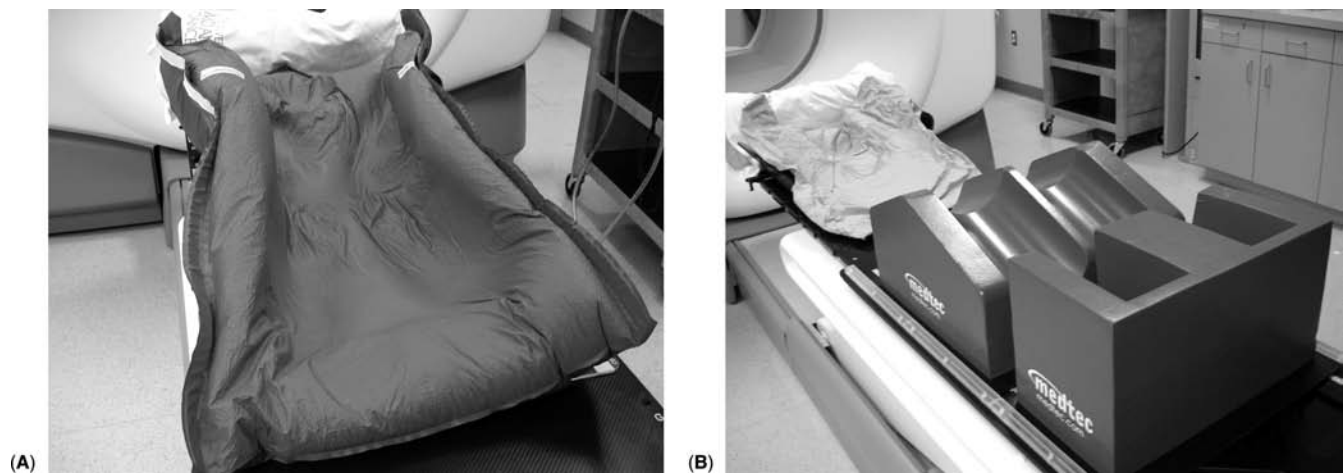
Figure 6   Immobilization devices used for reducing setup uncertainty in thoracic radiation therapy. (**A**) An extended vacuum bag indexed to the table. (**B**) A shoulder and leg immobilization device.
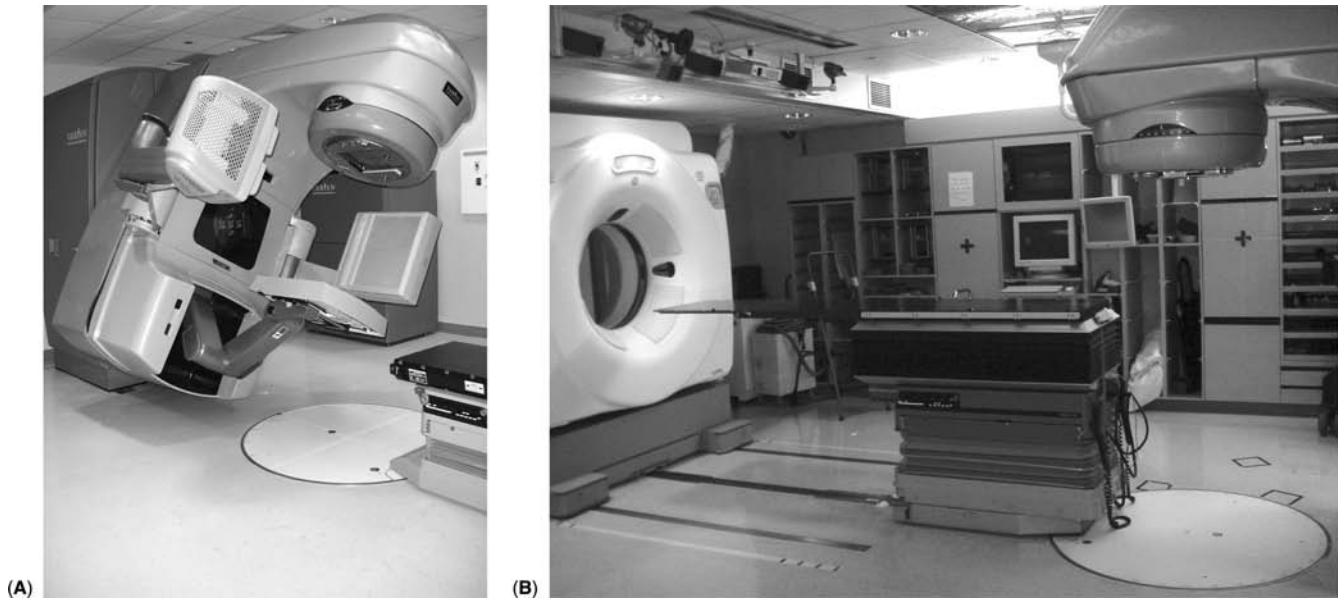
Figure 7 Devices used to implement image-guided setup to reduce setup uncertainty in thoracic radiation therapy. (**A**) A kilovoltage imaging device attached to the gantry of the linear accelerator. (**B**) An in-room CT scanner that shares a common the treatment table with the linear accelerator. *Source*: Courtesy of P. Balter (**A**) and T. Diel (**B**), M.D. Anderson Cancer Center.

For example, Hanley et al. (26) have investigated the use of a voluntary deep-inspiration breath hold to reduce tumor motion, but this technique does not guarantee that the breath hold occurs at the same place in the respiratory cycle. Wong et al. (27) have used an occlusion spirometer to force a breath hold at a specified point in the respiratory cycle. The experience with forced breath hold, however, has been with patients who have tumors in locations other than the lung, such as Hodgkin's lymphoma and liver cancer. It is not clear that a forced breath is effective in lung cancer patients, whose breathing may be compromised. Nelson et al. (28) have investigated the feasibility of using a feedback-guided breath hold. In this technique, the patient can view his or her respiratory trace, typically with a set of virtual reality goggles. The patient is then trained to effect a breath hold in a very narrow gating window. The extent to which residual tumor motion is reduced using this technique has not yet been determined, however.

CONCLUSIONS

Because respiration can cause tumors to move several centimeters, depending on the tumor location and patient factors, gating the delivery of radiation to the respiratory cycle can enable us to shrink treatment margins; consequently, we may then be able to increase the radiation dose to the tumor, decrease morbidity, or both. However, before respiratory gating can be deemed a useful technique in photon radiation therapy, several conditions need to be met. The first condition will be reflected in patient selection: Respiratory gating appears to be useful only for those patients with small tumors that move. The second condition is that the surrogate for respiratory motion must accurately reflect the tumor's position. This requirement may necessitate the use of fiducials implanted near the tumor. The final condition that must be met to make respiratory gating clinically effective is that it be combined with measures to reduce setup uncertainty and residual respiratory motion. Consequently, some sort of image-guided setup would be likely, along with the use of a breath-hold maneuver during treatment delivery.

Respiratory gating may be particularly suited to hypofractionated radiation therapy for stages I and II lung tumors, as these are likely to be the small tumors most affected by respiratory motion. Promising applications also may occur in proton therapy, as the range of the protons may be markedly affected by changes in tumor or tissue positions due to respiratory motion, but this possibility remains to be demonstrated dosimetrically. Finally, respiratory gating may be useful in the treatment of subdiaphragmatic tumors exhibiting marked respiratory motion, such as those in the liver, although again, dosimetric demonstration of such improvement is needed.

REFERENCES

1. Barker JL, Garden AS, Ang KK, et al. Quantification of volumetric and geometric changes occurring during fractionated radiotherapy for head-and-neck cancer using an integrated CT/linear accelerator system. Int J Radiat Oncol Biol Phys 2004; 59:960–70.

2. Huang E, Dong L, Chandra A, et al. Intrafraction prostate motion during IMRT for prostate cancer. Int J Radiat Oncol Biol Phys 2002; 53:261–8.

3. Ohara K, Okumura T, Akisada M, et al. Irradiation synchronized with respiration gate. Int J Radiat Oncol Biol Phys 1989; 17:853–7.

4. Ross CS, Hussey DH, Pennington EC, Stanford W, Doornbos JF. Analysis of movement of intrathoracic neoplasms using ultrafast computerized tomography. Int J Radiat Oncol Biol Phys 1990; 18:671–7.

5. Korin HW, Ehman RL, Riederer SJ, Felmlee JP, Grimm RC. Respiratory kinematics of the upper abdominal organs: A quantitative study. Magn Reson Med 1992; 23:172–8.

6. Davies SC, Hill AL, Holmes RB, Halliwell M, Jackson PC. Ultrasound quantitation of respiratory organ motion in the upper abdomen. Brit J Radiol 1994; 67:1096–102.

7. Liu HH, Balter P, Tutt T, Choi B, Zhang J, Wang C, Chi M, Luo D, Pan T, Hunjan S, Starkschall G, Rosen I, Prado K, Liao Z, Chang J, Komaki R, Cox JD, Mohan R, Dong L, "Assessing respiration-induced tumor motion and internal target volume using 4 DCT for radiation therapy of lung cancer," Int J Radiat Oncol Biol Phys 2007; 68:531–40.

8. Stevens CW, Munden RF, Forster KM, et al. Respiratory-driven lung tumor motion is independent of tumor size, tumor location, and pulmonary function. Int J Radiat Oncol Biol Phys 2001; 51:62–8.

9. Butler LE, Forster KM, Stevens CW, et al. Dosimetric benefits of respiratory gating: a preliminary study. J Appl Clini Med Phys 2004; 5:1–9.

10. Starkschall G, Forster KM, Kitamura K, Cardenas A, Stevens CW. Correlation of GTV excursion with the desirability of respiratory gating. Int J Radiat Oncol Biol Phys 2004; 60:1291–97.

11. Nelson C, Starkschall G, Chang JY. The potential for dose escalation resulting from reduction in margins used to generate the planning target volume. Int J Radiat Oncol Biol Phys 2006; 65:573–86.

12. Pan T, Lee TY, Rietzel E, Chen GTY. 4-D CT imaging of a volume influenced by respiratory motion on multi-slice CT. Med Phys 2004; 31:333–40.

13. Keall PJ, Starkschall G, Shukla H, et al. Acquiring 4D thoracic CT scans using a multislice helical method. Phys Med Biol 2004; 49:2053–67.

14. Kaus M, Pekar V, McNutt T, Bzdusek K. An efficient algorithm for image-based dose deformation and accumulations. Med Phys 2005; 32:1900 (abstract).

15. International Commission on Radiation Units and Measurements, Prescribing, recording, and reporting photon beam therapy (supplement to ICRU report 50), ICRU Report 62. Bethesda, MD: International Commission on Radiation Units and Measurements, 1999.

16. Lu W, Low DA, Parikh PJ, et al. Comparison of spirometry and abdominal height as four-dimensional computed tomography metrics in lung. Med Phys 2005; 32:2351–7.

17. Lu W, Parikh PJ, El Naqa IM, et al. Quantitation of the reconstruction quality of a four-dimensional computed tomography process for lung cancer patients. *Med Phys* 2005; 32:890–1.

18. Koch N, Liu HH, Starkschall G, et al. Evaluation of internal lung motion for respiratory-gated radiation therapy using magnetic resonance imaging (MRI). I—Correlation of motions of the internal anatomy and external fiducial. Int J Radiat Oncol Biol Phys 2004; 60:1459–72.

19. Shirato H, Shizumi S, Kitamura K, et al. Four-dimensional treatment planning and fluoroscopic real-time tumor tracking radiotherapy for moving tumor. Int J Radiat Oncol Biol Phys 2000; 48:435–42.

20. Balter JM, Wright JN, Newell LJ, et al. Accuracy of a wireless localization system for radiotherapy. Int J Radiat Oncol Biol Phys 2005; 61:933–7.

21. Barnes EA, Murray BR, Robinson DM, Underwood LJ, Hanson J, Roa WHY. Dosimetric evaluation of lung tumor immobilization using breath hold at deep inspiration. Int J Radiat Oncol Biol Phys 2001; 50:1091–8.

22. Graham MV, Purdy JA, Emami B, et al. Clinical dose-volume histogram analysys for pneumonitis after 3D treatment for non-small cell lung cancer (NSCLC). Int J Radiat Oncol Biol Phys 1999; 45:323–9.

23. Lai J, Starkschall G. The potential for dose reduction to normal lung in respiratory-gated radiation therapy. In Bissonnette J-P, ed., Proceedings of the XVth International Conference on the Use of Computers in Radiation Therapy, (Novel Digital Publishing, Oakville, Ontario, Canada, 2007) vol 2, pp. 124–8.

24. Nelson C, Starkschall G, Morice R, Stevens CW, Chang JY. Assessment of lung tumor motion during respiratory gating using implanted fiducials. Int J Radiat Oncol Biol Phys 2007; 67:915–23.

25. Court LE, Dong L. Automatic registration of the prostate for computed-tomography-guided radiotherapy. Med Phys 2003; 30:2750–7.

26. Hanley J, Debois MM, Mah D, et al. Deep inspiration breath-hold technique for lung tumors: the potential value of target immobilization and reduced lung density in dose escalation. Int J Radiat Oncol Biol Phys 1999; 45:603–11.

27. Wong JW, Sharpe MB, Jaffray DA, et al. The use of active breathing control (ABC) to reduce margin for breathing motion. Int J Radiat Oncol Biol Phys 1999; 44:911–19.

28. Nelson C, Starkschall G, Balter P, et al. Respiration-correlated treatment delivery using feedback-guided breath hold: a technical study. Med Phys 2005; 32:175–81.

Image-Guided Stereotactic Body Radiation Therapy for Early-Stage Non–Small Cell Lung Cancer

Joe Y. Chang
Department of Radiation Oncology, University of Texas M.D. Anderson Cancer Center, Houston, Texas, U.S.A.

Peter Balter
Department of Radiation Physics, University of Texas M.D. Anderson Cancer Center, Houston, Texas, U.S.A.

Ritsuko Komaki
Department of Radiation Oncology, University of Texas M.D. Anderson Cancer Center, Houston, Texas, U.S.A.

INTRODUCTION

Patients with early-stage non–small cell lung cancer (NSCLC) who cannot undergo surgery because of their lung function, cardiac function, bleeding tendency, or other comorbid conditions or who refuse surgery should be considered for definitive radiation therapy. Conventional fractionated radiotherapy (60–66 Gy in 1.8- or 2.0-Gy fractions) in these patients with stage I/II disease has resulted in 5-year local control rates of 30–50% and overall survival rates of 10–30% (1,2). Modern three-dimensional conformal radiotherapy (3D-CRT), however, may improve clinical outcome compared with two-dimensional radiotherapy (3). Several studies have reported a benefit from such a dose escalation, suggesting a dose–response relationship from the standpoint of both survival and local disease control in these patients (1,2,4,5). Because early-stage NSCLC is not inherently a systemic disease at the time of diagnosis and because local control is poor after conventional radiotherapy, research directed toward improving survival should put more emphasis on improving local tumor obliteration.

Three-dimenstional conformal radiotherapy and hypofractionated stereotactic body radiation therapy (SBRT) allow precise targeting and delivery of radiotherapy. SBRT for lung cancer integrates elements of 3D-CRT with systems for treating tumors in motion and for decreasing setup uncertainty through the use of image-guided radiation therapy (IGRT) techniques. These systems allow the reduction of treatment volumes, facilitate hypofractionation with markedly increased daily doses, and substantially reduce overall treatment time. Thus, SBRT combines multiple beam angles to achieve sharp dose gradients, high-precision localization, and a high dose per fraction in extracranial locations. This approach delivers a high biologically effective dose (BED) to the target while minimizing the normal tissue toxicities, which may translate into improved local control and survival rates. Preliminary data have shown local control rates of >85% and promising survival rates in patients with stage I NSCLC treated with SBRT. In this chapter, we discuss the rationale, indications, optimal BED, and image-guided techniques for SBRT in patients with NSCLC.

INDICATIONS FOR SBRT

In general, SBRT should be considered only for early-stage [stage I (T1–T2, N0, M0), selective stage II (T3 with chest wall involvement, N0, M0)], isolated, peripherally located recurrent or metastatic NSCLC. Because the ablative dose will be delivered to the target, the target should be away from critical structures such as the main bronchus, major vessels, trachea, heart, esophagus, spinal cord, and brachial plexus. When an extremely high-dose regimen is used, such as 60 Gy delivered in three fractions, the target should be at least 2 cm away from the bronchial tree (6) (see discussion below). If a milder-dose regimen such as 50 Gy in four fractions is used, the 2-cm rule is not required.

4D-CT-BASED SBRT PLANNING

SBRT requires sophisticated 3D-CRT, IGRT, and a reliable immobilization device. Immobilization is crucial in SBRT to reduce daily setup uncertainty. The appropriate immobilization should be chosen for each patient. We immobilize patients in an arms-up position using a commercially available vacuum

immobilization bag (Body-Fix, Elekta Inc.), which extends from the patient's head to the pelvis, combined with a wing board.

Consideration of tumor motion in SBRT is very critical in patients whose tumor moves substantially during radiotherapy. In a recent four-dimensional computed tomography (4D-CT) study of 72 patients with lung cancer, Liu et al. (7) showed tumor movement of more than 1 cm during breathing in 13% of the patients, particularly in those with small lower lobe tumors close to the diaphragm. An individualized tumor-motion margin should be considered for such patients. In addition, patients should be evaluated for regularity of breathing, responsiveness to feedback guidance, and breath-holding capability. On the basis of this evaluation, one of the following treatment-delivery techniques can be selected: (1) free-breathing approach (with or without feedback guidance), (2) respiratory-gated approach, (3) breath-holding approach (with or without feedback guidance), (4) abdominal compression, or (5) a combination of the above techniques.

For patients with tumor motion of <5 mm, simple expansion of the tumor-motion margin is adequate (free-breathing approach). However, for patients with considerable tumor motion, particularly movement of >1 cm, an individualized tumor-motion margin should be considered. A commercially available system can be used for these patients with a respiratory-gated approach (8). This technique uses an externally placed fiducial that is tracked as the patient breathes. The beam can be triggered at a chosen point in the respiratory cycle; this is typically done at the end of expiration because this is the longest and most reproducible portion of the respiratory cycle. This technique requires patients to be able to breathe slowly in a regular pattern. Active breathing control and deep-inspiration breath-holding are two techniques that have been pioneered to help patients hold their breaths at reproducible points in the respiratory cycle (9,10). The radiation beam is then initiated. These two techniques limit patient respiratory excursion to fixed volumes, and they limit diaphragm excursion to about 5 mm instead of 10–15 mm. These techniques, however, require very cooperative patients who are able to hold their breath for at least 15 sec. Abdominal compression has been used in some institutions to reduce the diaphragm movement.

With the advent of new technologies such as multislice detectors and faster imaging reconstruction, it is now possible to image real-time breathing and to assess organ motion using 4D-CT (11). This provides a more accurate design for respiratory-gated or breath-holding SBRT using a breathing cycle-guided procedure. For most patients who cannot breathe regularly or who cannot hold their breath, 4D-CT also provides an individualized approach to evaluate the exact tumor locations during the whole breathing cycle. At The University of Texas M.D. Anderson Cancer Center, all SBRT are conducted based on respiratory-correlated 4D-CT images. 4D-CT data are obtained by acquiring spatially oversampled CT data while simultaneously monitoring the patient's respiration. A collection of 3D-CT datasets is then created by either sorting or reconstructing the image data in a series of respiratory-phase bins. This gives us the motion of the tumor and the surrounding structures as a function of respiratory phase (Fig. 1A and 1B). Two abstractions are made of the 4D-CT data set: the average CT (avg-CT, Fig. 1C) and the maximum intensity projection (MIP, Fig. 1D). The average CT is a 3D-CT dataset created by performing a voxel-by-voxel numerical averaging over all the breathing phases. The MIP is a 3D-CT dataset created by assigning each voxel the value of the highest valued voxel at that location across the breathing phases. All 10 respiratory-phase datasets, the MIP, and the average CT along with extended range free-breathing CT acquired during the same imaging session are transferred to our treatment planning system. This information is crucial for our target delineation using the internal target volume (ITV) approach to take tumor motion into consideration (discussed in the following section).

SBRT Target Volume Delineation

Gross tumor volume
The gross tumor volume (GTV) should be delineated using CT. The pulmonary extent of lung tumors should be delineated on lung windows. PET should be used only for disease staging.

Internal gross target volume
If 4D-CT is available, we can design the internal gross target volume (IGTV) that is the volume containing the GTV throughout its motion during respiration. One method of combining the data from the multiple CT datasets is to create a maximal intensity projection, which can be used as an aid in contouring the IGTV (Figs. 1 and 2). Another approach is to use a deformable registration technique in which the tumor volume that is outlined on the expiratory phase of the 4D images is registered on other phases of the images to create a union of target contours, enclosing all possible positions of the target. In all cases the resulting IGTV contour should be evaluated across all phases, a very quick operation. The third approach is to contour the GTV with the end of inspiration and expiration breath-holding and then combine these two volumes to form the IGTV. The last approach can
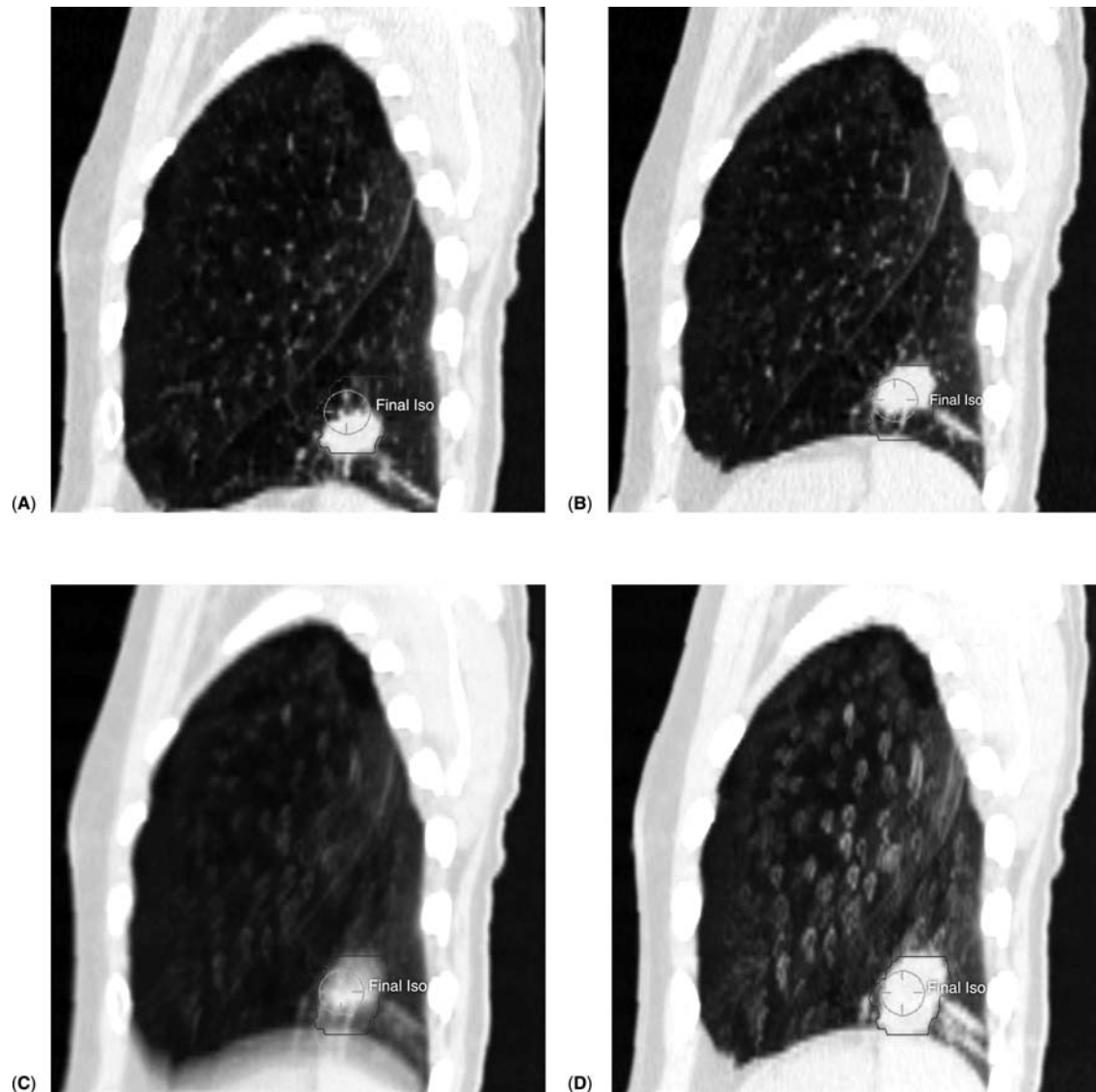
Figure 1 4D-CT simulation demonstrated tumor motion during breath cycle. (**A**) End of inspiration; (**B**) end of expiration; (**C**) average CT; (**D**) MIP. In this patient, MIP image was used to design IGTV (Fig. 2). Alternatively, SBRT can be delivered using respiratory-gated approach during end of expiration (**B**) or breath-hold approach at end of inspiration (**B**). *Abbreviations*: 4D-CT, four-dimensional CT; IGTV, internal gross target volume; MIP, maximum intensity projection; SBRT, stereotactic body radiation therapy.

be used with regular spiral CT without 4D. All CT datasets are transferred to the treatment-planning system for reference.

Clinical target volume
The clinical target volume (CTV) consists of the GTV plus an 8-mm margin that is edited as necessary to account for physical boundaries.

Internal target volume
The ITV consists of an IGTV plus an 8-mm margin that is edited as appropriate, as mentioned above.

Planning target volume
The planning target volume (PTV) consists of either a CTV plus a margin for tumor motion and for daily setup uncertainty or an ITV plus a margin for daily setup uncertainty.

DOSE–VOLUME CONSTRAINTS

To avoid acute and chronic toxicity, it is very important to keep the dose volume of normal critical structures under threshold. The long-term clinical data using SBRT in lung cancer are limited. Most dose volume
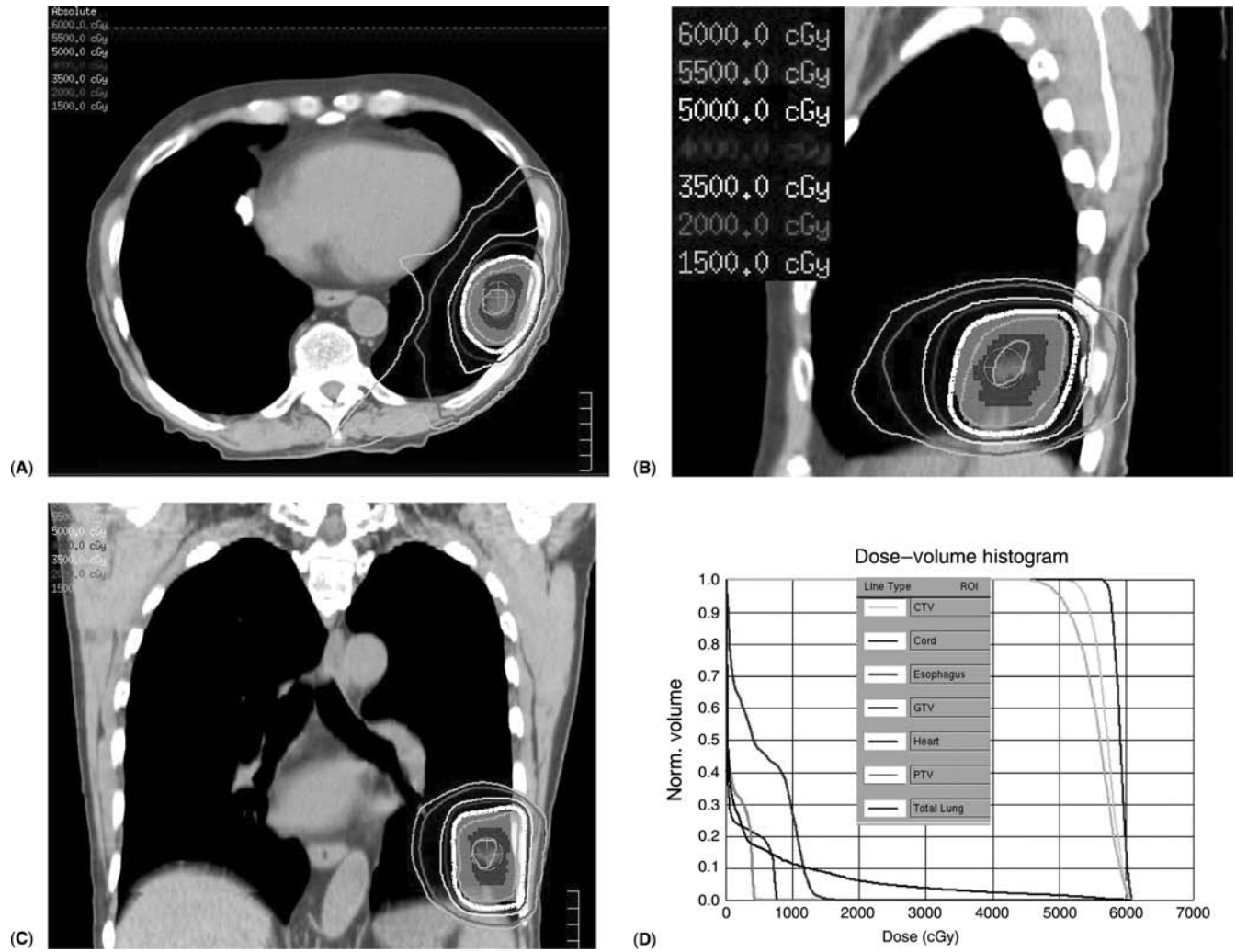
Figure 2 (*See color insert.*) SBRT planning based on ITV generated by 4D-CT using MIP approach. IGTV (red-color wash) was created based on MIP image (Fig. 1). CTV (yellow-color wash) = IGTV + 8 mm margin. PTV (blue-color wash) = CTV + 3 mm margin. 50 Gy (white line) in four fractions prescribed to PTV. (**A**) Transverse; (**B**) sagittal. (**C**) coronal; (**D**) dose–volume histogram. *Abbreviations*: 4D-CT, four-dimensional CT; CTV, clinical target volume; GTV, gross tumor volume; MIP, maximum intensity projection; PTV, planning target volume.

constraints have been developed based on experience with conventional fractionation regimens and RBE calculation. At M.D. Anderson Cancer Center, we treat patients with early-stage NSCLC with 50 Gy in four fractions prescribed to the PTV. With the use of this regimen, we recommend that the maximum dose to the esophagus, major vessels, heart, trachea, and main bronchus should be less than 50 Gy; the maximum dose to the spinal cord should be less than 25 Gy. Dose-volume constraints in critical structures are as follows:

Lung: V20 ≤ 20%
Esophagus: $40\,Gy \leq 1\,cm^3$, $36\,Gy \leq 10\,cm^3$
Trachea: $40\,Gy \leq 1\,cm^3$, $36\,Gy \leq 10\,cm^3$
Main bronchus: $48\,Gy \leq 1\,cm^3$, $40\,Gy \leq 10\,cm^3$
Heart: $48\,Gy \leq 1\,cm^3$, $40\,Gy \leq 10\,cm^3$
Brachial plexus and major vessels: $48\,Gy \leq 1\,cm^3$ $40\,Gy \leq 10\,cm^3$.

For patients who have received previous radiotherapy, the attending radiation oncologist needs to evaluate the previous treatment plan, particularly the dose delivered to critical structures, and make a clinical judgment based on BED, previous radiation therapy, and current SBRT doses using the above dose–volume constraints as a guide.

DAILY CT ON-BOARD IMAGE-GUIDED SBRT DELIVERY

Because SBRT delivers a very high fraction size of radiation each time, it is very crucial to target the tumor accurately and avoid normal critical structures. In such cases, very generous margins without image guidance may cause significant late toxicity. Daily image-guided SBRT delivery is important to ensure

adequate tumor coverage while sparing normal critical structures (12). Discrepancies larger than 3, 5, and 8 mm between the planned and actual tumor position during SBRT were reported in 47%, 27%, and 8% of cases, respectively, as measured by daily cone-beam CT images (13). In addition, displacements of tumor position relative to the bony anatomy with larger than 3, 5 and 8 mm were counted in 29%, 12%, and 3% respectively (13).

At M.D. Anderson Cancer Center, all patients treated with SBRT are imaged using either an in-room CT (GE Medical Systems) or a linac-mounted cone-beam CT (Trilogy, Varian Associates) before each fraction of SBRT. These are both slow acquisitions with respect to respiration (~1 min) and provide a randomly sampled CT (GE) or an average CT (Trilogy). Usually, the spinal vertebral body nearest the tumor is used as the anatomic reference structure for patient setup. In the case of rotations, a combination of transitions in the lateral and anterior/posterior

directions is generally used to achieve target coverage (Fig. 3). If there are nearby critical structures, the patient may have to be re-setup to eliminate the rotation. We have also observed that some tumors show monotonic positional changes during treatment. The treatment isocenter is moved to ensure coverage of these targets as they move day to day, with care being taken to ensure sparing of critical structures. The setup uncertainty can be kept to <3 mm using the daily CT on-rail image. If daily CT is not available, a larger setup margin is advised.

OMITTING PROPHYLACTIC LYMPH NODE IRRADIATION

For many years, standard radiation therapy in the United States, with some recent exceptions, consisted of 40–50 Gy delivered to electively irradiated regional-nodal areas (ipsilateral, contralateral, hilar, media-stinal, and occasionally supraclavicular), with an
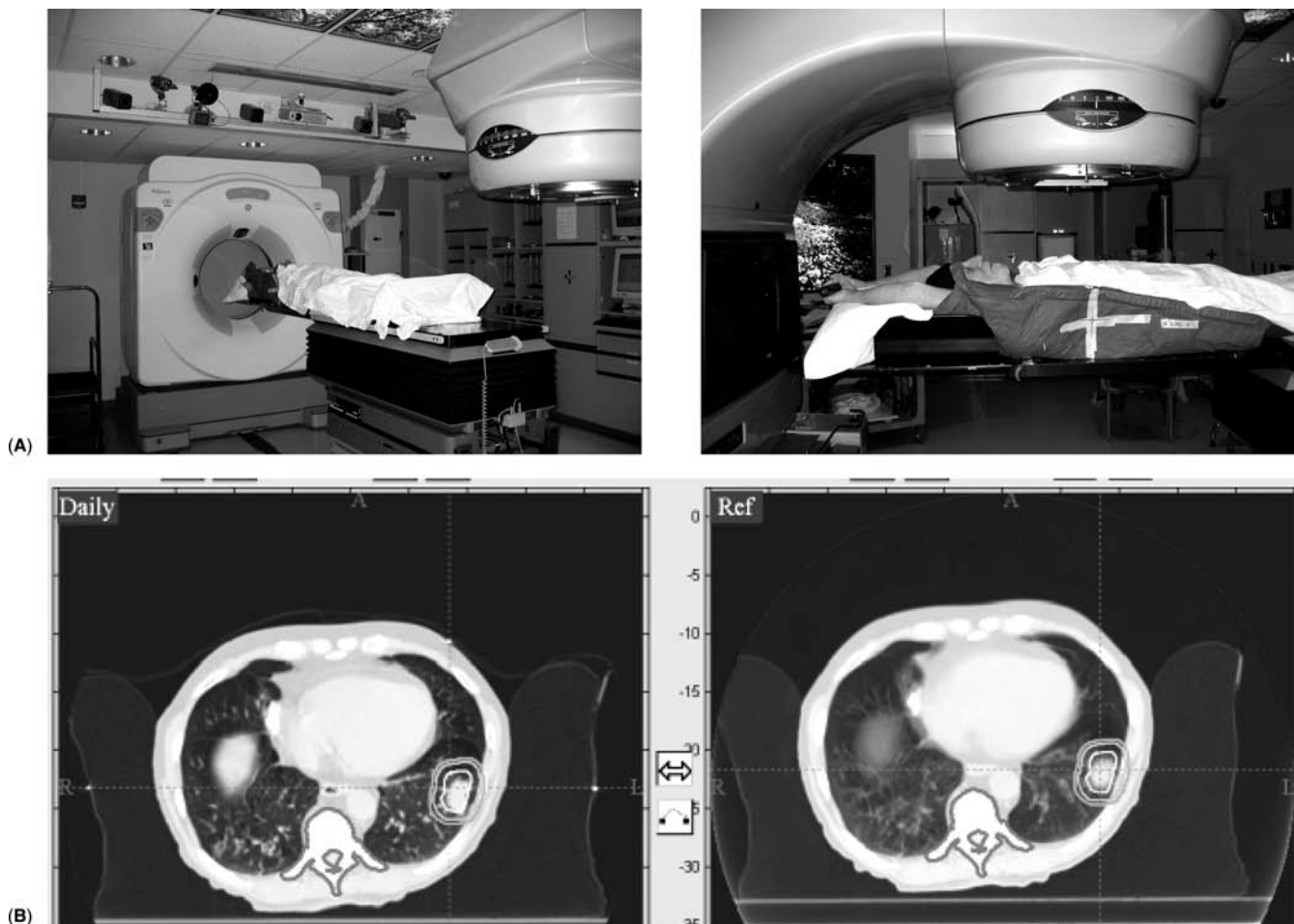
Figure 3 Daily on-board CT on-rail before each fraction of SBRT. (**A**) CT-rail; (**B**) daily on-board image for patient's set up. (*Bottom left*) daily CT for set up. (*Bottom right*) simulation CT. IGTV: Yellow contour. CTV: Blue contour. PTV: Green contour. *Abbreviations*: CT, computed tomography; CTV, clinical target volume; IGTV, internal gross target volume; PTV, planning target volume; SBRT, stereotactic body radiation therapy.

additional 20 Gy delivered to the primary tumor through reduced fields. This regimen was based on pathologic information regarding the high incidence of hilar and mediastinal node metastases in patients with bronchogenic carcinoma. The rationale opposing elective nodal irradiation has been the high local recurrence rates within the previously irradiated tumor volume and the high likelihood of distant metastasis; the thinking was that if gross disease cannot be controlled, why enlarge the irradiated volumes to include areas that may harbor microscopic disease?

Three major factors have changed the standards for radiation therapy in recent years: the use of chemotherapy, the advent of 3D-CRT, and better disease staging and target delineation with PET. In addition, emerging clinical data have shown that omitting prophylactic lymph node irradiation does not reduce the local control rate for patients receiving definitive radiotherapy who have isolated outside-field (field of radiotherapy) local recurrence rates of 3–8%, particularly in patients with stage I disease and in those who undergo PET for disease staging (14–16).

About 15–20% of patients with stage I NSCLC who receive SBRT develope distant metastasis, more commonly in those with T2 disease (17,18). Recent studies of adjuvant chemotherapy after surgical resection for early-stage NSCLC have shown a 4–15% survival benefit for patients with stage Ib NSCLC or higher who received postoperative chemotherapy (19–21). Therefore, adjuvant chemotherapy after SBRT should be considered in T2 disease if the patient can tolerate it.

CLINICAL OUTCOME AND BED CONSIDERATIONS

Several studies have shown considerably improved local control and survival rates in patients with stage I lung cancer treated with SBRT. For example, Uematsu et al. (22) reported their 5-year experience in patients with stage I NSCLC treated with CT-guided frameless SBRT. Fifty patients were treated with 50–60 Gy in 5 to 10 fractions over 1–2 weeks. At a median follow-up of 36 months, 6% of patients developed local failure. The 3-year overall survival and disease-specific survival rates were 66% and 88%, respectively. However, for patients with medically operable disease, the 3-year overall survival rate was 88%. No definite adverse effects were noted. Onishi et al. (17) reported on the delivery of 60 Gy to the PTV in 10 fractions (6 Gy/fraction) in patients with stage I NSCLC; 6% of these patients had local progression, and 14% had distant or regional lymph node metastasis. Also, 9% experienced grade 2 or higher toxic effects. The 2-year overall survival rates were 58% in

all patients and 83% in those with operable disease. Additionally, Nagata et al. (18) reported on the delivery of 48 Gy to the isocenter in four fractions (12 Gy/fraction) over 5 to 13 days in patients with early-stage NSCLC. The local control rate was 98%, and the 5-year overall survival rates were 83% in patients with stage Ia disease and 72% in those with stage Ib disease. In 6.7% of these patients, disease recurred in the regional lymph nodes, and 15–20% of patients developed distant metastases. None of the patients experienced grade 3 or higher toxic effects. In a ongoing multi-institutional phase II study conducted by the Japan Clinical Oncology Group, patients with T1 N0 M0 NSCLC receive 48 Gy delivered in four fractions to the tumor isocenter. In the United States, Timmerman's group (23) conducted a phase I dose-escalation study using SBRT for patients with stage I NSCLC. These researchers prescribed radiation to the 80% isodose line and escalated the dose from 24 to 72 Gy (delivered in three fractions over 2 weeks). The local failure rate was 21%, and the regional and/or distant metastasis rate was about 30%. Most of the local failures occurred in patients who received doses of ≤48 Gy. Grade 3 and higher toxic effects occurred in patients treated with doses of ≥48 Gy. Timmerman et al. (6) then conducted a phase II clinical study of 70 patients with stage I inoperable NSCLC treated with SBRT at doses of 60–66 Gy in three fractions over 1–2 weeks. The median follow-up was 17.5 months; the 2-year local control rate was 95%, and the overall survival rate was 54.7%. However, 20% of these patients developed grade 3–5 toxicity, most commonly patients with centrally located lesions. This dose regimen is therefore considered too toxic for centrally located tumors and should be used only for peripheral lesions (located at least 2 cm from the bronchial tree). Currently, the Radiation Therapy Oncology Group is conducting a phase II clinical study of 60 Gy delivered in three fractions, as described by Timmerman et al. (6), in patients with inoperable stage I and selective stage II peripherally located NSCLC. Recently, Xia et al. (24) reported results from a phase II study of SBRT in 43 patients with medically inoperable stage I/II peripherally and/or centrally located NSCLC. When 70 Gy was delivered at 7 Gy/fraction to the GTV, the 1-, 2-, and 3-year local control rates were 95% in all patients. The 1-, 2-, and 3-year overall survival rates were 100%, 91%, and 91%, respectively, in patients with stage I disease and 73%, 64%, and 64%, respectively, in those with stage II disease. Only 2.3% (1/43) of the patients had grade 3 pneumonitis (24).

The BED is a well-accepted means of evaluating the acute or late effects of radiation therapy. The BED is calculated with the following linear quadratic equation: BED = $n \times d$ [1 + $d/(\alpha/\beta)$] (where n is the

number of fractions, *d* is the dose per fraction, and *n* × *d* is the total dose delivered) using an α/β of 10 for acute effects and of 3 for late effects. The higher the BED, the better the chances of eliminating the cancer. There are two ways to increase the BED: (1) delivering a higher total dose by increasing the number of fractions while keeping the conventional dose per fraction, or (2) delivering a higher dose per fraction but lowering the total dose and the number of fractions, which is done in SBRT. As mentioned above, however, the primary concern about SBRT is chronic toxicity.

The optimal dose and fractionation for SBRT are unclear. Onishi et al. (25) retrospectively evaluated results from a Japanese multi-institutional SBRT study. At a total of 13 institutions, 245 patients with stage I NSCLC were treated with hypofractionated high-dose SBRT. A total dose of 18–75 Gy at the isocenter was administered in 1–22 fractions. The median calculated BED was 108 Gy (range, 57–180 Gy), and the median follow-up was 24 months. Greater than grade 2 pulmonary complications were observed in only six patients (2.4%). The local recurrence rate was 8.1% for those given a BED of ≥100 Gy but was 26.4% when the BED was <100 Gy (*P* < 0.05). The 5-year overall survival rate in patients with medically operable NSCLC was 88.4% for those given a BED of ≥100 Gy, compared with 69.4% when the BED was <100 Gy (*P* < 0.05). NSCLC recurred in the regional lymph nodes in 8.2% of the patients, and distant metastasis occurred in 14.7% of the patients. Recently, Onishi et al. updated their results at a median follow-up of 38 months. At 5 years, the local failure rate was 8.4% and the overall survival rate was 72% for patients with operable disease who received SBRT with a BED of >100 Gy (2006 SBRT workshop in Maui, Hawaii, sponsored by the International Association for the Study of Lung Cancer). Their data showed that hypofractionated high-dose SBRT with a BED up to 180 Gy was feasible and beneficial for the curative treatment of patients with stage I NSCLC. For all treatment methods and schedules, local control and survival rates were better in patients treated with a BED of ≥100 Gy than in those receiving a BED of <100 Gy. Survival rates in patients with medically operable disease treated with a BED of ≥100 Gy were comparable to those of patients who underwent surgery.

The BED, calculated with the linear quadratic equation using an α/β of 10, was 96 Gy with the delivery of 60 Gy in 10 fractions, 106 Gy with the delivery of 48 Gy in four fractions, 119 Gy with the delivery of 70 Gy in 10 fractions, and 180 Gy with the delivery of 60 Gy in three fractions. However, when we consider the optimal BED for SBRT, we also need to keep in mind the potential long-term toxicity associated with SBRT, particularly for lesions close to critical structures

such as the trachea, bronchus, vessels, nerves, esophagus, spinal cord, heart, and skin. The current consensus is that the BED must be >100 Gy and that the volume of the critical structures receiving the high BED (>80 Gy) should be minimized. Therefore, in general, only peripherally located disease should be treated with SBRT. When SBRT is used for patients with a centrally located tumor, a greater number of fractions and/or a lower BED should be considered, until further long-term toxicity data become available.

We reported our preliminary data for image-guided SBRT in patients with early-stage NSCLC (12). Thirty-seven patients with pathologically confirmed stage I disease were treated with SBRT. NSCLC in all patients was staged with chest CT, PET, and brain magnetic resonance imaging. 4D-CT images were obtained with a GE simulator with the Varian RPM system. The IGTV was delineated using a maximal intensity projection that was created by combining the data from the multiple 4D-CT datasets at different breath phases. The ITV consisted of the IGTV plus an 8-mm margin, and a 3-mm setup uncertainty margin was added to form the PTV. Daily CT on-rail simulation was conducted during each fraction of radiotherapy. SBRT was prescribed at a dose of 50 Gy to the PTV, delivered at 12.5 Gy/fraction for 4 consecutive days (the BED was 112.5 Gy). Critical structures such as the main bronchus, heart, and major vessels were excluded from the 40-Gy isodose line. Patients were followed up with chest CT every 3 months for 2 years. PET follow-up was recommended at 3–5 months after SBRT.

The progression-free survival rate at the treatment site in all patients was 100%, with a median follow-up of 10 months. In 22 patients with stage Ia (T1 N0 M0) disease, the complete response rate was 66.7% and the partial response rate was 28.8%; however, the complete response rate was 100% in 11 patients who underwent PET for post-SBRT evaluation. The rate of stable disease was 4.5%. Mediastinal lymph node metastasis and distant metastasis developed in 4% of the patients. There was no grade 2 or higher radiation-induced pneumonitis in patients with stage I disease, and no esophagitis was noted. Grade II/III dermatitis developed at the treatment site in 9.5% of the patients. All patients tolerated SBRT well, with no symptoms of toxicity during SBRT. More studies with long-term patient follow-up are needed. Figure 4 shows a representative patient with stage I NSCLC who received SBRT and achieved a complete clinical response as measured by PET.

ROLE OF SBRT IN OPERABLE STAGE I NSCLC

The role of SBRT in operable stage I NSCLC remains unclear. Currently, lobectomy with mediastinal

Before SBRT   3 months after SBRT
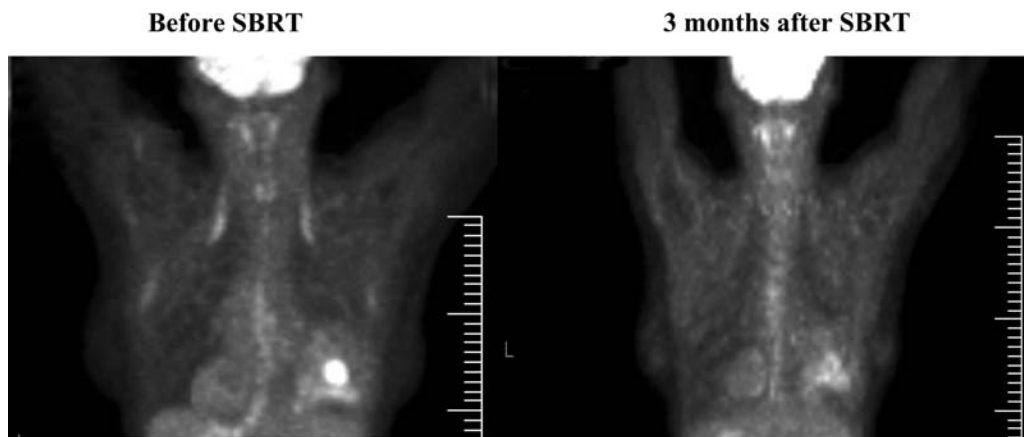
Figure 4   A representative patient case with stage I NSCLC who received SBRT (50 Gy in four fractions) and achieved a complete clinical response by PET. *Abbreviations*: NSCLC, non–small cell lung cancer; PET, positron emission tomography; SBRT, stereotactic body radiation therapy.

sampling or dissection is considered the standard treatment for this disease. Supporting this were the findings from a study conducted by the Lung Cancer Study Group, which consisted of a randomized comparison of an anatomic lobectomy versus limited (wedge or segmental) resection for peripheral T1 pulmonary carcinomas (26). The locoregional recurrence rate associated with limited resection was three times that associated with lobectomy, 17% compared with 6.4%. The potential advantages of surgical resection include the complete removal of the involved lobe, resulting in less chance of local recurrence, and the pathologic stage (maybe therapeutic in some cases) of hilar and/or mediastinal lymph nodes. If a lymph node is involved, adjuvant chemotherapy or radiotherapy (for N2 disease) may be considered. Compared with surgical resection, SBRT with a BED of >100 Gy achieves comparable results, with >90% local control and <10% regional nodal recurrence. When PET is used for staging, regional nodal recurrence is about 5%. If cancer recurs locally or regionally, salvage surgery and/or radiotherapy should still be considered, although these techniques are more challenging.

Multi-institutional phase II studies of SBRT for stage I NSCLC have begun in Japan (JCOG0403) and the United States (RTOG0236). Clinical data indicated an improved therapeutic ratio for SBRT in patients with inoperable stage I NSCLC. However, comparable data for patients with operable disease are scarce. To determine the role of SBRT in patients with operable stage I NSCLC, a randomized study is warranted. Currently, the International Association for the Study of Lung Cancer is considering such a study.

SUMMARY

Image-guided SBRT with the delivery of a BED >100 Gy is feasible and safe in the treatment of patients with peripherally located inoperable stage I NSCLC. The 3- to 5-year local control and overall survival rates for patients who receive SBRT seem to be much better than the rates for patients who receive conventional radiotherapy for stage I disease, and the toxicity rate is minimal. SBRT is becoming the standard treatment for patients with inoperable stage I NSCLC. However, its role in operable stage I NSCLC is not clear. To balance improved targeting accuracy with minimized treatment-related toxicity, a reliable immobilization device and consideration of image-guided tumor motion are crucial. The optimal dose regimen remains unclear, but a BED >100 Gy seems warranted.

REFERENCES

1. Dosoretz D, Galmarini D, Rubenstein J, et al. Local control in medically inoperable lung cancer: An analysis of its importance in outcome and factors determining the probability of tumor eradication. Int J Radiat Oncol Biol Phys 1993; 27:507–16.

2. Kaskowitz L, Graham M, Emami B, et al. Radiation therapy alone for stage I non-small cell lung cancer. Int J Radiat Oncol Biol Phys 1993; 27:517–23.

3. Fang L, Komaki R, Allen P, et al. Comparison of outcomes for patients with medically inoperable Stage I non-small-cell lung cancer treated with two-dimensional vs. three-dimensional radiotherapy. Int J Radiat Oncol Biol Phys 2006; 66:108–16.

4. Dosoretz D, Katin M, Blitzer P, et al. Medically inoperable lung carcinoma: The role of radiation therapy. Semin Radiat Oncol 1996; 6:98–104.

5. Sibley G, Jamieson T, Marks L, et al. Radiotherapy alone for medically inoperable stage I non-small-cell lung cancer: The Duke experience. Int J Radiat Oncol Biol Phys 1998; 40(1):149–54.

6. Timmerman R, McGarry R, Yiannoutsos C, et al. Excessive toxicity when treating central tumors in a phase II study of stereotactic body radiation therapy for medically inoperable early-stage lung cancer. J Clin Oncol 2006; 24(30):4833–9.

7. Liu H, Choi B, Zhang J, et al. Assessing respiration-induced tumor motion and margin of internal target volume for image-guided radiotherapy of lung cancers. Int J Radiat Oncol Biol Phys 2005; 63(Suppl. 1):S30.

8. Ramsey C, Scaperoth D, Arwood D, et al. Clinical efficacy of respiratory gated conformal radiation therapy. Med Dosim 1999; 24(2):115–9.

9. Rosenzweig K, Hanley J, Mah D, et al. The deep inspiration breath-hold technique in the treatment of inoperable non-small-cell lung cancer. Int J Radiat Oncol Biol Phys 2000; 48(1):81–7.

10. Sixel K, Aznar M, Ung Y. Deep inspiration breath hold to reduce irradiated heart volume in breast cancer patients. Int J Radiat Oncol Biol Phys 2001; 49(1):199–204.

11. Nehmeh S, Erdi Y, Pan T, et al. Four-dimensional (4D) PET/CT imaging of the thorax. Med Phys 2004; 31:3179–86.

12. Chang J, Balter P, Liao Z, et al. Preliminary report of image-guided hypofractionated stereotactic body radiotherapy to treat patients with medically inoperable stage I or isolated peripheral lung recurrent non-small-cell lung cancer. Int J Radiat Oncol Biol Phys 2006; 66(3):S480.

13. Guckenberger M, Richter A, Wilbert J, et al. Cone-beam CT based image guidance for hypofractionated radiotherapy of intrapulmonary lesions—evaluation of benefits and limitations. Int J Radiat Oncol Biol Phys 2006; 66(3, Suppl. 1):S154.

14. Bradley J, Thorstad W, Mutic S, et al. Impact of FDG-PET on radiation therapy volume delineation in non-small-cell lung cancer. Int J Radiat Oncol Biol Phys 2004; 59(1):78–86.

15. Krol A, Aussems P, Noordijk E, et al. Local irradiation alone for peripheral Stage I lung cancer: Could we omit the elective regional nodal irradiation? Int J Radiat Oncol Biol Phys 1996; 34(2):297–302.

16. Sulman E, Chang J, Liao Z, et al. Exclusion of elective nodal irradiation does not decrease local regional control of non-small-cell lung cancer. Int J Radiat Oncol Biol Phys 2005; 63(Suppl 1):S226–7.

17. Onishi H, Kuriyama K, Komiyama T, et al. Clinical outcomes of stereotactic radiotherapy for stage I non-small cell lung cancer using a novel irradiation technique: Patient self-controlled breath-hold and beam switching using a combination of linear accelerator and CT scanner. Lung Cancer 2004; 45(1):45–55.

18. Nagata Y, Takayama K, Matsuo Y, et al. Clinical outcomes of a phase I/II study of 48 Gy of stereotactic body radiotherapy in 4 fractions for primary lung cancer using a stereotactic body frame. Int J Radiat Oncol Biol Phys 2005; 63(5):1427–31.

19. Winton T, Livingston R, Johnson D, et al. Vinorelbine plus cisplatin vs. observation in resected non-small-cell lung cancer. N Engl J Med 2005; 352(25): 2589–97.

20. Strauss G, Herndon J, Maddaus M, et al. Randomized clinical trial of adjuvant chemotherapy with paclitaxel and carboplatin following resection in Stage IB non-small cell lung cancer (NSCLC): Report of cancer and leukemia group B (CALGB) protocol 9633. J Clin Oncol 2004 (meeting abstract):7019.

21. Arriagada R, Bergman B, Dunant A, et al. Cisplatin-based adjuvant chemotherapy in patients with completely resected non-small-cell lung cancer. N Eng J Med 2004; 350(4):351–60.

22. Uematsu M, Shioda A, Suda A, et al. Computed tomography-guided frameless stereotactic radiotherapy for stage I non-small cell lung cancer: A 5-year experience. Int J Radiat Oncol Biol Phys 2001; 51(3):666–70.

23. McGarry R, Papiez L, Williams M, et al. Stereotactic body radiation therapy of early-stage non-small-cell lung carcinoma: Phase I study. Int J Radiat Oncol Biol Phys 2005; 63(4):1010–5.

24. Xia T, Li H, Sun Q, et al. Promising clinical outcome of stereotactic body radiation therapy for patients with inoperable Stage I/II non-small-cell lung cancer. Int J Radiat Oncol Biol Phys 2006; 66:117–25.

25. Onishi H, Araki T, Shirato H, et al. Stereotactic hypofractionated high-dose irradiation for stage I non-small cell lung carcinoma: Clinical outcome in 245 subjects in a Japanese multi-institutional study. Cancer 2004; 101(7):1623–31.

26. Ginsberg R, Rubinstein L. Randomized trial of lobectomy versus limited resection for T1 N0 non-small cell lung cancer. Lung Cancer Study Group. Ann Thorac Surg 1995; 60:615–22.

The Physics Aspects of Intensity-Modulated Radiation Therapy for Lung Cancers

Helen H. Liu
Department of Radiation Physics, University of Texas M.D. Anderson Cancer Center, Houston, Texas, U.S.A.

INTRODUCTION

Radiation therapy for lung cancer has a unique set of requirements because of the anatomy in the thorax. First of all, lung is a very radiosensitive organ and exhibits a greater effect of volume dependency than other organs. Thus, designing effective radiation beams that can reach tumors surrounded by a large amount of normal pulmonary tissue has been a great challenge in radiation oncology. Second, in the normal thorax, critical structures such as the mediastinum, heart, esophagus, and spinal cord are often very close or adjacent to tumors. Thus the risk of developing potentially fatal toxicity in these normal structures poses a great concern for oncologists treating lung cancers. Often, normal tissue complication is a major impediment to dose escalation and further improvements in therapeutic efficacy. Treatment strategies must effectively address improving tumor control without significantly increasing toxicity and compromising quality of life in patients with lung cancers.

In the 1990s, three-dimensional conformal radiation therapy (3D-CRT) quickly changed the terrain of radiation therapy and dominated the technological development of radiation therapy for lung cancers. Radiation dose distributions are now shaped to conform to target volumes by the use of 3D treatment planning, multimodality imaging, and more sophisticated beam delivery techniques, such as multileaf collimators (MLCs). Improving the dose conformity to the target coverage could potentially reduce dose–volume of the irradiated normal tissues.

Along the same direction of the 3D-CRT, intensity-modulated radiation therapy (IMRT) has emerged as an exciting new modality for treating lung cancers. In IMRT, the intensity of the individual beamlets within the beams of radiation is modulated in the process of inverse planning or treatment planning optimization. The goals of the optimization process are to create more conformal dose distributions and avoid exposing critical structures. From a physics standpoint, the free parameters that can be optimized in an IMRT treatment plan are the weights of the beamlets in the beams and the angles of the beams. The number of free parameters to be optimized can easily exceed several thousand if beam-angle optimization is further considered.

However, typical 3D-CRT plans have many fewer free parameters and may include only beam weights, wedge angles, and beam angles. We can then easily imagine that the degree of difference between conventional 3D-CRT versus IMRT can be dramatic in terms of the capability to shape the dose distributions. In fact, most of the treatment planning optimization algorithms used in commercial planning systems nowadays have not been able to take full advantage of IMRT because the number of free parameters in optimization and thus the solution space to be explored often exceeds the capabilities of even modern computers.

IMRT has been used successfully in treating prostate and head and neck cancers and is quickly becoming the standard of practice for cancers at these sites. In treating prostate cancer, the intensity modulation of IMRT can be used to create an ideal dose distribution, one shaped around the prostate gland and seminal vesicles, with tissue sparing in the rectum and bladder. In treating head and neck, IMRT is ideal for generating complex dose distributions to surround target volumes and avoid adjacent normal structures, which typically include the parotid gland, brain stem, and optic nerves. The effectiveness of IMRT in managing tumors at these sites has been demonstrated in both treatment planning studies and clinical settings (1–4).

In principle, IMRT would be a desirable tool for treating lung cancers because of the need to reduce the normal tissue toxicity associated with chemoradiation, hypofractionated, or dose-escalated therapy. However, the role of IMRT in treating lung cancers has not been firmly established because of several issues unique to radiation therapy for lung cancers.

One major clinical concern is that, because of the low dose tolerance of lung tissue, IMRT may result in

the exposure of a large volume of normal lung to low yet still damaging radiation doses. Clinical studies have shown that radiation doses as low as 10–20 Gy can be associated with injury to lung tissues (5–8). In addition, the risk of radiation pneumonitis can increase substantially when the volume of lung irradiated at that dose level exceeds a certain threshold. The dose and volume thresholds at which lung injury may lead to radiation pneumonitis and other such conditions are likely to be significantly reduced by the use of chemoradiation and hypofractionated radiation therapies; however, to our knowledge, very few clinical studies have defined these thresholds.

Another practical issue is that respiration and cardiac pulsation may cause lung tumors to move significantly during radiation delivery. Besides using a large margin to accommodate such motion, the interplay between tumor and collimator motions may still lead to unexpected dose distributions. Nevertheless, it is debatable whether intrafractional lung motion has a perceptible effect on the cumulative dose delivered using many beams and fractions (9).

The third issue is that the tissue inhomogeneity in the thorax and use of large and highly modulated beams for advanced lung cancers will require a high degree of accuracy in the dose calculations for IMRT. Approximations made in the dose–calculation algorithms, which are often used to speed up IMRT optimization, may result in artificial treatment plans which may not be deliverable or may be associated with large dose errors especially to critical structures.

To address these valid concerns, we began to conduct research and implementing IMRT for lung cancers in our clinic in the earlier 2000s. We first evaluated the effectiveness of IMRT in a series of retrospective treatment planning studies (10,11) in addition to other similar studies published by other groups (12–14). Subsequently, we sought to improve the optimization and deliverability of IMRT treatment plans to facilitate the clinical implementation of the technology (15–18). In parallel, we also invested a substantial amount of effort in developing a Monte Carlo based dose calculation and quality assurance program for the use of IMRT in the lungs (19). Many interesting results were obtained from these dosimetry studies that will be discussed in the following sections.

In the mid-2004, the technology of four-dimensional computed tomography (4D-CT) was introduced in our clinic (20) that enabled us to study and understand the issues related to respiratory motion and to estimate their impact on treatment planning and delivery. The details of these studies and findings are described in other related chapters. Because the technology of IMRT and its clinical use have evolved to maturity up to date, currently, nearly half of our locally advanced lung cancer patients is treated with IMRT in our clinic. The clinical outcome of the treated patients is being closely followed up to date. We are now pursuing studies on toxicities, patient survival, and dose–response modeling of the various clinical endpoints. Detailed information about these studies is given in Chapter 9.

Clearly, whether high-volume of low dose or low-volume of high dose is more detrimental to the healthy lung is a critical question that needs to be addressed in using IMRT. The emerging clinical data from patients treated with IMRT will offer us extremely valuable information to resolve this question. Technological advancement in using image guidance, function imaging, and biological targeting may further enhance the effectiveness of IMRT for lung cancers, for which clinicians are eagerly awaiting for the actual clinical results to emerge and mature (21).

CLINICAL IMPLEMENTATION OF IMRT FOR LUNG CANCERS

The following sections, which are organized in the sequence considering the workflow of radiation therapy, offer some of our experience and insights developed in applying the new technologies related to IMRT in the treatment of lung cancers.

Patient Selection

Appropriate patient selection is an important prerequisite of using IMRT successfully in the radiation oncology clinic. In one study on the use of IMRT for non-small cell lung cancer (NSCLC), we found that patients who had locally advanced diseases or recurrent diseases may benefit most from IMRT among the lung cancer patients (11). The conclusions of the study are not surprising. Patients who have earlier stage disease usually have small lesions that are easily managed with conventional 3D-CRT, without exposing a large volume of normal lung tissue to radiation. However, patients who have more advanced or recurrent disease typically have either large lesions, additional lymph node involvement, or complex anatomy that require delicate dose shaping that can only be achieved by IMRT.

One way to understand the benefit of IMRT is to compare IMRT and 3D-CRT treatment plans for patients with advanced diseases, for example, adjacent to the mediastinum. Figure 1 shows the treatment plans of one such patient. It has been a challenge in using 3D-CRT to give dose in excess of 60 Gy to such a site because of the dose–volume constraints of healthy tissues (lung, esophagus, spinal cord, heart, etc.). If a typical 3D-CRT beam arrangement is planned, for example, using anterior–posterior (AP) direction plus oblique beams, the dose–volume of exposed lung
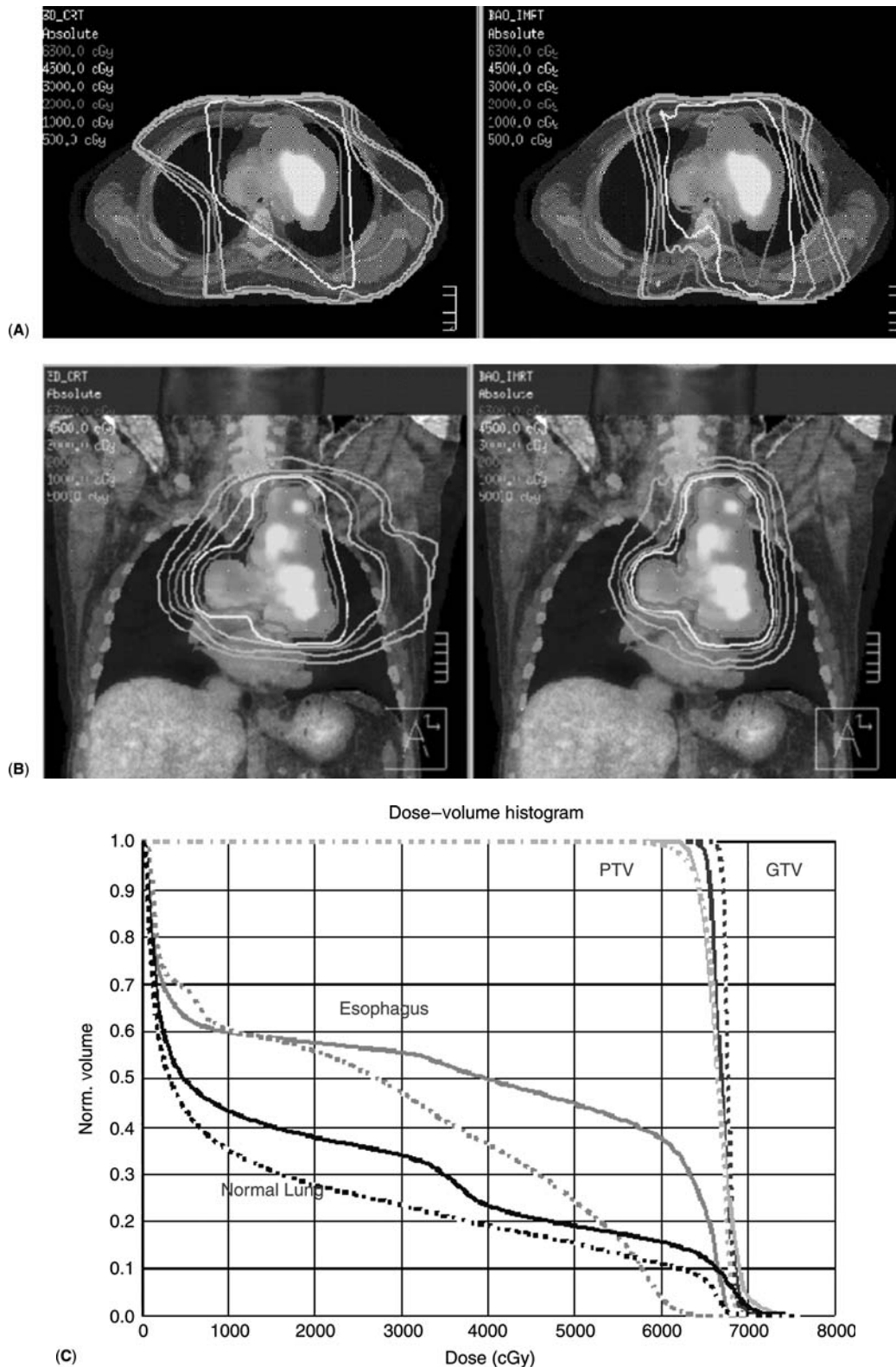
Figure 1 (*See color insert*.) Comparison of the 3D-CRT and IMRT treatment plans for a patient with NSCLC who had stage III disease involving the mediastinum. PET images were fused with planning CT images to show the SUV avid tumor regions. (**A**) Axial view of the dose distribution of the 3D-CRT plan (*left panel*) and the IMRT plan (*right panel*); (**B**) coronal view of the 3D-CRT dose distribution plan (*left panel*) and the IMRT plan (*right panel*); (**C**) comparison of the DVHs of the GTV, PTV, esophagus, and total lung from the 3D-CRT plan (*solid lines*) and IMRT plan (*dashed lines*). The isodose lines are given in cGy. *Abbreviations*: 3D-CRT, three-dimensional conformal radiation therapy; CT, computed tomography; DVH, dose–volume histograms; GTV, gross tumor volume; IMRT, intensity-modulated radiation therapy; NSCLC, non–small cell lung cancer; PET, positron emission tomography; PTV, planned treatment volume, SUV, standard update value.

would be very large, which exposes a high risk of developing pulmonary complication in such a patient. In the IMRT plan, however, 5 coplanar beams were used, with reduced dose–volume exposure to the lung and a higher degree of dose conformity and homogeneity to the target volume.

Based on our experience in treating lung cancers with mediastinum involvement and presence of multiple lesions, IMRT can be an effective tool in shaping dose distributions with reduced dose to the normal lung. The question on how to select IMRT beam angles and choosing appropriate dose–volume constraints for normal tissues will be discussed in more details later. For patients who have recurrent disease or who have undergone previous chest irradiation, IMRT can also be used to treat the present lesions without giving an excessive dose to the previously irradiated areas. In our clinic, we have also used IMRT in lung cancer patients who have moderate cardiopulmonary performance, small normal lungs, or other special clinical conditions that need to be considered, should these patients be managed aggressively with curative intent.

However, not all patients should be treated with IMRT. We have found, for example, that patients who have extensive disease in the chest may require the entire hemithorax be irradiated to treat the lesions with adequate beam margins. Figure 2 shows the
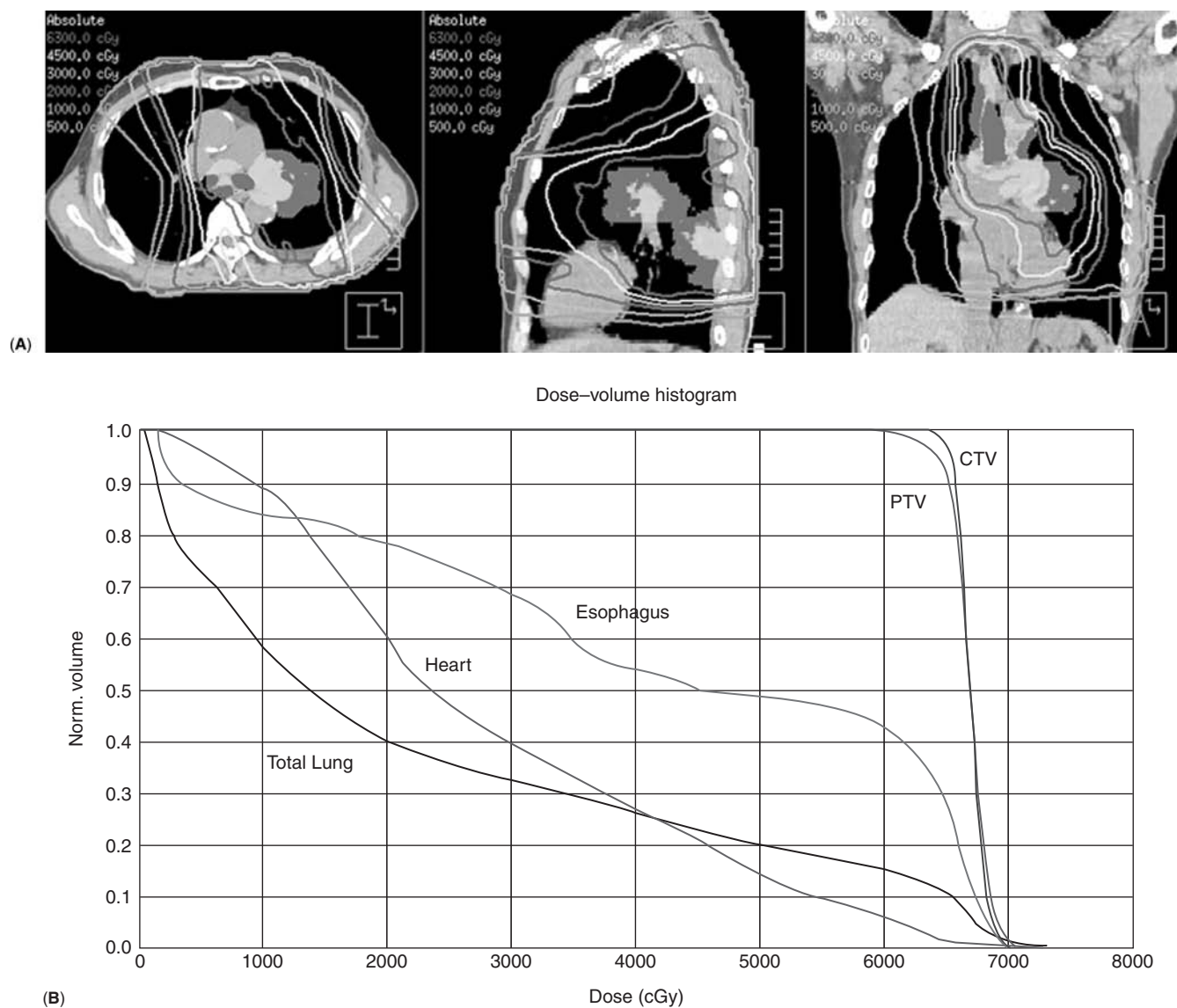
Figure 2 (*See color insert.*) Isodose distribution (**A**) and DVHs (**B**) of the IMRT plan of one NSCLC patient who developed severe pulmonary complication post-radiation therapy. The patient had disease extension from right apex of the lung to the left lower lobe of lung, with additional involvement of the mediastinum. A large volume of the normal lung had to be irradiated which may be one of the factors triggered the onset of pulmonary complication. *Abbreviations*: DVH, dose–volume histograms; IMRT, intensity-modulated radiation therapy; NSCLC, non—small cell lung cancer.

treatment plan of one lung cancer patient treated with IMRT who developed severe pulmonary complication as a result of the treatment. This patient had an extremely complex and large lesion extending from the right upper lobe to the left lower lobe of the lung. Though IMRT was successfully used to create a satisfactory dose conformation to the target volume, a large volume of lungs had to be treated inevitably that may have increased the risk of developing pulmonary complication for this patient. This topic will be discussed further in the treatment planning section of this chapter and in Chapter 9 on dose–response studies.

In patients who receive chemotherapy in the form of either induction, concurrent, or adjuvant therapy in combination with radiation therapy, they may be at a greater risk than patients treated with radiation therapy alone to develop cardiopulmonary complication because of possibly additive toxic effect from the use of chemotherapy agents. Thus, extreme caution should be exerted in the use of IMRT for patients who have extremely poor cardiac or pulmonary performance prior to chemoradiation. Finally, because the survival rate and life expectancy of patients with metastatic lung cancers are very poor, patient's post-treatment quality of life and dose-effectiveness of the treatment should be considered as some of the high priorities in choosing the appropriate forms of therapy. Clearly, IMRT does not offer a miracle but rather another tool that can better shape the dose distribution, provided we have a clear understanding of the desired clinical goals to be achieved for the patients.

Treatment Simulation

In this subsection, the topics related to patient setup and CT simulation for IMRT will be discussed. Topics on the use of advanced imaging technologies (4D-CT and PET/CT) for IMRT simulation will be also included.

Patient setup

In our clinic, treatment simulation procedure for IMRT is very similar to that for 3D-CRT. During both, patients undergo a routine CT simulation with immobilization devices. In this process, patients are instructed to lie down flat and supine, with their arms up above the head. The immobilization devices used to hold patients in this position typically include a body frame, arm and leg supports, and hand holders. During the process of implementing IMRT and other advanced technologies such as stereotactic radiosurgery and proton therapy in our clinic, we evaluated several commercial varieties of the patient setup and immobilization devices. Those devices that can be shaped easily to the thorax and upper abdomen, and provide comfortable yet rigid body support are ideal choices for the use with IMRT. We also found that because older patients usually experience discomfort in the arms-up position, having support for the arms and hands is important. For the patients who have lesions in the apex of the lungs, the arms-down position similar to those used in treating head-neck cancers may be a preferred option to allow treatment through the upper chest and shoulder regions.

Using the conventional patient setup and immobilization devices described above, we estimated the daily setup uncertainty to be approximately 7–8 mm in all three dimensions in our center. This margin can be reduced by more than half if daily or more frequent imaging is used during the treatment course. In IMRT, because of the dose conformity and the need to spare structures adjacent to the disease, typically the esophagus or spinal cord, the setup uncertainty should be kept as small as possible. In addition, during inverse planning for IMRT, safety margins can be created for certain organs, such as the spinal cord, to account for uncertainty of patient setup.

CT simulation

During CT simulation, we first choose a reference position near the patient's carina in the middle of the sternum, as this position is felt to be the most stable, considering the patient's breathing motion and skin movement. A high-density BB is then placed at the reference position with a fast CT scout taken. The patient's body is then adjusted to align straight by repeatedly checking the position of vertebral column in the CT scout image. Next, two lateral BBs are placed along each side of the patient on the same cranial-caudal plane as the first reference BB near the carina. The CT scan then proceeds, with the patient instructed to perform shallow free-breathing during the scan. Upon image acquisition, the visibility and alignment of the three BBs are verified on the CT images. The three BBs are used to mark the reference locations on the CT images, which may not always coincide with the center of the target volume. Rather, the isocenter is usually defined in the target in the treatment planning stage later on. The information on the shift of the isocenter from the reference point is given by the treatment planning system, which is then provided to the treatment machines. After the CT scanning is completed, the patient is tattooed to mark the positions of the three BBs.

4D simulation

In addition to conventional CT simulation, 4D-CT was added to the IMRT simulation procedure with the aim of assessing respiratory motion for lung cancer

patients. During 4D simulation, patients are immobilized and setup in a similar way as the conventional CT simulation. In our clinic, the CT room is equipped with a respiratory monitoring system (RPM, Varian Oncology Systems, Palo Alto, California), which is consisted of a small box with two infrared reflection markers, an infrared camera, and associated computer hardware and software. The reflection box is usually placed on top of the patient's abdomen near the umbilicus or wherever the greatest amount of respiratory motion is observed. The camera is mounted at the end of the CT couch and moves with the couch during CT scanning. Although the Varian RPM system is simple to operate and comfortable for patients, the principle of operation and thus the consistency of correlation between the measured skin movement versus internal organ motion still needs improvement, as discussed in one of our published study (22). A combinatory form of measurement using both signals from spirometry and surface movement may offer more reliable means of monitoring respiration.

The respiratory trace, as measured by the motion of the reflection box, is measured online in real time and interfaced with the CT scanner data so that each CT image can be associated with a particular phase in the respiratory cycle. In our clinic, we also evaluated the use of audio and video feedback to help the patient regulate his or her breathing during the CT scan, which is necessary for 4D-CT. With audio feedback, computer-generated instructions on breathing-in and breathing-out phases are provided to the patient continuously, and the respiratory cycle may be adjusted based on the patient's need. In video feedback, patients typically wear eye goggles that display real-time breathing traces, which allows the patient to modulate his or her breathing.

The overall simulation procedure starts with a conventional CT simulation with the patient performing free-breathing, followed by a 4D-CT procedure. Patients who cannot regulate their breathing or who require special treatment techniques, such as respiratory gating or breath-hold, undergo additional CT scanning as needed. The respiratory motion was evaluated from the 4D-CT images displayed in a cine-mode upon acquisition of the 4D images. Afterward, all data sets are archived and sent to the treatment planning system.

This 4D simulation procedure is dynamic and still evolving in our clinic because of the changes in technology and emergence of more clinical data. We still need to demonstrate the benefits of 4D-CT as how they are related to both dosimetry improvement and clinical outcome. Before 4D-CT becomes a more routine procedure, its operation must be automated and made more efficient, because in its current form, 4D-CT simulation requires a substantial amount of physicist support and computation resources than conventional CT simulation procedures.

PET/CT simulation

The Positron emission tomography/computed tomography (PET/CT) is increasingly used as an important modality for assessing lesions in lungs, disease staging, and treatment follow-ups. In our clinic, it has been incorporated as a component of the treatment simulation and planning process, although extra precaution should be taken during thoracic imaging (23). When PET/CT was introduced in our clinic, the PET/CT scanner (Discovery ST, GE Healthcare, Waukesha, Wisconsin) was configured as a CT simulator with in-room laser and simulation software. For patients who have combined PET/CT and conventional CT simulation (without 4D simulation), they will have immobilization devices made first and are setup in such devices with flat bed on the scanner couch. Next, radiation therapist aligns the patient in a way similar to that of a traditional CT simulation procedure. The radiology technician proceeds by acquiring a fast helical whole-body CT scan that will be used for PET attenuation correction. This is followed by PET acquisition which usually takes about 20 min to complete. Both CT and PET scans are acquired with the patient performing shallow free-breathing to minimize breathing artifacts. The CT images used for the PET attenuation correction are reconstructed with the parameters needed for radiation oncology applications and co-registered with the PET images. The final set of CT images can be used directly in treatment planning.

Because PET images are acquired with a considerably longer time than the helical CT images, respiratory motion may cause notable anatomic mismatch in the PET images. In later phases of our PET/CT development, we combined the 4D-CT simulation and PET/CT to avoid such a mismatching of anatomy (24). This procedure uses the average CT image set calculated from the 4D-CT images as the attenuation correction map for the PET images, replacing the conventional free-breathing CT images. In this procedure, patients are first instructed to regulate their breathing during the acquisition of 4D-CT images in the thoracoabdominal region. Then, conventional PET/CT is performed as described above. Upon image acquisition, the respiratory motion and image artifacts are assessed to determine which sets of CT and PET images will be used for treatment planning. As this chapter is written, this PET/CT simulation procedure is still evolving. In the near future, it may be made more automated and efficient, and offered as a commercial product.

Treatment Planning

In this subsection, three most important aspects of IMRT treatment planning for lung cancers will be discussed: Organ delineation, inverse planning, and selection of beam angles for IMRT treatment plans.

Organ delineation

In treating lung cancer, the assessment and delineation of the target volume are critical steps in treatment planning. In other chapters of this book, the use of CT, PET/CT, and other function-imaging modalities to delineate target volumes are addressed in more detail. In this section, only issues specifically related to IMRT treatment planning are discussed.

In the initial phase of treatment planning, we import multimodality images (typically simulation CT, PET/CT, 4D-CT if available, and other functional images such as SPECT/CT if available) into the treatment planning system. These images are first co-registered with the reference simulation CT images using the image fusion software in the treatment planning system or other available tools so that the patient coordinate system is consistent among the various datasets.

The target volume, typically the gross tumor volume (GTV), is outlined first. If 4D-CT images are available, the maximum excursion of the GTV, which we refer as the internal GTV (iGTV) is outlined. If PET/CT images are available, the iGTV will also be adjusted to include all the lesions demonstrated on PET. In essence, the iGTV is the largest enclosure of the disease extension that needs treatment from all image modalities. The iGTV is then expanded to a CTV by adding an isotropic margin, typically 8 mm wide, to account for microscopic disease. This definition of the CTV is equivalent to what is frequently called the internal target volume (ITV) (25). The CTV is then expanded to a planned treatment volume (PTV) by adding yet another margin, typically 8–10 mm isotropically, to account for the uncertainty of daily treatment setup and respiratory motion.

On the planning CT image, we outline normal lung (except for parts included in the GTV), esophagus, heart, spinal cord, liver, and kidney, if they are involved in the treatment fields. These organs could be outlined either on free-breathing CT images (for conventional CT simulations), or on one particular phase of the 4D-CT images (for 4D-CT simulations). For example, up to date, we have tested outlining the normal anatomy on the average CT (averaged from all phases of the 4D-CT images), mid-expiration or mid-inspiration phase of 4D-CT, or on the normal expiration or inspiration phase of 4D-CT. The mid-expiration CT images offers a more realistic approximation of the anatomy and dose distribution than other phases considering the motion during the respiration. However, the expiratory phase may offer more crispy and artifact-free images, and possibly more conservative estimation of dose distributions for lung and other normal organs than other phases of 4D-CT images.

We further expand the outlines for the esophagus and spinal cord by a 1-cm margin to account for the patient's movement. We also create an expanded PTV with an additional 1-cm margin referred to as the PTV moat. The normal tissue, which is enclosed by the skin and excludes the expanded PTV, is also outlined for planning purposes. Other structures are also added during the inverse planning process as needed.

IMRT inverse planning

The IMRT inverse planning process starts with the setup of radiation beams that can effectively treat the target volume with a minimal involvement of critical structures. As with the design of 3D-CRT plans, selecting and optimizing beam angles are very important steps in IMRT planning. Appropriately designed beam angles can improve the effectiveness of treatment plans tremendously and vice versa. This subject will be discussed more extensively later on. For lung cancers, we usually choose co-planar 6-MV photon beams unless the target volume and lung anatomy require a different beam arrangement and higher photon energy. In general, higher energy photon beams require a greater buildup distance to reach electron equilibrium. This may be detrimental for treating lung lesions with microscopic disease extending into the lung parenchyma. However, if achieving dose homogeneity in solid masses in soft tissues such as the mediastinum or sparing skin is clinically important, higher energy beams may be of benefit.

The most important aspect of IMRT planning is the understanding of the desired target coverage and tolerance of normal structures. In our clinic, we have a standard template of planning objectives for all lung cancer patients (Table 1). However, this generic template must be customized according to the clinical situations of each patient and requirements of the attending oncologists. In addition, keep in mind that the planning objectives are used to direct the inverse planning process. So they are naturally more restrictive and conservation than the actual clinical constraints. This is because in general, the optimization process usually stops when the goals are reached, in other words, it will not know automatically and will not attempt to obtain a solution better than what the planner is asking for.

Although we would ideally treat only the target volumes, it is physically impossible to avoid irradiation of other normal structures. The challenge is then

Table 1 Templates of Dose–Volume Objectives for Involved Structures Used in Initial IMRT Inverse Planning

Structure	Planning Objectives (more restrictive than actual clinical constraints)
CTV	Min dose > 95% prescription dose; max dose < 120% prescription dose
PTV	Min dose > 90% prescription dose; max dose < 120% prescription dose
PTV moat[a]	Max dose < 75% prescription dose (used to reduce dose outside PTV)
Lungs	V5 < 60%; V10 < 40%; V20 < 30%; mean lung dose < 19 Gy
Spinal cord	Max dose < 45 Gy
Heart	V40 < 40%
Esophagus	V40 < 40%
Liver	V30 < 25%
Kidney	V20 < 40% (both kidneys combined) V20 < 60% (for functional kidney if only one left)
Other tissue	Max dose < 120% prescription dose

Note: These objectives are used to direct the optimization process in achieving satisfactory isodose distributions and DVH constraints. Thus, the objectives listed are made more restrictive than the actual clinical goals. [a] PTV moat is a structure that is a 1-cm thick ring surrounding PTV. This structure is used to constraint the high dose from over-spilling outside the PTV. *Abbreviations*: CTV, clinical target volume; DVH, dose-volume histogram; PTV, planned treatment volume.

to make an intelligent and informed decision based on the trade-offs associated with the conflicting goals. Unfortunately, the tools available in current treatment planning systems are not developed enough to equip planners and clinicians to make such decisions easily. Also, because the solution space for alternative IMRT plans is often too large to be explored efficiently, researchers are still working on optimizing multi-objective treatment planning (17,26).

In treating lung cancers, two objectives are directly competing with each other. Namely, maintaining a conformal and uniform dose to the target volume and reducing the dose–volume of the irradiated healthy lung. The first goal reflects the need to deliver a high dose to the target volume with a curative intent. Meanwhile, radiation doses to the volume of the healthy lung should be limited as low as possible. The dose level at which lung damage appears is still being vigorously debated. However, we know from published data and clinical experience the exposed lung volume above 5 Gy and higher, as well as mean lung doses have been reported to be associated with an increased risk of radiation pneumonitis (6–8,27–29). Lung dose–volume histograms (DVHs) clearly show that the irradiated lung volume at these dose points and the mean lung dose are likely to be correlated. Thus, if we could reduce the volume of lung treated above 5 Gy, or V5, then we would more likely be able to reduce the amount of lung treated at higher doses (e.g. V10 and V20) and the mean lung dose.

When dose distribution, especially low-dose regions, are pushed away from the lung, the target conformity and dose uniformity have to be sacrificed to certain degree. In addition, when the volume of the lung exposed to low-dose radiation is reduced, the gradient of dose distribution becomes sharper near the edge of the target, and the likelihood of creating a hot spot (a small, isolated high-dose area) in other normal tissues is increased. Figure 1 has shown the example where a mediastinum target treated with minimum exposure to the normal lung and sharp dose gradient by the edge of the target. Here, planners must consider the connections between the goals of covering the target, protecting the normal lung, and reducing hot spots.

In multiobjective optimization, where multiple conflicting objectives are involved in the optimization process, current treatment planning systems usually use an approach in which a weighting factor is assigned to each objective and the individual objectives are combined into a single composite form in a simple arithmetic way. Although the weighting factor is sometimes called a priority or importance factor, those terms can be misleading in finding an appropriate weighting factors for the treatment objectives. Solutions to optimization problems depend on the subobjectives and their combined form. For example, if we assign a very high weight to the target coverage to make it a dominant objective, then the final plan will reflect that selection bias by paying little attention to the lungs and other structures. Assigning appropriate weighting factors is the key to obtaining a satisfactory compromise among conflicting objectives.

Based on the multiobjective nature of the IMRT inverse planning, we have performed in-depth research on how to achieve a reasonable treatment plan and determine the most sensitive objectives competing with the target coverage in a typical lung IMRT treatment plan (17). We found that protecting the lung is often the strongest objective in competition with the covering the target, while other objectives, such as reducing hotspots and protecting the heart, esophagus, and spinal cord, are easier to accomplish. Whether any objective is more or less competitive with the objective of covering the target depends on the size or volume of the structure involved and the desired dose–volume limit. The volumes of normal tissue hot spots, the spinal cord, and the esophagus are usually much smaller than the target and normal lung volumes. For the heart, the dose–volume limit is much greater than that of the lungs. Therefore, these structures can be more easily spared than the lungs. The same principle can be applied to the design of IMRT plans for tumors at other sites.

The treatment planning system we use (Pinnacle, version 7.4 Philips Medical Systems, Andover, Massachusetts) is well designed and provides the cost of individual objectives and the combined form. The total cost is simply the sum of the costs of the individual objectives, each multiplied by its weighting factor. These cost values are presented at each optimization iteration to guide treatment planners. Therefore, we took advantage of the information offered during the inverse planning iterations in the Pinnacle system and developed the following iterative process for designing IMRT plans with minimal trial-and-error.

In this process, we first assign a template of objectives (see Table 1) to the patient with a weighting factor of unity to all the objectives (the weighting procedure is updated during beam angle optimization (BAO), which will be discussed later). Starting with a standard, equally weighted template is a reasonable approach, because at this point in the process, we do not have a good idea of what can be accomplished for the patient. Next, the optimization is run for only one optimization iteration. At its completion, we obtain the IMRT plan's equivalent to a 3D-CRT plan with beam-eye-view collimation to the target and flat intensity within the beams. We then evaluate the cost of each objective to determine how to assign the weighting factors and adjust the dose–volume limits for each objective. In the first phase of the optimization process, the focus is to attain a reasonable target coverage with some degree of lung protection. Therefore, we choose a weighting factor such that the total cost for the target is approximately three times the total cost for the normal lungs. The other objectives, those concerning the spinal cord, esophagus, and heart, are ignored at this stage. The optimization is run through approximately five iterations, based on the existing plan's optimization solution. The plan is then evaluated to determine whether the weighting factors and dose–volume limits need to be readjusted. This process is repeated until the target is evaluated to have a reasonable coverage.

In the next phase of the planning process, which is focused on reducing the dose–volume of the normal lung, the weighting factors and dose–volume limits are adjusted to make the total cost for the lung equivalent to that for the target. The optimization is run for another five iterations based on the existing solution and (if necessary) repeated until the target coverage and lung sparing reach a reasonably acceptable compromise. The planner will need to check and balance between the objectives of these two competing structures.

In the third phase of the planning process, we evaluate the dose–volumes for the other structures (spinal cord, esophagus, and heart) and determine whether their weights and dose–volume limits need

to be adjusted. If they do, we increase the costs of their objectives to make them more important in the optimization. The optimization is run for several more iterations to achieve reasonable dose–volume sparing for these structures.

In the last phase of the planning process, we evaluate whether any of the hot spots in normal tissue pose a clinically significant problem. If yes, we create additional structures in the planning program to contour such hot spots, and add their objectives. We then assign appropriate weights, and designate dose–volume objectives for these hot spots to make those objectives more important. The optimization is run for a few more iterations until a reasonable compromise is reached between the target, lung, and hot spots. This will end the planning process with a solution that can be given to a physician for evaluation.

In the above process, we always repeat the optimization based on the existing plan without resetting the plan from the beginning. This is because the optimization algorithm used in the Pinnacle system and most other commercial systems is typically gradient-search based method that can speed up the optimization tremendously. Thus, the trade-off for the greater speed is an increased likelihood of trapping the optimization solution in the local minimum. In a sense, the solution is always the one closest to the starting point before optimization. Using this shortcoming to our advantage, we adjust the weighting and dose–volume objectives in the iterative and adaptive processes to take control of the optimization and achieve a reasonable compromise among the conflicting objectives. Unfortunately, this process has not been adopted to be an automated procedure in the commercial Pinnacle system. A great deal of progress must still be made to improve the above process. Ultimately, we hope to let the computer repeat the process and then provide the planner with a library of candidate plans. This approach would not demand the manual labor required by the current process and would explore the plan solution space in a much more efficient and productive manner (26).

Beam angle optimization

BAO is an important prerequisite for developing an effective IMRT plan involving the lungs. Unlike other cancer sites, such as the prostate and head and neck, the lungs are very sensitive to the selection of beam angles, and a good treatment plan should always minimize the exposure of lungs to low doses of radiation from the spread of multiple beam angles. Nine equally spaced beams should never be used in treating lung cancers except in hypothetical research situations. Such a beam arrangement may be used in treating, for example, head and neck cancers because

most commercial treatment planning systems lack efficient BAO tools. However, even in treating prostate and head and neck cancers, BAO has definite advantages that could improve the quality of IMRT treatment plans (30).

BAO is important in developing IMRT plans because IMRT is an advanced and sophisticated form of 3D-CRT, with intensity modulation added to the beams. In a 3D-CRT plan, BAO can determine the quality of the plan; the role of BAO in an IMRT plan is at least equally important. However, because the intensity modulation of IMRT beams can compensate for inferiorly planned beam angles, some argue that BAO is not needed for IMRT planning.

In a previously published study (15), we analyzed the role of BAO in lung IMRT planning and means of expediting the process for routine clinical operations. We learned that using fewer IMRT beams does not sacrifice the plan quality and that a general agreement exists between the best angle sets optimized in 3D-CRT and IMRT plans. In essence, the beam angles favored in 3D-CRT plans are generally preferred angles for IMRT plans as well, and BAO can be applied in a multiresolution setting (i.e. with various degrees of intensity modulation and angle resolution in the three-dimensional search space).

In IMRT plans for lung tumors, we found that the angles favoring the target volumes and normal tissues are usually more spread around to create more uniform dose distributions for these structures. However, the normal lung has sets of distinctively different angles that can be used to offer tissue protection. These angles in general are aligned in the AP direction, which minimizes the lung's exposure to radiation. Straight-lateral angles tend to pass through more lung tissue than AP beams. Thus, lateral beams should be avoided unless the target volume's location particularly calls for lateral beams.

Figure 3 shows a comparison of the IMRT plans generated using either five optimized beams versus nine equally spread beams. The isodose distributions indicate that the IMRT plans using fewer optimized beams can achieve essentially the same plan quality as those using more beams. However, the risk of low-dose radiation exposure to the lungs and thorax can be reduced using fewer beams. Also, with more beams, the monitor unit efficiency or the number of MUs for each beam is likely to be reduced, thus leading to more leakage from the MLCs and increased mechanical wear of the MLCs.

The complexity of BAO comes from another factor that the optimized angles and plans depend on the selection of the optimization objectives. It is apparent that if the planner puts more emphasis on certain structures, such as the target volume, the beam angle optimized will reflect that goal. Because each structure favors its own sets of angles, planners need to understand, again, the importance of balancing the competing structures when optimizing beam angles. In lung IMRT plans, as we have mentioned above, the target volume and normal lung are the two most heavily weighted competing structures; thus, the selection of beam angles must include consideration for these two structures, particularly the lungs, which are more sensitive to the beam selection than the target volume.

To make BAO a routine clinical operation, we developed the following procedure for the treatment planning process (manuscript in preparation):

1. A pair of equally weighted AP/PA parallel-opposed beams are set up to treat the PTV with appropriate beam eye view (BEV) collimation.
2. The dose and DVHs are calculated for this simple plan so that the minimal amount of the lung that must be exposed at various dose levels can be determined and the DVHs for other normal structures can be evaluated.

Figure 3 (*See color insert.*) Comparison of the isodose distributions of the IMRT plans using either five optimized beams (*left panel*) or nine equispaced beams (*right panel*). Fewer optimized beams can achieve essentially the same plan quality as more beams. However, the risk of spreading low-dose radiation exposure (e.g. 5 Gy) to the lungs and thorax can be reduced by using fewer beams.

3. A 3D template of beams is set up to treat the PTV with appropriate BEV collimation. This template consists of either 15–17 coplanar equispaced beams or additional non-coplanar beams in the anterior direction. We favor the coplanar beam arrangement unless the anatomy of the target volume calls for the non-coplanar arrangement, which typically happens with tumors located exclusively in the mediastinum with minimal lateral extension into the healthy lung.

4. With equal beam weights assigned to the 3D beam template, the doses and DVHs are calculated.

5. BAO objectives are created and include:
Minimum coverage of the PTV, for example, 95% of PTV covered by the prescribed dose; maximum allowed V5, V10, and V20 for the lungs; and mean lung dose. These criteria should come from the AP/PA plan that was initially evaluated. This approach uses the achievable limits from the AP/PA plan instead of requiring treatment planners to take a blind guess. Objectives for other structures can be entered, but usually are not necessary at this time.

6. Beam weight optimization (not intensity optimization) is performed for the 3D beams using the above objectives, with an equal weighting factor having been given to each objective. During the optimization process, the weighting factors for each objective can be adjusted to reflect the importance of each objective. The solution depends on the appropriate selection of the weighting factors for the objectives.

7. The beam weights for all the 3D beams are evaluated. The beams with the highest weights are those that favored by the current objectives. The angle arrangement is evaluated to determine its appropriateness and whether reoptimization is required.

8. All the beams with small weights are deleted and the 5 or 6 beams with the largest weights are kept.

9. If necessary, beam angles are fine-tuned and readjusted to avoid excessive overlap. For example, if a planner puts too much emphasis on sparing the lung, the beams with the largest weights may all end up aligned in the AP/PA direction, which may create too many hot spots and sacrifice more target conformity than necessary in order to spare the lungs. Slightly spreading the beams around the AP/PA direction can help balance the needs of target coverage and lung sparing.

10. Optimization is then run with intensity modulation added to the selected beams, making the process similar to the one discussed in the previous section.

Our current experience using BAO for the lungs indicates that most plans can be achieved using 5–7 beam angles. In fact, we limit the number of beams to fewer than six except in extraordinary cases. By using fewer beams, we will be able to control low-dose spread to the lungs and thorax. Here again, the conflict among many objectives—sparing the lungs, covering the target, and avoiding hot spots in normal tissues—must be considered. The closer the beams are arranged together, the more likely hot spots near the target will be created and target conformity will be sacrificed. This leads to a better sparing of the lungs. In some cases in which sparing the lung while attaining appropriate target coverage was difficult, we have had some success by adding one or two non-coplanar beams to spread the dose more, particularly for mediastinum targets that do not have much overlap with normal lung tissue.

Dosimetry Verification

When IMRT technology was introduced for treating lung cancer in our clinic, an in-depth dosimetry verification program was carried out to evaluate the accuracy of the dose distributions computed by the treatment planning systems. As mentioned earlier, IMRT for lung cancer has a set of requirements different from those for cancers at other sites. First, the dose–volume constraints for normal lung tissue require that the low dose in the lungs be calculated relatively accurately. Second, the lungs have low tissue density, which requires accurate heterogeneity correction in the thoracic region.

Our routine clinical IMRT QA program, which is carried out in the same way for cancers at all sites, consists of measuring the doses at several points in the high-dose target region using ion chambers and verifying intensity profile using radiographic film. In the first component, ion chamber measurements are taken in the center of a water phantom that mimics patient treatment conditions. In the second component, film measurements are taken using a solid water phantom that lets the IMRT beams incident perpendicularly on the phantom surface (31). This QA program has been replaced recently by a somewhat more efficient procedure that integrates the taking of chamber and film measurements using a single solid water phantom.

It is known that IMRT QA is time consuming and has many limitations, mainly caused by the fact that delivered doses are both time- and intensity-modulated. This requires that dosimeters have both high spatial and temporal resolutions. In addition, because of the variations in dose and energy spectra in an IMRT field, dosimeters that exhibit strong energy dependency, such as radiographic films and diodes, may over-respond in the low-dose region (manuscript

under preparation). Therefore, in the high-dose region, where the dose gradient is relatively small, ion chamber dosimetry is a reasonable option. In the low-dose region, where the dose gradient can be high, extra precautions must be taken to ensure measurements are meaningful, because ion chambers can give misleading results due to partial volume and other effects (32).

Because of the limitations of dosimetry measurements for IMRT QA, we also developed a full-scale Monte Carlo dose calculation system that was commissioned for clinical use (19,33). This Monte Carlo system was integrated with our existing treatment planning system and can be invoked within the Pinnacle planning system. Our system's components include: the conversion of Pinnacle beam parameters through Dicom-RT and other interfaces; the preparation of Monte Carlo simulation parameters; the completion of dose calculations on a Linux computer cluster; the conversion of doses to Pinnacle format; and the use of visualization and other data analysis tools. The accelerator heads are simulated with phase space data generated at a plane under the flattening filter. Later, MLCs and collimator jaws are simulated for specific IMRT fields by using an MLC model developed in-house (33). Dose calculations are performed in a patient phantom based on a patient's CT images.

The development of this Monte Carlo system required a great deal of effort to model the MLCs and understand the effect of MLCs on IMRT dose distributions. The results of our studies point to the fact that doses in IMRT fields are determined by three components: primary fluence that passes through the opening of the MLC leaves; secondary fluence (transmission and leakage) that passes through the MLC leaves; and tertiary fluence that is scattered from the MLC leaves by multiple Compton interactions.

In a typical 3D-CRT field with MLC collimation, the dose inside the field comes mainly from the primary fluence, while the dose at the penumbra and outside the field comes from the secondary and tertiary components. In an IMRT field, however, the contribution of the last two components depends on the degree of fluence modulation or MU efficiency (defined as the dose delivered to the target normalized by the number of MUs), as well as the size of the IMRT field. In a large IMRT field with a high degree of fluence modulation or low MU efficiency, the contribution from the transmission and leakage can be very high, while the dose at the penumbra and outside the field can be greatly increased by the presence of scatter from the MLC (34).

In a study that compared the dose distributions for thoracic IMRT plans from two treatment planning systems (the Pinnacle and Corvus systems) by using doses measured with ion chambers, TLDs, and films and by using Monte Carlo calculations (19), we found that the dose calculation accuracy of the commercial treatment planning systems in the high-dose target volume is more likely to meet clinical requirement. However, in the low-dose regions, such as in the normal lung tissue, a high degree of underestimation could occur because of the lack of sophisticated MLC modeling and therefore failure to account for MLC-contributed doses in such regions. Meanwhile, we found that the tissue heterogeneity effect was less important than the role of MLC modeling, even in the thoracic regions.

In a separate study, in which we focused on the low-dose regions of IMRT treatment plans
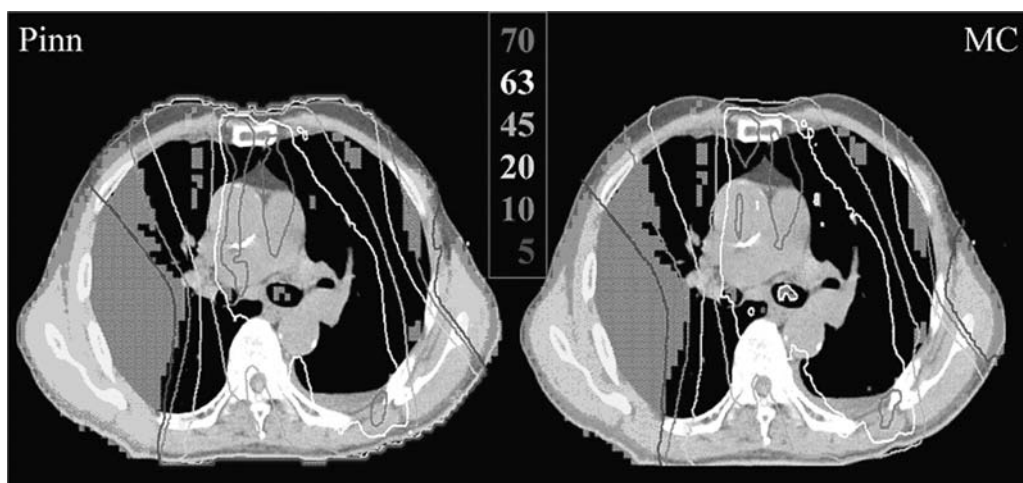
Figure 4 (*See color insert.*) Comparison of the dose distributions from the Pinnacle calculations (*left panel*) to the Monte Carlo calculations (*right panel*) for one patient with lung cancer who was treated with IMRT. The difference in the dose distribution, which either exceeded 5% in local dose or 5 mm in distance-to-agreement (because of the dose–gradient effect), is highlighted in yellow. The isodose is given in Gy. *Abbreviation*: IMRT, intensity-modulated rediation theraphy.

Table 2 Comparison of Dose to PTV, Mean Lung Dose, V5, V10, and V20 to Lung in IMRT Plans

Parameter	Monte carlo		TPS		Ratio or difference
PTV					
Dose to 95% volume (Gy)	Mean	Range	Mean	Range	Mean (Range)
Lung (with complication)	61.8	44.9–69.9	63.2	45.2–70.7	0.99 (0.96–1.02)
Lung (without complication)	65.5	60.3–70.0	66.0	61.7–70.1	0.99 (0.98–1.00)
Mesothelioma (Pinnacle)	45.0	42.9–54.2	45.2	44.3–54.2	0.99 (0.97–1.00)
Mesothelioma (Corvus)	46.7	44.4–52.6	48.3	47.2–52.0	0.97 (0.94–1.01)
Mean lung dose (Gy)					
Lung (with complication)	23.2	18.6–26.1	22.4	18.0–25.7	1.04 (1.01–1.06)
Lung (without complication)	9.1	8.3–10.2	8.7	7.9–9.5	1.05 (1.04–1.07)
Mesothelioma (Pinnacle)	9.7	8.7–9.9	8.4	7.8–8.8	1.15 (1.11–1.19)
Mesothelioma (Corvus)	9.5	9.3–10.0	8.7	8.1–9.3	1.09 (1.07–1.15)
V5 (%)					
Lung (with complication)	75.1	60.5–79.4	72.0	56.3–75.2	3.7 (1.6–7.2)
Lung (without complication)	33.8	29.5–34.2	31.7	28.5–33.0	1.2 (1.0–2.1)
Mesothelioma (Pinnacle)	77.1	61.0–97.3	54.5	42.4–72.3	22.5 (12.6–25.0)
Mesothelioma (Corvus)	94.7	83.7–99.2	83.4	62.9–93.8	11.3 (5.5–20.8)
V10 (%)					
Lung (with complication)	57.1	37.7–65.8	55.0	35.0–63.6	2.4 (−0.6–4.0)
Lung (without complication)	21.9	19.3–27.4	21.5	18.9–26.2	0.4 (0.4–1.2)
Mesothelioma (Pinnacle)	26.1	22.1–30.2	20.2	18.7–25.6	3.4 (2.5–7.4)
Mesothelioma (Corvus)	25.3	24.5–31.9	19.6	19.3–25.8	5.9 (4.9–6.1)
V20 (%)					
Lung (with complication)	38.5	28.9–44.5	37.0	28.3–43.7	0.9 (0.3–2.2)
Lung (without complication)	12.8	12.1–15.3	12.9	11.9–15.3	0.0 (−0.1–0.2)
Mesothelioma (Pinnacle)	8.4	6.1–10.3	7.8	6.1–9.4	0.6 (0.0–1.1)
Mesothelioma (Corvus)	7.7	4.9–8.8	7.2	4.7–8.5	0.5 (0.1–3.6)

Note: IMRT Plans computed by either Monte Carlo or commercial treatment planning systems (TPS, Pinnacle system version 7.6 or Corvus system version 5.0.). The ratio in case of PTV dose and mean lung dose, or difference in the lung DVH in case of V5, V10, and V20 for lung between the two different ways of dose calculations are listed. Four types of cases were studied: NSCLC cases with radiation pneumonitis developed (with complication) or without (without complication); Mesothelioma cases planned using the Pinnacle or Corvus treatment planning systems.
Abbreviations: PTV, planning target volume; V5, V10, V20, irradiated volume more than 5, 10, 20 Gy, respectively; TPS, treatment planning system; Difference, Monte Carlo–TPS; Ratio, Monte Carlo/TPS data presented as the mean value.

(manuscript under preparation), we found consistent and interesting results indicating how MLC scatter contributes to low-dose spread outside planned IMRT fields. For example, in comparing dose distributions from either Pinnacle or Corvus to distributions calculated in Monte Carlo systems, we found that the commercial systems underestimated the V5 for the normal lung (Fig. 4), particularly outside the IMRT beam penumbra. This underestimation was caused by ignoring the MLC scatter in the IMRT fields, which contributes to the low dose near the beam penumbra and outside the beams. Table 2 summarizes the results from this study, showing the treatment planning- and Monte Carlo-computed doses for lung cancer cases and mesothelioma cases that would be treated with IMRT. The degree of underestimation of V5 for the lungs depended on the size of the PTV and somewhat on the MU efficiency used in the beam delivery.

Although it is debatable whether such underestimation of low doses has clinical significance, for example, in terms of toxic effects on normal tissue, it is well established that low-dose spread to a large volume of normal tissue is detrimental and should thus be avoided in any IMRT treatment. In addition, for studies focused on the biological effects of IMRT treatments (e.g. secondary malignancies), dose estimation in low-dose areas far away from the main fields that nonetheless receive radiation due to scatter from the MLC and head-leakage will be important.

In reviewing the above results, we believe that clinics implementing IMRT for lung and thoracic cancers should examine the dose distributions obtained from the treatment planning systems carefully, particularly for IMRT fields with high fluence modulation and large target sizes. This explains why, in the treatment planning section, we emphasized the importance of simplifying IMRT plans by minimizing the over-modulation of fluence and the number of beam angles. Doing both can help reduce the number of MUs and thus MLC leakage and scatter that cause unnecessary increases in the low-dose exposure of normal tissues. In addition, it should be remembered that the low doses (particularly those below 10 Gy) calculated by the planning system could be significantly underestimated. Therefore, minimizing such low-dose volumes is even more important during IMRT treatment planning.

EFFECTS AND MANAGEMENT OF RESPIRATORY MOTION

As discussed in treatment simulation and planning section, 4D-CT has become more accessible to many of our patients and possibly other cancer centers. Respiratory motion has attracted a great amount of attention in those studying IMRT and IGRT for lung cancers because of the challenges of treating moving targets with precise doses of radiation. We have imaged and studied breathing motion patterns in patients with lung cancer, the behavior of the lung cancers during breathing, and the dosimetric effects and appropriate approaches for dealing with such motions.

In a recently completed research study, we analyzed 4D-CT images acquired from approximately 250 patients with lung cancer who were treated in our clinic (manuscript in press). Of these patients, approximately half underwent 4D-CT of the entire lung, which allowed the acquisition of information on how the entire lung moved during the imaging sessions. The patients were asked to perform normal free-breathing during CT scanning. The results of this important study showed that the primary direction of tumor motion was craniocaudal. The percentages of tumors that moved more than 0.5 cm along the SI, lateral, and AP axes were 39.2%, 21.8%, and 5.4%, respectively.

For 95% of the tumors studied, the tumor motion were less than 1.34, 0.40, and 0.59 cm, respectively, along the SI, lateral, and AP axes. These results are summarized in Table 3, which shows the ITV margins estimated to cover the motion of the tumors obtained from the 4D-CT study on the lung tumors.

The distribution of tumor motion in the three dimensions suggests that anisotropic treatment margins would be more appropriate than the uniform margin conventionally applied. We also found that the movement of tumors was most likely caused by diaphragm motion. A linear "rubber-band" effect was observed for the lung tumor movement, that is, the lung motion was initiated at the bottom of the lungs where the diaphragm exhibited the greatest amount of movement; this diaphragm movement was then propagated to the top of lung with the lung parenchyma serving as a non-elastic spongy rubber band to move the tumors along. Thus, the tumor location along the SI axis and the size of the tumors greatly influence the mobility of the tumors. Figure 5 shows the distribution of the tumor motion along three dimensions and the total motion as a vector sum of the 3D components for 166 lung tumors studied with 4D-CT (among which, 87 tumors were from stage III/IV NSCLC patients). The degree of tumor motion along the SI direction as a function of the GTV size is shown in Figure 6 for tumors located in the
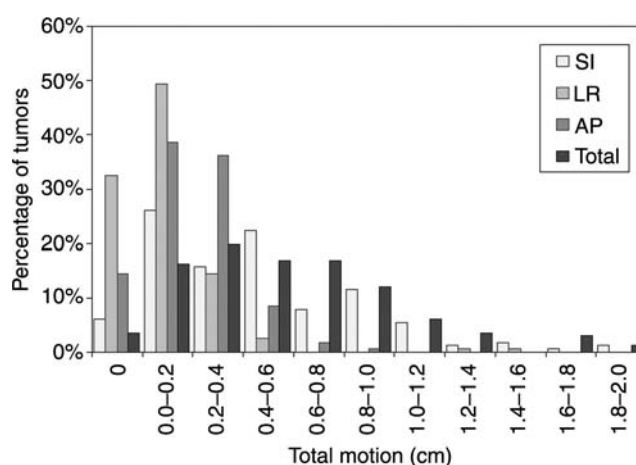
Figure 5 Distribution of the tumor motion along the SI, lateral (LR), and AP axes, along with the magnitude of the total motion vector (the vector sum of the motion component along the three dimensions). The results were summarized from 166 tumors of lung cancer patients simulated with 4D-CT and natural free-breathing. *Abbreviations*: 4D-CT, four-dimensional computed tomography; AP, anterior–posterior direction; LR, left–right direction; SI, superior–inferior direction.

Table 3 The Estimated Tumor Motion Along Each Dimension Based on 4D-CT Study of 166 Tumors from Lung Cancer Patients

	SI (cm)			All tumors (*N*)	
		GTV size (cm³)		LR (cm)	AP (cm)
fSI	<100 (*N*)	100–400 (*N*)	>400 (*N*)		
fSI < 0.25	0.6 (23)	0.3 (5)		0.4 (166)	0.6 (166)
0.25 < = fSI<0.5	1.3 (26)	0.7 (28)	0.4 (11)		
fSI > = 0.5	1.8 (28)	1.3 (28)	0.8 (7)		

Note: The motion margin was obtained to cover at least 95% of the tumors studied under each group of cases. The tumor motion in the SI direction was dependent on the GTV size and fractional SI direction, and was thus subdivided into 9 groups of cases. The number of tumors available for the study were also included in the brackets. The tumor SI location was quantified by fractional SI distance or fSI, which is the distance from the apex of the lung to the centroid of the GTV normalized by the distance from the apex of the lung to the diaphragm on the same plane as the GTV centroid.

Abbreviations: 3D, three-dimensional; 4D, four-dimensional; CT, computed tomography; SI, superior–inferior direction (axis is towards patient's feet); LR, left–right direction (axis is towards patient's right); AP, anterior–posterior direction (axis is toward anterior of patient).
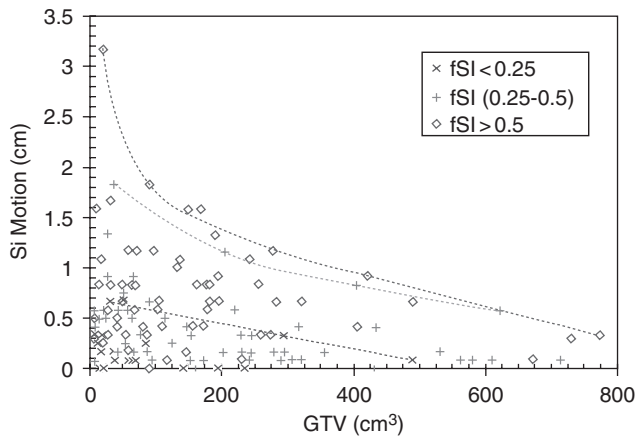
Figure 6 The scatter-plot of the tumor motion in the SI direction versus the GTV size for the same 166 tumors as those of Figure 5. Because the magnitude of tumor motion was found to be dependent on the SI tumor location and diaphragm motion as well, the data were further separated into three groups according to the fractional SI location (or fSI, defined as the ratio between the distance from the apex of the lung to the GTV centroid versus that from the apex to the diaphragm through the same plane of the GTV centroid): the upper lung tumors with fSI < 0.25; the upper-middle lung tumors with 0.25 < fSI < 0.5; and the mid-lower lung tumors with fSI > 0.5. The small lower lobe tumors exhibited the greatest amount of motion, in contrast to the upper larger tumors which were immobile. *Abbreviations*: GTV, gross tumor volume; SI, superior–inferior direction.

upper quadrant, upper to mid quadrant and low half of the lung. The mobility of the small tumors in the low lobe of the lung can be appreciated. In contrast, large tumors located in the apex of the lung were nearly still during breathing.

Following this study, we also have a concurrent research protocol for acquiring 4D-CT images of lung cancer patient during every week of his or her treatment; our goal is to document the changes in the tumor anatomy and respiratory motion that occur during the treatment course. Preliminary analysis of the data from this study confirmed our expectations that there is a high probability that tumors shrinkage may affect the respiratory motion during treatment course (35, manuscript under preparation). Therefore, the ITV margin determined from the initial treatment simulation may need to be assessed more frequently than current standards demand. An even safer approach is to use a wider and more conservation ITV margin for patients whose tumors are more likely to move, for example, those with tumors located in the lower lobes and the posterior portions of the lungs.

The potential interplay of effects between MLC and tumor motion during breathing may cause dose discrepancies in IMRT delivery. However, such interplay effects bear a stochastic nature for each interval of the dose delivery, for example, during the beam-on

of each fraction. Thus, the cumulative effect after the delivery of multiple beams and multiple fractions may quickly wash out (9). Although we acknowledge the existence of such an effect, in our experience, it has a very minor dosimetric impact for the use of IMRT for lung cancers beyond 10 fractions. In particular, data from our 4D-CT study show that the percentage of patients with free-breathing tumor motion greater than 1 cm may be less than 10%. Thus, for advanced lung cancers with large target volumes, the possibility of the tumor motion may affect the IMRT beam delivery is further reduced.

To understand the effect of breathing motion on the dose distributions of the treatment plans, we performed a separate preliminary study on 4D treatment planning (manuscript under preparation). In this study, patients who underwent 4D-CT for the entire lung had treatment plans that used all phases of their 4D-CT images. The dose distributions from the entire respiratory cycle were added together using the deformable registration technique (30). We computed the actual dose from one full cycle of respiration, which could then be applied to any phase of the 4D-CT images. In general, we chose the expiratory phase as the reference phase because of its longer duration and stability compared to other phases.

Figure 7 shows the comparison of dose distributions between inspiration and expiration for one patient treated with IMRT. This patient was found to have the largest change in dose distributions during the breathing cycle of all the cases studied. Such change is mainly caused by anatomic movement with respiration, in this case, the superior–inferior (SI) movement of the heart and ventilation of the lung during breathing.

The results from this study yielded a few important messages. First, the photon dose distribution plans does not change significantly with breathing motion because mega-voltage photon beams are not very sensitive to anatomic changes. However, the dose distribution may change noticeably when other organs, typically the heart, diaphragm, liver, and stomach, move in and out of the photon fields, as shown in Figure 7A and B.

Second, because lung volume constantly changes during breathing, the DVHs of the lung reflect such changes. For example, in comparing the DVHs between inspiration and expiration phases as seen in Figure 7C, the lung DVHs increase during exhalation because of lung volume reduction. However, the dose mass histogram computed, considering the mass of the lungs, would be more consistent across the breathing cycle because lung mass is relatively stable during breathing.

Third, considering the composite dose distributions, which are combinations of all the dose
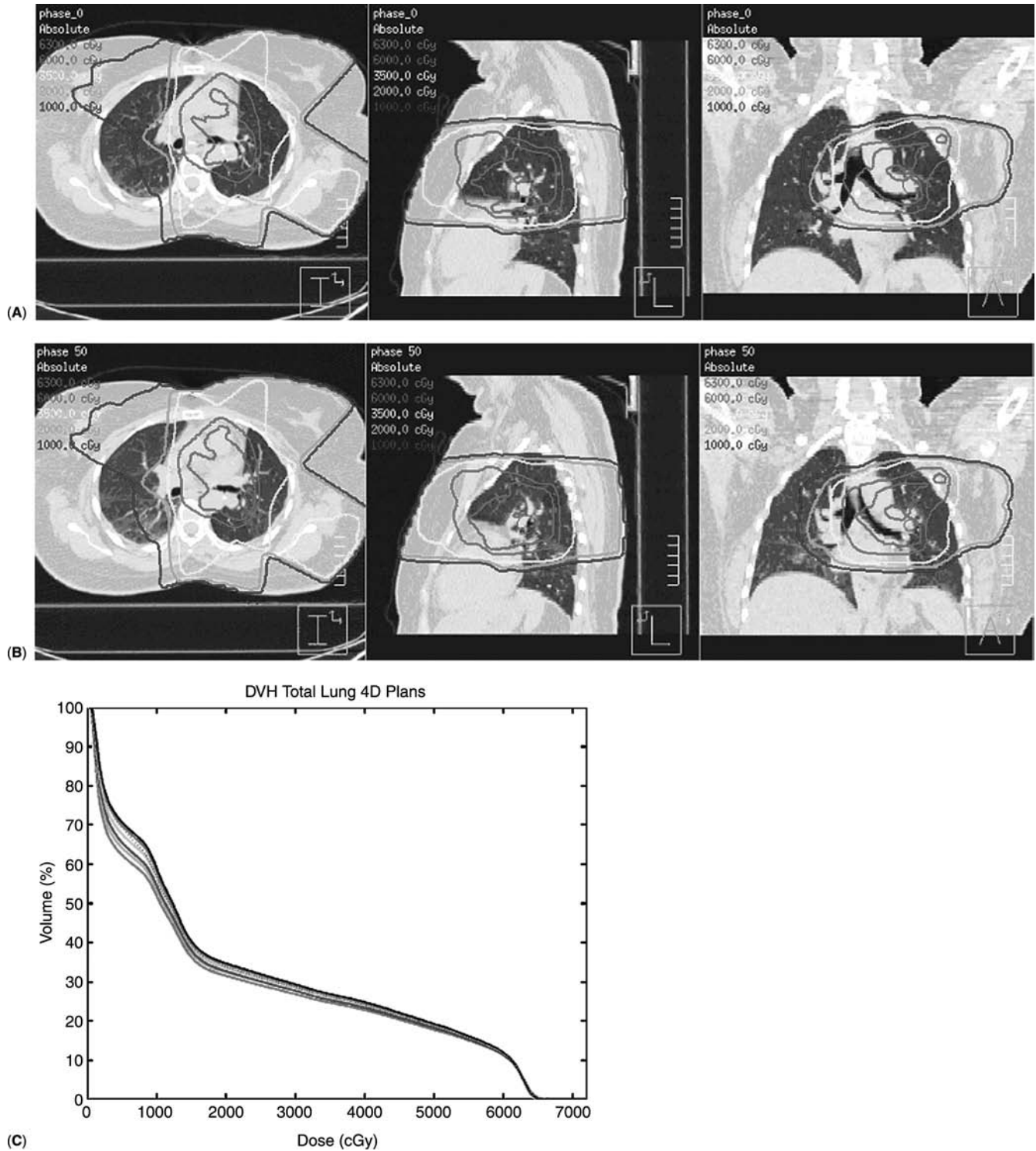
Figure 7 (*See color insert.*) Comparison of dose distributions between inspiration phase (**A**) and expiration phase (**B**) for one patient with lung cancer treated with IMRT. The change in dose distribution was mainly caused by anatomic movement (in this case, the heart) during breathing. The change in lung DVH is given (**C**), which shows the increase of the DVH during the expiration phase as a result of decreased lung volume. *Abbreviations*: DVH, dose–volume histogram; IMRT, intensity-modulated radiation therapy.

distribution phases, the actual dose distribution is more realistically represented by a mid-respiratory phase, such as the mid-inspiration or mid-expiration phases, than any other phases. One of these mid-

respiratory phases could have been used to compute the plan and estimate the approximate dose distribution without computing the plans for all the phases and deforming them together. Logically, this is

consistent with the fact that a mid-respiratory phase physically occurs between inspiration and expiration and thus could represent the "average" state of the anatomy and how the dose distributions move during the breathing cycle.

To best account for respiratory motion, we use 4D-CT to assess the ITV for the treatment planning process. Because 4D-CT is very demanding in terms of computational and staff resources, 4D-CT should be used for those patients who are most likely to present with a large degree of motion—those with small tumors, or lower-lobe tumors. In addition, the ITV margin should be enlarged to accommodate the uncertainty due to breathing motion during the treatment course. For patients with great tumor motion, although breath-hold and gating techniques may eventually be used in treatment, the combination of IMRT with these techniques may prolong treatment time and increase patient discomfort. Therefore, in our clinic, IMRT is usually delivered with patients instructed to perform shallow free-breathing.

USE OF FUNCTION IMAGING FOR IMRT PLANNING

The motivation for using IMRT to treat lung cancer comes mainly from the clinical need to spare normal and especially functional lung tissue. It is known that unlike normal lungs, a diseased lung does not have uniform function distribution (36,37). The ventilation of the lungs in general largely occurs in the lower portion of the lungs with diaphragmatic breathing, and the perfusion of the lung may change depending on vascular distribution, gravity, and other factors. If we are to spare the lung optimally from a functional point of view, the conventional CT images of the lung may have to be complemented by other modalities that offer information not only on the anatomy but also the function of the lung.

In the beginning stage of using 3D-CRT, lung function imaging, typically perfusion imaging using SPECT, was used in the treatment planning and dose–response assessment (37,38). SPECT imaging has revealed that even normal lung tissue in patients without lung cancers can be highly heterogeneous. In patients with lung cancer, large perfusion defects with hypo-perfusion could appear because of blockage of the tumors, to the pulmonary vessels, or to other tumor-associated structures. It has also been reported that patients with poor pulmonary function may be more at risk for such perfusion defects. It then becomes an interesting question: whether the existence of such perfusion defects can be used as a treatment advantage to better spare lung function.

In 3D conformal planning, optimal beam angles and dose distributions can be re-oriented considering the distribution of the lung perfusion. Theoretically,

given the distribution of lung perfusion, this would make sense for IMRT planning, which is much more flexible in accommodating and customizing dose distributions according to hypo-perfused regions, while sparing other hyper-perfused functioning lung (38,39). Recently, we completed a series of studies to clarify perfusion in the lungs of patients with lung cancer and understand whether the perfusion distribution could be used in IMRT planning.

In the process of using the SPECT for IMRT planning, the patients undergo SPECT/CT scanning (using such commercially available equipment as Hawkeye, GE Healthcare, Waukesha, Wisconsin and Symbia, Siemens Corporation, New York) with 185 MBq of technetium-99m-labeled macro-aggregated albumin. The treatment positions are duplicated in setting up the patients for the SPECT imaging. In addition, thoracic land markers are also used near the alignment points on the patients. The SPECT images are fused with the planning CT images, which are further used to evaluate the quality of the perfusion. We then visualize the distribution and quantify the perfusion using histograms and derivatives of the SPECT histograms. For example, one term that we have used in this qualification process is called "area-under-curve" or AUC. This is the area of the cumulative SPECT histogram. This index gives us an idea of how heterogeneous the SPECT appears (manuscript in press).

To use SPECT in IMRT planning, ideally, the SPECT count of each voxel in the normal lung (excluding the GTV) is used to assign a function weighting factor combined with the local dose distribution. This term gives the function-dose for the local voxel and can be used in constructing the dose–function histogram (DFH) (37) and the corresponding objective functions for IMRT planning. Unfortunately, most commercial treatment planning systems do not have this advanced application implemented, and we must incorporate this process into our own research platform.

A simple way of taking advantage of the lung perfusion distribution in the IMRT planning process is to directly contour the perfusion levels. For example, we normally contour the hyper-perfused regions, such as the lung volumes in the top 10th, 25th, and 50th percentile of lung volumes. The objectives for these structures are then created in the IMRT plans to signify their function status and the desire to protect them further. The IMRT plan can be run with BAO or in the routine process as described earlier. We have observed that the dose distributions in hyper-perfused regions can be pushed away by more aggressively protecting the regions and rearranging the dose given to the hypo-perfused areas. In this way, we may achieve better lung DVHs

and DFHs, while target coverage and other structures may not be affected significantly .

An example of a function-based IMRT plan is shown in Figure 8; the patient presented with a large perfusion defect caused by the tumor. SPECT images were fused with planning CT images to show the perfusion distribution in the lung. In general, we found that patients with non-uniform lung perfusion were more suitable for and benefited more clearly from SPECT based IMRT planning than patients with few perfusion defects or relatively regular perfusion distributions.

In addition to the possibility of using function images to optimize the intensity of IMRT beams, we also performed a separate study on BAO for IMRT to address whether information about lung perfusion distributions may alter the optimization of beam angles (manuscript under preparation). To summarize, the study showed that the optimized angles for lung IMRT plans are usually aligned with the AP axis of the lungs. And unless the perfusion defects meaningfully offset the lung function distribution, the beam angles optimized using lung perfusion images are very similar to those based on traditional CT images. Table 4 summarizes the difference between the beam angles used in plans generated using anatomic and function images with and without non-coplanar beams. In addition, Figure 9 shows the distribution of optimized angles from these plans and the similarity between the anatomic and functional plans. The results indicate that when using either anatomic CT images or perfusion SPECT images, the angles that most appeared to protect the normal lung tissue were those aligned with the AP/PA axis of the thorax. The benefits of using non-coplanar beams seemed to

be small if the functional images were not used in the planning process.

From extensive treatment planning studies using the function images on both early- and advanced-stage lung cancers, we found that patients who have a greater degree of heterogeneity in perfusion distribution and who have large perfusion defects may benefit most from function-based planning. In addition, the location of the defects is also very important. Additional sparing of the lungs may be difficult when perfusion defects caused by previous radiation treatment are located either too close to the tumor, which is common in advanced lung cancers, or too far away from the tumor, because the likelihood of successfully rearranging the dose distribution to accommodate these hypo-perfused regions is greatly reduced. In other words, the perfusion defects must be located in the regions where the low to medium doses (between 5 and 30 Gy) would typically be distributed. Only then can we take advantage of the presence of the hypo-perfused regions and reallocate the radiation dose. In addition, the perfusion defect must be large enough to be affected by a dose rearrangement. With these limitations, we found that fewer than one third of patients are ideal candidates for such function planning. As shown in an earlier study, patients with poor pulmonary function may be more likely to present with perfusion heterogeneity and perfusion defects than patients with healthier lungs.

The picture is somewhat more blurred considering the possible reperfusion of hypo-perfused regions, as has been found in existing clinical evidence. For perfusion defects caused by tumor blockage of the pulmonary vessels, tumor shrinkage may release and change blood distribution to the

(A)   (B)
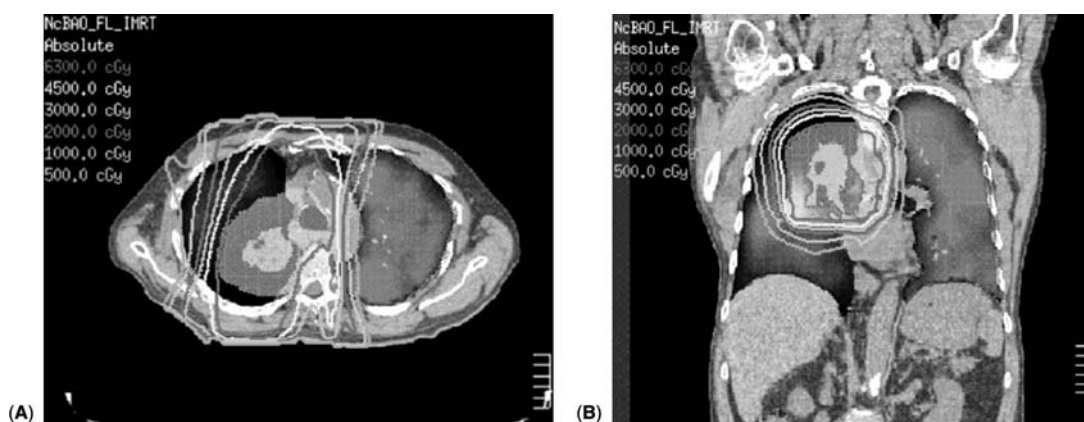
Figure 8 (*See color insert.*) An IMRT plan generated using the lung perfusion images fused with the planning CT images. The SPECT images were shown with high intensity areas indicating hyper-perfusion in the lungs. The perfusion defect can be seen in the apex of the right lung near the tumor. Isodose lines were made to conform to the target volume with minimal impact to the functional lung with hyper-perfusion. The axial view (**A**) and coronal view (**B**) of the dose distributions are given in cGy. *Abbreviations*: CT, computed tomography; IMRT, intensity–modulated radiation therapy; SPECT, single photon-emission completed tomography.

Table 4 Number of Beams That Were Different in Four Types of IMRT Treatment Plans

	Anatomical BAO	Differences	Functional BAO
Coplanar BAO	Coplanar: 6	1 (0–2)	Coplanar: 6
Differences	*3 (1–4)*	*3 (1–4)*	*3 (1–4)*
Non-coplanar BAO	Coplanar: 3 (2–6)	1 (0–2)	Coplanar: 3 (2–5)
	Non-coplanar: 3 (0–4)		Non-coplanar: 3 (1–4)

Note: Anatomic BAO: beam angles optimized with anatomical images only using either coplanar beams only or coplanar and non-coplanar beams; functional BAO: beam angles optimized with functional lung perfusion images using either coplanar beams only or coplanar and non-coplanar beams. In the coplanar plans, six beams were used with their angles optimized. In the non-coplanar plans, on average, three beams were coplanar (range, 2–6), and three beams were non-coplanar (range, 0–4). Results were based on studying 10 patients with NSCLC who had SPECT images showing remarkable perfusion defects near the tumors. The number of beams that were different among the four types of plans was given as an mean value and range (minimum–maximum). The results show that the beam angles optimized based on the anatomic and functional images were very similar among the plans.
Abbreviation: BAO, beam angle optimization.

previously non-functioning areas. If excessive doses are given to such areas, we may reduce the chance of that such tissue will function again.

Although the idea of using function images for IMRT treatment planning is appealing and clinically sound approach, limited applications for function images are currently available in clinical settings, particularly given that few patients are likely to benefit from such a procedure and that the procedure is associated with a high medical cost. More research is needed to improve the preselection and prescreening of patients and to understand the best way to utilize function images in the IMRT planning optimization process. For example implementing DFH and its associated objectives takes advantage of the voxel-by-voxel variations in perfusion distributions, but lung perfusion is reduced by radiation with dose dependency. As such, function images of the lung could be used to better quantify the performance of the lung and possibly correlated with other clinical endpoints, such as radiation pneumonitis and reduction in pulmonary function. Because the relationship between these different endpoints is not clear (40–42), further research is needed to clarify the biologic and pathophysiologic nature of radiation-related and radiation-caused lung injury; doing so would allow further improvements of treatment techniques using IMRT and IGRT to be developed.
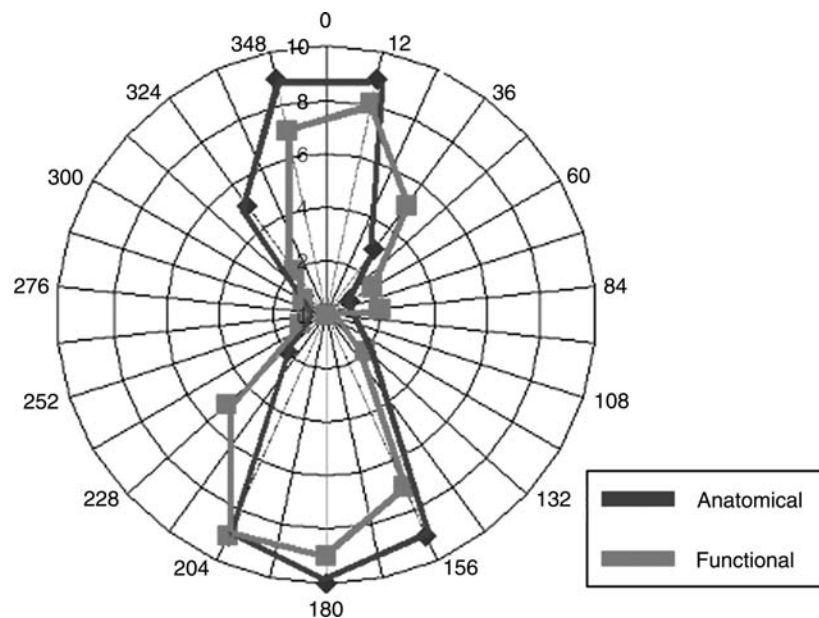
Figure 9 The pattern of beam angles most likely chosen in IMRT plans with beam angle optimized using either anatomic CT images only (anatomic) or with functional lung perfusion images added (functional). The plot shows the probability of choosing certain beams in IMRT plans versus the beam angle, with results generated using SPECT images from 10 patients with NSCLC with perfusion defects by the tumors. Only coplanar beams were used in this study. Results clearly demonstrate that the AP axis offers the most favorable angles for protecting normal lung tissue. There is an agreement among the angles optimized with either anatomic or functional images. *Abbreviations*: AP, anterior–posterior direction; CT, computed tomography; IMRT, intensity-modulated radiation therapy; NSCLC, non-small cell lung cancer. SPECT, single photon-emission computed tomography.

Apart from using the clinical standard of SPECT to obtain lung perfusion images, more recent breakthroughs have been made using 4D-CT to obtain the distributions of lung ventilation and perfusion (43,44). This research is currently underway with computer softwares possibly integrated with treatment planning systems to provide function distribution of the lung.

SUMMARY

In this chapter, we reviewed the rationales and techniques for using IMRT to treat lung cancers. IMRT is used independently and in combination with function imaging to achieve dose modulation and sculpting in the thoracic region and thus, dose conformity to thoracic target volumes and dose avoidance or function protection of normal lung, heart, spinal cord, and other normal tissues. Proper patient selection is a prerequisite to taking advantage of the benefits that IMRT could possibly offer. IMRT is ideally suitable for patients with locally advanced lung cancers to be treated with curative intent. In implementing IMRT for lung cancers, accounting for respiratory motion and the possibility of spreading low doses of radiation to a greater amount of normal tissues require close attention. Specifically, dealing with the spread of low dose radiation requires that the conflict among many clinical concerns—achieving target conformity, protecting normal lung tissue, and avoiding the creation of hot spots in normal tissue—be properly understood to reach a reasonable trade-off during treatment planning. BAO plays an important role of using IMRT for lung cancer. Planners must also consider that the low-dose regions in an IMRT plan can be further elevated by high modulation and large target size, which commercial treatment planning systems may not yet be properly designed to accommodate.

Other advanced technologies, such as IGRT and function imaging, are being incorporated into radiation therapy and IMRT. In the meantime that we embrace these new changes in the radiation oncology practice, we must evaluate the clinical outcomes for these technologies to understand the benefit versus costs offered by these new options and how much impact the technological advances truly bring to the lung cancer patients worldwide. Since we started using IMRT for lung cancers, we have been vigilant in collecting clinical outcome data and studying the clinical benefits of IMRT in terms of toxicity to normal tissue and local control versus survival. Preliminary results show that using IMRT for locally advanced NSCLC has promising advantages over 3D-CRT. As this chapter is written, the results of several studies are emerging and being prepared for publication. Some of these results, including the details of the outcome study, are discussed in a separate chapter, and others are to be published in the near future. Also needed are prospective and randomized phase III clinical trials, which may supply concrete clinical evidence on the outcome improvement and directions for future research; both are underway in our clinic.

ACKNOWLEDGMENTS

REFERENCES

1. Zelefsky MJ, Chan H, Hunt M, Yamada Y, Shippy AM, Amols H. Long-term outcome of high dose intensity modulated radiation therapy for patients with clinically localized prostate cancer. J Urol 2006; 176:1415–9.

2. Garden AS, Morrison WH, Rosenthal DI, Chao KS, Ang KK. Target coverage for head and neck cancers treated with IMRT: review of clinical experiences. Semin Radiat Oncol 2004; 14(2):103–9.

3. Puri DR, Chou W, Lee N. Intensity-modulated radiation therapy in head and neck cancers: dosimetric advantages and update of clinical results. Am J Clin Oncol 2005; 28:415–23.

4. Demanes DJ, Rodriguez RR, Schour L, Brandt D, Altieri G. High-dose-rate intensity-modulated brachytherapy with external beam radiotherapy for prostate cancer: California endocurietherapy's 10-year results. Int J Radiat Oncol Biol Phys 2005; 61:1306–16.

5. Kong FM, Hayman JA, Griffith KA, et al. Final toxicity results of a radiation-dose escalation study in patients with non-small-cell lung cancer (NSCLC): predictors for radiation pneumonitis and fibrosis. Int J Radiat Oncol Biol Phys 2006; 65: 1075–86.

6. Trodella L, Ramella S, Salvi G, et al. Dose and volume as predictive factors of pulmonary toxicity. Rays 2005; 30:175–80.

7. Mehta V. Radiation pneumonitis and pulmonary fibrosis in non-small-cell lung cancer: pulmonary function, prediction, and prevention. Int J Radiat Oncol Biol Phys 2005; 63:5–24.

8. Rodrigues G, Lock M, D'Souza D, Yu E, Van Dyk J. Prediction of radiation pneumonitis by dose–volume histogram parameters in lung cancer—a systematic review. Radiother Oncol 2004; 71:127–38.

9. Bortfeld T, Jiang SB, Rietzel E. Effects of motion on the total dose distribution. Semin Radiat Oncol 2004; 14:41–51.

10. Liu HH, Wang X, Dong L, et al. Feasibility of sparing lung and other thoracic structures with intensity-modulated radiotherapy for non-small-cell lung cancer. Int J Radiat Oncol Biol Phys 2004; 58:1268–79.

11. Murshed H, Liu HH, Liao Z, et al. Dose and volume reduction for normal lung using intensity-modulated radiotherapy for advanced-stage non-small-cell lung cancer. Int J Radiat Oncol Biol Phys 2004; 58:1258–67.

12. Grills IS, Yan D, Martinez AA, Vicini FA, Wong JW, Kestin LL. Potential for reduced toxicity and dose escalation in the treatment of inoperable non-small-cell lung cancer: a comparison of intensity-modulated radiation therapy (IMRT), 3D conformal radiation, and elective nodal irradiation. Int J Radiat Oncol Biol Phys 2003; 57:875–90.

13. Choi Y, Kim JK, Lee HS, Hur WJ, Chai GY, Kang KM. Impact of intensity-modulated radiation therapy as a boost treatment on the lung-dose distributions for non-small-cell lung cancer. Int J Radiat Oncol Biol Phys 2005; 63:683–9.

14. Schwarz M, Alber M, Lebesque JV, Mijnheer BJ, Damen EM. Dose heterogeneity in the target volume and intensity-modulated radiotherapy to escalate the dose in the treatment of non-small-cell lung cancer. Int J Radiat Oncol Biol Phys 2005; 62: 561–70.

15. Liu HH, Jauregui M, Zhang X, Wang X, Dong L, Mohan R. Beam angle optimization and reduction for intensity-modulated radiation therapy of non-small-cell lung cancers. Int J Radiat Oncol Biol Phys 2006; 65:561–72.

16. Wang X, Zhang X, Dong L, Liu H, Wu Q, Mohan R. Development of methods for beam angle optimization for IMRT using an accelerated exhaustive search strategy. Int J Radiat Oncol Biol Phys 2004; 60:1325–37.

17. Zhang X, Wang X, Dong L, Liu H, Mohan R. A sensitivity-guided algorithm for automated determination of IMRT objective function parameters. Med Phys 2006; 33:2935–44.

18. Zhang X, Liu H, Wang X, Dong L, Wu Q, Mohan R. Speed and convergence properties of gradient algorithms for optimization of IMRT. Med Phys 2004; 31:1141–52.

19. Jang S, Vassiliev ON, Liu HH, Mohan R. Development and commissioning of a multileaf collimator model in Monte Carlo dose calculations for intensity-modulated radiation therapy. Med. Phys. 2006; 33:770–81.

20. Rietzel E, Pan T, Chen GT. Four-dimensional computed tomography: image formation and clinical protocol. Med Phys 2005; 32:874–89.

21. Yom SS, Liao Z, Liu HH, Tucker SL, et al. Initial evaluation of treatment-related pneumonitis in advanced-stage non-small-cell lung cancer patients treated with concurrent chemotheraphy and intensity-modulated radiotheraphy. Int J Radiat Oncol Biol Phys 2007; 68(1):94–102.

22. Chi PC, Balter P, Luo D, Mohan R, Pan T. Relation of external surface to internal tumor motion studied with cine CT. Med Phys 2006; 33:3116–23.

23. Mawlawi O, Pan T, Macapinlac HA. PET/CT imaging techniques, considerations, and artifacts. J Thorac Imaging 2006; 21:99–110.

24. Pan T, Mawlawi O, Nehmeh SA, et al. Attenuation correction of PET images with respiration-averaged CT images in PET/CT. J Nucl Med 2005; 46:1481–7.

25. van der Geld YG, Senan S, van Sornsen de Koste JR, et al. Evaluating mobility for radiotherapy planning of lung tumors: a comparison of virtual fluoroscopy and 4DCT. Lung Cancer 2006; 53:31–7.

26. Rosen I, Liu HH, Childress N, Liao Z. Interactively exploring optimized treatment plans. Int J Radiat Oncol Biol Phys 2005; 61:570–82.

27. Seppenwoolde Y, Lebesque JV, de Jaeger K, et al. Comparing different NTCP models that predict the incidence of radiation pneumonitis. Normal tissue complication probability. Int J Radiat Oncol Biol Phys 2003; 55:724–35.

28. Kong FM, Ten Haken R, Eisbruch A, Lawrence TS. Non-small cell lung cancer therapy-related pulmonary toxicity: an update on radiation pneumonitis and fibrosis. Semin Oncol 2005; 32:S42–54.

29. Vujaskovic Z, Marks LB, Anscher MS. The physical parameters and molecular events associated with radiation-induced lung toxicity. Semin Radiat Oncol 2000; 10:296–307.

30. Wang X, Zhang X, Dong L, et al. Effectiveness of noncoplanar IMRT planning using a parallelized multiresolution beam angle optimization method for paranasal sinus carcinoma. Int J Radiat Oncol Biol Phys 2005; 63:594–601.

31. Childress NL, White RA, Bloch C, Salehpour M, Dong L, Rosen, II. Retrospective analysis of 2D patient-specific IMRT verifications. Med Phys 2005; 32:838–50.

32. Bouchard H, Seuntjens J. Ionization chamber-based reference dosimetry of intensity modulated radiation beams. Med Phys 2004; 31:2454–65.

33. Jang S, Liu HH, Wang X, et al. Dosimetric verification for intensity-modulated radiotherapy of thoracic cancers using experimental and Monte Carlo approaches. Int J Radiat Oncol Biol Phys 2006; 66:939–48.

34. Kim JO, Siebers JV, Keall PJ, Arnfield MR, Mohan R. A Monte Carlo study of radiation transport through multileaf collimators. Med Phys 2001; 28:2497–506.

35. Britton KR, Starkschall GTP, Time Trends in Mobility and Size of target Volumes for Locally Advanced Stage III Non-small-Cell Lung Cancer Patients Using Serial four-dimensional Computed Tomography (4-DCT). Int J Radiat Oncol Biol Phys 2006; 66:468 (Abstract).

36. Seppenwoolde Y, Muller SH, Theuws JC, et al. Radiation dose-effect relations and local recovery in perfusion for patients with non-small-cell lung cancer. Int J Radiat Oncol Biol Phys 2000; 47:681–90.

37. Marks LB, Spencer DP, Sherouse GW, et al. The role of three dimensional functional lung imaging in radiation treatment planning: the functional dose-volume histogram. Int J Radiat Oncol Biol Phys 1995; 33:65–75.

38. Seppenwoolde Y, Engelsman M, De Jaeger K, et al. Optimizing radiation treatment plans for lung cancer using lung perfusion information. Radiother Oncol 2002; 63:165–177.

39. Christian JA, Partridge M, Nioutsikou E, et al. The incorporation of SPECT functional lung imaging into inverse radiotherapy planning for non-small cell lung cancer. Radiother Oncol 2005; 77:271–7.

40. Seppenwoolde Y, De Jaeger K, Boersma LJ, Belderbos JS, Lebesque JV. Regional differences in lung radiosensitivity after radiotherapy for non-small-cell lung cancer. Int J Radiat Oncol Biol Phys 2004; 60:748–58.

41. Marks LB, Spencer DP, Bentel GC, et al. The utility of SPECT lung perfusion scans in minimizing and assessing the physiologic consequences of thoracic irradiation. Int J Radiat Oncol Biol Phys 1993; 26:659–68.

42. Marks LB, Munley MT, Spencer DP, et al. Quantification of radiation-induced regional lung injury with perfusion imaging. Int J Radiat Oncol Biol Phys 1997; 38: 399–409.

43. Guerrero T, Sanders K, Castillo E, et al. Dynamic ventilation imaging from four-dimensional computed tomography. Phys Med Biol 2006; 51:777–91.

44. Guerrero T, Sanders K, Noyola-Martinez J, et al. Quantification of regional ventilation from treatment planning CT. Int J Radiat Oncol Biol Phys 2005; 62:630–4.

Image-Guided Proton Radiotherapy in Lung Cancer

Joe Y. Chang
Department of Radiation Oncology, University of Texas M.D. Anderson Cancer Center, Houston, Texas, U.S.A.

Radhe Mohan
Department of Radiation Physics, University of Texas M.D. Anderson Cancer Center, Houston, Texas, U.S.A.

James D. Cox
Department of Radiation Oncology, University of Texas M.D. Anderson Cancer Center, Houston, Texas, U.S.A.

INTRODUCTION

Conventional photon radiotherapy with a dose of 60–66 Gy delivered in 30–33 fractions has been considered "standard" treatment for inoperable stage I/II/III non–small cell lung cancer (NSCLC). However, this dose regimen is associated with only 30–50% local control (1–3). Uncontrolled locoregional disease is a major source of continuous seeding to distant organs and is the eventual cause of treatment failure; thus, its eradication is essential for cure. Increasing clinical evidence suggests that a radiation dose–response relationship is involved in both survival and local control in patients with NSCLC (4–6). However, higher radiation doses, particularly with concurrent chemotherapy, are associated with higher levels of toxicity (7).

Advances in diagnostic imaging in the 1980s led to more individualized radiotherapy that was based on the specific anatomy of individual patients rather than on anatomic atlases. Commercial treatment-planning systems allowed three-dimensional conformal radiotherapy (3D-CRT) by the early 1990s. Computer simulations of dose distributions clearly showed that with 3D-CRT, higher total doses could be delivered to the gross tumor volume than were possible with two-dimensional (2D) treatment. Also, normal tissues could be spared or at least exposed to much lower doses with 3D-CRT than with 2D treatment. Recent clinical trials showed that 3D-CRT improved local control, increased overall survival in patients with stage I NSCLC (8), and allowed doses to be escalated from 63 to 74 Gy with concurrent chemotherapy in patients with stage III NSCLC (9,10).

The delivery of small X-ray beams with different intensities permitted further shaping of the high-dose volume. Physicists optimized the different intensities, and with use of dynamic multileaf collimators, intensity-modulated radiotherapy (IMRT) was fully realized. However, such precision in radiation delivery requires more careful target delineation, treatment planning, and quality assurance. Moreover, because of the risk of missing tumors that may move (e.g. during respiration) between daily fractions or during treatments, image-guided radiotherapy is required (see Chapter. 7 for details).

Although 3D-CRT and IMRT have the potential to reduce normal tissue toxicity, the relatively high exit dose from photon X-ray therapy limits the possibility of dose escalation or acceleration. A proton beam, on the other hand, is made up of charged particles (protons) that have a well-defined range of penetration into tissue. As the proton beam penetrates the body, its particles slow down and deposit a large portion of their energy near the end of their range. The resultant central axis depth dose distribution is known as the Bragg peak. By modulating the Bragg peak in both energy and time, a full, localized, uniform dose can be delivered to the target while sparing the surrounding normal tissue. Thus, proton beam treatment is ideal when organ preservation is a priority, particularly in patients with lung cancer.

Despite decades of clinical experience, proton therapy is still basic, and many questions remain, particularly about the effect of tumor motion during and between treatments. Thus, there are many opportunities to improve the distribution of proton doses. The use of intensity-modulated proton therapy (IMPT) and image-guided interventions for both interfractional and intrafractional variations should reduce some of the uncertainties and should considerably improve the therapeutic potential of proton therapy. In this chapter, we review the rationale for proton therapy, describe the image-guided treatment planning for and delivery of this therapy, and discuss the clinical outcome for patients with NSCLC who undergo this therapy.

RATIONALE FOR PROTON THERAPY

The fundamental property of proton beams that provides a substantial advantage over X-ray beams is that in homogeneous tissues, protons can be made to stop within a few millimeters past the distal surface of the target volume, whereas X-rays deposit their radiation dose in the healthy tissues and organs that lie in the beam's path beyond the target volume and then exit the patient on the side opposite to the beam's entrance. In addition, protons deposit a lower dose than do X-rays to normal tissues and organs that lie in the beam's path between the surface of the patient and the target volume.

The primary advantage of protons in cancer therapy is their highly localized dose distribution. For treatment-delivery techniques of similar complexity, protons typically deposit one half or less of the integral dose that X-rays deliver to uninvolved normal tissue (11). For a given level of radiation-induced toxicity in normal tissue, the maximal tolerated dose of proton radiotherapy is likely to be higher than that of conventional photon radiotherapy because of the physical characteristics of the proton beam (i.e. its Bragg peak). Therefore, the potential for proton radiotherapy to improve local tumor control and survival rates may be better than that for conventional photon therapy, including IMRT (12,13).

PHYSICAL CHARACTERISTICS OF PROTON BEAMS

As with all heavy charged particles (e.g. helium and carbon ions and negative pi-mesons), protons have a unique depth dose distribution, commonly referred to as the Bragg peak or the pristine Bragg peak. The depth dose is characterized by a low entrance dose (about 30–40% of the maximal dose), followed by a relatively flat dose plateau, which rises sharply to a narrow peak (the Bragg peak) as the protons slow down and then falls rather rapidly to a zero dose immediately after the maximal dose is reached, near the end of the range of proton penetration. The depth of the Bragg peak depends on the material being penetrated and the energy of the protons. The selection of the energy level of the protons to use for treating a specific target (i.e. the energy range required to reach the most distal edge of the target, including the margins) is based on the largest depth of penetration.

The width of the pristine Bragg peak is too narrow both laterally and along the depth of penetration to allow treatment of any but the smallest clinical targets. Therefore, range modulation [i.e. adding multiple Bragg peaks of sequentially lower energies and smaller weights (time duration)] is used to produce an extended region of depth dose
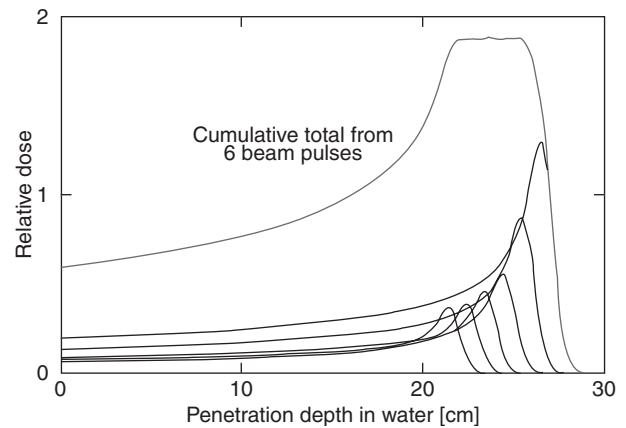
Figure 1 Energy modulation of multiple Bragg peaks to generate an SOBP. *Abbreviation*: SOBP, spread-out bragg peak.

uniformity called a spread-out Bragg peak (SOBP) (Fig. 1). SOBPs can be achieved by placing either a range-modulation wheel (for dynamic modulation) or a ridge filter (for passive modulation) in the beam or by changing the energy in the accelerator or energy-selection system while adjusting the weight of each individual Bragg peak. By appropriately selecting the range pullback and weight of each pristine Bragg peak, the desired uniformity as a function of depth can be achieved to cover the tumor. To achieve lateral uniformity in the tumor target, the beam must also be spread laterally either by passive scattering or by magnetically scanning a narrow pencil beam in a uniform pattern. In general, SOBPs of different widths, customized to individual target volumes, can be produced. It should be noted that as the width of the SOBP increases, the surface dose increases. An SOBP that extends to the surface (full modulation) would have a surface dose of 100%. For passively scattered proton beams of a given energy, fields of different widths can be achieved by different combinations of scatterers. The maximal range for a given energy depends on the degree of lateral scattering required and decreases with increasing field size. For instance, the maximal range for a 250-MeV beam scattered to produce a $10 \times 10\,cm^2$ field is 28.5 cm, compared with a range of 25 cm to produce a $25 \times 25\,cm^2$ field. For magnetically scanned beams, however, the range is independent of field size. For both passively scattered protons and scanned beams, the dose rate is inversely proportional to the square of the extent of lateral spreading.

TREATMENT DELIVERY USING PASSIVELY SCATTERED PROTON BEAMS

Until now, passive scattering has been the standard method for spreading the proton beam laterally for therapeutic applications (14). In passive scattering
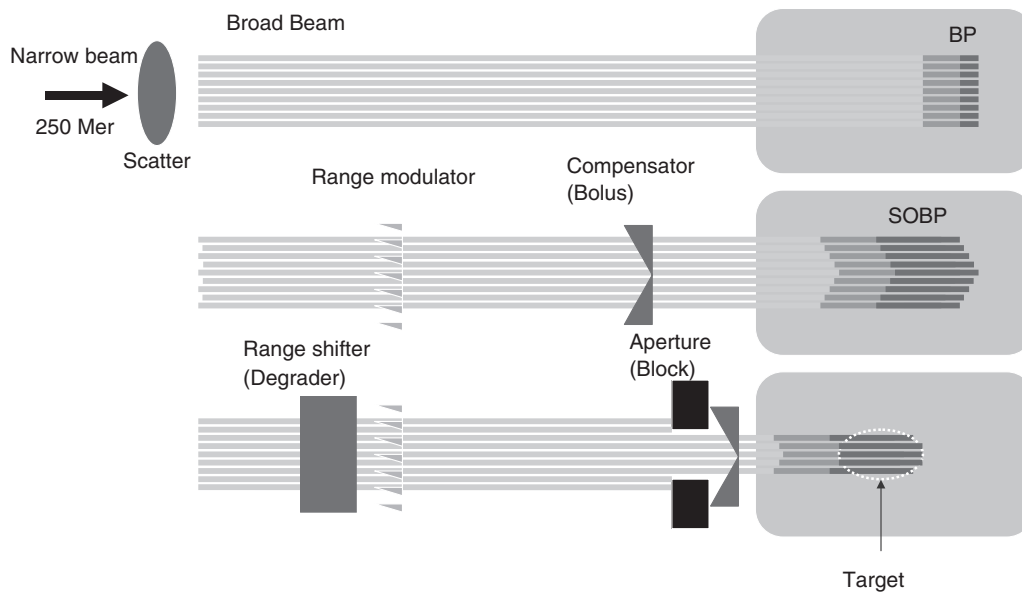
Figure 2 A proton beam passes through a passive scattering system to produce a 3D-CRT. *Abbreviations*: BP, Bragg peak; SOBP, spread-out Bragg peak.

systems, before the proton beam enters a patient, it is passed through a range-modulating wheel (which is often also a part of the first scatterer), a second scattering device, a range shifter, an aperture for shaping the beam laterally, and a customized compensator (Fig. 2). The double scattering system (range-modulating wheel or first scatterer and the second scattering device) creates a broad, flattened beam at the final aperture. The range shifter finely adjusts the maximal depth penetrated by the protons. The customized range compensator tailors the distal surface of the dose distribution to match the distal shape of the target volume with the necessary margins. The treatment-planning system in the range compensator calculates the water-equivalent (WE) path lengths between the patient's surface and the distal edge of the target volume by accounting for the shape of the patient's surface, all inhomogeneities between the patient's surface and the planning target volume (PTV), and the shape of distal surface of the target volume to yield the thicknesses of the range penetration at each point.

TREATMENT PLANNING FOR THE USE OF PASSIVELY SCATTERED PROTON BEAMS

In most ways, planning for proton- and photon-based treatments is similar. However, there are differences. The change in position of the patient as a whole along the path of the beam has virtually no effect on proton dose distribution, whereas tissue variation in the path

to the distal edge due to intrafractional motion and/or due to interfractional changes, such as tumor shrinkage, weight loss, and changes caused by nonrigidity of the body, may affect the range of protons. For this reason and because of other uncertainties that affect the range as discussed below, beam-specific distal and proximal margins are assigned to the clinical target volume (CTV) to ensure coverage of the CTV along the path of each beam. The magnitude of these margins is estimated on the basis of clinical experience and measurements and depends, for example, on the depth of the target, inhomogeneities in the path to the target, and image artifacts. Lateral margins depend on the anatomic variations orthogonal to the beam direction and are determined in the same manner as those for photons.

Another strategy to ensure coverage of the target in the presence of motion and variations of structures normal to the beam direction is the "smearing" of the compensator. Smearing allows for possible small misalignment of the compensator with the patient's anatomy due to changes in anatomy or positioning uncertainties. The smearing process essentially reduces the width of higher-thickness regions of the compensator to allow protons to penetrate deeper, even when adjacent higher-density tissues move into their path. This is a user-controlled parameter that can be adjusted during planning. Using smearing and including margins for range uncertainty ensures coverage of the target at the expense of a higher dose to normal tissue distal to the target.

The compensator design for a target that moves because of respiration should allow for the inadequate representation of the target's shape, size, and position on conventional computed tomographic (CT) images obtained during treatment. Increasingly, four-dimensional CT (4D-CT) scans that comprise multiple (e.g. 10) 3D-CTs in a sequence of phases of the respiratory cycle are being used in planning both photon-based and proton-based treatments that include a motion-integrated internal target volume (ITV) enveloping the moving target. For designing the compensator for proton-based treatment, the density at each point in the ITV should be set to the maximal density in any one of the phases, not to the average density of all the phases (Fig. 3). This strategy ensures that protons will penetrate deeply enough to cover the target adequately, regardless of its position.

In the overall treatment-planning process for a specified beam direction, a typical proton treatment-planning system first determines the maximal WE depth of penetration to the distal edge of the target plus the margin and the minimal WE depth to the target minus the margin. These quantities are then used to determine the range, and therefore the energy, of incident protons and the width of the SOBP. The range and SOBP are eventually used in selecting treatment machine parameters (e.g. range-modulation wheel, second scatterer, energy, range shifters) required for delivering the beam. For each beam, the proton treatment-planning system also creates a block conforming to the beam's eye view shape of the CTV plus appropriate margins for setup and motion uncertainties normal to the beam direction and for the beam penumbra. Dose distributions for each beam are then calculated and summed for plan evaluation. Dose calculations for the planning of proton treatments in the current state of the art generally use semiempirical pencil-beam models (15,16). Parameters of the analytical formalisms of the model are fitted with measured dose distributions. These models are quite accurate except for complex heterogeneities such as those in the thorax.

The advantages of passive scattering systems are their safety, simplicity, and lower sensitivity to the time structure of the accelerator. Although these systems have well served their intended purpose, they have a number of disadvantages, the most serious being that they are only about 20–40% efficient and therefore waste a large number of protons in the scattering system and in the beam-limiting aperture. This substantial loss of protons can pose a problem for synchrotron-based proton therapy systems, in which the dose rate is more limited than in cyclotrons. Passive scattering systems also tend to be sensitive to variations in the beam position. Furthermore, when protons are stopped in the scattering system and
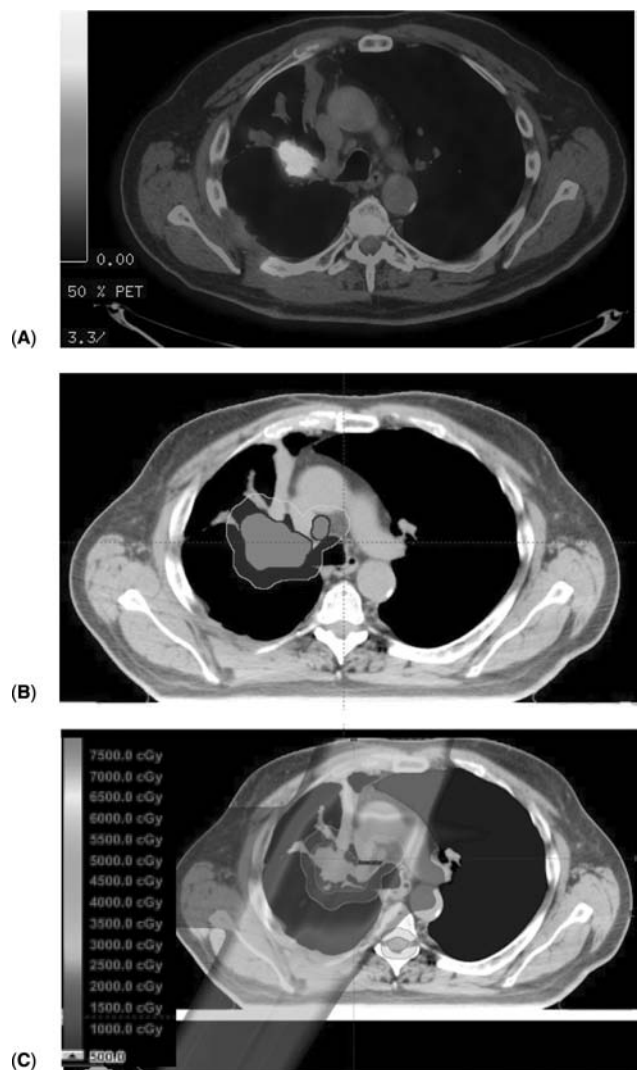
Figure 3 (*See color insert.*) CT-based MIP approach for treatment planning in patients with stage III NSCLC. (**A**) Positive emission tomographic/CT image shows a lesion in the upper lobe of the right lung with distal lung atelectasis and an adjacent right pretracheal lymph node. (**B**) Scan shows the MIP approach to create internal gross target volume (IGTV) (red color wash) and to design the proton compensator. The CTV (yellow contour) = IGTV + 8-mm margin. (**C**) Scan shows the isodose distribution based on a MIP IGTV compensator design and calculated in the time-averaged CT image using actual density. Right lateral, right posterior oblique, and left anterior oblique treatment beams were chosen to avoid the spinal cord, esophagus, and contralateral lung. *Abbreviations*: 4D-CT, four-dimensional computed tomography; CTV, clinical target volume; IGTV, internal gross target volume; MIP, maximal intensity projection; NSCLC, non–small cell lung cancer.

aperture, they produce secondary neutrons, many of which can contribute to the whole-body dose to the patient. Neutrons have a high relative biologic effectiveness (RBE) and are believed to be the source of secondary cancers in some patients (17).

Another disadvantage of this system is that it produces a single SOBP for the entire target volume; thus, during treatment of large irregular target

volumes with notable differences in their thickest and thinnest depths, the high-dose region is pulled back into normal tissues. For this reason, the dose-shaping properties of passive scattering techniques are often described as 2.5-dimensional. The solution to the disadvantages of passive scattering systems is found in dynamic spot scanning systems (see below).

As with X-ray and electron treatments, proton treatments use multiple fields, often noncoplanar, to keep the skin dose to reasonable limits and to spare normal tissues in the beam path. However, as mentioned above, treatment-planning strategies involving protons can be quite different from those involving X-rays and electrons because of the particular properties of proton beams. For example, in proton-based treatments, the rapid distal falloff of the proton dose distribution permits the planner to aim a proton beam directly toward a critical normal structure, as opposed to X-ray–based and electron-based therapies, which may deliver a toxic dose to critical structures distal to the target because of the higher exit dose. However, there is uncertainty about the travel range of protons in the body and about the possible increased RBE toward the end of the SOBP. Therefore, caution should be observed because of the behavioral interactions of the protons in the body and because of the various uncertainties encountered in this therapy. As mentioned above, motion and interfractional changes in inhomogeneous structures in the path of protons also affect the range of protons. The uncertainty about proton range may also be associated with the correlation between CT Hounsfield units and the proton mass stopping power of tissues. This uncertainty has a negligible effect on photon dose distributions; however, its effects on protons are much more important because of the protons' charge, weight, and manner of scattering.

Another factor is that the transport of protons through complex inhomogeneities, such as those encountered in the lung, degrades the proton range, and the protons do not stop at a sharp edge as they would in a homogeneous material. Range uncertainties can result in the beam stopping prematurely, the target being underdosed, or the beam extending beyond the target, possibly overdosing critical structures. Such concerns are particularly acute for low-density regions around lung tumors. A correlation between CT Hounsfield units and proton mass stopping powers, based on measurements of materials of known stopping powers on the CT scanner, is used to calculate proton ranges in tissue (18–20). However, the problem of reducing the uncertainty associated with CT Hounsfield units and proton mass stopping powers still needs to be solved.

With regard to uncertainty in the RBE, preliminary data show that the RBE of a proton beam depends on tissue type, dose, dose rate, energy, and depth of penetration (21). However, to date there is no unequivocal clinical evidence that the use of an average RBE value of 1.1 leads to higher-than-expected toxicity or poorer local control. RBE issues are discussed further below.

An important difference between photon and proton treatment planning is the use of margins to expand the CTV to the PTV. The concept of the PTV is inapplicable to proton therapy. Proton beams have essentially three edges: the two lateral penumbras resulting from coulomb multiple scattering and the distal edge. In contrast, photons have only lateral edges. Also, the depth dependence of the lateral penumbras in the proton beam is stronger than that of photon for WE depths greater than about 17 cm; for shallower depths, the proton lateral penumbra is generally smaller than that of photon.

As stated above, various factors contribute to the uncertainty in the range of protons; thus, a margin for range uncertainty must be applied. In general, each treatment beam must have its own distal and proximal margins that are dependent on the distance traveled by the beam in the tissue. Therefore, expanding the CTV to the PTV is not valid. However, the magnitude of lateral margins may be determined in the same manner as that for the CTV-to-PTV margin for photons.

DYNAMIC SPOT SCANNING AND INTENSITY-MODULATED PROTON THERAPY

In dynamic spot scanning, the Bragg peak of a narrow pencil beam entering the treatment nozzle is magnetically scanned across the target cross section, and the energy of the protons is adjusted to vary the depth of the spot to achieve the intended dose pattern. The beam can be either scanned continuously in a raster scan pattern or stopped at discrete, predetermined positions for a specified time to deliver the desired dose. In discrete spot scanning, the beam is then turned off during travel between the spots (22). The deepest layer is scanned by selecting the appropriate energy, and when scanning of that layer is completed, the energy is decreased and the next layer is scanned. In this manner, the entire target volume can be irradiated either to deliver a uniform dose distribution for each field, much like the passive scattering method, or to deliver a nonuniform dose distribution for each field in such a way that when the doses from all the fields are summed, the total dose distribution is uniform. This is called IMPT (23). Figure 4 shows a typical dynamic spot scanning system. To produce a nonuniform dose distribution with raster scanning, the intensity of the beam can be varied continuously as the spot is moved.
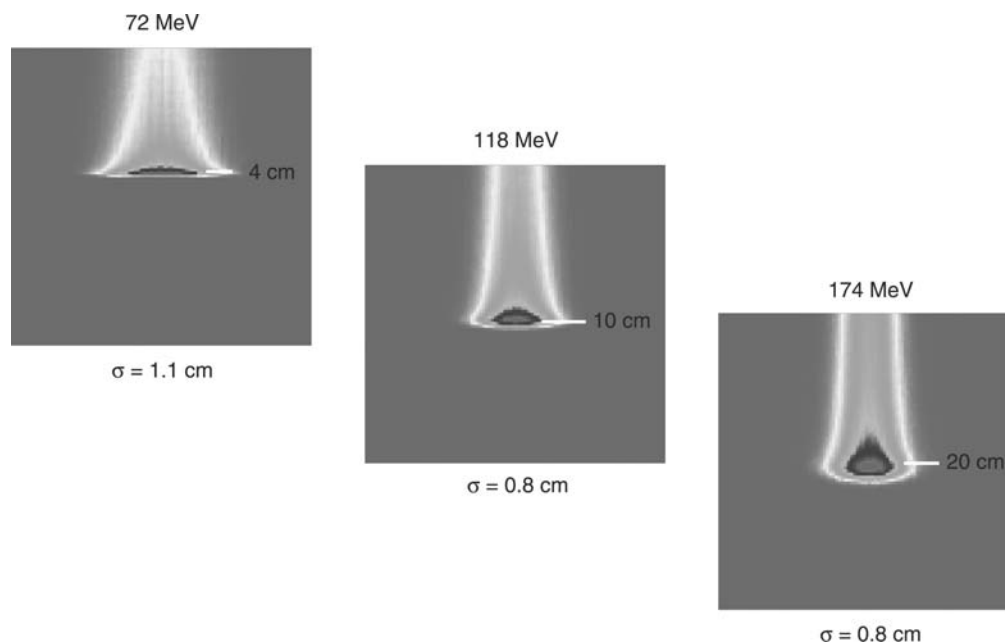
Figure 4   A typical dynamic spot scanning system. Pencil beam dose distribution with different energies in water and the contribution to the penumbra.

Dynamic spot scanning has several advantages: It provides full 3D shaping of the dose distribution to the target volume; no devices such as dose-limiting apertures or range compensators are required; the efficiency is high because very few protons are wasted; and very few neutrons are produced. One disadvantage of dynamic spot scanning is the difficulty in delivering a desired dose to tumors that move during irradiation; however, beam-gating techniques such as respiratory-gated proton beam radiotherapy (see the "4D-CT–Based Tumor Motion Consideration" section) should decrease the uncertainty in such treatments. Another way to decrease the effect of target motion is by scanning each layer multiple times—the dose error due to target motion decreases as the number of scans increases, although there is a practical limit to the number of times a layer can be rescanned.

IMPT plans are optimized with an "inverse" treatment-planning system that is similar to the inverse planning for IMRT (24,25). However, there is an additional degree of freedom in IMPT because the energy of each proton pencil beam, in addition to its intensity, can be varied, which increases the dose-shaping potential of the IMPT plans. Although IMPT and IMRT have equally complex treatment plans, the IMPT plans will always be superior to IMRT plans, especially in the sparing of normal tissue. The coverage of the target volume, however, can be quite similar for IMPT and IMRT. On average, IMPT uses half the integral dose used by IMRT, resulting in substantial sparing of critical tissues and organs (11).

RBE CONSIDERATION

Proton beams are essentially a form of low linear energy transfer radiation. Protons have nearly the same RBE as photons. Paganetti et al. (21) summarized findings from numerous experiments with protons and concluded that the RBE of protons is approximately 1.1; an RBE of 1.1 is considered standard in routine clinical practice. The computed physical dose distribution is multiplied by the RBE to obtain the cobalt Gray equivalent (CGE) dose distribution. However, the RBE has been shown to vary with the linear energy transfer, which increases as the energy of protons decreases with increasing depth (21). This effect may be particularly pronounced near the end of the proton range. This variation in RBE is ignored, and the biologically effective dose near the end of the range is likely to be higher than that seen in a treatment plan. For this reason and because of uncertainties in range, aiming the beams toward a normal critical structure in very close proximity of the target must be avoided, particularly when the number of beams in the treatment plan is small.

IMAGE-GUIDED PROTON DELIVERY

Proton dose distributions are highly localized because of the SOBP high-dose region that is followed by an abrupt falloff of the dose to a value of zero. However, protons are more sensitive than photons to motion, interfractional changes, and inhomogeneities. Therefore, much of their relative advantage may be

lost if the treatment-planning process, patient setup, or delivery are not optimized and accurate. An uncertainty in the calculated range of the proton beam can either cause a portion of the distal target volume to receive no dose (if the range is too short) or cause an overdose to a critical structure (if the range is too long). The accuracy of the patient setup for treatment and of the treatment delivery is usually ensured by the use of onboard image guidance and extensive monitoring and by the quality assurance of the beam-delivery process. Most proton treatment delivery systems contain three orthogonal imaging systems (X-ray tubes and flat-panel imagers), image analysis systems, and computerized couches with six degrees of freedom; with these aids, stereotactic techniques can be used to accurately position the patient, correct for misalignments, and verify the treatment setup daily for each treatment field.

CT-on-rails technology and cone-beam CT have been considered for CT imaging in the treatment room. However, considering the cost of proton facilities, it is necessary to maximize throughput. Alternatively, the patient may be immobilized and undergo CT on a transportable tabletop in one room and then be wheeled into the treatment room, where the tabletop is then docked to the treatment table. Such a system is in use at the Paul Scherrer Institut in Switzerland.

4D-CT BASED TUMOR MOTION CONSIDERATION

The use of proton radiotherapy in patients with lung cancer raises many important issues. Among the most challenging is tumor motion during treatment due to the patient's breathing (26–28). The development of multislice detectors and faster imaging reconstruction has enabled real-time imaging of breathing patients and the assessment of organ motion using 4D-CT (26).

A more interesting and challenging application for 4D-CT images is determining the actual dose distributions for free-breathing treatments (29). In this process, the dose distributions are calculated for each phase of the breathing cycle and then added by deformable image registration. The composite dose distribution and corresponding dose–volume histograms show the actual dose that the patient receives from the treatment if the patient breathes in the same way as shown in the 4D-CT images.

Another application of 4D-CT is ensuring that all cancer cells are adequately covered by the proton beam. This is accomplished by defining an ITV that combines the gross tumor volumes at different phases of the respiratory cycle that are customized to the tumor motion pattern of the patient. In the

treatment-planning process that uses the ITV, an internal gross target volume (IGTV) is first created with maximal intensity projection (MIP) for the compensator design, as shown in Figure 4 (27). In preliminary 4D treatment-planning studies, the IGTV MIP approach has been shown to achieve dose distributions similar to those actually delivered. Compared with the approach that uses a large smearing margin in highly mobile lung tumors, as proposed by Moyers et al. (14), the IGTV MIP approach achieves similar target coverage while sparing more normal tissue because a universally large smearing margin is not used. Instead, an individualized IGTV based on actual tumor motion is used for the compensator design (27). This approach may slightly overtreat the normal tissues behind the tumor when the tumor moves out of the field, but it ensures that the whole tumor is treated adequately, no matter where it moves during the different breathing phases.

To reduce the effect of motion in proton therapy, a virtual clinical study of 4D-based proton therapy was conducted to determine the extent of improvement in normal tissue sparing achieved with respiratory-gated proton beam radiotherapy compared with the free-breathing ITV approach in patients with mobile lung cancers (Chang et al., October 2006 presentation at the Particle Therapy Co-operative Oncology Group, Houston, Texas). An approximate 25% relative reduction of total mean lung dose and a 5–7% absolute improvement in the lung V5 (the volume of total lung that received at least 5 Gy), V10, and V20 were found in the gated proton treatment compared with the ITV approach ($P < 0.002$). The maximal dose to the spinal cord, the esophageal V55, and the heart V40 were also significantly improved ($P < 0.03$). Patients treated with the respiratory-gating approach, especially those with substantial tumor motion (>10 mm), benefited more in normal tissue sparing than did those treated with the ITV approach. These data indicated that respiratory-gated proton radiotherapy, compared with the nongated ITV approach, improved normal tissue sparing for the lung, heart, esophagus, and spinal cord. The respiratory-gating approach allows for further reduction in normal tissue toxicity and/or dose escalation or acceleration in patients who experience large tumor motion.

To evaluate the change in dose distribution from tumor motion and/or shrinkage over weeks of radiotherapy, a tumor motion study using weekly 4D-CT during radiotherapy is currently under way. The preliminary data show that repeated computer simulation is indicated in selected patients who have substantial tumor shrinkage, a changing breathing pattern, or lung atelectasis (Fig. 5).
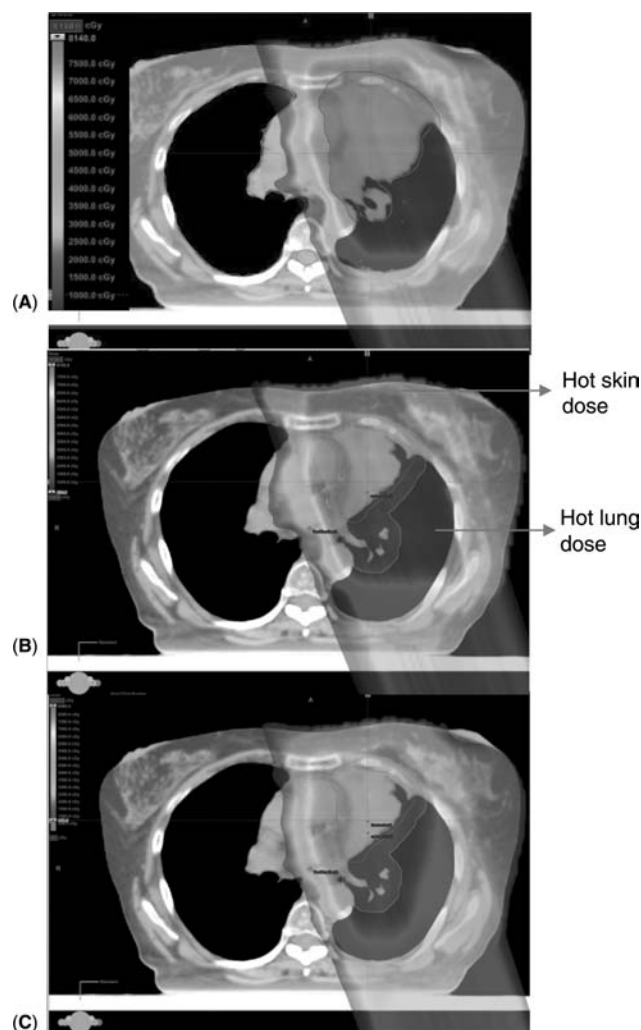
Figure 5 (*See color insert.*) Images illustrate adapted proton therapy in a patient with stage III NSCLC. (**A**) Isodose distribution based on the initial proton treatment plan using a MIP approach. (**B**) The tumor shrank substantially 3 weeks after the initiation of proton therapy; this would result in clinically significant higher skin and lung doses if the patient continued to be treated according to the initial plan. (**C**) An adapted proton treatment, based on new 4D-CT at 3 weeks, shows the reduction in skin and lung doses compared with doses in (**B**) that are achieved with the adjustments to account for the tumor shrinkage. *Abbreviations*: 4D-CT, four-dimensional computed tomography; MIP, maximal intensity projection NSCLC, non-small wall lung cancer; NSCLC, non–small cell lung cancer.

VIRTUAL CLINICAL TRIAL AND CLINICAL STUDIES

Virtual Clinical Trial Comparing Proton Therapy, 3D-CRT, and IMRT

As mentioned earlier, increasing evidence (4–6) suggests that dose escalation in radiotherapy improves local disease control and survival rates in patients with NSCLC. Toxicity in normal tissues, especially in important organs such as the lungs, spinal cord, esophagus, and heart, limits the potential for dose escalation (9). As we know, 3D-CRT, compared with 2D radiation therapy, has been shown to spare more normal tissues and to more effectively reduce toxicity in patients with lung cancer. However, more improvement is needed to allow substantial dose escalation without increasing toxicity.

IMRT may offer the benefit of dose escalation without causing greater toxicity to surrounding normal tissue in selected patients with lung cancer (30–32). The use of IMRT for the treatment of lung cancer, however, has been delayed because of two concerns: (1) the interplay between the moving tumor and the moving leaves of the multileaf collimator and (2) low-dose radiation exposure to the normal lung. For the delivery of IMRT, the interplay between the moving tumor and the moving leaves of the multileaf collimator may lead to hot and cold spots in the tumor (33,34). However, recent studies (30,31,35,36) have shown that IMRT may allow greater dose escalation than 3D-CRT without notably increasing the incidence of adverse effects in selected patients with locally advanced disease and tumor motion of <10 mm. In addition, it has been demonstrated that the interplay effect washes out over multiple fields and over several fractions. A virtual clinical trial was conducted to compare dose–volume histograms from patients with either stages I or IIIA/B NSCLC treated with standard-dose 3D-CRT or IMRT or with simple 3D (without IMPT) proton radiotherapy at standard or escalated doses (37). Proton treatment reportedly improved the dose–volume histograms of all of the critical organs, particularlythe lungs, with about 10–20% absolute improvement. Compared with standard-dose photon therapy, proton treatment statistically significantly reduced the dose to normal lungs, esophagus, spinal cord, and heart, even with dose escalation. In addition, there was a 33–60% absolute improvement of the nontarget integral dose with proton therapy. The reduction was more notable in stage I disease and in the contralateral lung. Findings from this trial indicated that proton therapy with dose escalation and/or acceleration may translate to better local control and survival rates without increasing the toxicity in patients with NSCLC.

A second concern about the use of IMRT for the treatment of lung cancer is low-dose radiation exposure to normal lung. As our previous studies showed, IMRT, compared with 3D-CRT, increased the lung V5 in half the patients we tested (30,31,36). Chang et al. (37) demonstrated that proton therapy, compared with IMRT, spared an additional 15–17% of the total lung and that 19–23% of the contralateral lung received 5 Gy. These findings show that proton therapy, compared with IMRT, may substantially reduce lung toxicity.

Clinical Studies and Patient Outcome

Several clinical trials have been conducted involving patients with NSCLC who underwent proton radiotherapy. These trials focused on dose-escalated or accelerated proton therapy in early stage disease and showed promising clinical results that were comparable to surgical resection in stage IA cases.

Bush et al. (38) studied 68 patients with clinical stage I disease who were treated with 51 or 60 CGEs delivered in 10 fractions over 2 weeks. No cases of symptomatic radiation pneumonitis or late esophageal or cardiac toxicity were seen. The 3-year local control and disease-specific survival rates were 74% and 72%, respectively. Significant improvement was seen in local tumor control in T1 (87%) and T2 (49%) tumors, with a trend toward improved survival rates. Local tumor control appeared to improve compared with historical results from conventional radiotherapy, with a good expectation of disease-specific survival 3 years after treatment. Currently, Bush et al. are conducting a phase I/II study of patients with stage I NSCLC who are receiving 70 CGEs delivered in 10 fractions.

Shioyama et al. (39) described 51 patients with NSCLC who were treated with proton therapy. The median fraction and total doses given were 3.0 and 76.0 Gy, respectively. The 5-year overall survival rates were 70% for 9 stage IA patients and 16% for 19 stage IB patients ($P < 0.05$). The 5-year in-field local control rate was higher in patients with stage IA disease (89%) than in those with stage IB disease (39%). Forty-seven patients (92%) experienced acute lung toxicity of grade 1 or less; three had grade 2, one had grade 3, and none experienced grade 4 or higher toxicity. Patients in this study showed very little late toxicity.

Nihei et al. (40) recently reported the results from their preliminary study of 37 patients with stage I NSCLC who received 70–94 CGEs delivered in 20 fractions. The 2-year progression-free survival and overall survival rates were 80% and 84%, respectively. The 2-year locoregional relapse-free survival rate was 79% in patients with stage IA disease and was 60% in those with stage IB disease. No serious acute toxicity was observed, and only three patients developed grade 2/3 chronic lung toxicity.

These reported clinical studies showed the safety and efficacy of proton therapy in early stage NSCLC. However, the optimal regimen has not been well defined. In addition, simple 3D proton therapy was used in these studies; optimized proton therapy such as respiratory-gated therapy was not available, and image-guided radiotherapy was not strictly applied. Clinically, minimal data are available about proton therapy for patients with stage III NSCLC, the most common stage requiring radiotherapy.

At the University of Texas M.D. Anderson Cancer Center, phase II clinical trials using image-guided proton radiotherapy for patients with NSCLC are ongoing (36). Twenty-three patients with medically inoperable stage I NSCLC and 56 patients with stage IIIA/B NSCLC will receive this therapy. Positron emission tomographic and CT studies will be used in all patients for both staging and treatment planning. We plan to deliver a total dose of 87.5 CGEs in 2.5-CGE fractions for patients with stage I disease and a total dose of 74 CGEs in 2-CGE fractions with concurrent chemotherapy followed by adjuvant chemotherapy for patients with stage III disease. In addition, a 4D-CT study is required to plan for tumor motion and to decide on the treatment-delivery technique (free-breath ITV, breath-hold, or gated treatment). The IGTV MIP approach is being used for the compensator design (Fig. 4).

Optimization of proton therapy with the appropriate management of uncertainties is being actively investigated. Image-guided respiratory-gated proton therapy and IMPT will be implemented soon. We plan to conduct randomized studies to compare IMRT with proton therapy using dose-escalated radiotherapy. In addition, image-guided stereotactic hypofractionated proton radiotherapy will be implemented for patients with early stage NSCLC and will be compared with hypofractionated stereotactic photon-based body radiotherapy, particularly for those with centrally located early stage NSCLC.

SUMMARY

The dose distributions of proton Bragg peaks led to the development of proton therapy that was superior to photon therapy for reducing the radiation dose to normal tissue adjacent to the target, such as those of the esophagus, lung, heart, and spinal cord, and to intervening tissues in the path of the radiation beams. However, image-guided proton therapy planning and delivery are crucial for the appropriate management of various sources of uncertainties induced by anatomic variations and by organ or tumor motion.

Reduced tumor motion is required for optimal image-guided proton therapy. 4D-CT planning is recommended for all proton therapy, particularly for IMPT. Respiratory-gated proton treatment further improves normal tissue sparing. More efficient CT imaging that will be performed before each treatment is being developed and will lead to greater accuracy in treatment delivery. Re-simulation during treatment is recommended for selected patients with substantial tumor shrinkage and possible lung expansion.

Because of the reductions in the "dose bath" and in the volume of normal tissues irradiated with proton

therapy, patients' tolerance of radiation and/or chemoradiotherapy would be enhanced, allowing the delivery of higher doses of these treatments. These higher doses, combined with the increased accuracy obtained from image-guided targeting and the greater avoidance of normal tissues, would lead to less toxicity and better local disease control and survival rates in patients with NSCLC.

REFERENCES

1. Kaskowitz L, Graham M, Emami B, et al. Radiation therapy alone for stage I non-small cell lung cancer. Int J Radiat Oncol Biol Phys 1993; 27:517–23.

2. Dosoretz D, Katin M, Blitzer P, et al. Medically inoperable lung carcinoma: The role of radiation therapy. Semin Radiat Oncol 1996; 6:98–104.

3. Dosoretz D, Galmarini D, Rubenstein J, et al. Local control in medically inoperable lung cancer: An analysis of its importance in outcome and factors determining the probability of tumor eradication. Int J Radiat Oncol Biol Phys 1993; 27:507–16.

4. Rosenman J, Halle J, Socinski M, et al. High-dose conformal radiotherapy for treatment of stage IIIA/IIIB non-small-cell lung cancer: Technical issues and results of a phase I/II trial. Int J Radiat Oncol Biol Phys 2002; 54(2):348–56.

5. Kong F, Ten Haken R, Schipper M, et al. High-dose radiation improved local tumor control and overall survival in patients with inoperable/unresectable non-small-cell lung cancer: Long-term results of a radiation dose escalation study. Int J Radiat Oncol Biol Phys 2005; 63(2): 324–33.

6. Choi N, Doucette J. Improved survival of patients with unresectable non-small-cell bronchogenic carcinoma by an innovated high-dose en-bloc radiotherapeutic approach. Cancer 1981; 48:101–9.

7. Curran W, Scott C, Langer C, et al. Long term benefit is observed in a phase III comparison of sequential vs concurrent chemo-radiation for patients with unresectable NSCLC:RTOG 9410. Proc Am Soc Clin Oncol; 2003. p. 621a.

8. Fang L, Komaki R, Allen P, Guerrero T, Mohan R, Cox J. Comparison of outcomes for patients with medically inoperable stage I non-small-cell lung cancer treated with two-dimensional vs. three-dimensional radiotherapy. Int J Radiat Oncol Biol Phys 2006; 66(1):108–16.

9. Schild S, McGinnis W, Graham D, et al. Results of a phase I trial of concurrent chemotherapy and escalating doses of radiation for unresectable non-small-cell lung cancer. Int J Radiat Oncol Biol Phys 2006; 65(4):1106–11.

10. Belderbos J, Heemsbergen W, De Jaeger K, Baas P, Lebesque J. Final results of a phase I/II dose escalation trial in non-small-cell lung cancer using three-dimensional conformal radiotherapy. Int J Radiat Oncol Biol Phys 2006; 66(1): 126–34.

11. Lomax A, Bortfeld T, Goitein G, et al. A treatment planning inter-comparison of proton and intensity modulated photon radiotherapy. Radiother Oncol. 1999; 51 (3):257–71.

12. Thames H, Schultheisis T, Henry J, Tucker S, Dubray B, Brock W. Can modest escalations of dose be detected as increased tumor control. Int J Radiat Oncol Biol Phys 1992; 22:241.

13. Fowler J. What can we expect from dose escalation using protons beam? Clin Oncol 2003; 15(1):S10–5.

14. Moyers M, Miller D, Bush D, Slater J. Method-ologies and tools for proton beam design for lung tumors. Int J Radiat Oncol Biol Phys. 2001; 49(5):1429–38.

15. Hong L, Goitein M, Bucciolini M, et al. A pencil beam algorithm for proton dose calculations. Phys Med Biol 1996; 41:1305–30.

16. Schaffner B, Pedroni E, Lomax A. Dose calculation models for proton treatment planning using a dynamic beam delivery system: an attempt to include density heterogeneity effects in the analytical dose calculation. Phys Med Biol 1999; 44: 27–41.

17. Hall E. Intensity-modulated radiation therapy, protons, and the risk of second cancers. Int J Radiat Oncol Biol Phys 2006; 65(1):1–7.

18. Schneider U, Pedroni E, Lomax A. The calibration of CT Hounsfield units for radiotherapy treatment planning. Phys Med Biol 1996; 41:111–24.

19. Kanematsu N, Matsufuji N, Kohno R, Minohara S, KanaiT. A CT calibration method based on the polybinary tissue model for radiotherapy treatment planning. Phys Med Biol 2003; 48:1053–64.

20. Chen G, Singh A. Treatment planning for heavy ion radiotherapy. Int J Radiat Oncol Biol Phys 1979; 5:1809–19.

21. Paganetti H, Niemierko A, Ancukiewicz M, et al. Relative biological effectiveness (RBE) values for proton beam therapy. Int J Radiat Oncol Biol Phys 2002; 53(2): 407–21.

22. Kanai T, Kawachi K, Kumamoto Y, et al. Spot scanning system for proton radiotherapy. Med Phys 1980; 7(4):365–9.

23. Goitein M, Lomax A, Pedroni E. Treating cancer with protons. Phys Today 2002; 55:45–50.

24. Oelfke U, Bortfeld T. Inverse planning for photon and proton beams. Med Dosim 2001; 26(2):113–24.

25. Bortfeld T. An analytical approximation of the Bragg curve for therapeutic proton beams. Med Phys 1997; 24:2024–33.

26. Liu H, Wei X, Jang S. Impact of respiratory motion on dose distributions and DVHs of thoracic structures-evaluation using 4DCT. Med Phys 2005; 32(6): 1924.

27. Kang Y, Zhang X, Wang H. Proton treatment planning for mobile lung tumors. Med Phys 2005; 32(6):2144.

28. Chang J, Dong L, Mohan R, Liao Z, Cox J, Komaki R. Image-guided proton radiotherapy for medically inoperable stage I non-small cell lung cancer. Int J Radiat Oncol Biol Phys 2005; 63(2):S41.

29. Engelsman M, Rietzel E, Kooy H. Four-dimensional proton treatment planning for lung tumors. Int J Radiat Oncol Biol Phys 2006; 64(5):1589–95.

30. Murshed H, Liu H, Liao Z, et al. Dose and volume reduction for normal lung using intensity-modulated radiotherapy for advanced-stage non-small-cell lung cancer. Int J Radiat Oncol Biol Phys 2004; 58(4):1258–67.

31. Liu H, Wang X, Dong L, et al. Feasibility of sparing lung and other thoracic structures with intensity-modulated radiotherapy for non-small-cell lung cancer. Int J Radiat Oncol Biol Phys 2004; 58(4):1268–79.

32. Grills I, Yan D, Martinez A, Vicini F, Wong J, Kestin L. Potential for reduced toxicity and dose escalation in the treatment of inoperable non-small-cell lung cancer: A comparison of intensity-modulated radiation therapy (IMRT), 3D conformal radiation, and elective nodal irradiation. Int J Radiat Oncol Biol Phys 2003; 57(3):875–90.

33. Chui C, Yorke E, Hong L. The effects of intra-fraction organ motion on the delivery of intensity-modulated field with a multileaf collimator. Med Phys 2003; 30(7):1736–46.

34. Bortfeld T, Jokivarsi K, Goitein M, Kung J, Jiang S. Effects of intra-fraction motion on IMRT dose delivery: statistical analysis and simulation. Phys Med Biol 2002; 47 (13):2203–20.

35. Yom SS, Liao Z, Hu C, et al. Preliminary report of radiation pneumonitis (RP) in patients with non-small cell lung cancer (NSCLC) treated with intensity modulated radiotherapy (IMRT) and concurrent chemotherapy (ConChT). Int J Radiat Oncol Biol Phys 2005; 63(Suppl. 1):S407.

36. Chang J, Liu H, Komaki R. Intensity modulated radiation therapy and proton radiotherapy for non-small-cell lung cancer. Curr Oncol Rep 2005; 7:255–9.

37. Chang J, Zhang X, Wang X, et al. Significant reduction of normal tissue dose by proton radiotherapy compared with three-dimensional conformal or intensity-modulated radiation therapy in stage I or stage III non-small-cell lung cancer. Int J Radiat Oncol Biol Phys 2006; 65(4):1087–96.

38. Bush D, Slater J, Shin B, Cheek G, Miller D, Slater J. Hypofractionated proton beam radiotherapy for stage I lung cancer. Chest 2004; 126(4):1198–203.

39. Shioyama Y, Tokuuye K, Okumura T, et al. Clinical evaluation of proton radiotherapy for non-small-cell lung cancer. Int J Radiat Oncol Biol Phys 2003; 56 (1):7–13.

40. Nihei K, Ogino T, Ishikura S, Nishimura H. High-dose proton beam therapy for stage I non-small-cell lung cancer. Int J Radiat Oncol Biol Phys 2006; 65(1):107–11.

Evaluation of Treatment-Related Toxicity and Clinical Outcome in Lung Cancer Treated by Image-Guided Radiotherapy and Chemotherapy

Zhongxing Liao
Department of Radiation Oncology, University of Texas M.D. Anderson Cancer Center, Houston, Texas, U.S.A.

Helen H. Liu
Department of Radiation Physics, University of Texas M.D. Anderson Cancer Center, Houston, Texas, U.S.A.

Ritsuko Komaki
Department of Radiation Oncology, University of Texas M.D. Anderson Cancer Center, Houston, Texas, U.S.A.

INTRODUCTION

Radiochemotherapy has become the treatment of choice for locally or regionally advanced, surgically unresectable lung cancers, which make up the greatest proportion of cases. Compared with radiotherapy alone, this therapeutic combination has resulted in increased local tumor control and an improved survival rate (1,2). This approach increased median survival time from 8 to 9 months in the 1980s (3) to about 18 months in the early 21st century (1,2), and long-term survival has increased from 9% to about 15% (1,2). However, these improvements have been achieved at the expense of increased frequency and severity of normal tissue toxicity. The most common and dose limiting toxicities related to radiochemotherapy to lung cancer include treatment-related pneumonitis (TRP) and esophagitis. Grades 3 and 4 pneumonitis and fibrosis, which are sometimes fatal, have been observed in about 25–30% of patients (4,5). Treatment-related toxicity from radiation and chemotherapy as well as from lung cancer itself has become one of the major factors limiting therapeutic effectiveness. Here we summarize the current studies evaluated the toxicity and treatment outcome in non–small cell lung cancer (NSCLC) patients treated with conformal radiochemotherapy.

TREATMENT-RELATED PULMONARY TOXICITY AFTER RADIOCHEMOTHERAPY

Overview

Radiation-induced lung damage is characterized by acute pneumonitis, which occurs 2–6 months after treatment, and fibrosis, which may develop slowly after initiation of treatment over a period of several months to several years. The process is divided into three stages: a latent period, lasting up to 4 weeks; an exudative phase, lasting from 3 to 8 weeks; and an acute pneumonitic phase, lasting between 2 and 6 months. The latter is an inflammatory reaction with intra-alveolar and septal edema accompanied by epithelial and endothelial desquamation (6). Mild (grade 1) pneumonitis is characterized by opacity or infiltration in the chest radiographic images. More severe (grade 2 or 3) pneumonitis is usually accompanied by such symptoms as cough, fever, chest pain, shortness of breath, and respiratory difficulty. Patients may become oxygen dependent or even crippled by pulmonary insufficiency, especially patients treated with concurrent chemoradiation. The severity of lung damage depends on four factors: the total radiation dose, the volume of the lung irradiated, fraction size (the radiation dose of each treatment), and whether chemotherapy was given together with radiation (5,7).

Lung damage may occur following use of chemotherapy drugs, such as bleomycin, cyclophosphamide, and mustine. The deterioration of lung function progresses with time and is generally irreversible. The most likely target cells are the pulmonary endothelial cells and type II pneumocytes, which are involved in the production of surfactant during the first few days after irradiation. Currently, there is no effective therapeutic option for lung damage caused by cancer treatment. The fact that both chemotherapy and radiotherapy contributes to the development and severity of the lung injury, we propose to replace "radiation pneumonitis" with "TRP" in patients who received combined radiochemotherapy.
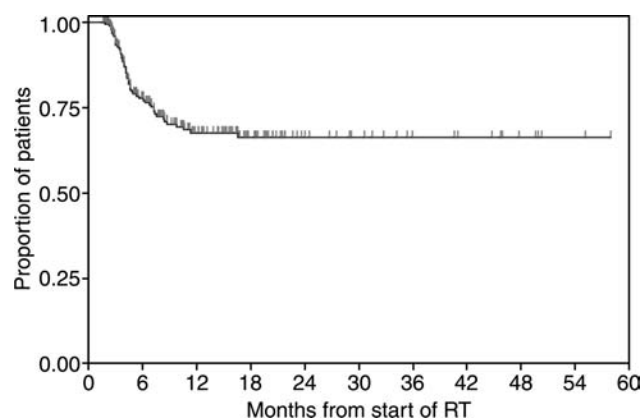
Figure 1 Freedom from grade ≥3 TRP among 222 NSCLC patients treated with concurrent chemoradiotherapy. *Abbreviations*: RT, radiation therapy; TRP, treatment-related pneumonitis. *Source*: From Ref. 8.

TRP is one of the major acute, dose-limiting toxicities resulting from chemotherapy and thoracic radiotherapy. The diagnosis of TRP, which typically occurs 3–9 months after radiotherapy (Fig. 1) (8), is established by a history of chemotherapy and radiotherapy, radiographic evidence, and clinical presentation. The typical radiological manifestation is areas of ground-glass opacity and/or consolidation in the irradiated lung that conforms to the shape and size of the treatment portals (9). The symptoms of TRP are dry cough, low-grade fever, chest pain, and shortness of breath. TRP can also present as ipsilateral pleural effusion and consolidation of the lung. Treatment for TRP is largely empirical and nonspecific, consisting of oral or intravenous steroids, oxygen, and sometimes assisted ventilation. TRP can be lethal if patients are not responsive to treatment. The clinical symptoms of TRP can lead to a poor quality of life for lung cancer patients (10).

3D Radiochemotherapy and TRP

The incidence of TRP ranges from 13% to 44%. This variance is due to inconsistencies in criteria used, heterogeneity in patient populations enrolled, and differences in treatment regimens and RT techniques employed (11–16). Clinical factors thought to predict TRP include poor ECOG performance status (17), poor pulmonary function before RT, concurrent cigarette smoking (18,19), chronic obstructive pulmonary disease (COPD) (20), lower-lobe tumors (21), concurrent chemotherapy (21), high total radiation dose, and high radiation dose per fraction. Dosimetric factors thought to predict TRP include mean lung dose (MLD) (20,22–24) and percentage volume of lung receiving more than a threshold dose (V_{dose}) (16,18,22,24–27). In most combined analyses of these clinical and dosimetric factors, many clinical factors

lost their ability to predict TRP; the only ones that did not were concurrent smoking, history of COPD, and induction chemotherapy with mitomycin. However, most of those studies included patients who were treated with RT alone or with some combination of chemotherapy and RT; only in one small study were all patients treated with concurrent chemoradiation therapy (27). Meanwhile, reports of other studies failed to describe important treatment details (e.g. whether patients received any kind of chemotherapy) (12,28). This lack of information on important variables (chemotherapy) that might influence the occurrence of TRP has led to confusion in the definition, measurement, and prediction of TRP in radiation oncology clinics.

Predictive radiotherapy dosimetric parameters range from the simple to the complex. MLD is both simple and clinically useful. So are the volumes of total lung irradiated to doses of ≥20 Gy (V_{20}) and ≥30 Gy (V_{30}) (29). All 3 of these parameters have the advantage of being easily calculated. Other parameters that involve more complicated calculations include Dose–volume histograms (DVH) reduction (i.e. reduction of the DVH of an organ to a single effective uniform dose), effective lung dose (V_{eff}), normal tissue complication probability (NTCP) (30–32), and the functional subunit model of Niemierko (33). These more complicated parameters have not been clinically confirmed and are technically difficult to calculate.

Number of studies (8,12,15,18,23,26) showed that MLD is an important dosimetric factor associated with the incidence of severe TRP and that a dose near 20 Gy (16.5 Gy) is a critical MLD cut point in predicting the incidence of TRP. It has been reported that when the MLD exceeds 20 Gy, the incidence of TRP is more than 20% (Table 1), although different grading systems for TRP were used in the aforementioned studies. Also, Oetzel et al. (12) and Willner et al. (24) found that the MLD of the ipsilateral lung is more important than the MLD of the total lung in predicting the risk of TRP.

In a recent single institution study included 222 patients with NSCLCs of similar stage and uniformly treatment with concurrent RT and chemotherapy (8), dosimetric factors were the only factors found to be associated with grade ≥3 TRP (as defined according to National Cancer Institute-Common Toxicity Criteria for Adverse Events [NCI-CTCAE] version 3.0.). Despite its retrospective nature, the study was unique because the patient population is quite homogeneous compared with most published studies to date: 96% of the patients had stage III or IV NSCLC, 65% had Karnofsky performance status ≥70, 96% received platinum-based concurrent chemotherapy and 79% had no COPD. The homogeneity of the study

Table 1 Effect of MLC and Incidence of TRP

Author, year (Ref.)	Treatment	Criteria (grade)	Incidence of RP for the whole group (%)	MLD (Gy)	Observed rate of RP for MLD subgroup (%)
Oetzel et al., 1995 (12)	28% 3D-CRT, chemotherapy not mentioned	RTOG 1+	15	≤15	0
				17.5–20	13
				22.5–25	21
				≥27.5	43
Kwa et al., 1998 (15)	100% 3D-CRT, 14% chemotherapy	SWOG 2+	16	0–8	5
				8–16	11
				16–24	24
				24–36	25
Graham et al., 1999 (26)	100% 3D-CRT 42%, chemotherapy	RTOG 2+	14 at 6 months	<20	8
				>20	24
Hernando et al., 2001 (18)	100% 3D-CRT <18%, concurrent chemotherapy, 51% surgery	Symptomatic CTC 2.0 1+	19	<10	10
				10–20	16
				21–30	27
				>30	44
Kim et al., 2005 (23)	100% 3D-CRT, 58% concurrent chemotherapy, 26% surgery	RTOG 3+	16	<10	0
				10–14.9	11
				≥15	45
Wang et al. 2006 (8)	100% 3D-CRT, 100% concurrent chemotherapy	CTC 3.0 3+	22 at 6 months	<20	16
				>20	40

Abbreviations: 3D-CRT, three-dimensional conformal radiation therapy; CTC, clinical tumor volume; MLC, multileaf collimators; MLD, mean lung dose; RTOG, Radiation Therapy Oncology Group; SWOG, Southwest Oncology Group; TRP, treatment-related pneumonitis.
Source: From Ref. 117.

population probably minimized variation in patient-, disease-, and treatment-related variables that might be associated with risk of TRP, allowing a relatively pure analysis of dosimetric factors.

Interestingly, the only significant factor associated with time to grade ≥3 TRP on multivariate analysis was the relative volume of total normal lung treated to 5 Gy (rV5). For rV5 ≤42% and rV5 >42%, the 1-year actuarial incidence of grade ≥3 TRP was 3% and 40%, respectively ($P = 0.001$) (Fig. 2). The frequent high correlation of dose–volume parameters suggests that the shape of the DVH may be more
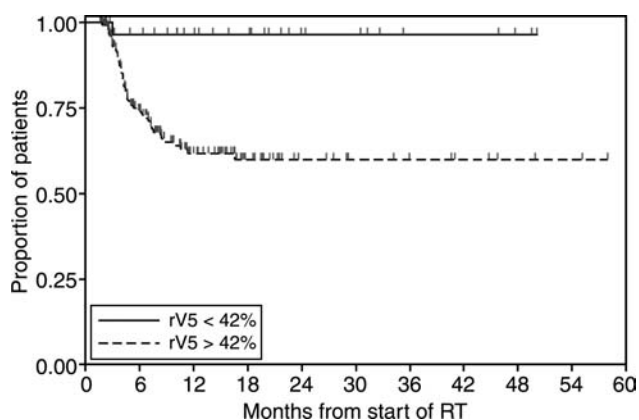
Figure 2 Effects of volume of lung receiving 5 Gy on freedom from grade ≥3 TRP in 222 patients with stage III NSCLC after undergoing concurrent radiotherapy and chemotherapy. *Abbreviations*: TRP, treatment-related pneumonitis; RT, radiation therapy. *Source*: From Ref. 8.

important than single points on the DVH curve (e.g. V20, rV5, or MLD) in predicting the probability of TRP (8). It also suggests that delivery of even a small dose of radiation as low as 5 Gy to a large volume of lung is not safe. This finding is supported by findings of Gopal et al. (34), who observed a sharp loss in the carbon monoxide diffusing capacity of normal lung exposed to as little as 13 Gy. The investigators concluded that a small dose of radiation to a large volume of lung could be much more damaging than a large dose to a small volume. Yorke et al. (28) reported that the risk of complications rose steeply when the MLD exceeded 10 Gy, indicating the need to limit widespread irradiation of normal lung tissue even at low doses. In contrast, Willner et al. (24) reported a sharp increase in the risk of TRP at higher doses, as shown on logistic regression curves for V10, V20, V30, and V40, and concluded that a small dose (e.g. 10 Gy) to a large volume of normal lung is preferable to a large dose (e.g. 40 Gy) to a small volume.

Although rV5 was the only factor selected by the mulitvariate recursive partioning analysis, many of the other dosimetric factors investigated in the study by Wang et al. (8), including MLD and rV10–rV65 were significantly associated with the incidence of grade ≥3 TRP; these factors are highly correlated with one another and with rV5 (Table 2). In fact, the high level of correlation makes it impossible to reach a definitive conclusion which dose level is most strongly associated with the risk of grade ≥3 TRP. Although the partitioning analysis suggests that very

Table 2 Incidence of Grade ≥3 TRP in Patient Subgroups Defined by Univariate Partitioning Analysis of MLD, GTV, Lung Volume and rV5–rV65

Variable	Median (range)	Group	No. of patients	Incidence of RP at 1 year (95% CI) (%)	P value
MLD	22.4 Gy (5.1–44.6 Gy)	≤16.5 Gy	30	13 (4–35)	0.018
		>16.5 Gy	193	36 (28–44)	
GTV	143 cc (1.5–1186 cc)	≤310 cc	181	28 (21–36)	0.003
		>310 cc	42	54 (37–73)	
Lung volume	3349 cc (1639–7871 cc)	≤5040 cc	200	35 (28–44)	0.023
		>5040 cc	23	6 (1–33)	
rV5	57% (12–98%)	≤42%	32	3 (<1–22)	0.001
		>42%	191	38% (30–47)	
rV10	47% (18–76%)	≤33%	25	5 (1–28)	0.007
		>33%	198	37 (29–45)	
rV15	43% (9–90%)	≤31%	26	4 (1–27)	0.005
		>31	197	37 (29–46)	
rV20	38% (8–78%)	≤28%	30	4 (1–24)	0.003
		>28%	193	37 (30–54)	
rV25	34% (7–71%)	≤27%	33	3 (<1–22)	0.001
		>27%	190	38 (30–47)	
rV30	32% (7–66%)	≤22%	28	10 (3–35)	0.014
		>22%	195	36 (28–44)	
rV35	29% (6–59%)	≤24%	56	12 (5–28)	<0.001
		>24%	167	39 (31–49)	
rV40	27% (6–56%)	≤22%	54	12 (5–27)	<0.001
		>22%	169	39 (31–49)	
rV45	24% (1–52%)	≤20%	61	14 (6–28)	<0.001
		>20%	162	39 (31–49)	
rV50	21% (0–48%)	≤14%	35	14 (6–37)	0.021
		>14%	188	36 (28–44)	
rV55	18% (0–46%)	≤15%	75	16 (8–30)	<0.001
		>15%	148	40 (31–50)	
rV60	15% (0–45%)	≤12%	58	18 (9–35)	0.008
		>12%	165	37 (29–46)	
rV65	10% (0–43%)	≤11%	119	25 (17–56)	0.021
		>11%	104	40 (30–52)	

Abbreviations: GTV, gross tumor volume; MLD, mean lung dose.
Source: From Ref. 8.
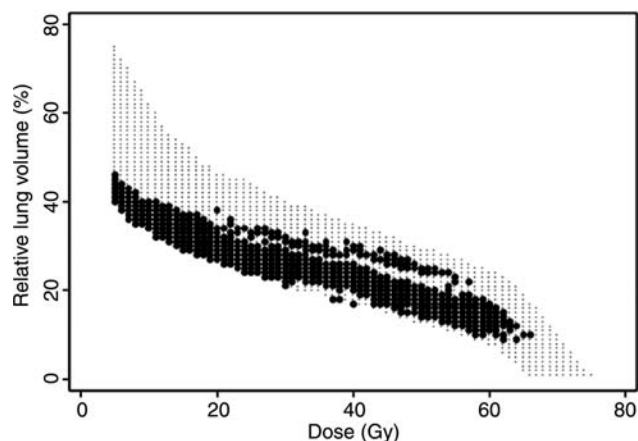
Figure 3 Comparison of time to grade ≥3 RP in patients subgroups divided according to magnitude (%) of rVD, for $D = 5$ to 80 Gy at 1 Gy increment. Small dots indicate comparisons for which each subset of the cohort included at least 10% of the patients; solid circles indicate comparisons for which $P < 0.05$ (log-rank test). *Source*: From Ref. 8.

low doses, near 5 Gy, might be most relevant, there was a wide variety in the dose–volume criteria corresponding to significant differences in time to grade ≥3 TRP. Figure 3 illustrates all partitions considered (small dots) as well as the dose–volume cut-points (solid circles) for which the comparison of time to grade ≥3 TRP in the corresponding subgroups reached statistical significance ($P < 0.05$, log-rank test). In view of the high correlation among relative lung volumes exposed to different doses, it was not yet possible to conclusively determine which dose range is most important in inducing grade ≥3 TRP.

Intensity Modulated Radiochemotherapy and TRP

Normal lung tissue is highly sensitive to low doses of radiation. Therefore, whereas the probability of tumor control may be predicted by the high-dose distribution around the tumor target, the NTCP might be predicted by the dose–volume relationship in the low-dose region. It is believed that the volume of normal

lung receiving low-dose irradiation should be minimized to avoid severe TRP. Techniques that decrease the volume of lung covered by a threshold dose include intensity-modulated radiotherapy (IMRT) and proton therapy.

The emerging technology of IMRT is rapidly gaining in popularity (35). Its increased conformality allows greater sparing of normal tissue at a number of sites (36). This approach may be useful in boosting radiation doses to lung tumors or in retreating previously irradiated sites (37,38) However, the clinical experience with IMRT has been limited to treating malignancies of the head and neck, brain, and pelvis; tumor excursion secondary to ventilatory and/or cardiac motion is considered problematic in IMRT for thoracic and abdominal malignancies. One planning study demonstrated a higher conformity index for IMRT than for three-dimensional conformal radiation therapy (3D-CRT) in the definitive treatment of lung and esophageal cancers (39). Another study comparing IMRT and 3D-CRT concluded that IMRT could be delivered at a 25–30% higher dose in node-positive patients while still meeting a conservative set of normal tissue constraints (40).

Based on planning studies demonstrating that IMRT could improve target coverage and reduce the volume of normal lung irradiated above low doses (41,42), IMRT with concurrent chemotherapy has been used in the definitive treatment of advanced NSCLC patients. In one of these previous studies, IMRT plans were generated for 41 patients with recurrent or Stages III–IV NSCLC who had undergone 3D-CRT. IMRT planning produced median absolute reductions in the relative percentages of normal lung volume irradiated to >10 and >20 Gy of 7% and 10%, respectively, corresponding to a decrease of >2 Gy in the total lung mean dose and a significant decrease in the model-based risk of TRP (42). However, to this point, no substantial clinical data have been available to assess IMRT in the treatment of advanced NSCLC.

Yom et al. (43) was the first to report clinical data regarding rates of high-grade TRP experienced in advanced NSCLC patients treated with IMRT and concurrent chemotherapy. The incidence of TRP in 68 NSCLC patients treated with IMRT and concurrent radiochemotherapy was compared with 222 similar patients treated with 3D-CRT. The median follow-up durations for the IMRT and 3D-CRT patients were 8 (range, 0–27) and 9 months (range, 0–56), respectively. The median IMRT and 3D-CRT doses were 63 Gy. The median gross tumor volume (GTV) was 194 mL (range, 21–911) for IMRT versus 142 mL (range, 1.5–1186) for 3D-CRT ($P = 0.002$). Despite the IMRT group's larger GTV, the rate of grade ≥3 TRP at 12 months was 8% (95% CI, 4–19%), compared to 32% (95% CI, 26–40%) for 3D-CRT ($P = 0.002$). (Fig. 4).
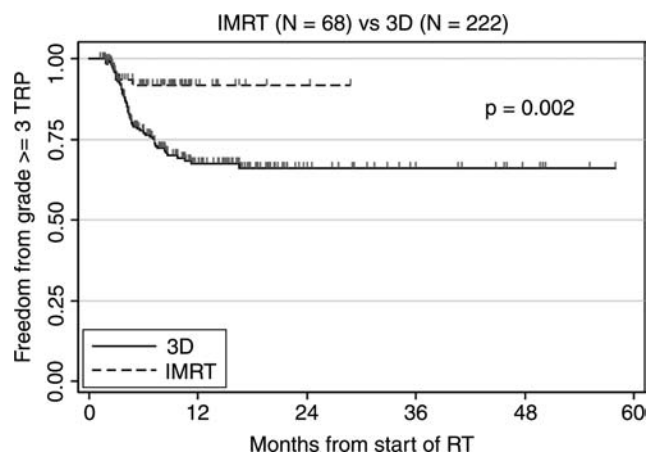
Figure 4 Freedom from grade ≥3 TRP after treatment of advanced NSCLC with concurrent chemotherapy and either 3D-CRT or IMRT. *Abbreviations*: 3D-CRT, three-dimensional conformal radiation therapy; IMRT, intensity-modulated radiation therapy; TRP, treatment-related pneumonitis; RT, radiation therapy. *Source*: From Ref. 44.

Interestingly, V5 (i.e. >70%) was again found to be significantly predictive of TRP (44).

In a previous planning study, toxicity modeling using parameters such as rV20, total lung mean dose, and NTCP predicted a risk of high-grade TRP after IMRT ranging from 7% to 16% (41). The clinical results of IMRT from study of Yom et al. approximated this earlier prediction. The strong patient selection biases in this retrospective study might have been expected to militate against the IMRT group, which was comprised of patients whose tumors could not be treated optimally with a conventional plan. IMRT patients had frequent need for coverage of large, bilaterally involved tumor volumes and had a larger GTV, more advanced stage of disease, and more debilitated performance status. In addition, patients with special medical conditions or a history of previous or synchronous surgical intervention or radiation treatment were often treated with IMRT. Though the clinical data is limited, it appears that IMRT can be safely used to treat very large tumors with the result of a lower risk of TRP than would be achieved with 3D-CRT. Figure 5 demonstrate a typical dose volume histogram and summarizes the dose constraints used in 3D-CRT or IMRT treatment planning for NSCLC at our institution.

The potential benefits of IMRT remain to be explored. For patients with locally advanced NSCLC, rates of locoregional failure remain high, and dose escalation has been limited by concerns about potentially deadly or permanently disabling lung toxicity (10). Dose escalation could lead to benefits in cancer eradication (45). One modeling study proposed that, at 2 Gy per fraction five times a week, 90–100 Gy would provide 30-month survival rates of

Dose–volume histogram

Parameter	Constraints
V5	<70%
V20	<35%
MLD	<20 Gy
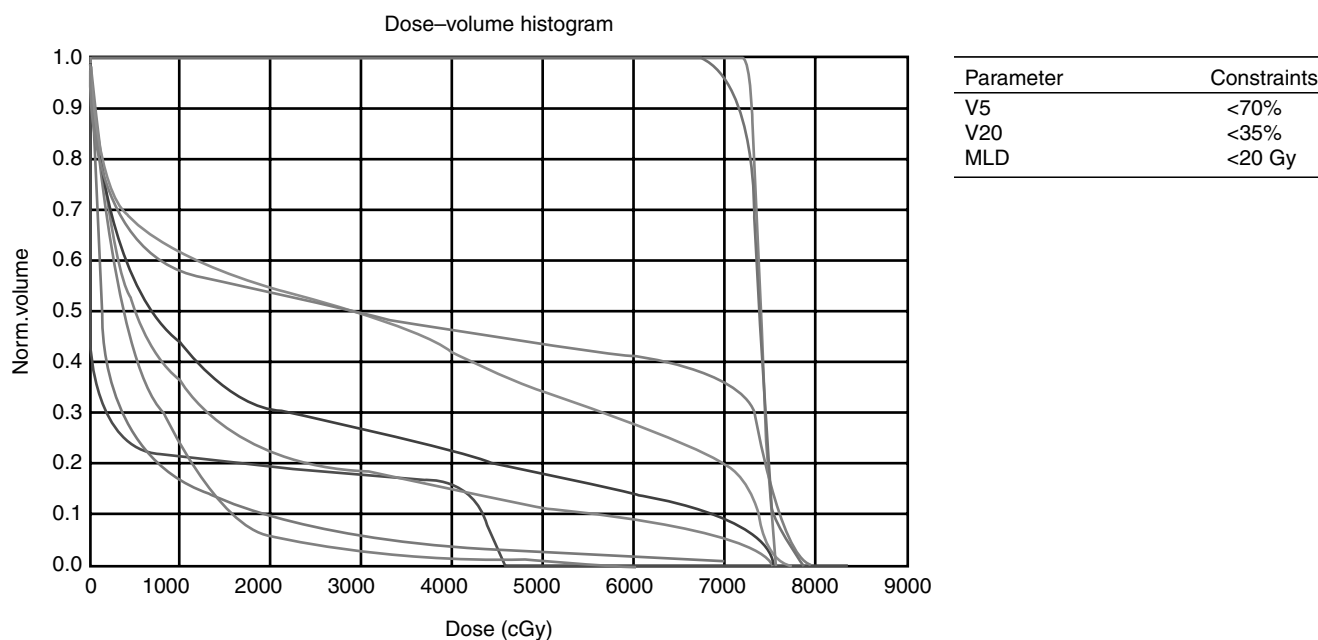
Figure 5   (*See color insert.*) Typical dose-distribution and DVHs (left) and dose constraints for use in planning treatment of stage III NSCLC. *Abbreviations*: DVH, dose–volume histograms; MLD, mean lung dose, NSCLC, non–small cell lung cancer.

60–70% (46). IMRT has been proposed as a means of improving the therapeutic ratio or allowing dose escalation (47). For example, a phase I study explored IMRT on an accelerated fractionation schedule to a dose of 84 Gy in 35 fractions preceded by induction paclitaxel. However, one patient experienced a fatal pulmonary toxicity at 3 months and the study was terminated (48).

To address the selection biases and confounding issues of contemporaneous technological evolution during the clinical implementation of IMRT at our institution, a randomized chemoradiation trial will compare 3D-CRT and IMRT for advanced NSCLC and is currently under review. A phase II trial of IMRT in combination with the tyrosine kinase inhibitor, cetuximab, is underway in Germany (49). Study of the effects of low-dose irradiation on the lung may benefit from more sophisticated dose calculation algorithms such as Monte Carlo (50). Proton therapy may offer a more advanced means of reducing peripheral dose delivery to the normal lung, because of the negligible dose delivery past the end of its targeted range (51). These are additional emerging areas for investigation.

ESOPHAGEAL TOXICITY

The radiotherapeutic management of thoracic malignancies often exposes the esophagus to high levels of ionizing radiation. After 2–3 weeks of conventionally fractionated RT, patients will often complain of acute reactions such as dysphagia, odynophagia, or both. These reactions can cause significant morbidity due to dehydration and weight loss that may necessitate treatment interruption. Late reactions of the esophagus to radiation generally involve fibrosis that can lead to stricture. Patients may experience various degrees of dysphagia and may require endoscopic dilation. In rare instances, acute and late responses may both involve esophageal perforation or obstruction.

The clinical and dosimetric predictors of acute and late esophagitis are not well characterized. Emami and colleagues (52) have reported $TD_{5/5}$ and $TD_{50/5}$ values for stricture and perforation of the esophagus but have not addressed the issues of acute and late esophagitis. The scarcity of data regarding the clinical and dosimetric predictors of acute and late esophagitis has become particularly important in the era of radiation dose escalation and combined chemoradiation therapy. Further intensification of these regimens will not be possible without further characterization of dose-limiting toxicities such as esophagitis.

Clinical Studies of Esophageal Toxicity
Seaman and Ackerman noted that radiologic findings of esophagitis, though rare, usually appeared as luminal narrowing. These investigators also inferred that the esophagus could tolerate a radiation dose of up to 6000 cGy, at a rate of 1000 cGy per week. These figures are remarkably similar to those later suggested by Emami and associates (53–55).

Goldstein and colleagues (56) reported on 30 patients who developed esophagitis after thoracic RT. Most showed no abnormality on barium swallow esophagrams; those who did usually showed altered esophageal motility. Lepke and associates (57) reported on 250 patients who received thoracic RT with or without chemotherapy. Forty patients had abnormal esophagrams. Patients treated with combined chemotherapy and RT had a nearly 5-fold higher incidence of esophageal abnormalities than did those treated with RT alone (7.7% [10/132] vs. 1.6% [1/63]).

Several large trials have shown that the esophagus can tolerate relatively high doses of conventionally fractionated radiation alone. Other trials suggest that platinum-based induction chemotherapy does not significantly lower esophageal tolerance. In a randomized trial of combination induction chemotherapy (vinblastine and cisplatin) and RT (total dose of 60 Gy) versus RT alone, Dillman and colleagues observed a similar incidence of severe esophageal toxicity (<1%) in both treatment arms (58). These findings were similar to those of the comparable studies summarized by Choy (59).

Several trials have shown that adding concurrent chemotherapy to RT increases esophageal toxicity. In trials of concurrent chemotherapy and RT versus conventionally fractionated RT alone (i.e. daily fractions of 1.8–2 Gy to a total dose of <60 Gy), the concurrent regimen markedly increased the incidence of esophagitis (60,61). Choy and colleagues reported a 46% incidence of acute grades 3–4 esophagitis in a trial of concurrent chemotherapy and RT consisting of weekly paclitaxel and carboplatin and daily 2-Gy fractions to a total dose of 66 Gy (62).

Byhardt et al. (60) reported on the toxicity results from five RTOG lung cancer trials of combined RT and cisplatin-based chemotherapy. The investigators segregated patients into three groups according to treatment: neoadjuvant chemotherapy and definitive radiation (group 1), neoadjuvant chemotherapy followed by concurrent chemoradiation (group 2), and concurrent chemotherapy and hyperfractionated radiation (group 3). The incidence of grade ≥3 acute esophagitis was significantly higher in group 3 than in either of the other two groups. Similarly, the incidence of late esophagitis in group 3 showed a trend toward significance (2% vs. 4% vs. 8%, $P = 0.077$).

Clinical and Dosimetric Studies of Esophageal Toxicity

There have been recent attempts to define the clinical and dosimetric predictors of esophagitis. In a recent report from M.D. Anderson Cance Center, investigators noted a 20.5% incidence of grade 3 acute esophagitis in 215 NSCLC patients treated with concurrent 3D-CRT and chemotherapy (Fig. 6) (63). They also identified three significant predictive
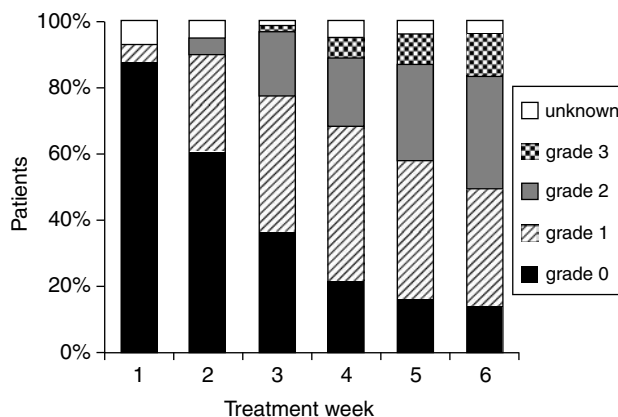
Figure 6 Incidence of acute esophagitis (grades 0–3) during each week of concurrent chemoradiotherapy. The incidence of severe acute esophagitis increased with time. *Source*: From Ref. 63

factors on univariate analysis (i.e. mean esophageal dose, absolute esophageal volume receiving 10–45 Gy, and relative esophageal volume receiving 10–45 Gy) (Fig. 7) and one significant predictive factor on multivariate analysis (i.e. relative V20) (63). In their report on 91 patients (61), Maguire and colleagues noted an 11% (10/91) incidence of acute grade ≥ 3 esophagitis and a 13% (12/91) incidence of late grade ≥ 3 esophagitis. In that study, 48% of patients received concurrent chemotherapy and 57% received hyperfractionated RT. Univariate analysis revealed no significant predictive factors for acute esophagitis but did identify one predictive factor for late esophagitis (i.e. length of 100% circumference receiving >50 Gy). In addition, multivariate analysis revealed two other predictive factors for late esophagitis (i.e. percentage of organ volume treated receiving >50 Gy and maximum percentage receiving >80 Gy).

Werner-Wasik and associates analyzed clinical and dosimetric predictors of esophagitis in 105 patients treated for lung cancer (64). They noted that 55% (58/105) received concurrent chemotherapy and that 7% (7/105) received twice-daily fractionated RT. They found that concurrent chemotherapy and twice-daily fractionation were associated with higher grades and longer durations of acute esophagitis, but that the absolute length of esophagus exposed to radiation did not predict esophagitis.

In a Washington University study of 207 patients treated with definitive RT or chemoradiation therapy, multivariate analysis revealed concurrent chemotherapy to be the predominant factor in treatment-related esophagitis (65). Overall, 8% of patients (16/207) in the study developed acute or late grades 3–5 esophagitis, and most of those ($N = 14$) had received concurrent chemoradiation therapy. Table 3 summaries the published results for risk factors associated with grade ≥ acute esophagitis (61,63,64–71).
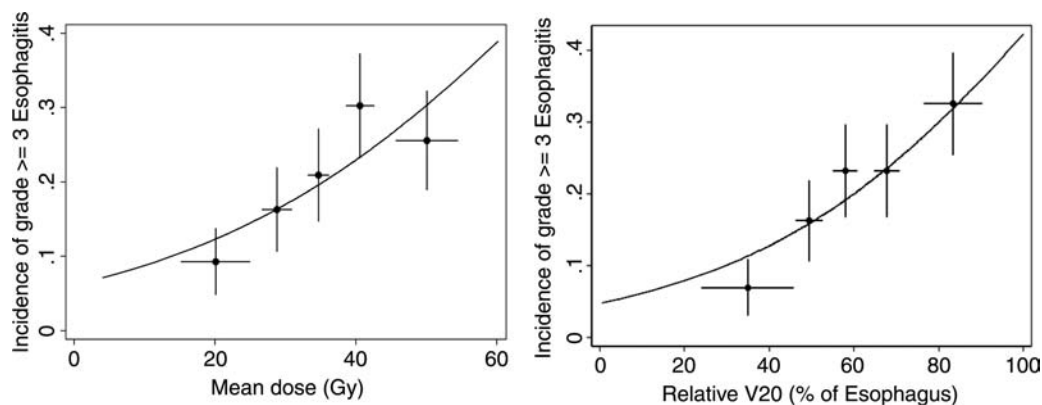
Figure 7 Effects of mean esophagus dose (*left*) and volume of esophagus receiving 20 Gy (*right*) on freedom from grade ≥3 acute esophagitis in 215 patients with stage III NSCLC after undergoing concurrent radiotherapy and chemotherapy. *Source*: From Ref. 63.

TUMOR RESPONSE AND SURVIVAL OF LUNG CANCER AFTER 3-D RADIOCHEMOTHERAPY

With the advent of 3D-CRT, traditionally recommended portals, target volumes, and beam arrangements have come into question. Because of NSCLC's reportedly high local failure rates, one goal of 3D-CRT is to increase the radiation dose delivered to the gross tumor while minimizing the radiation dose delivered to normal tissues. 3D-CRT has several significant advantages over traditional RT techniques: improved delineation of tumor and normal tissue, image segmentation and display, accurate dose calculation, and the ability to manipulate beam geometry and weighting through forward planning. The importance of improved target delineation cannot be overemphasized. Once the patient is immobilized and can undergo CT in the treatment position, the radiation oncologist can delineate the tumor and adjacent tissues in three dimensions; choose beam angles that maximize tumor coverage, minimize the amount of normal tissue exposed to radiation, or both;

Table 3 Published Results for Risk Factors Associated with Grade ≥3 Acute Esophagitis

First author, year (Ref.)	Criteria used	Overall incidence (%)	Total no. patients	Incidence of AE CCT + RT (qd) (%)	Incidence of AE CCT + RT (bid) (%)	Risk factors identified
Wei et al., 2006 (63)	CTC 30	20.5	215	18.3	31.8	Mean dose to esophagus, V20, bid
Belderbos et al., 2005 (66)	RTOG	6	156	27	N/A	CCT, V35
Qiao et al., 2005 (67)	RTOG	12	208	46	N/A	CCT, Dmax 60
Bradley et al., 2004 (68)	RTOG	5	166	N/A	N/A	CCT, A55, V60
Patel et al., 2004 (69)	RTOG	5	36	N/A	5	V50
Singh et al., 2003 (65)	RTPG	8	207	26	N/A	CCT, Dmax >58
Hirota et al., 2001 (70)	CTC 2.0	7	26	7	N/A	L45, V45
Werner-Wasik et al., 2000 (64)	RTOG	13	105	18	43	CCT, bid
Maguire et al., 1999 (61)	RTOG	11	91	N/A	N/A	Pre-RT dysphagia, bid
Werner-Wasik et al., 1999 (71)	RTOG	7	682	N/A	41	CCT

Abbreviations: A55, esophageal area receiving radiation dose >55 Gy; bid, twice daily; CCT, concurrent chemotherapy; CTC 2.0, National Cancer Institute-Common Toxicity Criteria for Adverse Events version 2.0; Dmax >58, maximal dose to the esophagus treated with >58 Gy; Dmax 60, maximal dose to the esophagus treated with >60 Gy; L45, esophageal length receiving radiation dose >45 Gy; N/A, not available; qd, daily; RT, radiation therapy; RTOG, Radiation Therapy Oncology Group; V35, esophageal volume receiving radiation dose >35 Gy; V45, esophageal volume receiving radiation dose >45 Gy; V50, esophageal volume receiving radiation dose >50 Gy; V60, esophageal volume receiving radiation dose >60 Gy.

alter beam weighting; and perhaps alter couch angles for noncoplanar beam delivery. This conformal technique also enables the fusion of complementary imaging modalities, such as PET to aid in tumor delineation and single photon emission computed tomography to choose beam angles. Purdy and colleagues have provided an excellent overview of 3D-CRT (72).

Planning for 3D-CRT in NSCLC has benefited from the application of target-defining guidelines published by the International Commission on Radiation Units (73). The GTV is defined as the primary tumor and any grossly involved lymph nodes. The clinical tumor volume (CTV) is defined as the anatomically defined area thought to harbor micrometastases (hilar or mediastinal lymph nodes or a margin around the grossly visible disease). The planning target volume (PTV) accounts for physiologic organ motion during treatment and the uncertainties of daily setup for fractionated therapy. When 3D treatment planning is done with the goals of conformal high-dose irradiation of the GTV and minimal irradiation of surrounding normal organs (especially lungs), unique portals, beam arrangements, and beam weights result.

3D-CRT Clinical Study Results

Several reports of recent 3D-CRT trials have been published. The most recent is M.D. Anderson Cancer Center's experience with 3D-CRT and concurrent chemotherapy in patients with predominantly stage III NSCLC (74). Of 265 patients enrolled, 127 (48%) were initially treated with 2 or 3 cycles of dual-agent induction chemotherapy; most of those ($N = 121$) received platinum and taxane. However, all 265 patients received 3D-CRT and concurrent chemotherapy (typically a weekly platinum- and taxane-based regimen). Radiation therapy typically targeted the GTV and involved lymph nodes. Uninvolved lymph nodes were not electively irradiated. The CTV was defined as the GTV plus an 8-mm margin, and the PTV was defined as the CTV plus a 10–15 mm margin. The radiation dose that was prescribed covered at least 95% of the PTV. Patients received radiation either daily in 1.8- or 2-Gy fractions ($N = 183$) or twice daily in 1.2-Gy fractions ($N = 82$), to a median dose of 63 Gy (range, 34.8–72 Gy). Nine patients who were unable to complete RT because of toxicity or disease progression and who thus received doses of >60 Gy were nevertheless included in the final analysis. The rates of overall survival, distant metastasis-free survival (DMFS), and local regional control (LRC) for the entire group of 265 patients were 41%, 43%, and 57%, respectively, at 2 years and 19%, 33%, and 51%, respectively, at 5 years (Fig. 8) (74).
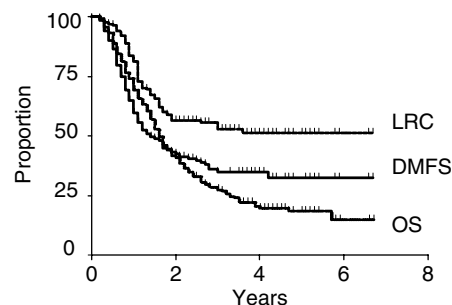
Figure 8 OS, DMFS, and LRC rates for 265 patients who were treated with 3D-CRT and concurrent chemotherapy at a single institution. The 2-year OS, DMFS, and LRC rates for the entire group were 41%, 43%, and 57%, respectively; the 5-year rates, 19%, 33%, and 51%, respectively. *Abbreviations*: OS, overall survival; DMFS, distant metastasis-free survival; LRC, local regional control. *Source*: From Ref. 74.

Another trial of 3D-CRT, reported by Bradley et al. (75), involved 207 patients with stage I-III inoperable bronchogenic carcinoma. The overall survival at 1 and 2 years was 59% and 41%, respectively. On multivariate analysis, the most important prognostic factor was GTV; tumor, nodal, and overall stage were not significant factors. Tumor doses of ≥70 Gy resulted in improved local control and cause-specific survival rates but did not improve overall survival. Care must be taken, however, in interpreting the dose data from this trial. Larger tumors were often treated with lower doses to keep normal tissues within their tolerance limits. Nonetheless, 3D dose-escalation data from other institutions support the notion that doses ≥60 Gy improve local control (14,76–79).

Elective Nodal Iirradiation

In many respects, surgery and external-beam RT play similar roles in the treatment of lung cancer. The intent of both modalities is local control in the treated field. Thus, for many years and with only a few recent exceptions (76,80–84), standard RT practice in the United States was to deliver 40–50 Gy to electively irradiated regional lymph nodes (e.g. ipsilateral hilum, ipsilateral and contralateral mediastinum, supraclavicular fassa) and an additional 20 Gy to the primary tumor through reduced fields. This approach was based on pathologic data indicating a high incidence of hilar and mediastinal node metastases in patients with bronchogenic carcinoma. Indeed, up to 26% of patients with stage I NSCLC may have pathologically proven nodal metastases (85,86), and an estimated 25% of T1N0 tumors and 35% of T2N0 tumors are consistently upstaged on the basis of surgical and pathological findings (87,88). Moreover, the risk of lymphatic metastasis increases with tumor size: from 0% at <1.0 cm to 17% at 1.1–2.0 cm and 38% at >2.0 cm (89). Poorly differentiated tumors have a

higher rate of nodal micrometastasis, which in itself is an independent prognostic factor for survival (90,91). In one trial, patients treated with lobectomy rather than with limited resection had significantly lower rates of local and regional failure and showed a trend toward improved survival, suggesting that the improvements were due to removal of both the primary tumor and the draining lymphatics (87). This conclusion is supported by a recent meta-analysis of four randomized trials of systemic nodal dissection versus more limited mediastinal lymph node sampling, which revealed an association between more aggressive treatment of the mediastinal lymphatics and significantly better 5-year overall survival (92).

The principle that adequate surgical resection of a T1N0 tumor requires systematic removal of all hilar and mediastinal lymph nodes (87,89) suggests that radiation fields should encompass the draining nodal areas. In an analysis of protocol compliance among patients with radiographically negative lymph nodes in the RTOG 73–01 trial, (93) Perez and associates observed better ($P = 0.35$) survival among patients whose treatment did not vary from the protocol and who had adequate coverage of the hilar/mediastinal lymph nodes. Together, such findings provide a rationale for elective nodal irradiation (ENI).

The major argument against ENI is the high rate of local recurrence within previously irradiated tumor volumes. If one cannot control gross disease, why enlarge the irradiated volumes to include areas that might harbor microscopic disease? Such concerns have been allayed by several major changes in lung cancer therapy since the RTOG 73-01 first established the standards for radiation doses and volumes: namely, the use of chemotherapy, the advent of 3D-CRT, and the incorporation of PET into NSCLC staging protocols.

According to a review of the patterns of failure after definitive RT in early-stage NSCLC, isolated regional failure occurs in no more than 15% of cases. (94,95) This suggests the possibility of creating localized radiation fields without utilizing ENI.

In one trial, Zhang et al. (84) observed 3- and 5-year overall survival rates of 55% and 32%, respectively, in selected patients with bronchogenic carcinoma whose primary tumors were irradiated but whose lymphatics were not. In another trial, Dosoretz et al. (76) observed no correlation between field size and treatment outcome, even after stratifying their data according to tumor size. In a third trial, Krol and colleagues (81) reported 3- and 5-year overall survival rates of 31% and 15%, respectively, in 108 patients with stage I lung cancer who underwent definitive RT encompassing the primary tumor but no ENI. More notably, the 3- and 5-year cancer-specific survival rates were 42% and 31%, respectively. These results

are comparable to results achieved in trials of RT encompassing both traditional fields and regional lymphatics. They have also been confirmed by Senan et al. (83), who reported similarly low failure rates in untreated elective nodal areas in stage III patients.

Nevertheless, the results of ENI trials to date need to be examined carefully because of the significant radiation doses ($\geq$40 Gy) delivered electively to regions outside the intended CTV (82,96). In their series of 171 patients in which involved field volumes were treated definitively with 3D-CRT but without ENI, Rosenzweig and coworkers reported an overall elective nodal failure rate of only 6.4%, including 1% in the ipsilateral supraclavicular region, 3% in the contralateral supraclavicular region, 4% in the ipsilateral inferior mediastinal region, and 1% in the contralateral inferior mediastinal region (82). However, these investigators also estimated that the ipsilateral superior mediastinum, inferior mediastinum, and subcarinal regions received incidental doses of at least 40 Gy (a median dose of 18 Gy to all elective regions) in 34%, 63%, and 41% of cases, respectively (82). Similar analyses by others found that the ipsilateral hilum, subcarinal region, low paratracheal region, and contralateral hilum and AP window received incidental doses of at least 50 Gy in 100%, 97%, 59%, and 57% of cases, respectively (77,97). It may be that these incidental doses were not delivered in standard fractions and that the biologically effective dose may not have been sufficient to control any disease that may have been present. Nevertheless, the impact of incidental radiation should be explored further before discounting its possible contribution to nodal failure. Dosimetric analyses (e.g. prospective analyses that correlate nodal failures with dose received) might be helpful in this regard.

There are at least two possible explanations for the lower-than-expected elective nodal failure rates observed in trials of ENI. First, incidental doses to the ipsilateral hilar, paratracheal, and subcarinal nodes approach 40–50 Gy when these regions are not intentionally irradiated (96). Second, lung cancer patients face multiple competing causes of death (e.g. local failure, distant failure, or intercurrent illness) that may kill them without elective nodal failures ever being detected.

Role of Positron Emission Tomography in Nodal Treatment Planning

The efficacy of ENI may be improved upon by utilizing PET in lung cancer treatment planning. PET has been a major innovation in lung cancer imaging, mainly because of its ability to supplement the structural information provided by traditional anatomical imaging (e.g. CT scans) with functional

information about the tumor cells themselves. PET images have added significantly to the accuracy of conventional imaging in estimating the true extent of NSCLC tumors (98). More accurate clinical staging with PET may allow radiation oncologist to include involved hilar and mediastinal nodes that are not appreciated on the CT scan and reduce the probability of elective nodal failures. As more and more facilities acquire dedicated fluorodeoxyglucose (FDG)-PET scanners and, more specifically, combined PET-CT units, radiation oncologists will be better able to delineate PTVs. Accurate definition and delineation of nodal metastases are crucial for planning curative RT, particularly since routine ENI is no longer recommended in patients NSCLC (99). Systematic review of the available evidence suggests that FDG-PET is superior to conventional mediastinal staging by CT and esophageal ultrasonography (98,100–102). One recent modeling study suggests that treating only FDG-positive mediastinal areas would decrease the volumes of lung and esophagus exposed to radiation, thus allowing for radiation dose-escalation and hence an improved radiotherapeutic ratio (103). In one prospective clinical trial of this approach, the rate of isolated nodal failure was only 2% (1/44) (104). However, in other trials, the rate of false-positive mediastinal nodes on PET scans has ranged as high as 39% (105,106). This suggests that histological confirmation of nodal failure is critical when it would have a major impact on the treatment. Figure 9 shows a PET scan of a right upper lobe tumor contiguous with a hilar mass, metastasis to an upper paratracheal node, and incidentally found right-sided adrenal metastasis.

PET's potential role in planning RT for primary NSCLC is under investigation. PET scanning would certainly help to delineate the GTV in the presence of significant obstructive atelectasis. However, its relatively low spatial resolution (presently 6–8 mm and physically limited to ~2 mm) and the resulting

blurring of tumor edges make PET-based contouring difficult. Autocontouring using predefined standard uptake value (SUV) thresholds has been reported (107,108). However, at present, the threshold-defining criteria for contouring GTVs in NSCLC lack pathological correlates. One attractive area of research concerns the use of PET SUV thresholds in planning "metabolic boosts" (i.e. delivery of higher radiation doses to areas with high SUV thresholds while sparing "hypodense" regions identified on FDG-PET scans). However, there is little pathological evidence that "hypodense" regions represent exclusively sites of necrosis and/or atelectasis. Thus, before the concept of modulating radiation doses to tumor subvolumes can be tested rationally in clinical trials, there will have to be studies that correlate pathology with PET images and studies that correlate PET tracer uptake with the molecular characteristics of tumor cells.

Role of Chemotherapy in Treating Microscopic and Nodal Disease

There is mounting evidence that chemotherapy can effectively control microscopic disease in NSCLC. In several trials, patients receiving chemotherapy for completely resected NSCLC derived an overall survival benefit (109–113). In a randomized trial of sequential therapy (chemotherapy followed by RT) versus RT alone for unresectable lung cancer, microscopic control was achieved (114). In a randomized RTOG trial of chemotherapy (vinblastine and cisplatinum) plus RT versus RT alone, analysis of failure patterns revealed a significant improvement in the rate of distant metastases for patients treated with the combination therapy ($P < 0.04$) (115). However, the RT regimen used in both of these randomized trials included ENI and had no effect on local control even with the addition of chemotherapy. Now that combined chemotherapy and radiotherapy has become

Figure 9 PET/CT scan image of a patient with a right upper lobe tumor contiguous with the right hilum, and an incidental finding of right adrenal metastasis.

the established treatment of choice for patients with locally advanced NSCLC, it is reasonable to suggest that chemotherapy may adequately address regional disease and that ENI may not be necessary, particularly in patients whose tumors will be treated with a combination of chemotherapy and RT after CT and PET staging.

CONCLUSION

Treatment-related pulmonary and esophageal toxicities are the two most important dose limiting factors in radiochemotherapy for NSCLC patients. TRP occurs in 13–44% of patients, and often irreversible and sometimes fatal. In applying 3D-CRT, it is extremely important not to exceed the maximum doses tolerated by sensitive intrathoracic structures such as the lungs, spinal cord, and heart. Unfortunately, partial-volume normal tissue tolerances are not well understood. Special care should be taken to restrict the radiation dose to the normal lung whenever possible. DVHs for all normal thoracic organs should be evaluated for dose and volume of irradiation. Although DVH analysis is still a developing technique, preliminary results indicate that it can be used to predict complications such as pneumonitis and to improve treatment planning (8,11,26,96,116). The potential benefits of 3D-CRT currently are being investigated in prospective trials.

IMRT is a useful technique to sparing normal lung for treating advanced NSCLC, especially for tumors not amenable to treatment with 3D-CRT. IMRT is appropriate for large-volume disease with fixation to the mediastinum and relatively minimal tumor motion, or for patients with complex medical conditions or other special conditions necessitating more complex planning. IMRT resulted in improved rates of high-grade TRP as compared to 3D-CRT. However, precautions should be taken to minimize exposure of large volumes of normal lung to low doses, to avoid potential serious pulmonary complications. It is critical to practice strict dose constraints in the treatment planning of NSCLC using 3D-CRT of IMRT: V5 < 70%, V20 < 35%, and MLD < 20 Gy.

There is no randomized study comparing 2D versus 3D radiochemotherapy for NSCLC. Data from retrospective reviews, and prospective phase I or II studies demonstrated 2- and 5-year survival of about 50% and 19%. Elective nodal irradiation in conformal radiochemotherapy era appears unnecessary, especially when functional image is used in guiding the target volume delineation.

Image-guided radiation therapy provides a tool to improve target accuracy, reduce normal tissue toxicity while increasing radiation dose to tumor that would increase therapeutic ratio of thoracic radiation therapy. Future investigation in radiation therapy include image guided adaptive radiation, and proton beam therapy.

REFERENCES

1. Furuse K, Fukuoka M, Kawahara M, et al. Phase III study of concurrent versus sequential thoracic radiotherapy in combination with mitomycin, vindesine, and cisplatin in unresectable stage III non-small cell lung cancer. J Clin Oncol 1999; 17:2692–9.

2. Curran W, Jr, Scott C, Langer C, et al. Phase III comparison of sequential vs concurrent chemoradiation for patients with unresectable stage III non-small cell lung cancer (NSCLC): Intial Report of Radiation Therapy Oncology Group (RTOG) 9410. ASCO. Vol 19; 2000: 484a.

3. Dillman RO, Herndon J, Seagren SL, Eaton WL, Green MR. Improved survival in stage III non-small-cell lung cancer: Seven-year follow-up of cancer and leukemia group B (CALGB) 8433 trial. J Natl Cancer Inst 1996; 88:1210–15.

4. Komaki R, Lee JS, Milas L, et al. Effects of amifostine on acute toxicity from concurrent chemotherapy and radiotherapy for inoperable non-small-cell lung cancer: report of a randomized comparative trial 1. Int J Radiat Oncol Biol Phys 2004; 58:1369–77.

5. Graham MV, Pajak TF, Herskovic A, Emami B, Perez CA. Phase I/II study of treatment of locally advanced (T3/T4) non-oat cell lung cancer with concomitant boost radiotherapy by the radiation therapy oncology group (RTOG 83-12): Long-term results. Int J Radiat Oncol Biol Phys 1995; 31:819–25.

6. Coogle J, Lambert B, Moores S. Radiation effects in the lung. Environ Health Perspect 1986; 70:261–91.

7. Liao Z, Travis E, Tucker S. Damage and morbidity form pneumonitis after irradiation of partial volumes of mouse lung. Int J Radiat Oncol Biol Phys 1995; 32:1359–70.

8. Wang SL, Liao ZX, Liu H, et al. Intensity-modulated radiation therapy with concurrent chemotherapy for locally advanced cervical and upper thoracic esophageal cancer. World J Gastroenterol 2006; 12(34):5501–8.

9. Choi YW, Munden RF, Erasmus JJ, et al. Effects of radiation therapy on the lung: radiologic appearances and differential diagnosis. Radiographics 2004; 24: 985–97.

10. Movsas B, Raffin T, Epstein A, Link C, Jr. Pulmonary radiation injury. Chest 1997; 111:1061–76.

11. Martel M, Ten Haken R, Hazuka M. Dose-volume histogram and 3-D treatment planning evaluation of patients with pneumonitis. Int J Radiat Oncol Biol Phys 1994; 28:575–81.

12. Oetzel D, Schraube P, Hensley F, Sroka-Perez G, Menke M, Flentje M. Estimation of pneumonitis risk in three-dimensional treatment planning using dose-volume histogram analysis. Int J Radiat Oncol Biol Phys 1995; 33:455–60.

13. Marks LB, Munley MT, Bentel GC, et al. Physical and biological predictors of changes in whole-lung function following thoracic irradiation. Int J Radiat Oncol Biol Phys 1997; 39:563–70.

14. Armstrong J, Raben A, Zelefsky M, et al. Promising survival with three-dimensional conformal radiation therapy for non-small cell lung cancer. Radiother Oncol 1997; 44:17–22.

15. Kwa S, Lebesque J, Theuws J, et al. Radiation pneumonitis as a function of mean lung dose: an analysis of pooled data of 540 patients. Int J Radiat Oncol Biol Phys 1998; 42:1–9.

16. Fu X, Huang H, Bentel G, et al. Predicting the risk of symptomatic radiation-induced lung injury using both the physical and biologic parameters V(30) and transforming growth factor beta. Int J Radiat Oncol Biol Phys 2001; 50:899–908.

17. Robnett TJ, Machtay M, Vines EF, McKenna MG, Algazy KM, McKenna WG. Factors predicting severe radiation pneumonitis in patients receiving definitive chemoradiation for lung cancer. Int J Radiat Oncol Biol Phys 2000; 48:89–94.

18. Hernando ML, Marks LB, Bentel GC, et al. Radiation-induced pulmonary toxicity: a dose-volume histogram analysis in 201 patients with lung cancer. Int J Radiat Oncol Biol Phys 2001; 51:650–9.

19. Johansson S, Bjermer L, Franzen L, Henriksson R. Effects of ongoing smoking on the development of radiation-induced pneumonitis in breast cancer and oesophagus cancer patients. Radiother Oncol 1998; 49:41–7.

20. Rancati T, Ceresoli GL, Gagliardi G, Schipani S, Cattaneo GM. Factors predicting radiation pneumonitis in lung cancer patients: a retrospective study. Radiother Oncol 2003; 67:275–83.

21. Yamada M, Kudoh S, Hirata K, Nakajima T, Yoshikawa J. Risk factors of pneumonitis following chemoradiotherapy for lung cancer. Eur J Cancer 1998; 34:71–5.

22. Claude L, PerolPérol D, Ginestet C, et al. A prospective study on radiation pneumonitis following conformal radiation therapy in non-small-cell lung cancer: clinical and dosimetric factors analysis. Radiother Oncol 2004; 71:175–81.

23. Kim TH, Cho KH, Pyo HR, et al. Dose-volumetric parameters for predicting severe radiation pneumonitis after three-dimensional conformal radiation therapy for lung cancer. Radiology 2005; 235:208–15.

24. Willner J, Jost A, Baier K, Flentje M. A little to a lot or a lot to a little? An analysis of pneumonitis risk from dose-volume histogram parameters of the lung in patients with lung cancer treated with 3-D conformal radiotherapy. Strahlenther Onkol 2003; 179:548–56.

25. Armstrong J, Zelefsky M, Leibel S, et al. Strategy for dose escalation using 3-dimensional conformal radiation therapy for lung cancer. Ann Oncol 1995; 6: 693–7.

26. Graham M, Purdy J, Emami B, Harms W, Bosch W, Lockett M. Clinical dose-volume histogram analysis for pneumonitis after 3D treatment for non-small cell lung cancer (NSCLC). Int J Radiat Oncol Biol Phys 1999; 45:323–9.

27. Tsujino K, Hirota S, Endo M, et al. Predictive value of dose-volume histogram parameters for predicting radiation pneumonitis after concurrent chemoradiation for lung cancer. Int J Radiat Oncol Biol Phys 2003; 55:110–15.

28. Yorke ED, Jackson A, Rosenzweig KE, et al. Dose-volume factors contributing to the incidence of radiation pneumonitis in non-small-cell lung cancer patients treated with three-dimensional conformal radiation therapy. Int J Radiat Oncol Biol Phys 2002; 54:329–339.

29. Munley M, Marks L, Scarfone C, et al. Multimodality nuclear medicine imaging in three-dimensional radiation treatment planning for lung cancer: challenges and prospects. Lung Cancer 1999; 23:105–14.

30. Kutcher G, Burman C. Calculation of complication probability factors for non-uniform normal tissue irradiation: the effective volume method. Int J Radiat Oncol Biol Phys 1989; 23:105–14.

31. Lyman J. Complication probability as assessed from dose-volume histograms. Radiat Res 1985; 8:S13–19.

32. Seppenwoolde Y, Lebesque J, De Jaeger K, et al. Comparing different NTCP models that predict the incidence of radiation pneumonitis. Int J Radiat Oncol Biol Phys 2003; 55:724–35.

33. Niemierko A. Reporting and analyzing dose distributions: a concept of equivalent uniform dose. Med Phys 1997; 24:103–10.

34. Gopal R, Tucker SL, Komaki R, et al. The relationship between local dose and loss of function for irradiated lung. Int J Radiat Oncol Biol Phys 2003; 56:106–13.

35. Mell L, Mehrotra A, Mundt A. Intensity-modulated radiation therapy use in the U.S., 2004. Cancer 2005; 104:1296–303.

36. Hong L, Alektiar KM, Hunt M, Venkatraman E, Leibel SA. Intensity-modulated radiotherapy for soft tissue sarcoma of the thigh. Int J Radiat Oncol Biol Phys 2004; 59:752–9.

37. Choi Y, Kim J, Lee H, Hur W, Chai G, Kang K. Impact of intensity-modulated radiation therapy as a boost treatment on the lung-dose distributions for non-small-cell lung cancer. Int J Radiat Oncol Biol Phys 2005; 63:683–9.

38. Beavis A, Abdel-Hamid A, Upadhyay S. Re-treatment of a lung tumour using a simple intensity-modulated radiotherapy approach. Br J Radiol 2005; 78:358–61.

39. Wu VWC, Sham JST, Kwong DLW. Inverse planning in three-dimensional conformal and intensity-modulated radiotherapy of mid-thoracic oesophageal cancer. Br J Radiol 2004; 77:568–72.

40. Grills I, Yan D, Martinez A, Vicini F, Wong J, Kestin L. Potential for reduced toxicity and dose escalation in the treatment of inoperable non-small-cell lung cancer: a comparison of intensity-modulated radiation therapy (IMRT), 3D conformal radiation, and elective nodal irradiation. Int J Radiat Oncol Biol Phys 2003; 57:875–90.

41. Murshed H, Liu H, Liao Z, et al. Dose and volume reduction for normal lung using intensity-modulated radiotherapy for advanced-stage non-small-cell lung cancer. Int J Radiat Oncol Biol Phys 2004; 58:1258–67.

42. Liu H, Wang X, Dong L, et al. Feasibility of sparing lung and other thoracic structures with intensity-modulated radiotherapy for non-small-cell lung cancer. Int J Radiat Oncol Biol Phys 2004; 58:1268–79.

43. Yom S, Liao Z, Hu C, et al. Preliminary report of radiation pneumonitis (RP) in patients with non-small cell lung cancer (NSCLC) treated with intensity modulated radiotherapy (IMRT) and concurrent chemotherpy (ConChT). ASTRO 2005; 63:S407.

44. Yom S, Liao Z, Liu H, et al. Initial evaluation of treatment-related pneumonitis in advanced-stage non-small cell lung cancer patients treated with concurrent chemotherapy and intensity-modulated radiation therapy. Int J Radiat Oncol Biol Phys 2007; 68(1):94–102.

45. Ling CC, Yorke ED, Amols H, et al. High-tech will improve radiotherapy of NSCLC: A hypothesis waiting to be validated. Int J Radiat Oncol Biol Phys 2004; 60:3–7.

46. Mehta M, Scrimger R, Mackie R, Baliwal B, Chappell R, Fowler J. A new approach to dose escalation in non-small-cell lung cancer. Int J Radiat Oncol Biol Phys 2001; 49:23–33.

47. Schwartz M, Alber M, Lebesque JV, Mijnheer BJ, Damen EMF. Dose heterogeneity in the target volume and intensity-modulated radiotherapy to escalate the dose in the treatment of non-small-cell lung cancer. Int J Radiat Oncol Biol Phys 2005; 62:561–70.

48. Holloway C, Robinson D, Murray B, et al. Results of a phase I study to dose escalate using intensity modulated radiotherapy guided by combined PET/CT imaging with induction chemotherapy for patients with non-small cell lung cancer. Radiother Oncol 2004; 73:285–7.

49. Jensen A, Munter M, Bischoff H, et al. Treatment of non-small cell lung cancer with intensity-modulated radiation therapy in combination with cetuximab: The NEAR protocol (NCT00115518). BMC Cancer 2006; 6:122.

50. Liu CH, Chang S-H, Narko K, et al. Overexpression of cyclooxygenase-2 is sufficient to induce tumorigenesis in transgenic mice. J Biol Chem 2001; 276:18563–9.

51. Chang JY, Zhang X, Wang X, et al. Significant reduction of normal tissue dose by proton radiotherapy compared with three-dimensional conformal or intensity-modulated radiation therapy in Stage I or Stage III non-small-cell lung cancer. Int J Radiat Oncol Biol Phys 2006; 65:1087–96.

52. Emami B, Lyman J, Brown A, et al. Tolerance of normal tissue to therapeutic irradiation. Int J Radiat Oncol Biol Phys 1991; 21:109–22.

53. Englestad R. Uber die wikungender rontgenstrahlung auf osophagus und trchea. Acta Radiol 1934; 15:608–14.

54. Phillips T, Ross G. Time-dose relationships in the mouse esophagus. Radiology 1974; 113:435–40.

55. Northway M, Libshitz H, West J, et al. The opossum as an animal model for studying radiation esophagitis. Radiology 1979; 131:731–5.

56. Goldstein H, Rogers L, Fletcher G, Dodd G. Radiological manifestations of radiation-induced injury to the normal upper gastrointestinal tract. Radiology 1975; 117:135–40.

57. Lepke R, Libshitz H. Radiation-induced injury of the esophagus. Radiology 1983; 148:375–8.

58. Dillman RO, Hemdon J, et al. Improved survival in stage III non-small-cell lung cancer: Seven-year follow-up of cancer and leukemia group B (CALGB) 8433 trial. Journal of the National Cancer Institute 1996; 88(17):1210–5.

59. Choy H, LaPorte K, Knill-Selby E, Mohr P, Shyr Y. Esophagitis in combined modality therapy for locally advanced non–small cell lung cancer. Seminars in Radiation Oncology 1999; 9(2 Suppl 1):90–6.

60. Byhardt R, Scott C, Sause W, et al. Response, toxicity, failure patterns, and survival in five Radiation Therapy Oncology Group (RTOG) trials of sequential and/or concurrent chemotherapy and radiotherapy for locally advanced non-small-cell carcinoma of the lung. Int J Radiat Oncol Biol Phys 1998; 42: 469–78.

61. Maguire P, Sibley G, Zhou S, et al. Clinical and dosimetric predictors of radiation-induced esophageal toxicity. Int J Radiat Oncol Biol Phys 1999; 45: 97–103.

62. Choy H, Akerley W, Safran H, et al. Multiinstitutional phase II trial of paclitaxel, carboplatin, and concurrent radiation therapy for locally advanced non-small-cell lung cancer. J Clin Oncol 1998; 16:3316–22.

63. Wei X, Liu HH, Tucker SL, Liao ZX, Hu CS, Mohan R, et al. Risk factors for acute esophagitis in non–small-cell lung cancer patients treated with concurrent chemotherapy and three-dimensional conformal radiotherapy. Int J Radiat Oncol Biol Phys 2006; 66(1):100–7.

64. Werner-Wasik M, Pequignot E, Leeper D, Hauck W, Curran W. Predictors of servre esophagitis include use of concurrent chemotherapy, but not the length of irradiated esophagus: a multivariate analysis of patients with lung cancer treated with noniperative therapy. Int J Radiat Oncol Biol Phys 2000; 48:689–96.

65. Singh A, Lockett M, Bradley J. Predictors of radiation-induced esophageal toxicity in patients with non-small-cell lung cancer treated with three-dimensional conformal radiotherapy. Int J Radiat Oncol Biol Phys 2003; 55:337–41.

66. Belderbos J, Heemsbergen W, Hoogeman M, Pengel K, Rossi M, Lebesque J. Acute esophageal toxicity in non-small cell lung cancer patients after high dose conformal radiotherapy. Radiother Oncol 2005; 75:157–64.

67. Qiao W-B, Zhao Y-H, Zhao Y-B, Wang R-Z. Clinical and dosimetric factors of radiation-induced esophageal injury: radiation-induced esophageal toxicity. World J Gastroenterol 2005; 11:2626–9.

68. Bradley J, Thorstad W, Mutic S, et al. Impact of FDG-PET on radiation therapy volume delineation in non-small-cell lung cancer. Int J Radiat Oncol Biol Phys 2004; 59:78–86.

69. Patel AB, Edelman MJ, Kwok Y, Krasna MJ, Suntharalingam M. Predictors of acute esophagitis in patients with non-small-cell lung carcinoma treated with concurrent chemotherapy and hyperfractionated radiotherapy followed by surgery. Int J Radiat Oncol Biol Phys 2004; 60:1106–12.

70. Hirota S, Tsujino K, Endo M, et al. Dosimetric predictors of radiation esophagitis in patients treated for non-small-cell lung cancer with carboplatin/paclitaxel/radiotherapy. Int J Radiat Oncol Biol Phys 2001; 51:291–5.

71. Werner-Wasik M, Scott C, Graham ML, et al. Interfraction interval does not affect survival of patients with non-small cell lung cancer treated with chemotherapy and/or hyperfractionated radiotherapy: a multivariate analysis of 1076 rtog patients. Int J Radiat Oncol Biol Phys 1999; 44:327–31.

72. Purdy J, Perez C, Klein E. Three-dimensional Con-formal Radiation Therapy and Intensity Modulated Radiation Therapy: Practical Potential Benefits and Pitfalls. New York: Lippincott Williamsand Wilkins; 2000.

73. ICRU Report 50. Prescribing, recording, and reporting photon beam. Bethesda, MD; 1993.

74. Huang E, Liao ZX, Cox JD, et al. Comparison of outcomes for patients with unresectable locally advanced non-small-cell lung cancer treated with induction chemotherapy followed by concurrent chemoradiation versus concurrent chemoradiation alone. Oncology 2007; 68(3):779–85.

75. Bradley JD, Ieumwananonthachai N, Purdy JA, et al. Gross tumor volume, critical prognostic factor in patients treated with three-dimensional conformal radiation therapy for non-small-cell lung carcinoma. Int J Radiat Oncol Biol Phys 2002; 52:49–57.

76. Dosoretz D, Galmarini D, Rubenstein J, et al. Local control in medically inoperable lung cancer: an analysis of its importance in outcome and factors determining the probability of tumor eradication. Int J Radiat Oncol Biol Phys 1993; 27:507–16.

77. Hayman JA, Martel MK, Ten Haken RK, et al. Dose escalation in non-small-cell lung cancer using three-dimensional conformal radiation therapy: Update of a phase I trial. J Clin Oncol 2001; 19:127–36.

78. Maguire P, Marks L, Sibley G, et al. 73.6 Gy and beyond: hyperfractionated, accelerated radiotherapy for non-small-cell lung cancer. J Clin Oncol 2001; 19: 705–11.

79. Robertson J, Ten Haken R, Hazuka M, et al. Dose escalation for non-small cell lung cancer using conformal radiation therapy. Int J Radiat Oncol Biol Phys 1997; 37:1079–85.

80. Dosoretz DE, Katin MJ, Blitzer PH, et al. Medically inoperable lung carcinoma: The role of radiation therapy. Semin Radiat Oncol 1996; 6:98–104.

81. Krol A, Aussems P, Noordijk E, Hermans J, Leer J. Local irradiation alone for peripheral stage I lung cancer: could we omit the elective regional nodal irradiation? Int J Radiat Oncol Biol Phys 1996; 34:297–302.

82. Rosenzweig K, Sim S, Mychalczak B, Braban L, Schindelheim R, Leibel S. Elective nodal irradiation in the treatment of non-small-cell lung cancer with three-dimensional conformal radiation therapy. Int J Radiat Oncol Biol Phys 2001; 50:681–5.

83. Senan S, Burgers S, Samson M, et al. Can elective nodal irradiation be omitted in stage III non-small-cell lung cancer? Analysis of recurrences in a phase II study of induction chemotherapy and involved-field radiotherapy. Int J Radiat Oncol Biol Phys 2002; 54:999–1006.

84. Zhang H, Yin W, Zhang L, et al. Curative radiotherapy of early operable non-small cell lung cancer. Radiother Oncol 1989; 14:89–94.

85. Conces DJJ, Klink JF, Tarver RD, Moak DG. T1B0JM0 lung cancer: evaluation with CT. Radiology 1989; 170:643–6.

86. Heavey L, Glazer G, Gross B, Frances I, Orringer M. The role of CT in staging radiographic T1N0M0 lung cancer. Am J Roentgenol 1995; 146:285–90.

87. Ginsberg R, Rubinstein L. Randomized trial of lobectomy versus limited resection for T1 N0 non-small cell lung cancer. Lung Cancer Study Group. Ann Thorac Surg 1995; 60:908–13.

88. Naruke T, Goya T, Tsuchiya R, Suemasu K. Prognosis and survival in resected lung carcinoma based on the new international staging system. J Thorac Cardiovasc Surg 1988; 96:440–7.

89. Ishida T, Yano T, Maeda K. Strategy for lymphadenopathy in lung cancer 3 cm or less in diameter. Ann Thorac Surg 1991; 50:708–71.

90. Chen Z, Perez S, Holmes E, et al. Frequency and distribution of occult micrometastases in lymph nodes of patients with non-small-cell lung carcinoma. J Natl Cancer Inst 1993; 85:493–8.

91. Maruyama R, Sugio K, Mitsudomi T, Saitoh G, Ishida T, Sugimachi K. Relationship between early recurrence and micrometastases in the lymph nodes of patients with stage I non-small-cell lung cancer. J Thorac Cardiovasc Surg 1997; 114:535–43.

92. Yang H, Wu Y, Yang X, Chen G. A meta-analysis of systematic lymph node dissectrion in resectable NSCLC. J Clin Oncol 2004; 22:7190 (abstract).

93. Perez C, Stanley K, Grundy G, et al. Impact of irradiation technique and tumor extent in tumor control and survival of patients with unresectable non-oat cell carcinoma of the lung: report by the Radiation Therapy Oncology Group. Cancer 1982; 50:1091–9.

94. Jeremic B, Classen J, Bamberg M. Radiotherapy alone in technically operable, medically inoperable, early-stage (I/II) non-small-cell lung cancer. Int J Radiat Oncol Biol Phys 2002; 54:119–30.

95. Koto M, Miyamoto T, Yamamoto N, Nishimura H, Yamada S, Tsujii H. Local control and recurrence of stage I non-small cell lung cancer after carbon ion radiotherapy. Radiother Oncol 2004; 71:147–56.

96. Martel M, Strawderman M, Hazuka M, Turrisi A, Fraass B, Lichter A. Volume and dose parameters for survival of non-small cell lung cancer patients. Radiother Oncol 1997; 44:23–9.

97. Martel M, Sahijdak W, Hayman JA, Ball D. Incidental doses to clinically negative nodes from conformal treatment fields for nonsmall cell lung cancer. Proc Am Soc Clinic Oncol 1999; 45:244 (abstr 186).

98. Dwamena BA, Sonnad SS, Angobaldo JO, Wahl RL. Metastases from non-small cell lung cancer: mediastinal staging in the 1990s–meta-analytic comparison of PET and CT. Radiology 1999; 213:530–6.

99. Senan S, De Ruysscher D, Giraud P, Mirimanoff R, Budach V. On behalf of the Radiotherapy Group of the European Organization for Research and Treatment of C. Literature-based recommendations for treatment planning and execution in high-dose radiotherapy for lung cancer. Radiother Oncol 2004; 71:139–46.

100. Fischer BMB, Mortensen J, Hojgaard L. Positron emission tomography in the diagnosis and staging of lung cancer: a systematic, quantitative review. Lancet Oncol 2001; 2:659–66.

101. Gould MK, Kuschner WG, Rydzak CE, et al. Test performance of positron emission tomography and computed tomography for mediastinal staging in

patients with non-small-cell lung cancer: a meta-analysis. Ann Inter Med 2003; 139:879–92.

102. Toloza EM, Harpole L, McCrory DC. Noninvasive staging of non-small cell lung cancer: a review of the current evidence. Chest 2003; 123:137S–46S.

103. van der Wel A, Nijsten S, Hochstenbag M, et al. Increased therapeutic ratio by 18FDG-PET-CT planning in patients with clinical CT stage N2/N3 M0 non-small cell lung cancer (NSCLC): a modelling study. Int J Radiat Oncol Biol Phys 2005; 61:648–54.

104. De Ruysscher D, Wanders S, van Haren E, et al. Selective mediastinal node irradiation on based on FDG-PET scan data in patients with non-small cell lung cancer: a prospective clinical study. Int J Radiat Oncol Biol Phys 2005: 62(4): 988–94.

105. Roberts PF, Follette DM, von Haag D, et al. Factors associated with false-positive staging of lung cancer by positron emission tomography. Ann Thorac Surg 2000; 70:1154–9.

106. Graeter TP, Hellwig D, Hoffmann K, Ukena D, Kirsch C-M, Schafers H-J. Mediastinal lymph node staging in suspected lung cancer: comparison of positron emission tomography with F-18-fluorodeoxyglucose and mediastinoscopy. Ann Thorac Surg 2003; 75:231–6.

107. Paulino AC, Johnstone PAS. FDG-PET in radiotherapy treatment planning: Pandora's box? Int J Radiat Oncol Biol Phys 2004; 59:4–5.

108. Caldwell CB, Mah K, Skinner M, Danjoux CE. Can PET provide the 3D extent of tumor motion for individualized internal target volumes? A phantom study of the limitations of CT and the promise of PET. Int J Radiat Oncol Biol Phys 2003; 55:1381–93.

109. Arriagada R, Bergman B, Dunant A, The International Adjuvant Lung Cancer Trial Collaborative G. Cisplatin-based adjuvant chemotherapy in patients with completely resected non-small-cell lung cancer. N Engl J Med 2004; 350:351–60.

110. Niiranen A, Niitamo-Korhonen S, Kouri M, Assendelft A, Mattson K, Pyrhonen S. Adjuvant chemotherapy after radical surgery for non-small-cell lung cancer: a randomized study. J Clin Oncol 1992; 10:1927–32.

111. Wada H, Hitomi S, Teramatsu T. Adjuvant chemotherapy after complete resection in non-small cell lung cancer. J Clin Oncol 1996; 14:1048–54.

112. Winton T, Livingston R, Johnson D, et al. A prospective randomized trial of adjuvant vinorelbine (VIN) and cisplatin (CIS) in completely resected stage 1B and II non small cell lung cancer (NSCLC). J Clin Oncol 2004; 22:7018 (abstract).

113. Keller SM, Adak S, Wagner H, et al. A randomized trial of postoperative adjuvant therapy in patients with completely resected stage II or IIIa non-small-cell lung cancer. N Engl J Med 2000; 343:1217–22.

114. Le Chevalier T, Arriagada R, Quoix E, et al. Radio-therapy alone versus combined chemotherapy and radiotherapy in nonresectable non-small-cell lung cancer: First analysis of a randomized trial in 353 patients. J Natl Cancer Inst 1991; 83:417–23.

115. Komaki R, Scott C, Ettinger D, et al. Randomized phase II study of chemotherapy/radiation therapy combinations for favorable patients with locally advanced inoperable nonsmall cell lung cancer: Radiation Therapy Oncology Group (RTOG) 92-04. Int J Radiat Oncol Biol Phys 1997; 38:149–55.

116. Graham M, Matthews J, Harms WS, Emami B, Glazer H, Purdy J. Three-dimensional radiation treatment planning study for patients with carcinoma of the lung. Int J Radiat Oncol Biol Phys 1994; 29:1105–17.

Future Development: Deformable Image Registration to Track Tumor Motion and 4-D Radiotherapy Planning and Verification

Lei Dong
Department of Radiation Physics, University of Texas M.D. Anderson Cancer Center, Houston, Texas, U.S.A.

BACKGROUND

Three-dimensional conformal radiotherapy (3D-CRT) is one of the targeted therapy techniques which geometrically conforms the three-dimensional radiation dose distributions to the target volume while minimizing the radiation dose to nearby normal organs (1,2). With recent interests in using the advanced form of 3D-CRT, the intensity-modulated radiation therapy (IMRT) (3), for lung cancer radiotherapy (4–7), it is concerned that respiratory induced organ motion may have an impact on the final dose distribution. It is well established that variations in organ shape and position can occur due to inter- and intrafractional motion. Typical interfractional anatomy variations include tumor shrinkage, weight loss, bowel/bladder filling, etc. Typical sources of intrafractional motion include respiration, cardiac motion, peristalsis, etc. Better dose conformality and steeper dose gradients make IMRT plans potentially more sensitive to setup errors and motion of the internal organs (8–12). In a simulation study by Flampouri et al. (13), it was demonstrated that the difference in the equivalent uniform dose of clinical target volume (CTV) between the planed and the delivered doses could be as high as 33 Gy if a plan is designed inappropriately for a patient with large motion effect. Therefore, it is important to understand the impact of organ motion on final dose distribution. The current treatment planning and delivery techniques, which do not correct for such daily and the moment-to-moment volumetric variations adequately, may lead to suboptimal treatments.

To study organ motion in the thorax, certain measures of anatomy in the fourth dimension, time, are required. Fortunately, with the invention of four-dimensional computed tomography (4D–CT) imaging, it becomes possible to quantify respiratory-correlated organ motion voxel-by-voxel in a breathing cycle.

4D-CT is a series of 3D-CT images of the patient at a number of breathing phases. In most situations, 4D-CT images were acquired using a reference external

signal from the up/down motion of a patient's abdomen (or where the motion was considered most relevant). A box with infrared reflectors was placed on the patient's skin surface and the motion of the box was captured by an infrared camera (Real-time Position Management system, RPM™, Varian Oncology Systems, Palo Alto, California) (14–16). Then the 2D projections of x-ray images can be sorted and reconstructed into 3D-CT images at various phases of the breathing cycle. Typically, 10 equispaced phases are used to describe the temporal motion of the thoracic anatomy. 4D-CT scans can be used for 4D treatment planning to explicitly account for respiratory motion. The 4D-CT imaging technology was described by Keall et al. (16,17) for the helical scanning mode and by Pan et al. (18) for the cine scanning mode. The application of 4D-CT for tracking internal organ motion and 4D treatment planning was described by Rietzel et al. (19–21). Although 4D-CT explicitly describe organ motion and deformation in different breathing phases, it is cumbersome and difficult to delineate target or normal organs and cumulate doses in different phases because each phase was treated as an independent time event. With the recent advance in deformable image registration, it is becoming possible to track organ motion and cumulating doses automatically. In the following sections, we will discuss the concept of deformable image registration and its application to thoracic cancer radiotherapy.

DEFORMABLE IMAGE REGISTRATION

Introduction

Image registration is a process to determine the spatial correspondence between two images collected at different times. In this application for treatment planning of thoracic cancers, the images of interest are 4D-CT images collected at different phases. Historically, image-registration has been classified as being "rigid" (where images are assumed to be of

objects that simply need to be rotated and translated with respect to one another to achieve correspondence) or "non-rigid" (where correspondence between structures in two images cannot be achieved without some localized stretching of the images). The "non-rigid" image registration is also referred here as deformable" image registration.

Deformable image registration algorithms can be categorized into two classes: model-based and grayscale image-based algorithms. Model-based algorithms use contours, fiducial points, or landmark points common in both images as constraints to the model. The one-to-one correspondence for other points in the image space will be determined by the model. In contrast, grayscale image-based algorithms use pixel or voxel intensity directly, assuming that image intensities alone contain enough information for image registration. Usually, the model-based algorithms are faster than image intensity-based algorithms when performing image registration because they usually operate on a sparse set of features. However, the time spent on feature-extraction (contours or anatomic landmarks on both images) can be significant and error prone. Most recent algorithms used automatic feature extraction, which can certainly improve the speed; however, the accuracy of the models based on limited control points is still not well studied. Examples of model-based image registration algorithms used in radiotherapy were described by Christensen et al. (22), Schaly et al. (23,24), Kaus et al.(25), Liang et al. (26), Yan et al. (27), Schreibmann et al. (28,29), Brock et al. (30,31), and Xiong et al. (32).

CT images are used in calculating radiation doses because Hounsfeld units (CT pixel values) are calibrated to the attenuation coefficient of water and therefore the pixel values are well defined. Because of the consistency in CT image intensities, it is advantageous to use a grayscale image-based algorithm for radiotherapy applications. Grayscale image-based algorithm has one big advantage, which is the automatic processing of the image data. Typical image-based algorithms used for radiotherapy applications are described by Lu et al. (33–35), Foskey et al. (36), Guerrero et al. (37), Gao et al. (38), and Wang et al. (39,40)

An Accelerated-Demons Algorithm for Image-Based Deformable Image Registration

To give an example of image-based deformable image registration, we describe a method we implemented (40), which was primarily based on Thirion's diffusing model, also known as the "demons" algorithm (41,42). Conceptually, the diffusing model assumes that local "demons" at every voxel location are applying invisible "forces" that push the voxels of the moving image into matching up with the reference

(static) image. This is illustrated in Figure 1. The rule to determine the force to move each voxel is based on the Equation 1 (40):

$$\vec{\mu} = (m - s) \times \left(\frac{\vec{\nabla}_s}{\left|\vec{\nabla}_s\right|^2 + (S - m)^2} + \frac{\vec{\nabla}_m}{\left|\vec{\nabla}_m\right|^2 + (S - m)^2} \right) \quad (1)$$

where s is the voxel intensity in the static image S and m is the intensity of the moving image M. The estimated displacement is $\vec{u} = (u_x, u_y, u_z)$, which is required for point P to match the corresponding point in M. $\vec{\nabla}_S$ is the gradient of the static image and $\vec{\nabla}_m$ is the gradient of the moving image. $\vec{\nabla}_S$ and $\vec{\nabla}_m$ represent the gradient information in the neighboring points (analog to the edge enhancement). The (m-s) term is the differential force of the interaction between the static and the moving images; hence, it is an "external" force. Equation 1 will be solved iteratively and the final result is the (deformation) displacement mapping vector $\vec{u} = (u_x, u_y, u_z)$, which describes the spatial relationship between the moving image and the reference static image. This displacement map can be used to translate the geometry information from one image into another. In addition, information related to geometry, such as the spatial distribution of doses and contours delineated by physicians, can be mapped as well. Therefore, deformable image registration is a powerful tool for calculating cumulative dose distributions to a deformed organ or for auto-delineation of target structures in subsequent imaging sessions. We will discuss these topics in more detail in the sections below.
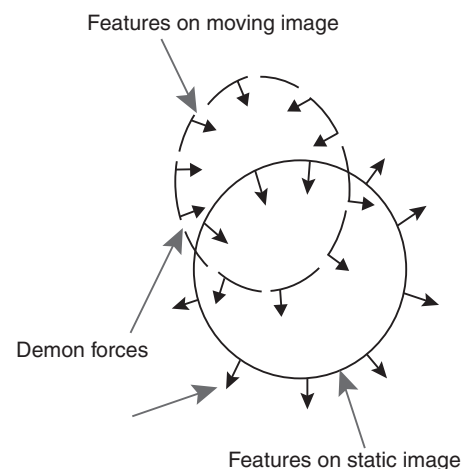
Figure 1 An image intensity-based diffusing model for deformable image registration by the demons algorithm. The voxels in the moving image is deformed based on "demons" forces of Equation 1. The modified, accelerated demons algorithm used both passive force contributed by static image and active force contributed by moving image.

A Multi-Resolution Approach

One of the assumptions made in deriving the force calculation in Equation 1 was that the deformation should be reasonably small. This is not always the case in clinical situations. One way to minimize the effect of large deformations is to use a coarse-to-fine multi-resolution approach (43). This approach uses low-resolution images derived from the original image (usually a high-resolution volumetric CT image) to begin the iterative demons diffusion process. After the solution converges, the displacement field is passed to the next higher resolution as the starting solution. The number of scales used can be easily extended to 4–6 scales when a larger deformation is observed or a higher resolution is used in the original image. This pyramidal multiresolution approach not only allows for large deformations between two images, but also significantly improved convergence and the speed of the calculation. The algorithm developed using the multi-resolution, accelerated demons algorithm can achieve the automatic deformable image registration for a lung cancer case between the inhale and exhale CT images to within 40 sec on a single CPU Intel processor.

DEFORMABLE IMAGE REGISTRATION FOR TRACKING ANATOMIC CHANGES

Tracking Intrafractional Anatomy Variations

One of the key applications of deformable image registration is to automatically track anatomy changes during a breathing cycle (intrafraction). The application is made possible by using 4D-CT, which defines the anatomy in space from the moment-to-moment breathing motion. In order to apply deformable image registration for this application, a reference phase CT should be identified. In addition, anatomies of interest, such as gross tumor volume (GTV), CTV, or normal organs (lung, esophagus, heart, etc.) to be tracked, should be delineated on this reference CT. Then the deformable image registration method, such as the one described by Equation 1 (44) or other methods (21,29,34,45,46), can be used to register each phase of the 4D-CT with the reference phase CT. The result of the deformable image registration is a matrix of mapping vectors (sometimes also called the deformable maps), which describes the displacement of the same voxel relative to its location in the reference phase CT $\vec{u} = (u_x, u_y, u_z)$.

The second step in tracking the anatomy requires the use of these displacement vectors for mapping the new positions of the anatomy of interest in each phase of the 4D-CTs. In order to do this, the region of interest (ROI) containing the anatomy of interest in the reference CT should be segmented as a binary mask: a value of 0 outside of the ROI and a value of 1 inside the ROI. The resolution of the mask should be equal to the same CT resolution, which the deformable mapping vectors were obtained. After creating each binary mask, the displacement vectors can be used to transform the binary mask from the reference CT to other CT images. This allows the binary mask (representing the ROI) to be deformed to match with the CT images of other respiratory phases. These deformed binary masks provide the surfaces of the new objects (ROIs) in the CT images to be registered. Then the last step of the auto-segmentation is to extract contours from these deformed masks in the new CT images. Image processing techniques can be used to obtain the outer boundary of a binary mask. Alternatively, the vertices of the surfaces can be reconstructed using a triangulated surface reconstruction method and then sliced through each CT slice (34). In order to view the contours overlaid with each axial CT slice, the contours must be extracted for each CT slice location.

An example of using the deformable image registration method to track anatomy from inspiration CT to the expiration CT is illustrated in Figure 2. In this case, the inspiration CT was used as the reference CT. Target volume is shown in red and a portion of the diaphragm is shown in brown color. For simplicity of illustration, other contoured organs were not displayed. The region of the deformable image registration is shown in the red box. The deformable mapping vectors were illustrated using the red arrows inside the registration region. The mapping vector illustrates the displacement of the same voxel position from the inspiration CT to the expiration CT. Using these mapping vectors, the target volume (red) and normal organs (such as the contoured diaphragm in brown) can be mapped automatically from the inspiration CT to the expiration CT. Similarly, the anatomy in the reference CT can be automatically transferred to other 4D-CT images of different breathing phases, which significantly reduce the target delineation time. After obtaining the auto-delineated target volume in 10 phases of 4D-CT, the internal target volume (ITV) can be composed and used for planning, accounting to organ motion and target deformation explicitly.

Tracking Interfractional Anatomy Variations

With the availability of in-room imaging techniques used in radiation therapy, it becomes obvious that patient's anatomy and tumor volume change during the course of radiation therapy. Recently, there were studies indicating that GTVs of lung cancers can shrink 60–80% during the course of radiotherapy (47,48). It may be important to take these interfractional anatomic variations into considerations for

| Inspiration | Mapping vectors | Expiration |
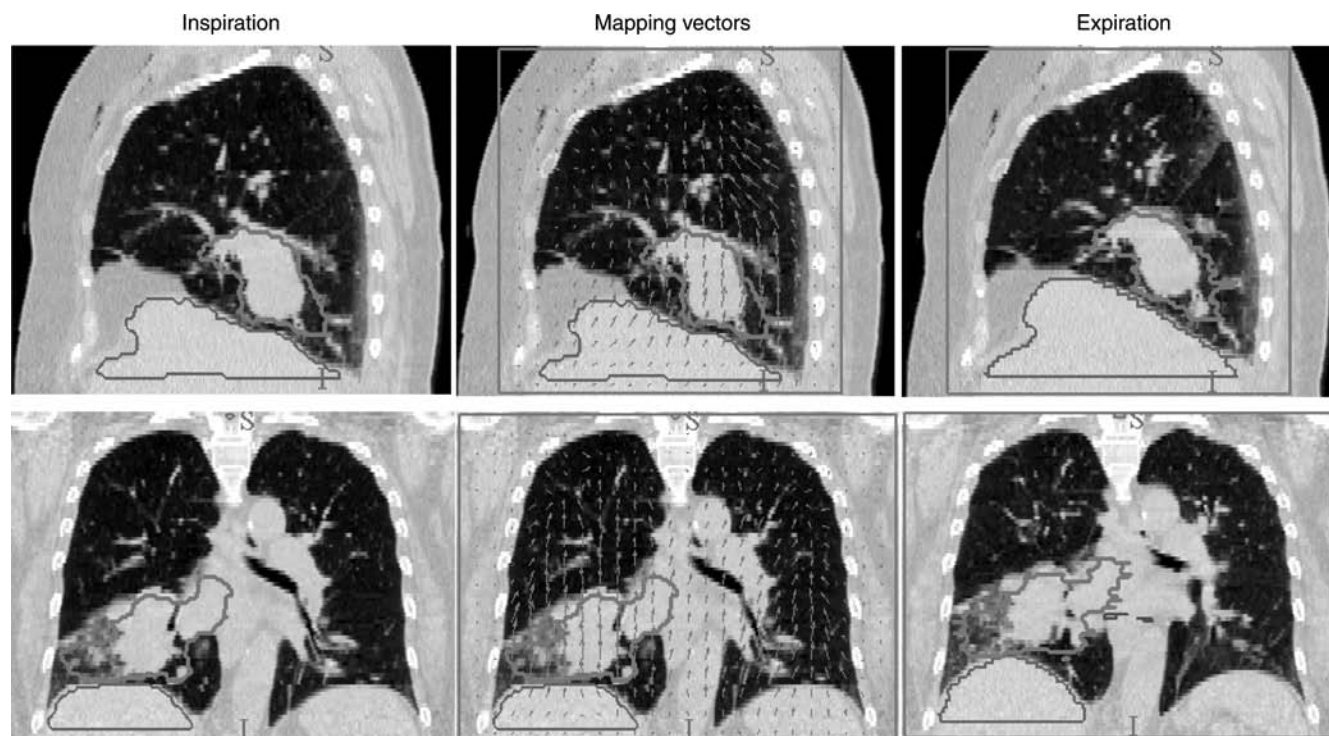
Figure 2   (*See color insert.*) An example of tracking anatomy using a deformable image registration method. The inspiration CT was used as the reference CT in this case. Target volume is shown in red and a portion of the diaphragm is shown in brown color. The region of deformable image registration is shown in red box, in which the deformable mapping vectors were shown in red arrows. The mapping vector is a displacement of the same voxel from the inspiration CT to the expiration CT. Using the mapping vectors, the target volume (red) and normal organs (such as the contoured diaphragm in brown) can be mapped automatically from the inspiration CT to the expiration CT. *Abbreviation*: CT, computed tomography.

adaptive radiotherapy strategies. In this case, the auto-segmentation of anatomy on repeat CT or 4D-CT becomes an important application.

With deformable image registration method, tracking interfractional anatomy variations is similar to tracking intrafractional anatomy variations. Again, a reference CT is required to deform the anatomy from the reference CT to the subsequent (repeat) CT or 4D-CT images acquired during the course of treatment. Figure 3 illustrates an example of a weekly repeat 4D CT study for a patient with NSCLC. The GTVs for the weeks 4 and 6 are shown in one CT slice in the end of expiration phase of the weekly repeat 4D-CT. The green contour around the tumor was created automatically using the image-based deformable image registration method, and the red contour was manually drawn by a physician. As it can be seen, there is an excellent agreement between the computer-drawn contours and the physician's manual delineation.

Figure 4 is the same case as shown in Figure 3, but it plotted the volume of the GTV week-by-week using repeat 4D-CT measurements. The horizontal axis indicates the elapsed treatment days from the start of radiation therapy. At the treatment simulation CT (prior to treatment), the tumor volume (GTV) was approximately 30 cc, but near the end of the treatment (6th week), the tumor volume was approximately 18 cc, a reduction to 60% of the original volume. In Figure 4, we also compared human contours (red; open circle) with the computer-generated contours using the deformable image registration method (blue; solid circle), which indicates reasonable agreement (considering the small size of the tumor). The Pearson correlation between the target volumes determined by the physician and the deformable image registration method is 0.988 ($P = 0.0002$).

In summary, tracking anatomy in 4D-CT or repeat CT using the deformable image registration method is a very effective and efficient method. Currently, deformable image registration methods are unable to delineate the reference phase anatomy alone, especially for the tumor or treatment volumes, which still require human intervention to determine the target volume.

Week 4   Week 6

Figure 3 (*See color insert*.) Tumor volume can also shrink during the course of radiotherapy. The CT images show the tumor volume in week 4 (*left*) and Week 6 (*right*) of the radiotherapy. The red contours were drawn by a radiation oncologist and the green contours were automatically created by a deformable image registration method.

DEFORMABLE IMAGE REGISTRATION FOR DOSE TRACKING

Cumulating Doses in a Breathing Cycle

With the availability of 4D-CT, dose calculations can be performed on each individual 3D-CT, which describes the dosimetric effect of organ motion explicitly in each individual phase. Although this is a possible approach; however, it may require significant effort in delineating target volumes and normal organ structures for each CT. The real problem is that the final dose distribution to the same volume element (containing the same cells) cannot be easily summed
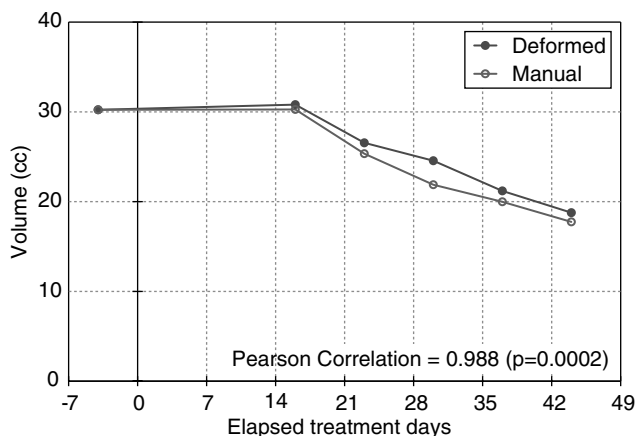
Figure 4 Tracking tumor volumes during treatment course. The volumetric variation of the tumor for the case shown in Figure 3 is plotted against the elapsed treatment days. The red line was the tumor volume delineated by a physician; and the blue line was the same volume tracked by the deformable image registration method. The Pearson correlation between time-trend tumor volume determined by the physician and the image registration method is 0.988 ($P = 0.0002$).

because organ motion is not uniform across all phases. Organ deformation has to be considered when creating a cumulative dose distribution over a breathing cycle. A more efficient (perhaps also a more accurate) method is to use the deformable image registration method to track the cumulative doses.

To evaluate the 4D dose distribution delivered to one breathing cycle, the dose distributions were calculated first for each of the 10 phases of the 4D-CT. Then, the dose distributions of all 10 phases were time-weight-summed onto the single reference phase CT using a deformable image registration method. For typical 4D-CT data sets, 10 reconstructed phases had an equal weight in time (duration of the phase), which means that a simple average of dose for each tracked voxel across the 10 phases would be adequate. Otherwise, the data sets will have a weighting factor for the duration of the phase. Assuming the 4D-CT data sets were constructed in 10 phases: T0, T10, T20,..., T90, we usually observed that T30–T70 phases were similar to the end of expiration phase (T50) which indicated that patients usually spent more time in the end of expiration. When evaluating 4D cumulative dose distribution, we can pick any phase as a reference phase for evaluating target coverage. T50, being the most stable phase, was chosen to calculate the cumulative dose distribution and analyze target coverage.

The voxel-by-voxel displacement vector linking the geometric coordinates between each single phase of 4D-CT and the reference phase of 4D-CT was obtained by the image intensity-based, automatic deformable image registration method. We refer to this time-averaged dose accumulation method as the full 4D dose calculation and the resultant dose distribution as the 4D dose distribution, which

contains the cumulative dosimetric effect of internal organ motion.

To give an example of this method, we calculated a proton treatment plan, which is more sensitive to the anatomy variations for each 4D-CT images. Figure 5 shows a proton plan calculated on each of the 10 4D-CT phases. For simplicity, the prescription isodose line (yellow) was shown as well as the tumor volumes (also propagated/tracked using the deformable image registration method) on each CT. As it can be seen, the isodose line (yellow) changes differently for each 4D-CT image due to organ motion/deformation in the beam path of the proton plan. The final cumulative (4D) dose distribution was shown in the bottom row of Figure 5, which was calculated on the T50 (end of expiration phase) CT. The prescription isodose line between the directly calculated T50 image and the cumulative T50 image (taking into account for organ motion through the entire breathing cycle) may appear to be similar, a closer look at the inferior portion of the target, as indicated by the black arrow near the top of the diaphragm, revealed that the cumulative dose distribution was tighter than the directly calculated dose distribution. This was primarily due to the dominate motion effect in the superior-inferior direction.

The dosimetric consequence of intrafractional breathing motion when using IMRT for lung cancer treatment can be demonstrated in Figure 6. In Figure 6, we show a case study that used a free-breathing CT image to design a treatment plan with an inadequate 8-mm margin to cover the CTV (shown in yellow). The dose distribution for each breathing phase was calculated using the 4D-CT data set. Due to the extensive excursion of tumor in this case (movement in excess 2.5 cm), the actual dose distribution did not cover the entire target volume in some of the breathing phases due to respiratory motion which was not detected by the single free-breathing CT. To illustrate the dosimetric impact of organ motion, we performed deformable image registration to calculate the cumulative dose distribution from the 10 individual phases. The cumulative dose was mapped to a free-breathing fast CT scan, which is very close to the end of exhale phase of the 4D-CT data set (T50). The resultant composite (cumulative) dose distribution summed from the entire breathing cycle is illustrated in the bottom row of Figure 6. This row shows the dose deficiency in the composite plan for the CTV target (as shown by the red arrows) if respiratory motion was not adequately compensated in the treatment planning process. For this case, we also
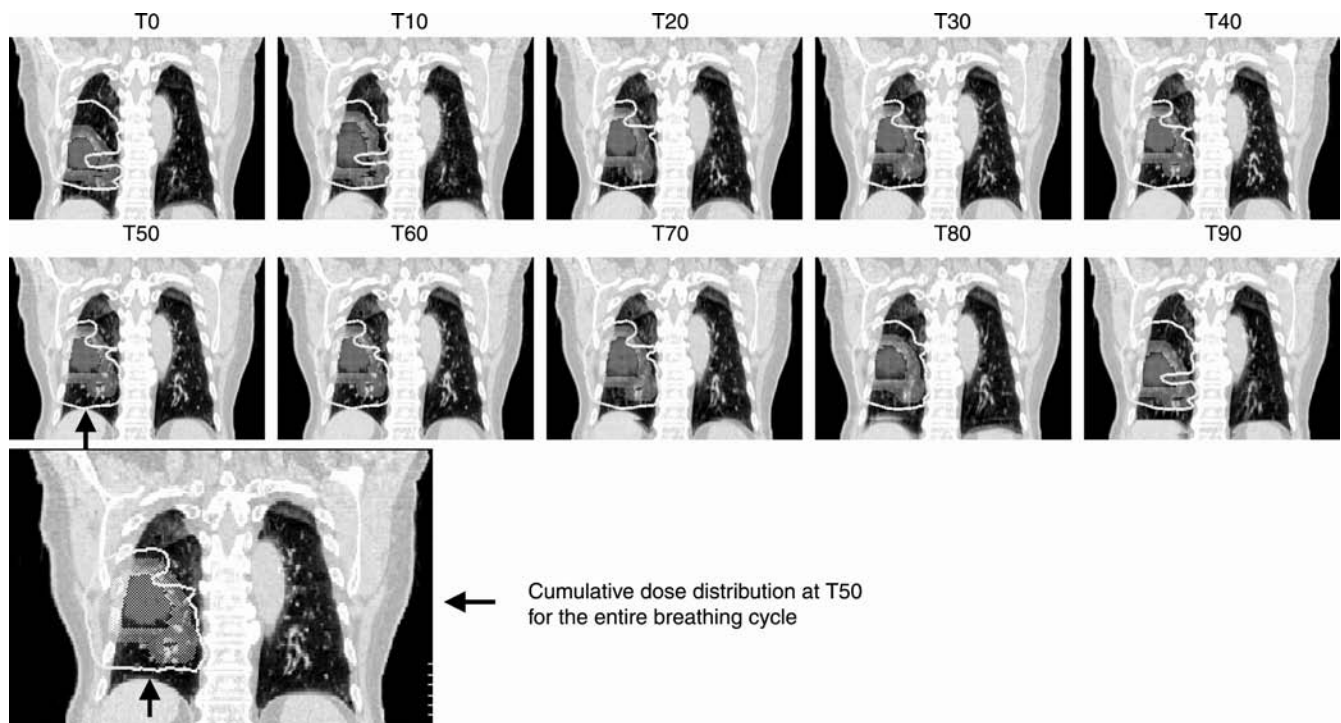
Figure 5 (*See color insert.*) Dose calculations to each phase of 4D–CT images. T0 phase represents the end of inspiration and T50 phase represents the end of expiration, which was used as a reference phase for calculating the cumulative dose distribution of all 10 phases using the deformable image mapping method. The prescribed dose isodose lines is shown in yellow. The maroon (inner) colorwash represents the GTV, the khaki (Middle) colorwash represents the CTV, and the aquamarine (large) colorwash represents the PTV. The final cumulative dose distribution is shown in the bottom row. *Abbreviations*: T0 and T50, 0% and 50% phases of the breathing cycle, respectively; GTV, gross tumor volume; CTV, clinical tumor volume; PTV, planning tumor volume.
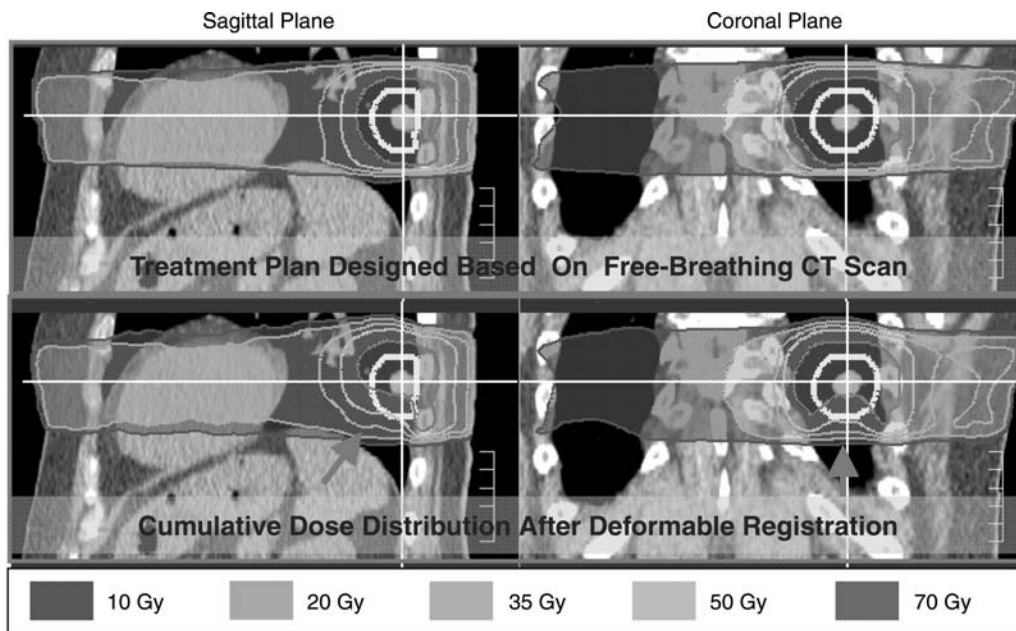
Figure 6 (*See color insert.*) Comparison of a treatment plan as perceived on a free-breathing CT (top row) and as realized after accounting for breathing motion in all 10 phases (bottom row). The latter was obtained by summing dose distributions computed on individual phases of the 4D CT image, and mapped to a reference CT image (T50) using the deformable image registration method.

calculated the cumulative dose distribution when using the ITV, determined from the full-range of motion for the target in all 10 phases of the 4D-CT, for treatment planning. The use of ITV-based "4D planning" did not underdose the target (but treated a large volume). This example illustrates the importance of quantifying patient-specific organ motion so that adequate treatment margins can be used for treatment planning.

Mapping Doses During Treatment Course

As we described previously, tumor volumes and normal anatomy in lung cancer treatment can vary significantly during the course of treatment due to radiation therapy and aggressive chemotherapy. It becomes necessary to evaluate the original dose plan which is designed based on a single CT or a set of 4D-CT images prior the start of treatment. Repeat CT or 4D-CT imaging allows for designing adaptive radiotherapy strategies by replanning or taking into account the cumulative dose distributions delivered to the patient.

Mapping repeat 4D dose is similar to the method of calculating the cumulative dose distribution during a respiratory cycle using the deformable image registration method, with one additional step to map the cumulative dose to another data set. The process involves three steps: (1) calculate the cumulative dose distributions to a reference phase CT for the 4D-CT images acquired at different times (this is the same step as described in the "Mapping Doses During Treatment Course" section); (2) perform deformable

image registration between the two reference phase CT images acquired at different times; (3) mapping the cumulative dose distribution from the later reference phase CT to the original planning CT.

To give an example, Figure 7 illustrates one patient case which we have acquired repeat 4D-CT images during the treatment course. The original 4D proton dose plan is shown in Figure 7(A). The same treatment plan was calculated onto the week 4 repeat 4D-CT images using a bony alignment technique to position the isocenter of the original proton treatment plan. Bony registration was used to simulate a daily image-guided treatment using orthogonal x-ray imaging to align the bony structures for each treatment. Then the same treatment plan was recalculated for each phase of the 4D-CT acquired on Week 4. Cumulative 4D dose was calculated and displayed in Figure 7(B) using the method described in the previous section. It can be seen that significant tumor shrinkage occurred in this case, although the cumulative dose distribution did not appear to change too much from the original treatment plan. However, after mapping the week 4 cumulative dose distributions to the original treatment planning CT, as shown in Figure 7(C), the actual dose distribution for Week 4 was shown quite differently from the original plan. The dose distribution was bulging out in the inferior portion of the treatment volume. This was due to the fact that tumor shrinkage dragged a significant lung tissue into the high dose region, as seen in Figure 7(B). After mapping dose back to the original plan, we can
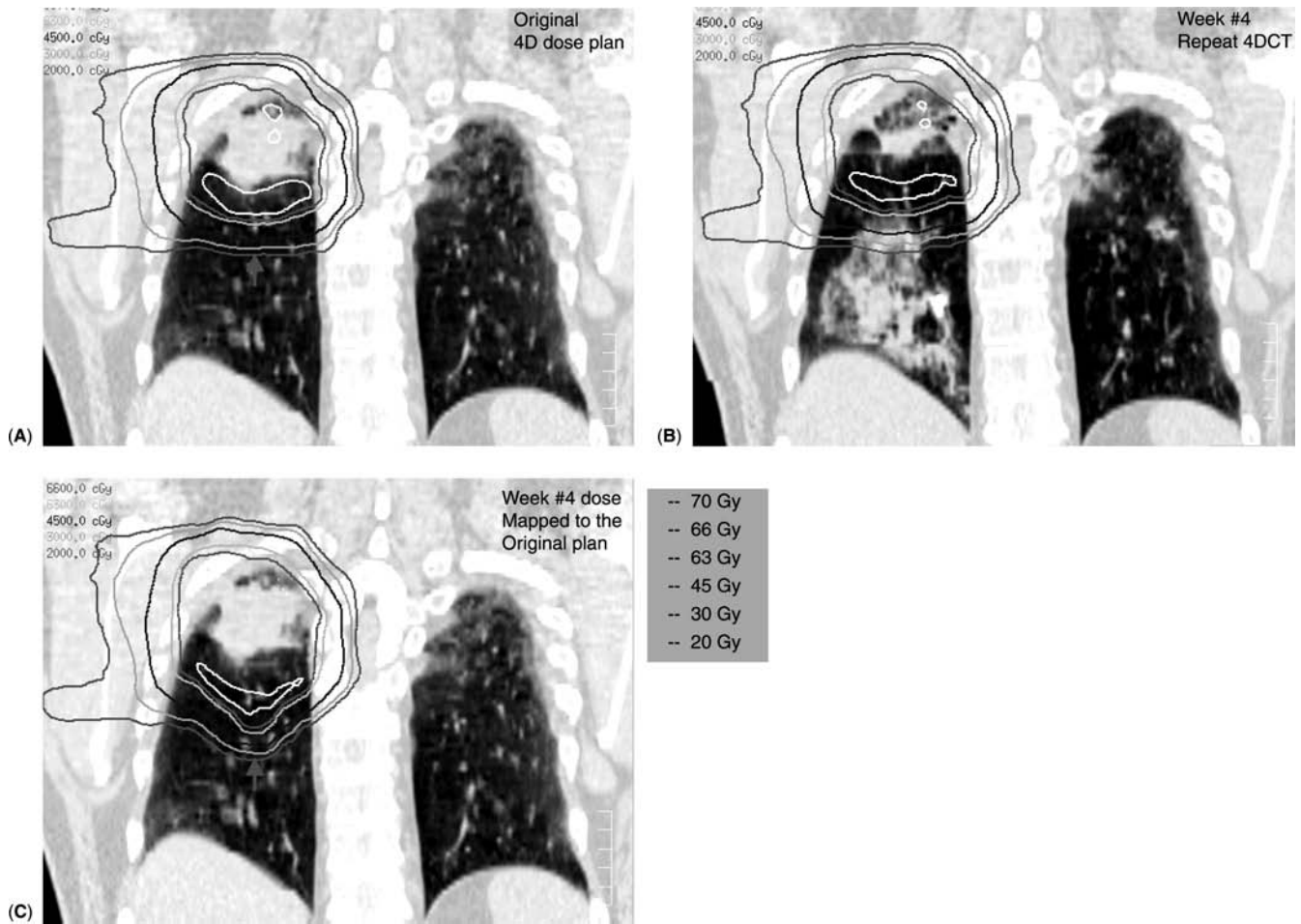
Figure 7 (*See color insert.*) Comparing the 4D dose distributions at treatment simulation (**A**) and at the week 4 of the radiotherapy. The original 4D (cumulative) dose distribution was calculated for the end of expiration phase (T50) in (**A**). The same treatment plan was calculated for the anatomy defined by the week 4 repeat 4D-CT (**B**). The cumulative 4D dose is shown in (**B**) for week 4. A dose mapping was done using the deformable image registration method, which maps the 4D cumulative dose distribution in (**B**) back to the original 4D plan (**C**). It can be seen that the dose distributions are different between (**A**) and (**C**) primarily due to tumor shrinkage, which dragged normal lung tissue into the high dose region. All plans shown are 4D cumulative dose distributions, which already included the breathing motion during a respiratory cycle.

see that the original plan was not reproduced truthfully due to anatomy changes during the course of the treatment.

The example in Figure 7 illustrates the importance to evaluate treatment plans during the course of therapy if significant anatomy changes are observed. To further illustrate the dosimetric impact of anatomy variations, we calculated the dose–volume histograms for the dose distributions in Figure 7(A) and (C). Figure 8 illustrated the CTV coverage and doses to the ipsilateral lung, spinal cord, and body dose. The solid line represents the original plan and the dashed line represents the week 4 dose distribution to the same structures in the original treatment plan. It can be seen that the target coverage becomes worse, although most of tumor volume was still treated to high dose of 66 Gy (prescription dose line). In contrast, normal tissue doses were all increased. In particular, the ipsilateral lung dose at 20 Gy was increased from 30% to 35%, which might be significant. The patient may benefit by replanning using the week 4 repeat 4D-CT images so that the new treatment plan will better match with the anatomy for the rest of the treatment.
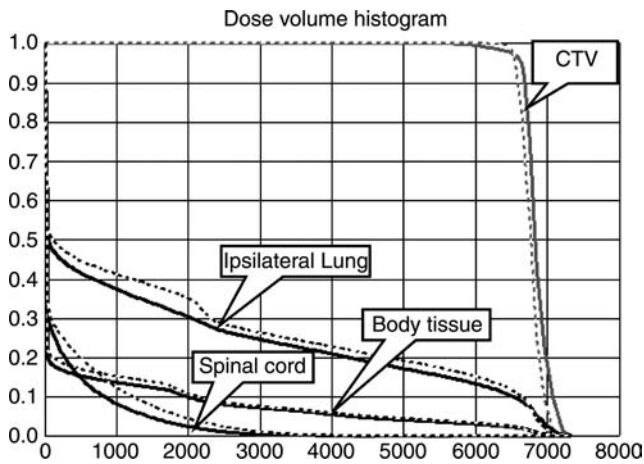
Figure 8 A dose–volume histogram comparison between the 4D dose distribution of the original treatment plan (Fig. 7A) and the actual dose plan delivered to the week 4 repeat 4D CT images after mapping doses back to the original CT (Fig. 7C). The CTV coverage was slightly worse and all normal structures received higher doses. *Abbreviations*: 4D, four-dimensional; CT, computed tomography; CTV, clinical target volume.

SUMMARY

We expect that deformable image registration techniques will rapidly become more mature and practical. Deformable registration and automated delineation of targets and normal structures, which only a few short years ago was just a fantasy, appear to be well within reach. Deformable image registration is the key technology for image-guided adaptive radiotherapy. Deformable image registration would also make auto-segmentation easier, which should lead to a great improvement in efficiency and consistency of delineation of anatomic structures for adaptive re-planning. We expect that image-guided adaptive radiotherapy will provide further benefits for lung cancer radiotherapy due to the significant anatomy variations and tumor volume changes during the course of chemoradiation treatment.

REFERENCES

1. Purdy JA. Advances in three-dimensional treatment planning and conformal dose delivery. Semin Oncol 1997; 24(6):655–71.

2. Purdy JA. 3D treatment planning and intensity-modulated radiation therapy. Oncology (Huntington) 1999; 13(10 Suppl 5):155–68.

3. Intensity Modulated Radiation Therapy Collaborative Working G. Intensity-modulated radiotherapy: current status and issues of interest. Int J Radiat Oncol Biol Phys 2001; 51(4):880–914.

4. Schild SE, Korte SM, Wong WW, Vora SA, Younggren JA, Ezzell GA. Treatment planning for dose escalation in non-small cell lung cancer (NSCLC). Med Dosim 2004; 29(3):196–203.

5. Tai P, Yu E, Battista J, Van Dyk J. Radiation treatment of lung cancer–patterns of practice in Canada. Radiother Oncol 2004; 71(2):167–74.

6. Chang JY, Liu HH, Komaki R. Intensity modulated radiation therapy and proton radiotherapy for non-small cell lung cancer. Curr Oncol Rep 2005; 7(4): 255–9.

7. Chang JY, Zhang X, Wang X, et al. Significant reduction of normal tissue dose by proton radiotherapy compared with three-dimensional conformal or intensity-modulated radiation therapy in Stage I or Stage III non-small-cell lung cancer. Int J Radiat Oncol Biol Phys 2006; 65(4):1087–96.

8. Keall PJ, Joshi S, Vedam SS, Siebers JV, Kini VR, Mohan R. Four-dimensional radiotherapy planning for DMLC-based respiratory motion tracking. Med Phys 2005; 32(4):942–51, 2005.

9. Keall PJ, Kini VR, Vedam SS, Mohan R. Potential radiotherapy improvements with respiratory gating. Australas Phys Eng Sci Med 2002; 25(1):1–6.

10. Giraud P, Yorke E, Jiang S, Simon L, Rosenzweig K, Mageras G. Reduction of organ motion effects in IMRT and conformal 3D radiation delivery by using gating and tracking techniques. Cancer Radiother 2006; 10(5):269–82.

11. Mechalakos J, Yorke E, Mageras GS, et al. Dosimetric effect of respiratory motion in external beam radiotherapy of the lung. Radiother Oncol 2004; 71(2):191–200.

12. Yorke E, Rosenzweig KE, Wagman R, Mageras GS. Interfractional anatomic variation in patients treated with respiration-gated radiotherapy. J Appl Clin Med Phys 2005; 6(2):19–32.

13. Flampouri S, Jiang SB, Sharp GC, Wolfgang J, Patel AA, Choi NC. Estimation of the delivered patient dose in lung IMRT treatment based on deformable registration of 4D-CT data and Monte Carlo simulations. Phys Med Biol 2006; 51(11):2763–79.

14. Pan T, Lee TY, Rietzel E, Chen GTY. 4D-CT imaging of a volume influenced by respiratory motion on multi-slice CT. Med Phys 2004; 31(2):333–40.

15. Rietzel E, Pan TS, Chen GTY. Four-dimensional computed tomography: Image formation and clinical protocol. Med Phys 2005; 32(4):874–89.

16. Keall P. 4-dimensional computed tomography imaging and treatment planning. Semin Radiat Oncol 2004; 14(1):81–90.

17. Keall PJ, Starkschall G, Shukla H, et al. Acquiring 4D thoracic CT scans using a multislice helical method. Phys Med Biol 2004; 49(10):2053–67.

18. Pan T, Lee TY, Rietzel E, Chen GT. 4D-CT imaging of a volume influenced by respiratory motion on multi-slice CT. Med Phys 2004; 31(2):333–40.

19. Rietzel E, Rosenthal SJ, Gierga DP, Willet CG, Chen GT. Moving targets: detection and tracking of internal organ motion for treatment planning and patient set-up. Radiother Oncol 2004; 73(Suppl. 2):S68–72.

20. Rietzel E, Pan T, Chen GT. Four-dimensional computed tomography: image formation and clinical protocol. Med Phys 2005; 32(4):874–89.

21. Rietzel E, Chen GT, Choi NC, Willet CG. Four-dimensional image-based treatment planning: Target volume segmentation and dose calculation in the presence of respiratory motion. Int J Radiat Oncol Biol Phys 2005; 61(5): 1535–50.

22. Christensen GE, Carlson B, Chao KS, et al. Image-based dose planning of intracavitary brachytherapy: registration of serial-imaging studies using deformable anatomic templates. Int J Radiat Oncol Biol Phys 2001; 51(1):227–43.

23. Schaly B, Kempe JA, Bauman GS, Battista JJ, Van Dyk J. Tracking the dose distribution in radiation therapy by accounting for variable anatomy. Phys Med Biol 2004; 49(5):791–805.

24. Schaly B, Bauman GS, Battista JJ, Van Dyk J. Validation of contour-driven thin-plate splines for tracking fraction-to-fraction changes in anatomy and radiation therapy dose mapping. Phys Med Biol 2005; 50(3):459–75.

25. Kaus MR, Pekar V, Lorenz C, Truyen R, Lobregt S, Weese J. Automated 3-D PDM construction from segmented images using deformable models. IEEE Trans Med Imaging 2003; 22(8):1005–13.

26. Liang J, Yan D. Reducing uncertainties in volumetric image based deformable organ registration. Med Phys 2003; 30(8):2116–22.

27. Yan D, Jaffray DA, Wong JW. A model to accumulate fractionated dose in a deforming organ. Int J Radiat Oncol Biol Phys 1999; 44(3):665–75, 1999.

28. Schreibmann E, Xing L. Image registration with auto-mapped control volumes. Med Phys 2006; 33(4):1165–79.

29. Schreibmann E, Chen GT, Xing L. Image interpolation in 4D CT using a BSpline deformable registration model. Int J Radiat Oncol Biol Phys 2006; 64(5): 1537–50.

30. Brock KK, Dawson LA, Sharpe MB, Moseley DJ, Jaffray DA. Feasibility of a novel deformable image registration technique to facilitate classification, targeting, and monitoring of tumor and normal tissue. Int J Radiat Oncol Biol Phys 2006; 64(4): 1245–54.

31. Brock KK, Sharpe MB, Dawson LA, Kim SM, Jaffray DA. Accuracy of finite element model-based multi-organ deformable image registration. Med Phys 2005; 32(6):1647–59.

32. Xiong L, Viswanathan A, Stewart AJ, et al. Deformable structure registration of bladder through surface mapping. Med Phys 2006; 33(6):1848–56.

33. Lu W, Chen ML, Olivera GH, Ruchala KJ, Mackie TR. Fast free-form deformable registration via calculus of variations. Phys Med Biol 2004; 49(14):3067–87.

34. Lu W, Olivera GH, Chen Q, Chen ML, Ruchala KJ. Automatic re-contouring in 4D radiotherapy. Phys Med Biol 2006; 51(5):1077–99.

35. Lu W, Olivera GH, Chen Q, et al. Deformable registration of the planning image (kVCT) and the daily images (MVCT) for adaptive radiation therapy. Phys Med Biol 2006; 51(17):4357–74.

36. Foskey M, Davis B, Goyal L, et al. Large deformation three-dimensional image registration in image-guided radiation therapy. Phys Med Biol 2005; 50(24): 5869–92.

37. Guerrero T, Zhang G, Segars W, et al. Elastic image mapping for 4-D dose estimation in thoracic radiotherapy. Radiat Protect Dosim 2005; 115(1–4):497–502.

38. Gao S, Zhang L, Wang H, et al. A deformable image registration method to handle distended rectums in prostate cancer radiotherapy. Med Phys 2006; 33(9):3304–12, 2006.

39. Wang H, Dong L, Lii MF, et al. Implementation and validation of a three-dimensional deformable registration algorithm for targeted prostate cancer radiotherapy. Int J Radiat Oncol Biol Phys 2005; 61(3):725–35.

40. Wang H, Dong L, O'Daniel J, et al. Validation of an accelerated 'demons' algorithm for deformable image registration in radiation therapy. Phys Med Biol 2005; 50(12):2887–905.

41. Thirion JP. Non-rigid matching using demons. In Computer Vision and Pattern Recognition, 1996 Proceedings CVPR '96, 1996 IEEE Computer Society Conference on; 1996:245–51.

42. Thirion JP. Image matching as a diffusion process: an analogy with Maxwell's demons. Medical Image Analysis 2(3):243-260, 1998.

43. Kostelec PJ, Weaver JB, Healy DM. Multiresolution elastic image registration. Med Phys 1998; 25(9):1593–604.

44. Wang H, Dong L, O'Daniel J, et al. Validation of an accelerated 'demons' algorithm for deformable image registration in radiation therapy. Phys Med Biol 2005; 50(12):2887–905.

45. Rietzel E, Chen GTY, Choi NC, Willet CG. Four-dimensional image-based treatment planning: Target volume segmentation and dose calculation in the presence of respiratory motion. Int J Radiat Oncol Biol Phys 2005; 61(5):1535–50.

46. Zhang T, Orton NP, Tome WA. On the automated definition of mobile target volumes from 4D-CT images for stereotactic body radiotherapy. Med Phys 2005; 32(11):3493–502.

47. Ramsey CR, Langen KM, Kupelian PA, et al. A technique for adaptive image-guided helical tomotherapy for lung cancer. Int J Radiat Oncol Biol Phys 2006; 64 (4):1237–44.

48. Kupelian PA, Ramsey C, Meeks SL, et al. Serial megavoltage CT imaging during external beam radiotherapy for non-small-cell lung cancer: observations on tumor regression during treatment. Int J Radiat Oncol Biol Phys 2005; 63(4):1024–8.

Index

Figure 2.3 PET-CT guided target volume delineation. Please refer to full legend on page 23.
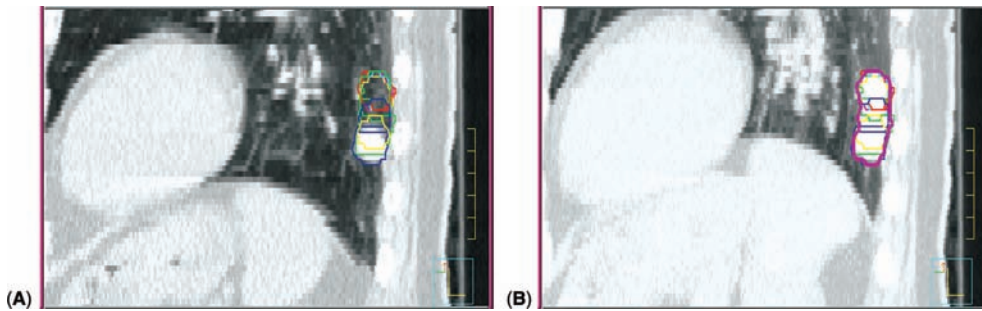
Figure 2.4 Breath evaluation and tumor-motion consideration using 4D-CT. Please refer to full legend on page 24.
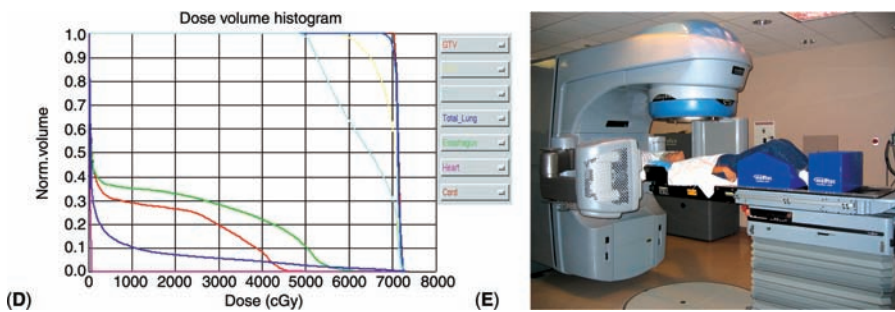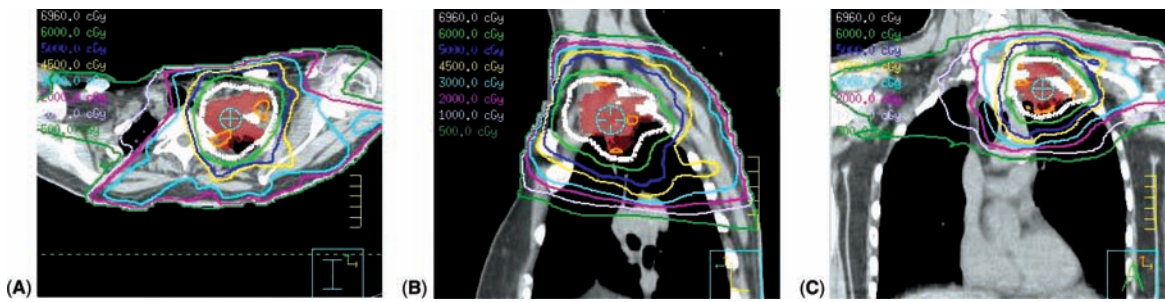
Figure 2.5 Onboard image-guided IMRT for superior sulcus cancer treated with concurrent chemotherapy; 69.6 Gy was prescribed and delivered as 1.2 Gy/fraction twice a day. Please refer to full legend on page 30.
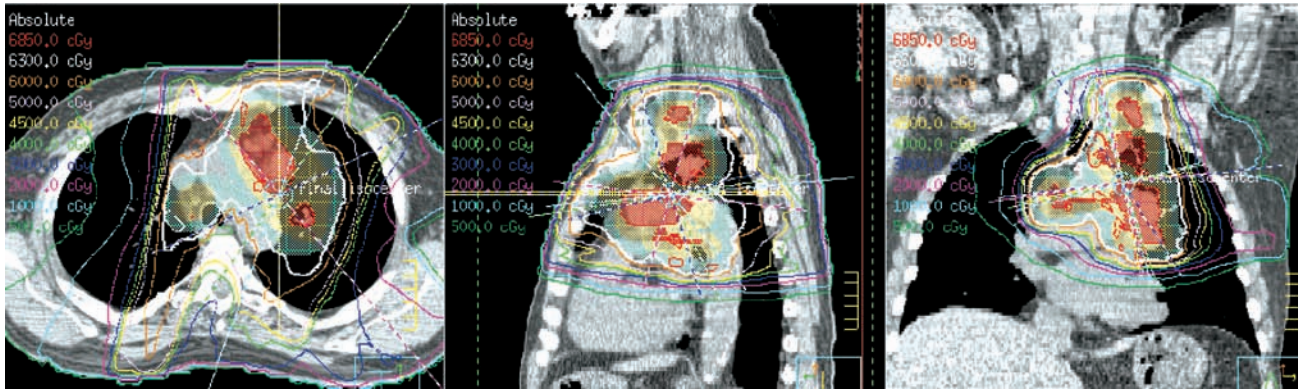
Figure 2.6 Image-guided therapeutic efficacy evaluation for stage III NSCLC treated with IMRT. Please refer to full legend on page 31.
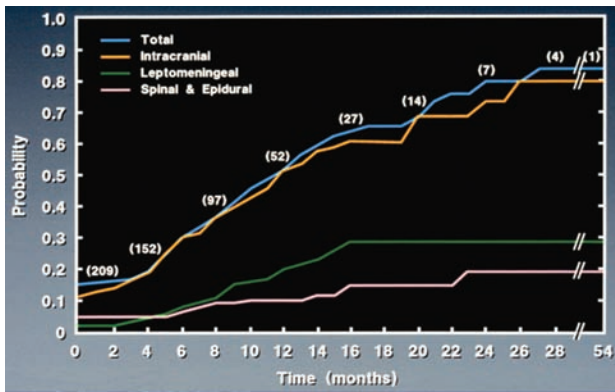
Figure 3.13 Analysis of autopsy series by Nugent et al. Please refer to full legend on page 54.
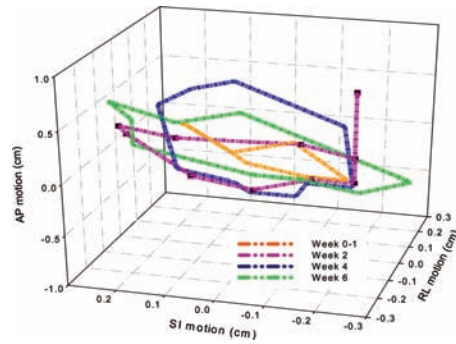
Figure 4.6A
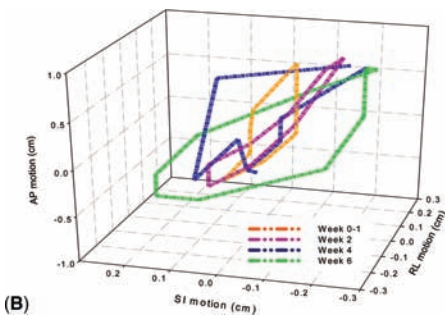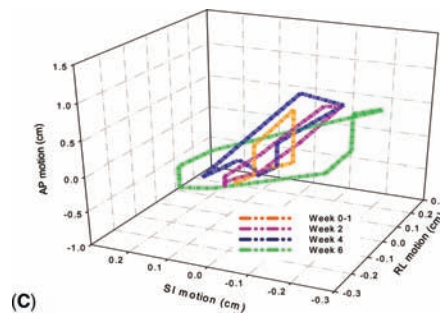
Figure 4.6 A–C Three-dimensional paths of GTV centroid motion. Please refer to full legend on page 71.
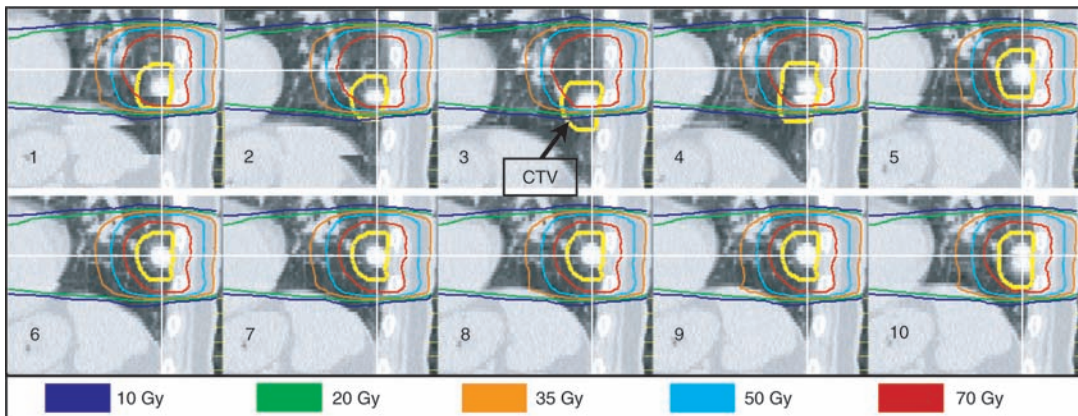
Figure 4.9 4D-CT scans showing the intrafractional effects of tumor motion on the dose distributed by IMRT. Please refer to full legend on page 74.
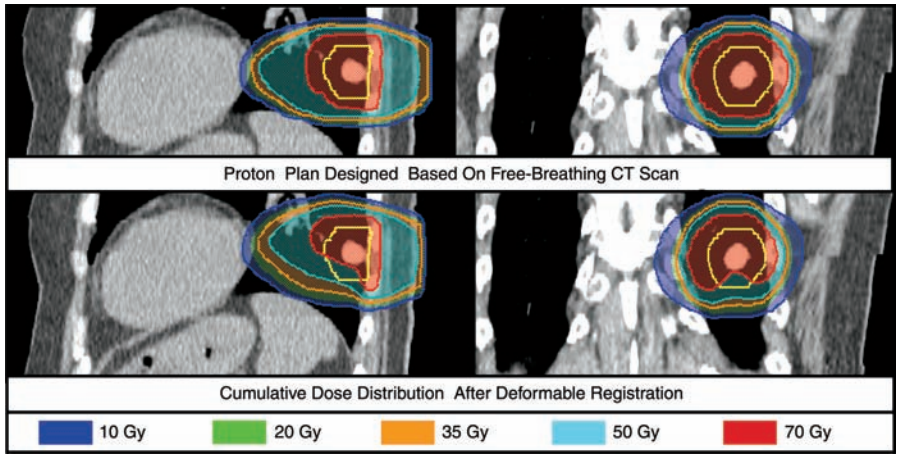
Figure 4.10 4D-CT scans showing a comparison of dose distributions of an IMRT plan for a patient with NSCLC. Please refer to full legend on page 74.
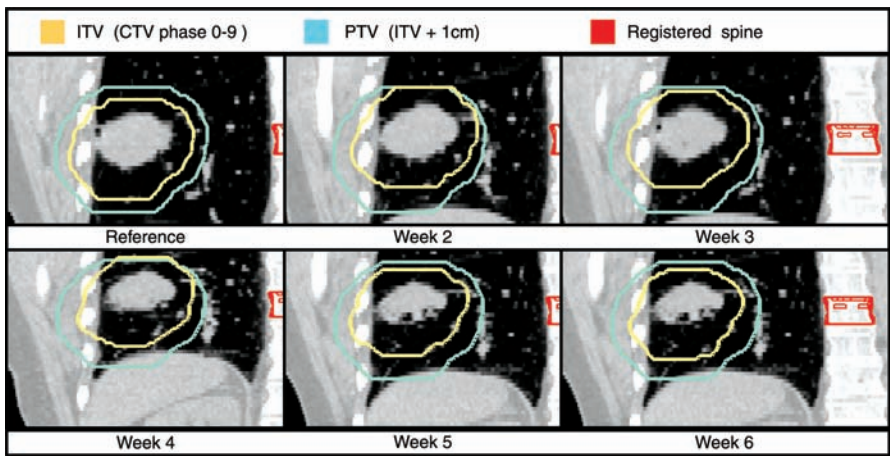
Figure 4.11 Serial 4D-CT scan (coronal view) of a non–small cell primary lung tumor with the reference planning target volume (PTV in cyan) geometrically correlated with the internal target volume (ITV in khaki). Please refer to full legend on page 76.
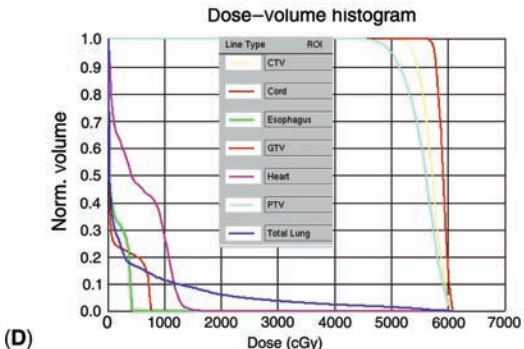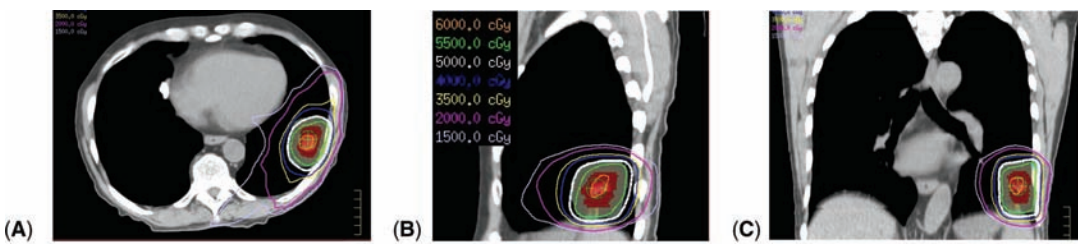
Figure 6.2 SBRT planning based on ITV generated by 4D-CT using MIP approach. Please refer to full legend on page 96.
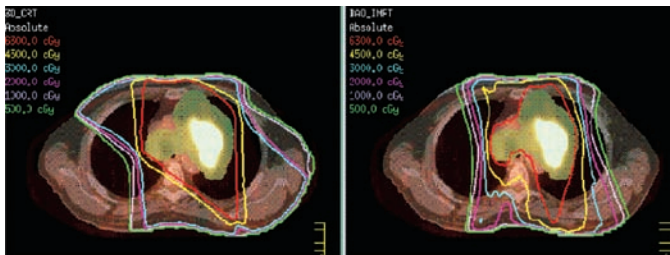
Figure 7.1A Axial view of the dose distribution of the 3D-CRT plan (*left panel*) and the IMRT plan (*right panel*). Please refer to full legend on page 105.
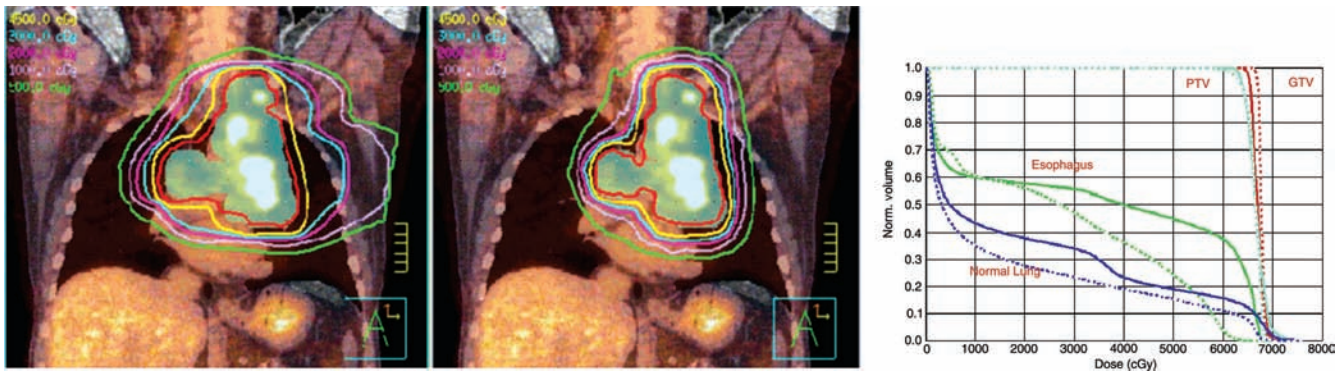
Figure 7.1 (**B**) Coronal view of the 3D-CRT dose distribution plan (*left panel*) and the IMRT plan (*right panel*); (**C**) comparison of the DVHs of the GTV, PTV, esophagus, and total lung from the 3D-CRT plan (*solid lines*) and IMRT plan (*dashed lines*). Please refer to full legend on page 105.
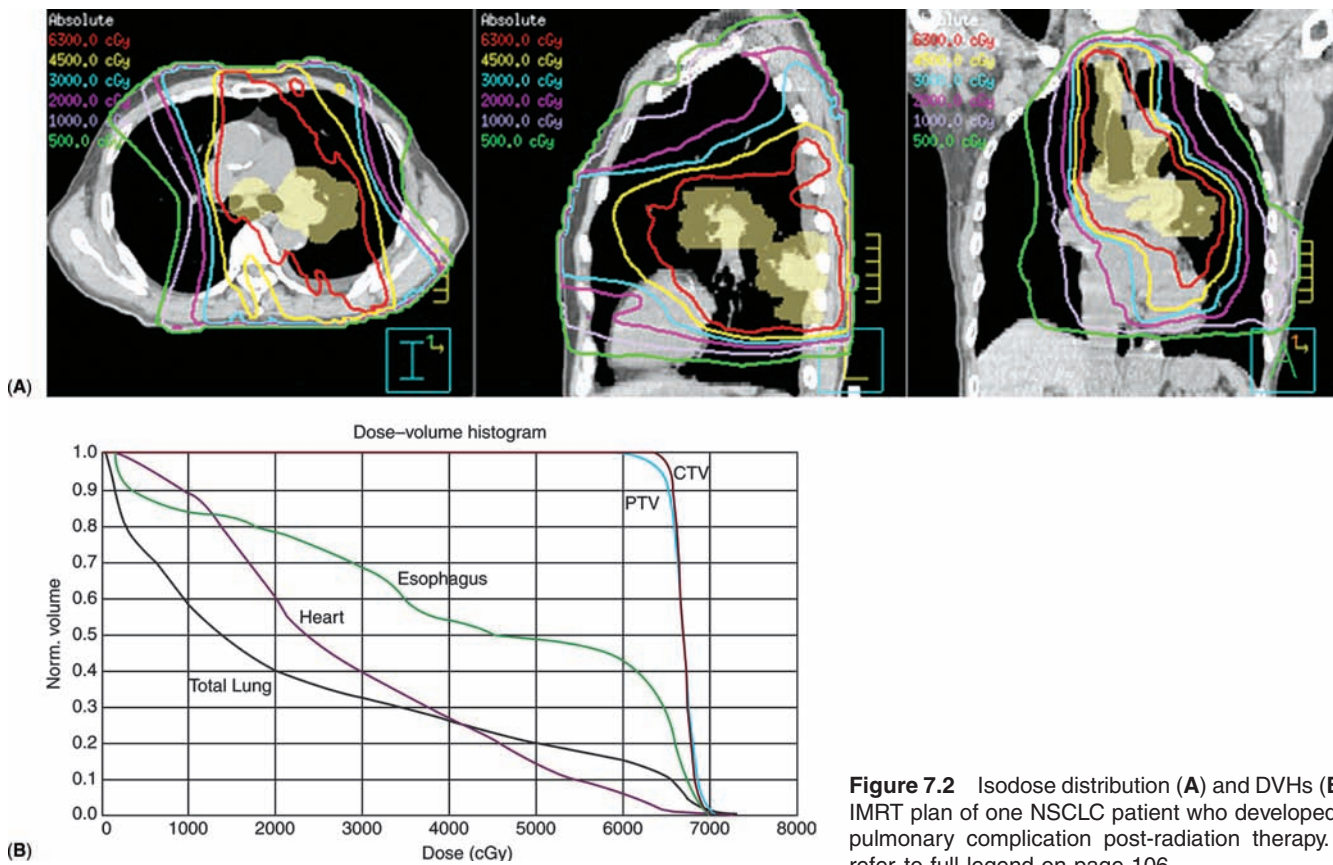
Figure 7.2 Isodose distribution (**A**) and DVHs (**B**) of the IMRT plan of one NSCLC patient who developed severe pulmonary complication post-radiation therapy. Please refer to full legend on page 106.
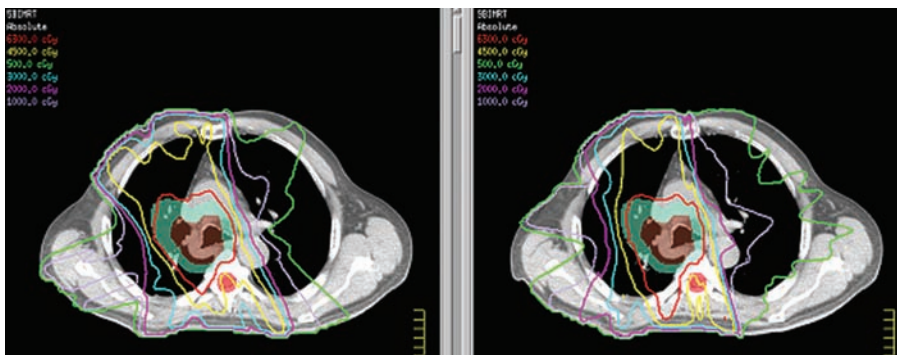
Figure 7.3 Comparison of the isodose distributions of the IMRT plans using either five optimized beams (*left panel*) or nine equi-spaced beams (*right panel*). Please refer to full legend on page 112.
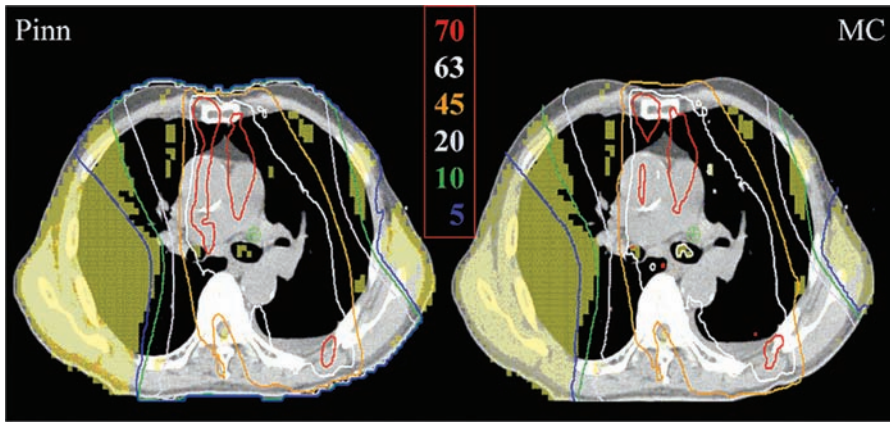
Figure 7.4 Comparison of the dose distributions from the Pinnacle calculations (*left panel*) to the Monte Carlo calculations (*right panel*) for one patient with lung cancer who was treated with IMRT. Please refer to full legend on page 114.
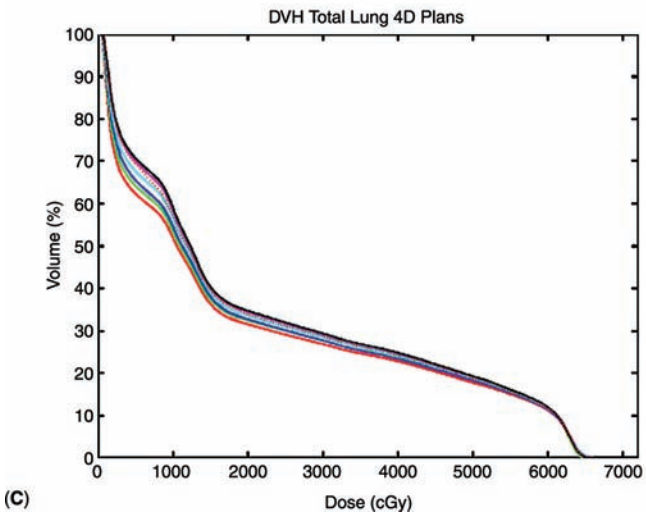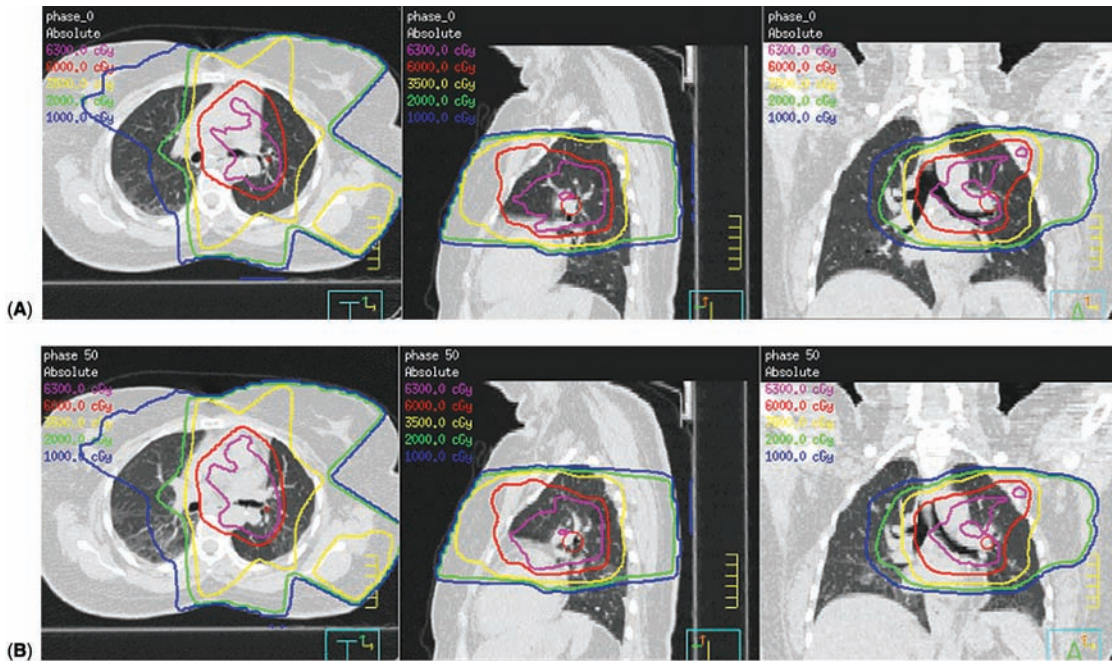

Figure 7.7 Comparison of dose distributions between inspiration phase (**A**) and expiration phase (**B**) for one patient with lung cancer treated with IMRT. Please refer to full legend on page 118.
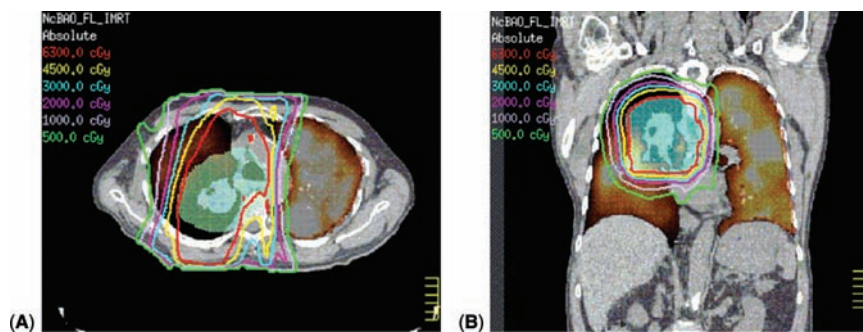
Figure 7.8 An IMRT plan generated using the lung perfusion images fused with the planning CT images. Please refer to full legend on page 120.
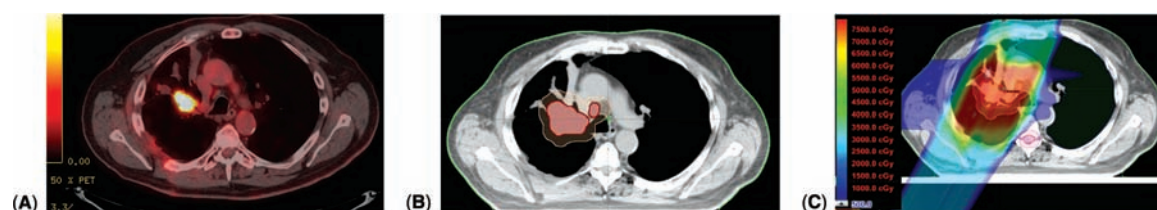

Figure 8.3 CT-based MIP approach for treatment planning in patients with stage III NSCLC. Please refer to full legend on page 130.
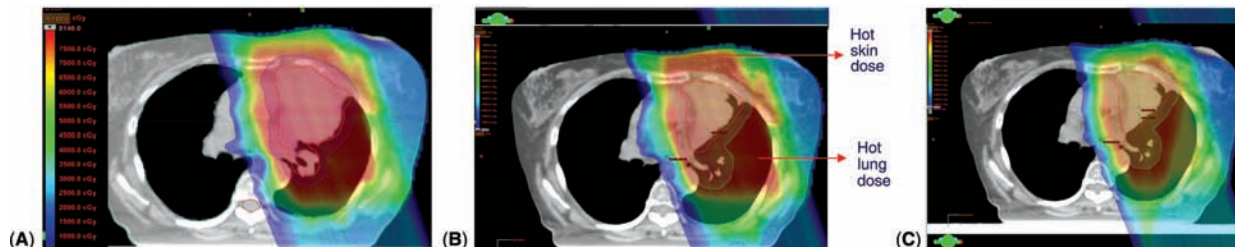

Figure 8.5 Images illustrate adapted proton therapy in a patient with stage III NSCLC. Please refer to full legend on page 134.

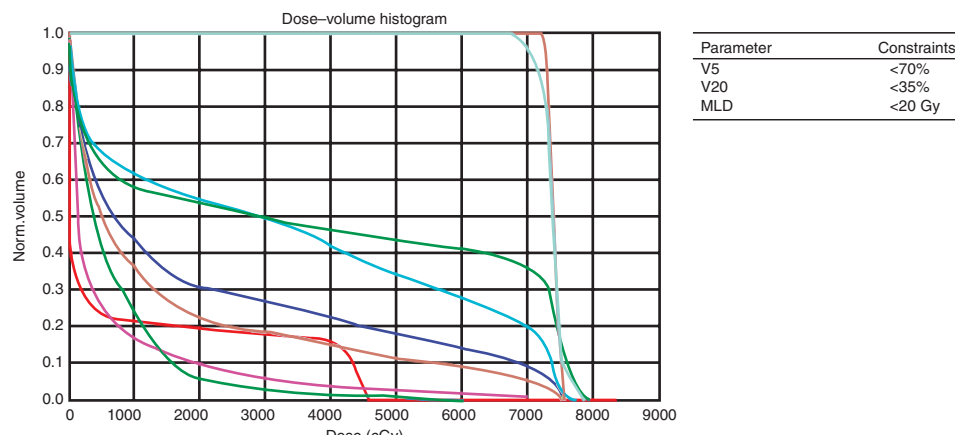| Parameter	Constraints
V5	<70%
V20	<35%
MLD	<20 Gy

Figure 9.5 Typical dose-distribution and DVHs (left) and dose constraints for use in planning treatment of stage III NSCLC. Please refer to full legend on page 146.
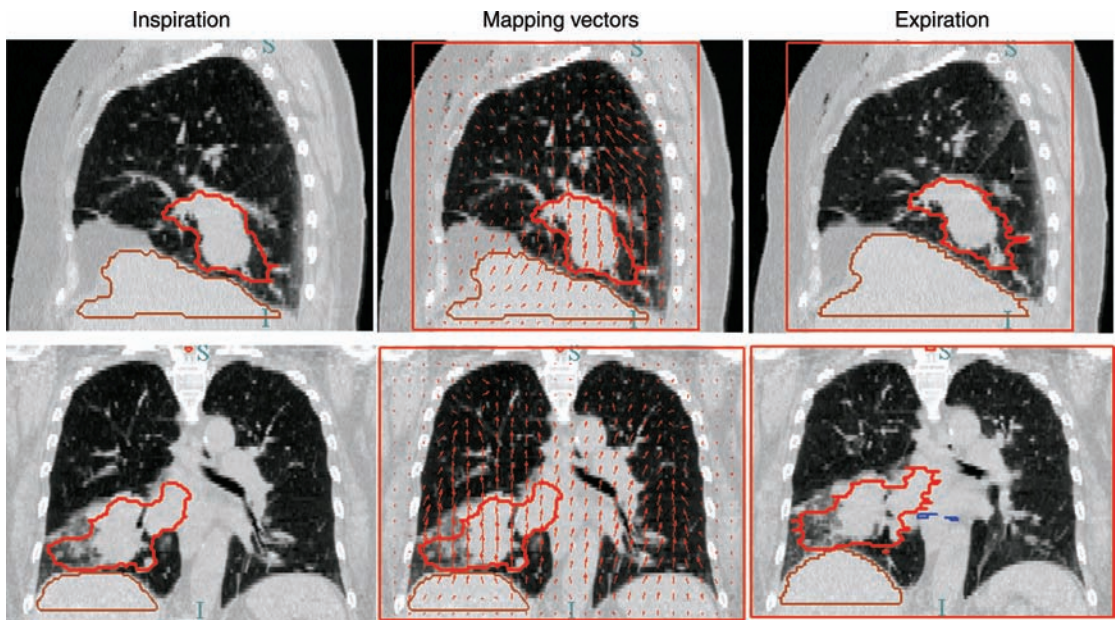
Figure 10.2 An example of tracking anatomy using a deformable image registration method. Please refer to full legend on page 164.
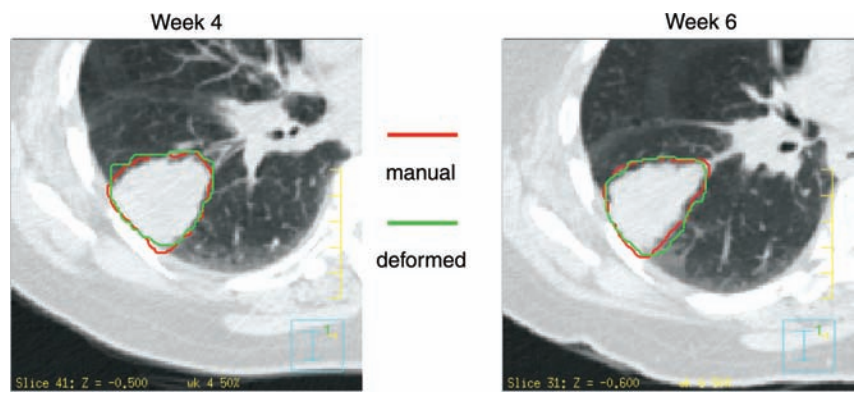

Figure 10.3 Tumor volume can also shrink during the course of radiotherapy. Please refer to full legend on page 165.
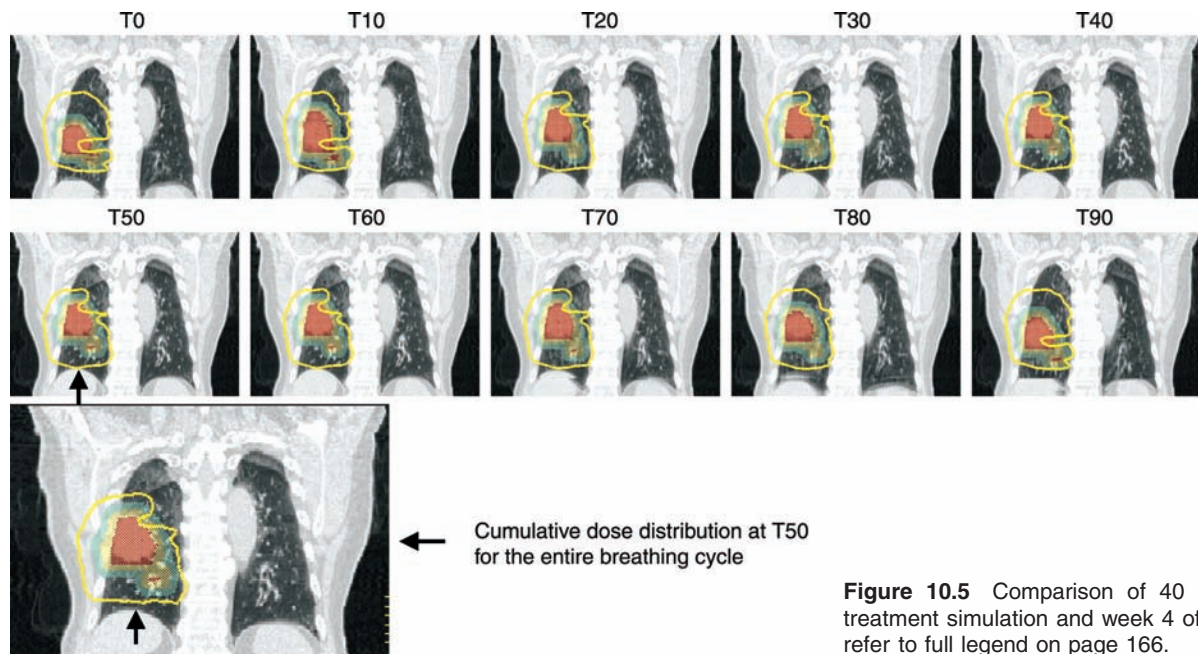

Cumulative dose distribution at T50 for the entire breathing cycle

Figure 10.5 Comparison of 40 dose distributions at treatment simulation and week 4 of radiotherapy. Please refer to full legend on page 166.

Sagittal Plane   Coronal Plane

Treatment Plan Designed Based On Free-Breathing CT Scan

Cumulative Dose Distribution After Deformable Registration
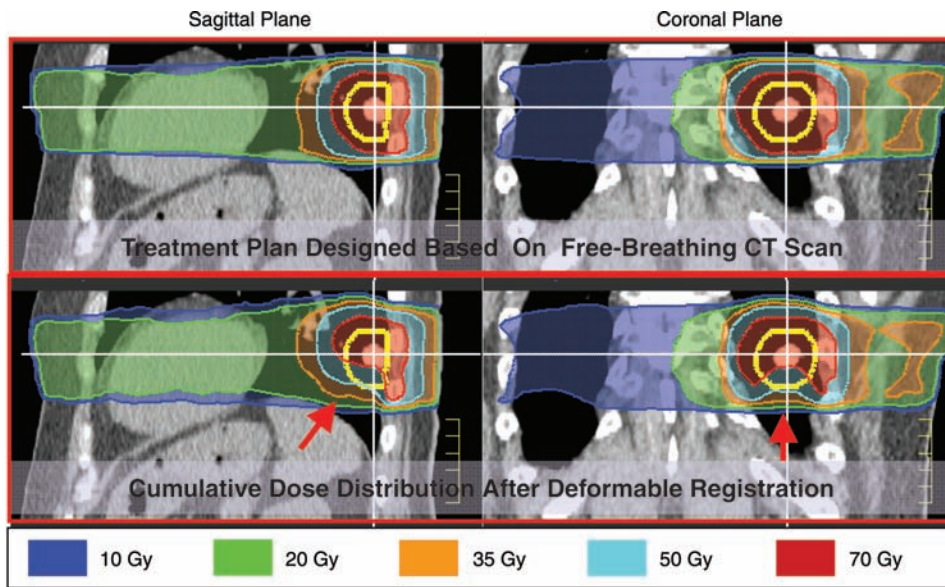
| 10 Gy | 20 Gy | 35 Gy | 50 Gy | 70 Gy |

Figure 10.6 Comparison of a treatment plan as perceived on a free-breathing CT (top row) and as realized after accounting for breathing motion in all 10 phases (bottom row). Please refer to full legend on page 167.
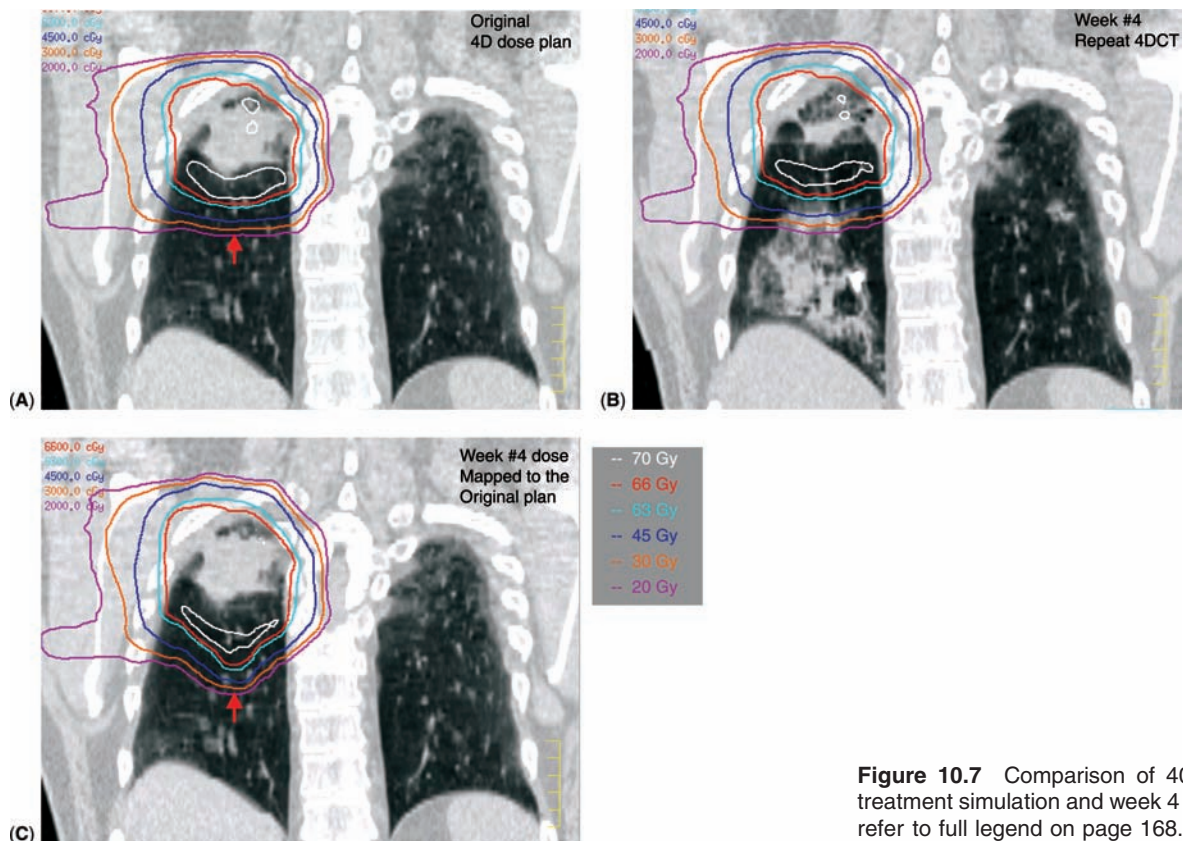

Original 4D dose plan

Week #4 Repeat 4DCT

Week #4 dose Mapped to the Original plan

-- 70 Gy
-- 66 Gy
-- 63 Gy
-- 45 Gy
-- 30 Gy
-- 20 Gy

Figure 10.7 Comparison of 40 dose distributions at treatment simulation and week 4 of radiotherapy. Please refer to full legend on page 168.

about the book...

Lung cancer is the leading cause of cancer death in the United States, but IGRT (image-guided radiation therapy) offers the possibility of more aggressive and enhanced treatments. The only available source on the subject that emphasizes new imaging techniques, and provides step-by-step treatment guidelines for lung cancer, this source helps clinicians locate and target tumors with enhanced speed, improve the accuracy of radiation delivery, and correctly target cancerous masses while avoiding surrounding structures.

Edited by radiation oncology experts from the renowned M.D. Anderson Cancer Center, this guide focuses on novel approaches using IGRT, particularly PET/CT, SPECT, 4-D CT, stereotactic body radiation therapy, IMRT and proton radiotherapy, and offers expert guidance on the dose, fractionation, target volume delineation (including recommended margins with and without respiratory gating based on our new 4-D CT study), and normal tissue tolerances...stands as the first step-by-step guide for radiation oncologists to implement new image-guided techniques into their day-to-day clinical practice, and considers the practical issues of implementing these approaches into their routine...helps clinicians use imaging technologies to detect changes in tumor size, shape, position, or metabolism over a course of radiotherapy treatment...provides disease stage-specific treatment guidelines and clearly lays out imaging techniques...and serves as a roadmap for future research and development.

about the editors...

JAMES D. COX is Professor and Head, Hubert L. and Olive Stringer Distinguished Chair for Oncology in Honor of Sue Gribble Stringer, Department of Radiation Oncology, The University of Texas M.D. Anderson Cancer Center, Houston. Dr. Cox received the M.D. degree from the University of Rochester School of Medicine and Dentistry, New York.

JOE Y. CHANG is Assistant Professor, Clinical Service Chief of Thoracic Radiation Oncology, Department of Radiation Oncology, The University of Texas M.D. Anderson Cancer Center, Houston. Dr. Chang received the M.D. degree from Shanghai Medical University and Ph.D. degree from The University of Texas M.D. Anderson Cancer Center, Houston.

RITSUKO KOMAKI is Professor of Radiation Oncology and the Gloria Lupton Tennison Distinguished Professorship in Lung Cancer, The University of Texas M.D. Anderson Cancer Center, Houston. Dr. Komaki received the M.D. degree from Hiroshima University School of Medicine, Japan.

Printed in the United States of America